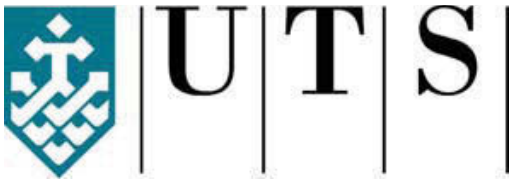

University of Technology Sydney

Advanced Control of Three-Phase Full-Bridge Converter in Microgrids

Xiaolong Shi

M.E. (Electrical Engineering), B.E. (Electrical Engineering)

School of Electrical, Mechanical and Mechatronic Systems
University of Technology Sydney, Australia

A thesis submitted to the University of Technology Sydney
for the Degree of Doctor of Philosophy

March 2017

CERTIFICATE OF AUTHORSHIP/ORIGINALITY

I certify that the work in this thesis has not previously been submitted for a degree nor has it been submitted as part of requirements for a degree except as fully acknowledged within the text.

I also certify that the thesis has been written by me. Any help that I have received in my research work and the preparation of the thesis itself has been acknowledged. In addition, I certify that all information sources and literature used are indicated in the thesis.

Signature of Candidate

Acknowledgements

First and foremost, I would like to express sincere gratitude and appreciation to my supervisor, Professor Jianguo Zhu, for providing tremendous levels of support over the years. I am so grateful for his mentoring in the discipline of power electronics and renewable energy systems with great encouragement and persistence. His enthusiasms on research and deep insight in multiple research areas benefited me a lot and broadened my thoughts, which will be most useful for my future study and life.

I am also thankful to Dr. Li Li, the co-supervisor, for his fruitful discussions, invaluable guidance, enthusiastic help, and consistent encouragement throughout the entire research project, which helped me a lot in research and in daily life.

Also, I would like to thank Associate Professor Dylan Dah-Chuan Lu, the co-supervisor, His rich experience and advices in power electronics area, which had a very precious direction on my work. His rigorous and professional attitudes towards research influenced me a lot.

I am also grateful for the valuable technical support, advices and kind helps from my laboratory colleagues and friends in the Centre for Electrical Machines and Power Electronics, University of Technology Sydney (UTS), in particular Associate Professor Youguang Guo, Dr. Jiefeng Hu, Dr. Gang Lei, and Dr. Jingyang Zheng.

I want to express my deepest gratitude to my parents for their support and encouragement in my whole student life. Their consideration and dedication stimulated me to challenge myself.

Finally, I want to express my deepest love to Jing Xu, for her accompany, sacrifice and tolerance throughout the most valuable years.

TABLE OF CONTENTS

LIST OF SYMBOLS

C	Filter capacitance [μF]
$d_a^{'}, d_b^{'}$	Duty ratio of voltage vector $V_a^{'}, V_b^{'}$
dp, dq	Digitized signals of tracking errors of active and reactive power
e_a, e_b, e_c	Three-phase AC source voltages [V]
$e_{\alpha\beta}$	Input source voltage vector [V]
f	Source voltage frequency
H_1 H_2.... H_5	Three-phase full-bridge converter module
I_a, I_b, I_c	AC source three phase current [A]
$I_{\alpha\beta}$	Line current vector [A]
i_L	AC inductor current [A]
L	Line inductance [mH]
P_i, Q_i	Active and reactive power with i-th voltage space vector
P^* Q^*	Active and reactive power reference value.
Q_1, Q_4	Switches in IBDC converter
R	Line resistance [Ω]
R_L	Load resistance [Ω]
S_1, S_2	Switches of power converter.
S_{ia}, S_{ib}, S_{ic}	Switching states of three-phase full-bridge converter.
S_n	Sector number
T_c	Computing time of control strategy [μs]
T_s	Sampling period [μs]
t_a, t_b, t_c	Duration time of space voltage vector [μs]
V_a, V_b, V_c	AC terminal voltages of the three-phase bridge [V]
$V_{\alpha\beta}$	Three-phase converter input voltage vector [V]
$V_{i\alpha}$,$V_{i\beta}$	Voltage space vector for each switching state [V]
V_0,V_1..V_7	Voltage space vector

V_{-a}, V_{-b}	Reverse vector of V_a, V_b
V_{dc}	DC terminal Voltage [V]
V_1, V_2	Input and Output Voltage [V]
V_α, V_β	Voltage vectors in the stationary reference frame [V]
ΔP ΔQ	Variation of active and reactive powers
ΔI_α ΔI_β	Variation of AC source current.
δ_{pi}, δ_{qi}	Active and reactive power slopes of i-th voltage space vector
δ_{pa}, δ_{qa}	Active power and reactive power slopes of the voltage vector
λ, λ_1, λ_2, λ_3	Weighting factors

LIST OF ABBREVIATIONS

AC	Alternating Current
BIL	Basic Insulation Level
CDPC	Conventional Direct Power Control
CEC	California Energy Commission
CFPP	Current Fed Push-pull
CMPC	Conventional Model Predictive Control
CPUC	California Public Utilities Commission
CPDCC	Conventional Predictive Duty Cycle Control
CSVMDPC	Conventional Space Vector Modulation based Direct Power Control
DAB	Dual Active Bridge
DC	Direct Current
DFIG	Doubly-Fed Induction Generator
DER	Distributed Energy Resource
DG	Distributed Generation
DPS	Dual-phase-shift
DSP	Digital Signal Processor
DTC	Direct Torque Control
ESS	Energy Storage System
ESPS	Extended Single-Phase-Shift
EPRI	Electric Power Research Institute
FCS-MPC	Finite Control Set MPC
IC	Internal Combustion
IBDC	Isolated Bidirectional Full-bridge DC-DC Converter
ISVMDPC	Improved SVM based Direct Power Control
IPDCC	Improved Predictive Duty Cycle Control
ISS	International Space Station
MPC	Model Predictive Control

MPCDDC	Model Predictive Control based Direct Duty Control
MMPC	Multi-functional Model Predictive Control
MPDCC	Model Predictive Duty Cycle Control
MPDPC	Model Predictive based Direct Power Control
MPCPDCC	Model Predictive Control based Predict Duty Cycle Control
MPPT	Maximum Power Tracking Point
MV	Medium Voltage
PEI	Power Electronic Interface
PDCC	Predictive Duty Cycle Control
PV	Photovoltaic
PWM	Pulse Width Modulation
RTDX	Real Time Data Exchange
STDPC	Switching Table based Direct Power Control
SST	Solid State Transformer
SIWG	Smart Inverter Working Group
SVM	Space Vector Modulation
SVMDPC	Space Vector Modulation based Direct Power Control
RES	Renewable Energy Sources
RPDCC	Reversible Predictive Duty Cycle Control
RMPCPDCC	Reversible Model Predictive Control based Predict Duty Cycle Control
SPDDC	Simplified Predictive Duty Cycle Control
SMPDDC	Simplified Model Predictive Direct Duty Cycle
THD	Total Harmonic Distortion
UPS	Uninterruptible Power Supply
VOC	Voltage-Oriented Control
VSC	Voltage Source Converter
ZVS	Zero Voltage Switching

LIST OF FIGURES

LIST OF TABLES

ABSTRACT

This thesis focused on application and control of three-phase full-bridge converter in renewable energy system (RES). Current challenges and application of the converter are reviewed, novel concept of smart converter and novel microgrid topology with modular design are proposed. Various kinds of control strategies are comprehensively researched and proposed to improve the performance.

Through review of power electronic interface (PEI) and control strategies in RES, it is concluded that three-phase full-bridge converter is generally utilized for AC/DC bi-directional conversion and could realize DC/DC conversion with high frequency transformer. Novel topology of microgrid is proposed with modular structure and wireless communication ability by using three-phase full-bridge converter modules, which is extremely reliable, expandable and flexible. The control modes, the control strategies for each module and system control strategy are discussed. Meanwhile, the smart converter concept is proposed for RES to improve the utility power quality and system stability.

For ancillary services and advanced functions, control strategies of three-phase full-bridge AC/DC converter play an important role. Firstly, the conventional switching table based direct power control (STDPC) and model predictive based direct power control (MPDPC) are compared. Though MPDPC has advantages such as fast dynamic response and lack of modulator, the mutual influence of control objectives is obvious and switching frequency is high. Thus novel advanced multi-functional MPDPC for improving both the dynamic and steady state performances simultaneously is proposed. Not only the novel control can improve the steady-state performance while impeding switching frequency increment, but it can also eliminate mutual influence between active and reactive powers during dynamic instant.

Due to finite number of vectors, the single vector selection based method still bears with variable switching frequency, relatively higher power ripple and spread spectrum nature of harmonics. Therefore, the three-vector based conventional predictive duty

cycle control (PDCC) uses prediction value of power slope and square error minimization method to calculate duration time of adjacent two none-zero vectors, which are selected based on sector information. However, incorrect vector selection cannot be avoided and negative duration time exists. Improved PDCC is presented to solve this issue by reselection of none-zero vector and recalculation of duration time, while the complexity and computation burden increase significantly. Finally, reversible PDCC method is proposed, which does not recalculate the power slope and duration time, it reduces the control complexity significantly while achieving better dynamic and steady performance.

However, there are still some inherent disadvantages of above mentioned methods. Firstly, the mutual influence inherits. Secondly, the calculated negative duration time cannot be wholly eliminated. Thirdly, the computation burden is quite high. Lastly, it limits the method to three vectors based approach only. Therefore, model predictive based vector selection is proposed to avoid incorrect vector selection, simplified duration time calculation method without power slope calculation is proposed, the dynamic and steady-state performance are further improved. Two vector based simplified model predictive duty cycle control (SMPDCC) is proposed with comparison of conventional two vector based approach, improved space vector modulation based DPC (ISVMDPC) is presented. Three vector based approaches with mutual influence elimination and simplified calculation are proposed. Comprehensive comparisons of each methods with simulation and experimental results are conducted.

CHAPTER 1

INTRODUCTION

1.1 Research Background

With the fast consumption of fossil fuels — the coal, oil and natural gas, which accounts for 81% of the total energy consumption in 2012 [1.1], fossil resources are experiencing a quick reduction as the environment crisis becomes more and more serious. To overcome these problems, great research efforts have been made in order to discover new ways to make more efficient use of renewable energy sources (RES), such as photovoltaic (PV) and wind energy, hydrogen fuel cell and lithium ion battery systems [1.2]-[1.5], and more advanced technologies for power integration in the utility grid.

In recent years, more and more RES are integrated into the power grid. For example, in 2015, the United States experienced continuous growth in total PV capacity with expected new installations reaching almost 9,000 MW [1.6]. The installed capacity of distributed generation (DG) is predicted to be doubled by 2023 [1.7]. However, the adaptation of the utility grid to integrate DGs in a efficient, distributed, and reliable way still remains a challenge and the key solution relies upon the advanced control of power converters in RES to provide better power quality with good control ability.

Meanwhile, the power electronics research has experienced a rapid development, because of the fast evolution of semiconductors that improved the transient response of the power, and high speed digital signal processors (DSPs) enabling to decrease the processing time and increase the control complexity [1.8]-[1.10]. A widespread use of the power electronic interface (PEI) in DG units can not only act as cost-effective and flexible DG interfaces, but also enable the control and management of the power and efficient power flows in renewable energy systems [1.11]-[1.13].

1.2 Challenges with High Penetration of Renewable Sources

With the growing deployment of RES, the larger reliance on variable, weather-dependent and distributed resources instead of the traditional energies will introduce more complications into the power regulation of distribution systems [1.14]-[1.17].

In earlier times with low-penetration of renewable energy systems, the PEI served the basic functions of power conversion and energy feeding, and would be disconnected from the grid during abnormal grid conditions or power outages [1.18]-[1.20]. For example, when the grid tied PV systems were rare, the inverter was required to produce a unity power factor and get out of the way quickly if anything bad happened as there was no requirement for fault ride-through in response to grid voltage or frequency excursions.

With more and more grid integrations of small-scale DGs, e.g. residential PV inverters, the utility power systems are experiencing divergent grid modernization with a transition towards a decentralized and distributed grid structure [1.21]. Thus, some issues appear more frequently and cannot be ignored as they were before. For example, if there is an increase in system frequency, the increased risk could trigger the power converters to disconnect a large amount of PV capacity from the grid simultaneously. In Germany, if the system frequency were to rise above the maximum level defined by the current PV interconnection standards (50.2 Hz), several gigawatts of PV capacity could potentially be disconnected instantly. This problem is known as the “50.2 Hz problem” [1.22]. Besides, as the amount of PV generation increases, it is required to ramp the conventional generating resources down at sunrise and to ramp them up quickly at sunset.

The development of DER requires the PEI in renewable energy systems to have more advanced functions with regard to the costs, rescale, power quality and system reliability improvement. In addition, in order to solve the above mentioned issues, the smart inverter was developed to provide multi-functions and various ancillary services

such as fault ride-through and reactive power compensation, to improve the reliability, stability and efficiency of the power distribution system [1.23-1.25].

1.3 Three-phase Full-bridge Converter for Renewable Energy Systems

The three-phase full-bridge converter as shown in Fig.1.1, which is also widely named as voltage source converter (VSC), has been widely used for integration of RES, active power filters, electric drives, and energy storage systems (ESS) due to its advantages such as four-quadrant power flow control, natural power factor correction, flexible DC-link voltage adjustment, and relatively low DC filter capacitance when compared to uncontrolled AC/DC converters [1.26].

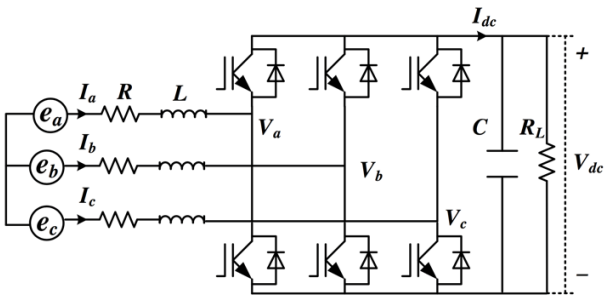

Fig. 1.1 Three phase PWM AC/DC converter

Through series connection of the three-phase full-bridge converter module with a high frequency transformer, the isolated bidirectional full-bridge DC/DC converter (IBDC) can be formed, as shown in Fig.1.2, and the DC/DC conversion can be realized. This has been verified to be more suitable as DC/DC converters in RES because of its the advantages of high power density, high efficiency, high reliability, zero voltage switching (ZVS), wide operation range, and galvanic isolation by a high-frequency transformer [1.27], [1.28]. It should be noted that the IBDC shown in Fig.1.2 is three-phase based topology, in terms of single phase based IBDC, which is more suitable for low power levels as we can just disable the control signals of one leg in each bridge, such as the IBDC converter for control of the ESS as shown in Fig.1.3.

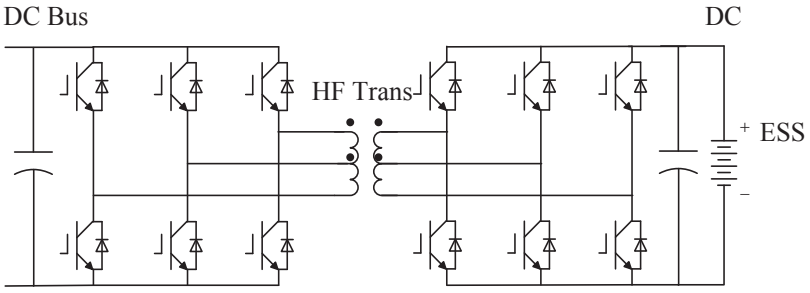

Fig. 1.2 Topology of dual active bridge converter (three phase topology)

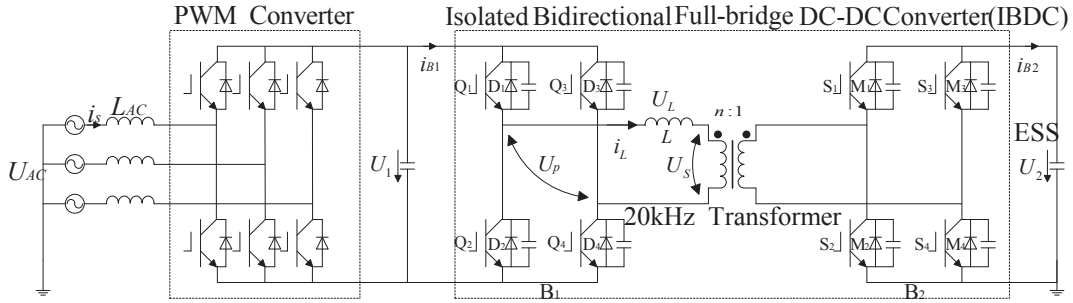

Fig. 1.3 Energy storage system based on IBDC in a microgrid

To form a microgrid, the IBDC converter and three-phase full-bridge AC/DC converter can also be applied as the PEI module for power integration and distribution, for instance, in the microgrid structure as shown in Fig.1.4 [1.29].

1.4 Advanced Control Strategies

Since the three-phase full-bridge converter plays an important role in RES, the control strategies for the three-phase full-bridge converter for bi-directional AC/DC conversion have attracted a lot of attentions with wide applications of the topology. Thus, some representative control strategies are worth discussing.

For single vector based control strategies, the switching table based direct power control (STDPC) and voltage-oriented control (VOC) are two typical control methods [1.30]-[1.32]. The VOC controls the input active and reactive powers through regulating

the input current. Although it has good dynamic response and stability in steady-state, the inner current controller has a large influence on system performance, as shown in Fig.1.5.

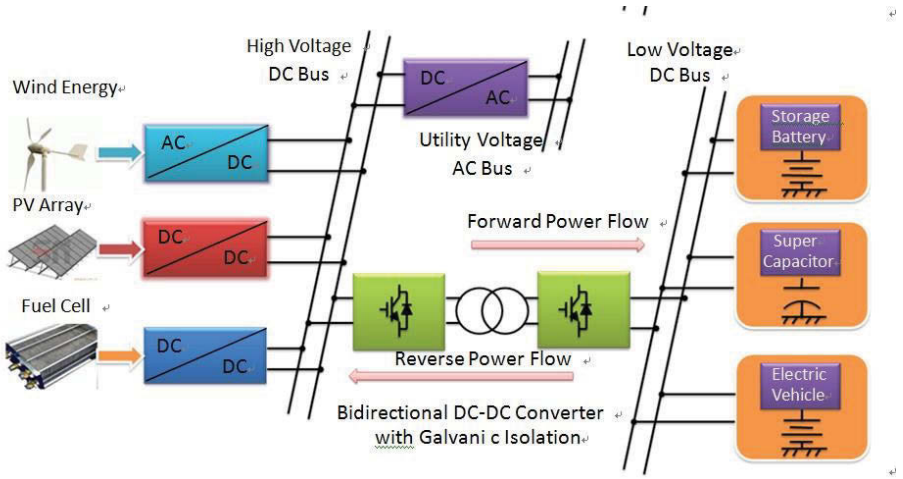

Fig. 1.4 Typical application of IBDC for power distribution in microgrid

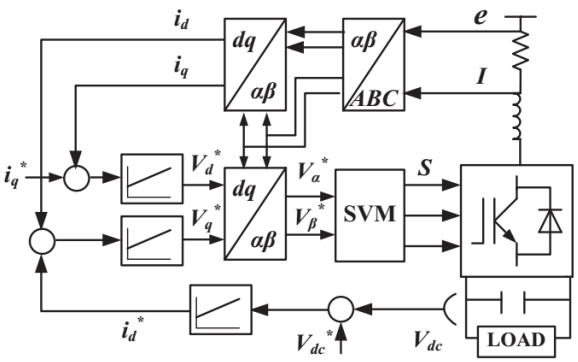

Fig. 1.5 Block diagram of VOC

The STDPC regulates the active and reactive powers directly by selecting an appropriate space voltage vector from the preset switching table based on the instantaneous errors between the reference and instantaneous values of active and reactive powers, and the voltage vector location [1.33], as shown in Fig.1.6. It has a simple control algorithm and does not need an internal controller while retaining good dynamic performance. However, the control accuracy cannot be guaranteed.

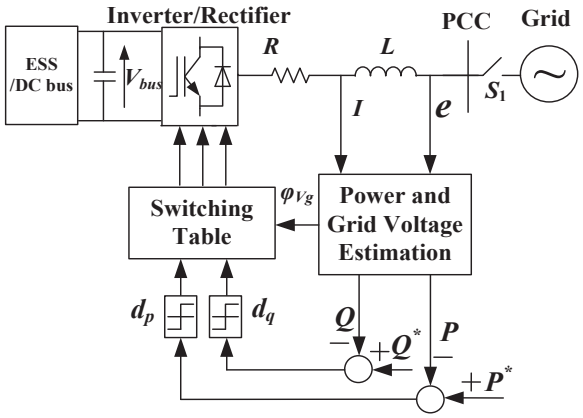

Fig. 1.6 Block diagram of conventional DPC-based power regulation

Without using a predefined switching table, some methods have been incorporated into direct power control (DPC) to achieve better performance, such as fuzzy logic rules, space vector modulation, sliding mode, virtual flux and predictive control [1.34]-[1.38], among which the predictive control strategy has attracted lots of attentions among power electronics researchers [1.39]-[1.47]. It is a flexible control method that allows simple inclusion of system nonlinearities and constraints. In model predictive control (MPC) based DPC control, the system model and cost function of errors between the reference and the actual active and reactive powers are evaluated for a finite set of voltage space vectors, the best voltage space vector that minimizes the cost function is selected for actuation, as shown in Fig.1.7. It has some advantages, such as fast dynamic response, lower power ripple, more sinusoidal current, lack of modulator, and flexibility to include other requirements or constraints in the controller [1.39]-[1.43].

For single vector based control strategies mentioned above, selecting one vector in a sampling period results in variable switching frequency and the spread spectrum nature of harmonics and thus complicating further the filter design [1.44]-[1.45]. The sampling frequency also has to be relatively high to achieve satisfactory performance. In order to overcome the disadvantages of MPDPC and further improve the performance, more efforts have recently been made to select two or three voltage vectors in one sampling period to reduce power ripples and achieve constant switching frequency.

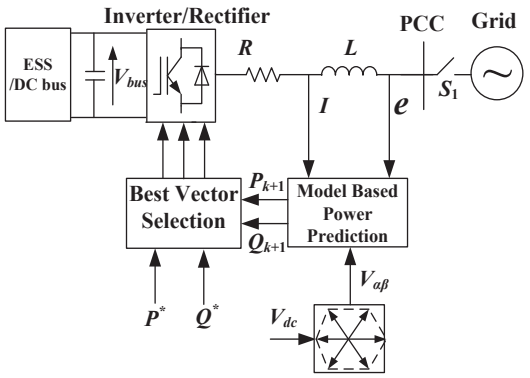

Fig.1.7 Block diagram of MPC-based power regulation

For two vector based control strategy, one best none-zero vector is firstly selected, and a second vector could be zero vector as presented in [1.46] or be selected from the rest of the vectors as in [1.47]. For instance, in [1.46], the best none-zero vector has been selected by a cost function of model predictive control and the corresponding switching duration time is calculated by minimizing the squared errors of the instantaneous active and reactive power between reference value, which is also known as the lease square minimization method. Fig.1.8 illustrates the control diagram, which considers the one step delay compensation for practical applications.

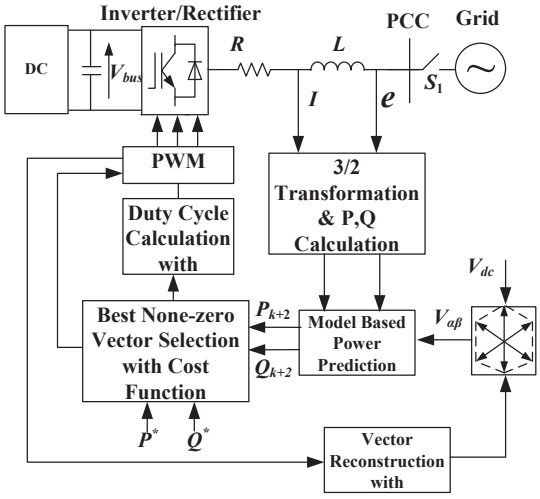

Fig.1.8 Block diagram of the SPDCC for the AC/DC converter

For the three vector based control strategy, the control method as shown in Fig.1.8 can also be expanded to a three vector based method similarly with the main difference

being that the adjacent vector pair is selected using different cost functions and then the duration time could be calculated by using a similar method. The space vector modulation (SVM) based DPC and predictive duty cycle control are also two typical control methods [1.48]-[1.51]. In terms of SVMDPC, it tracks errors of the active and reactive powers and puts them into two separate PI regulators. Its control block diagram is illustrated in Fig.1.9. The PI regulators are used to transform the input tracking errors to V_α and V_β in the stationary reference frame. Then SVM module is used to generate the switching signals, though the PI controller and coordinate transformation to increase the control complexity.

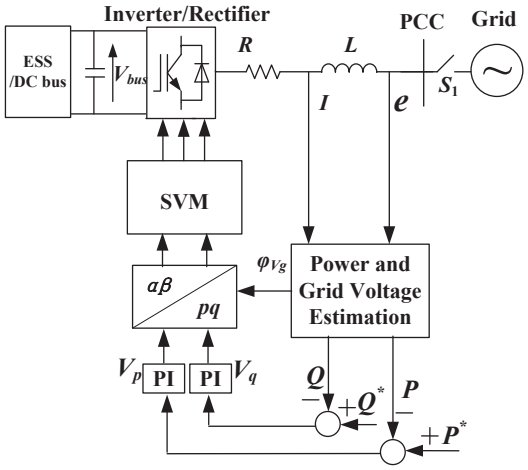

Fig. 1.9 Block diagram of SVMDPC-based power regulation

The predictive control selects the best adjacent two none-zero vectors based on the sector information. The least square method is employed to calculate the duty cycle of each vector. However, it may select incorrect voltage vectors based on the conventional vector sequence table, which will further result in the negative value of optimal duration time, and deteriorate the control performance.

It is concluded that each method has its advantages and disadvantages. To overcome the disadvantages, some novel control method should be developed.

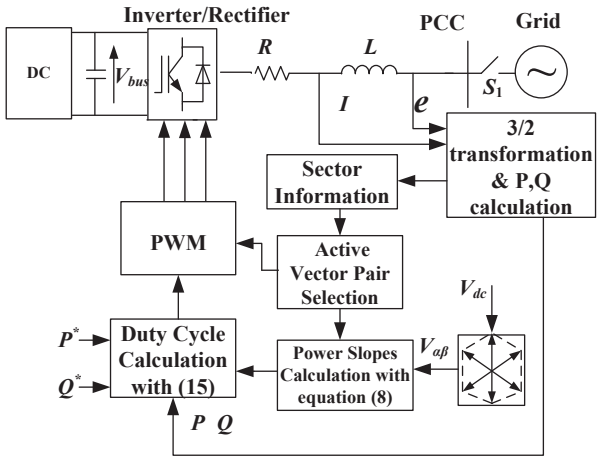

Fig.1.10 Block diagram of PDCC for the AC/DC converter

1.5 Research Objectives

In order to exploit the control and integration of DG in renewable energy systems, this thesis is focused on the application of the three-phase full-bridge converter in renewable energy systems and development of control strategies to solve technical problems related to the modelling, control, and power management. The main objectives of this research project can be described as:

(1) Development of applications of three-phase full-bridge converters for renewable energy systems,

(2) Discussion of three-phase full-bridge converter as a converter module for application with various scenarios in the microgrid, and

(3) Development of advanced control techniques for three-phase full-bridge converters to achieve good power quality and control performance.

1.6 Outline of the Thesis

The thesis is organized as follows:

In Chapter 1 (this chapter), the research background and significance of this thesis are discussed, determining the main focus of the three-phase full-bridge converter for renewable energy applications. The challenges of current AC/DC converters for DG

integration and its control strategies are also introduced. The objectives of the thesis are then presented.

Chapter 2 presents a comprehensive review of the power electronic interface for AC/DC and DC/DC conversions as well as the corresponding control strategies. The topology of the microgrid is also briefly reviewed.

Chapter 3 proposes the microgrid topology with modular design. The control modes of the microgrid and control strategies of the converter module are discussed. A comprehensive discussion of the challenges of the current grid-tied converter for DG integration and a review of the smart inverter are presented. The smart converter concept is proposed.

Chapter 4 presents the analyses of conventional control strategies for three-phase full-bridge AC/DC converters. Then, the advanced multi-objective MPC is proposed to enhance both the dynamic and steady state performances simultaneously. A novel generalized mutual influence elimination constraint is proposed to eliminate the mutual influence. Simulation and experimental results are presented as the verification of new method.

Chapter 5 discusses the conventional three-vector based predictive duty cycle control and the corresponding improved method to further enhance the control performance. To solve the incorrect vector selection and control complexity of the conventional method and the improved method, correspondingly, the reversible predictive duty cycle control (RPDCC) method is proposed. It can reduce significantly the control complexity and achieve much better steady state and dynamic performances.

Chapter 6 applies the MPC for vector selection of the two- and three-vector based control methods. A simplified method is proposed for duration time calculation without the need for calculating the power slope value. The improved space vector modulation (SVM) based DPC (ISVMDPC) method is discussed. Novel two- and three-vector based approaches with mutual influence elimination and simplified calculation are proposed. Comprehensive comparisons between various methods are conducted by simulation and experimental studies.

Chapter 7 concludes this thesis with a general summary of the contributions. Future works that require further investigations are also presented in this Chapter.

REFERENCES

[1.1] International Energy Agency. Key World Energy Statistics; 2014

[1.2] X. Tan, Q. Li, and H. Wang, ‘‘Advances and trends of energy storage technology in microgrid,’’ *Int. J. Electr.Power Energy Syst*., vol. 44, no. 1, pp. 179–191, Jan. 2013

[1.3] H. Jiayi, J. Chuanwen, and X. Rong, ‘‘A review on distributed energy resources and MicroGrid,’’ *Renew. Sustain. Energy Rev*., vol. 12, no. 9, pp. 2472–2483, 2008

[1.4] L. Xu and D. Chen, ‘‘Control and operation of a DC microgrid with variable generation and energy storage,’’ *IEEE Trans. Power Del.*, vol. 26, no. 4, pp. 2513–2522, Oct. 2011

[1.5] J. M. Carrasco, L. G. Franquelo, J. T. Bialasiewicz, E. Galvan, R. C. Portillo Guisado, M. A. M. Prats, J. I. Leon, N. Moreno-Alfonso, "Power-electronic systems for the grid integration of renewable energy sources: A survey", *IEEE Trans. Ind. Electron.*, vol. 53, no. 4, pp. 1002-1016, Jun. 2006

[1.6]. (December 2014). Solar Industry Data. Available at www.seia.org/researchresources/solarindustrydata

[1.7] I.Navigant Consulting. Global distributed generation deployment forecast; 2014

[1.8] J. Leon, S. Kouro, L. G. Franquelo, J. Rodriguez, B. Wu, "The essential role and the continuous evolution of modulation techniques for voltage source inverters in past present and future power electronics", *IEEE Trans. Ind. Electron.*, vol. 63, no. 5, pp. 2688-2701, May 2016

[1.9] G. A. Papafotiou, G. D. Demetriades, V. G. Agelidis, "Technology readiness assessment of model predictive control in medium- and high-voltage power electronics", *IEEE Trans. Ind. Electron.*, vol. 63, no. 9, pp. 5807-5815, Sep. 2016

[1.10] E. Van Brunt, et al, “Development of Medium Voltage SiC Power Technology for Next Generation Power Electronics,” GOMAC 2015

[1.11] F. Blaabjerg, Z. Chen, S. Kjaer, "Power electronics as efficient interface in dispersed power generation systems", *IEEE Trans. Power Electron.*, vol. 19, no. 5, pp. 1184-1194, Sep. 2004

[1.12] B. Kroposki, C. Pink, R. DeBlasio, H. Thomas, M. Simes, P. K. Sen, "Benefits of power electronic interfaces for distributed energy systems", *IEEE Trans. Energy Convers.*, vol. 25, no. 3, pp. 901-908, Sep. 2010

[1.13] W. Kramer, S. Chakraborty, B. Kroposki, H. Thomas, "Advanced power electronic interfaces for distributed energy systems—I: System and topologies", *National Renewable Energy Laboratory Golden CO Tech. Rep. NREL/TP-58142672*, 2008-Mar.

[1.14] S. X. Carvajal, J. Serrano, and S. Arango, "Colombian ancillary services and international connections: Current weaknesses and policy challenges," *Energy Policy*, vol. 52, pp. 770–778, Jan. 2013

[1.15] S Appert: "Advanced inverter technologies report", California public utilities commission, 18 January 2013, http://www.cpuc.ca.gov/WorkArea/DownloadAsset.aspx?id=3342

[1.16] W. Zhang et al., "Survey on fault-tolerant techniques for power electronic converters," *IEEE Trans. Power Electron.*, vol. 29, no. 12, pp. 6319-6331, Dec. 2014

[1.17] M. Braun, T. Stetz, R. Bründlinger, C. Mayr, K. Ogimoto, H. Hatta, H. Kobayashi, B. Kroposki, B. Mather, M. Coddington, K. Lynn, G. Graditi, A. Woyte, and I. MacGill, "Is the distribution grid ready to accept large-scale photovoltaic deployment? state of the art, progress, and future prospects," in *Progress in Photovoltaics: Research and Applications*, 2011, DOI: 10.1002/pip. 1204

[1.18] L. Hassaine, E. OLias, J. Quintero, and V. Salas, "Overview of power inverter topologies and control structures for grid connected photovoltaic systems," *Renewable and Sustainable Energy Reviews*, vol. 30, pp. 796–807, Feb. 2014

[1.19] J. Li and K. Corzine, "Development of grid-connected inverters for micro-grid", *Power Systems Conference (PSC)*, 2014 Clemson University. IEEE, pp. 1-6

[1.20] Z. Ming, L. Ximei, and P. Lilin, "The ancillary services in China: An overview and key issues," *Renewable and Sustainable Energy Reviews*, vol. 36, pp. 83–90, Aug. 2014

[1.21] F. Wang, J. Duarte, M. Hendrix, "Grid-interfacing converter systems with enhanced voltage quality for microgrid application;concept and implementation", *IEEE Trans. Power Electron.*, vol. 26, no. 12, pp. 3501-3513, Dec. 2011

[1.22] Time P O. Advanced Inverter Functions To Support High Levels of Distributed Solar[J]. Accessed Feb. 2017: http://www.oregonrenewables.com/Publications/NREL-smart-inverters-62612.PDF

[1.23] M. Prodanovic, K. De Brabandere, J. Van Den Keybus, T. Green, J. Driesen, "Harmonic and reactive power compensation as ancillary services in inverter-based distributed generation", *IET Gen. Transm. Distrib.*, vol. 1, no. 3, pp. 432-438, May 2007

[1.24] G. Jóos (Joos), B. T. Ooi, D. McGillis, F. D. Galiana, R. Marceau, "The potential of distributed generation to provide ancillary services", *Proc. IEEE Power Eng. Soc. Summer Meeting*, 2000

[1.25] Y. G. Rebours, D. S. Kirschen, M. Trotignon, S. Rossignol, "A survey of frequency and voltage control ancillary services—Part I: Technical features", *IEEE Trans. Power Syst.*, vol. 22, no. 1, pp. 350-357, Feb. 2007

[1.26] J. R. Rodriguez, J. W. Dixon, J. R. Espinoza, J. Pontt, and P. Lezana, "PWM regenerative rectifiers: State of the art," *IEEE Trans. Ind. Electron.*, vol. 52, no. 1, pp. 5–22, Feb. 2005

[1.27] H. Bai and C. Mi, "Eliminate reactive power and increase system efficiency of isolated bidirectional dual-active-bridge DC-DC converter using novel dual-phase-shift control," *IEEE Trans. Power Electron*., vol. 23, no. 6, pp. 2905-2914, Nov. 2008

[1.28] G. G. Oggier, G. O. Garc´ıa, and A. R. Oliva, "Switching control strategy to minimize dual active bridge converter losses," *IEEE Trans. Power Electron*., vol. 24, no. 7, pp. 1826–1838, Jul. 2009

[1.29] X. Shi, J. Jiang, and X. Guo, "An efficiency-optimized isolated bidirectional dc-dc converter with extended power ranger for energy storage systems in microgrids," *Energy*, vol. 6, pp. 27–44, 2012

[1.30] J. Alonso-Martinez, J. E. Carrasco, and S. Arnaltes, "Table-based direct power control: A critical review for microgrid applications," *IEEE Trans. Power Electron.*, vol. 25, no. 12, pp. 2949–2961, Dec. 2010

[1.31] M.Malinowski, M.P.Kazmierkowski, and A.M.Trzynadlowski,"A comparative study of control techniques for PWM rectifiers in AC adjustable speed drives," *IEEE Trans. Power Electron.*, vol. 18, no. 6, pp. 1390–1396, Nov. 2003

[1.32] J. Hu, J. Zhu, and D. G. Dorrell, "A Comparative Study of Direct Power Control of AC/DC Converters for Renewable Energy Generation," in Proc. *IEEE IECON Conf.*, pp. 3453–3458, 2011

[1.33] J. Hu, J. Zhu, and D. Dorrell, "In-depth study of direct power control strategies for power converters, *IET Power Electronics*," vol. 7, no. 7, 2014, pp. 1810–1820

[1.34] Bouafia, F.Krim, and J. P.Gaubert, "Fuzzy-logic-based switching state selection for direct power control of three-phase PWM rectifier," *IEEE Trans. Ind. Electron*., vol. 56, no. 6, pp. 1984–1992, Jun. 2009

[1.35] J. Restrepo, J. Viola, J. M. Aller, and A. Bueno, "A simple switch selection state for SVM direct power control," in Proc. *IEEE ISIE*, Montreal, QC, Canada, Jul. 2006, vol. 2, pp. 1112–1116

[1.36] J. Hu, L. Shang, Y. He, and Z. Q. Zhu, "Direct active and reactive power regulation of grid-connected dc/ac converters using sliding mode control approach," *IEEE Trans. Power Electron*.,vol. 26, no. 1, pp. 210–222, Jan. 2011

[1.37] S. Vazquez, J.A. Sanchez, J.M. Carrasco, J.I. Leon, and E. Galvan, "A model-based direct power control for three-phase power converters," *IEEE Trans. Ind. Electron.*, vol. 55, no. 4, pp. 1647–1657, Apr. 2008

[1.38] P. Antoniewicz and M. P. Kazmierkowski, "Virtual flux predictive direct power control of three phase AC/DC converter," in *Proc. Human Syst.Interactions*, 2008, pp. 510–515

[1.39] S. Vazquez *et al.*, "Model predictive control: A review of its applications in power electronics," *IEEE Ind. Electron. Mag.*, vol. 8, no. 1, pp. 16–31, Mar. 2014

[1.40] R. Aguilera, P. Lezana, and D. Quevedo, "Finite-control-set model predictive control with improved steady-state performance," *IEEE Trans. Ind. Informat*., vol. 9, no. 2, pp. 658 –667, may 2013

[1.41] J. Rodriguez, M. P. Kazmierkowski, J. R. Espinoza, P. Zanchetta, H. Abu-Rub, H. A. Young, and C. A. Rojas, "State of the art of finite control set model predictive control in power electronics," *IEEE Trans. Ind. Informat.*, vol. 9, no. 2, pp. 1003–1016, May 2013

[1.42] J. Hu, J. Zhu, G. Platt, and D. G. Dorrell, "Multi-objective model-predictive control for high power converters," *IEEE Trans. Energy Convers.,* vol. 28, no. 3, pp. 652-663, Sep. 2013

[1.43] A. Bouafia, J.-P. Gaubert, and F. Krim, "Predictive direct power control of three-phase pulse width modulation (PWM) rectifier using space-vector modulation (SVM)," *IEEE Trans. Power Electron*., vol. 25, no. 1, pp. 228–236, Jan. 2010

[1.44] A. Bouafia, J.-P. Gaubert, and F. Krim, "Predictive direct power control of three-phase pulse width modulation (PWM) rectifier using space-vector modulation (SVM)," *IEEE Trans. Power Electron*., vol. 25, no. 1, pp. 228–236, Jan. 2010

[1.45] S. Kwak and J.-C. Park, "Switching strategy based on model predictive control of VSI to obtain high efficiency and balanced loss distribution," *IEEE Trans. Power Electron.*, vol. 29, no. 9, pp. 4551–4567, Sep. 2014

[1.46] Y. Zhang, W. Xie, Z. Li, and Y. Zhang, "Low-complexity model predictive power control: Double-vector-based approach," *IEEE Trans. Ind. Electron.*, vol. 61, no. 11, pp. 5871–5880, 2014

[1.47] Y. Zhang, Y. Peng, and H. Yang, "Performance improvement of two-vectors-based model predictive control of PWM rectifier," *IEEE Trans. Power Electron.*, vol. 31, no. 8, pp. 6016–6030, 2016

[1.48] Restrepo, J., Viola, J., Aller, J.M., Bueno, A.: 'A simple switch selection state for SVM direct power control'. *IEEE ISIE* 2006, 2006, pp. 1112–1116

[1.49] A. Bouafia, J.P. Gaubert, F. Krim, 'Predictive direct power control of three-phase pulsewidth modulation (PWM) rectifier using space-vector modulation (SVM)', *IEEE Trans. Power Electron*., 2010, 25, (1), pp. 228–236

[1.50] S. Aurtenechea, M. A. Rodriguez, E. Oyarbide, and J. R. Torrealday,"Predictive control strategy for DC/AC converters based on direct power control," *IEEE Trans. Ind. Electron.*, vol. 54, no. 3, pp. 1261–1271, Jun. 2007.

[1.51] J. Hu and Z. Zhu, "Improved voltage-vector sequences on dead-beat predictive direct power control of reversible three-phase grid-connected voltage-sourced converters," *IEEE Trans. Power Electron.*, vol. 28, no. 1, pp. 254–267, Jan. 2013.

Chapter 2

LITERATURE REVIEW

2.1 Introduction

The microgrid is an approach to integrate distributed generation (DG), renewable energy sources (RES), distributed energy storage devices or systems, and local loads by means of network management. Renewable energy based microgrids are a better way of utilizing renewable energy. There are kinds of renewable energy sources and energy storage devices that can be integrated into microgrids, such as photovoltaic (PV), wind energy, fuel cells, and battery systems, etc. Different kinds of renewable energy systems have different connection interfaces to the microgrid according to the voltage types of output power. For instance, the doubly fed induction generator (DFIG) and AC/DC inverter are used to generate wind power, thus for power flow control and high power quality in the microgrid, it is important to control the DFIG and inverter more efficiently with high power quality.

Many types of renewable power, such as PV and wind energy, vary with time, weather and environment of nature, thus results in the not stable and somehow discontinuous feature. The peaks of power demand do not necessarily coincide with the peaks of DG. To overcome the issues which lead to power fluctuation and the voltage sags, energy storage systems (ESS) stabilizing the power supplement are essential. In terms of the connection methods of the DG, energy storage devices, and loads in a microgrid, there are mainly three types of microgids: the DC bus based microgrids, AC bus based microgrids, and multiple-bus based microgrids. Of these, the DC bus is the simplest interconnection bus [2.1] with high efficiency, high reliability, and no frequency or phase control requirements compared with the AC inter-connection bus [2.2], [2.3], which is also a hot research area.

For integration of distributed generations, the three-phase full-bridge converter is most generally utilized and plays an important role in renewable energy systems. With more and more distributed generation (DG) integration nowadays, it requires the AC/DC converter with more advanced functions in regard to the cost, rescale, power quality, and system reliability improvement. Thus, the control strategies for three-phase full-bridge AC/DC converters have a great influence on system performance and need to be fully researched.

With ESS, the DC/DC converter is usually required to actively control the power flow between ESS and the load or DC bus while regulating a bus voltage during source and load voltage changes. The DC/DC converter must be very efficient, easy to control with wide power and voltage range, and should offer redundancy if required. Moreover, the galvanic isolation with high-voltage basic insulation level (BIL) requirements is required not only for safety reasons but also when several converters operate in series or parallel connection. [2.4] For distribution grids and storage systems, a DC/DC converter must also provide bidirectional power flow. As the input power and power demand are not always regulated, the DC/DC converter has to operate under a wide range of input voltages. It requires the converter to have the capacity to deliver power over a wide power range. Therefore, a suitable DC/DC converter and control strategy for the microgrid are also very important. Also, the interleaved structure of AC/DC/DC converter for high power transfer efficiency and control flexibility are necessary for the microgrid [2.5], [2.6].

Although the control of AC/DC inverter and DC/DC converter are very important in microgrids, the analyses of microgrid structure and converter control for better power flow and power quality are much more significant. In the first step, the structure of the microgrid will be fully discussed and reviewed. Then, the relative control strategy of the converter reviewed.

2.2 Control of Power Converters for Distributed Generation

2.2.1 AC/DC converter in renewable energy systems

For AC/DC conversion in renewable energy systems, the most general utilized topology is the three-phase full-bridge AC/DC converter. The single-phase AC/DC converter is less used in distributed generation due to capacity limitation and phase mismatch. Thus, for larger systems over 10 kW in renewable energy systems, the three-phase full-bridge converter is a popular option for integration of renewable energy sources, active power filters, electric drives and ESS due to its advantages such as four-quadrant power flow, natural power factor correction, flexible DC-link voltage adjustment, and relatively low DC filter capacitance in comparison with uncontrolled AC/DC converters [2.7]-[2.10]. The isolation from the grid can be realized by using either a line-frequency transformer or a high-frequency transformer.

For wind power generation and integration to utility grid, the configuration of synchronous generator plus power electronics is generally used as illustrated in Fig. 2.1 [2.11].

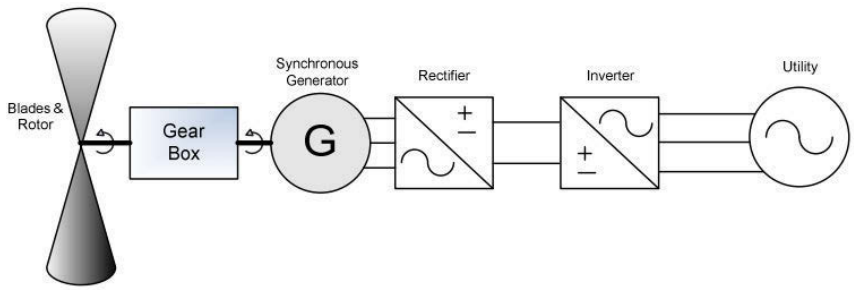

Fig. 2.1 Synchronous generator plus power electronics configuration

The corresponding power electronics topology is presented in Fig 2.2. It converts the AC power to DC voltage and the three-phase DC/AC inverter is applied for power feed to the utility grid. Fig. 2.3 presents the power electronic AC/DC/AC converter for the DFIG [2.11].

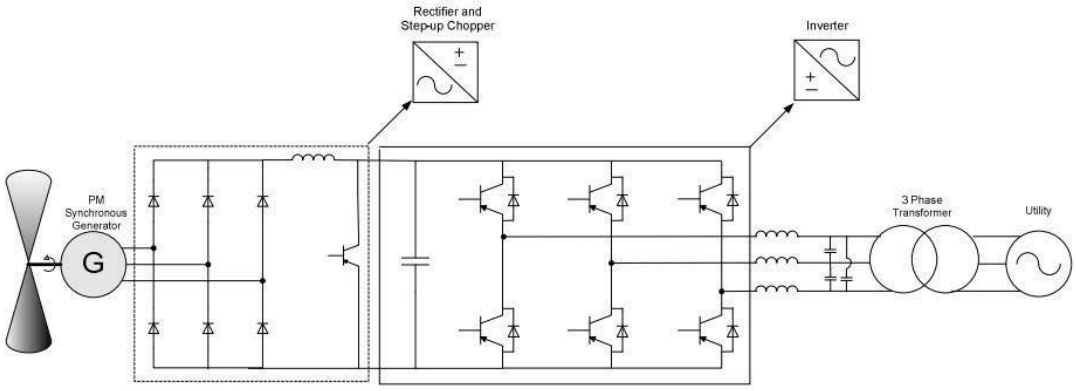

Fig. 2.2 The topology of three-phase full bridge power electronic converter for synchronous wind turbine generator

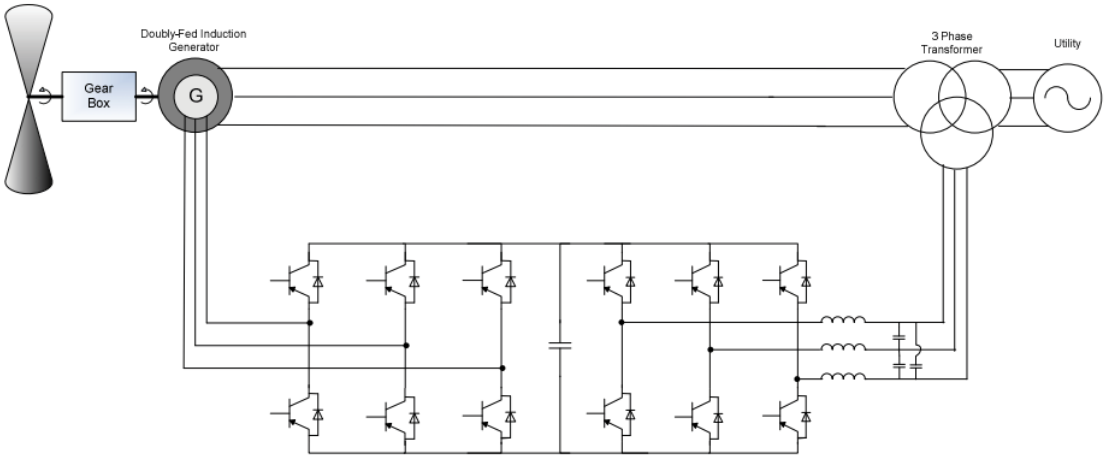

Fig. 2.3 Power electronic AC/DC/AC converter for doubly-fed wind turbine generator

For PV power generation, there are also various types of topology for power conversion. Usually, to avoid bulky, low-frequency transformers, which is generally quite large size and low efficiency, the multiple stage (two-stage) conversion systems are used for PV generation. The most generalized form of power electronics topology for the PV application is the DC/DC converter in consist of high-frequency transformer, along with the DC/AC inverter. Generally, the maximum power point tracking (MPPT) and voltage boost are done by the DC/DC converter. The power flow control to the utility and the unity power factor are produced by the DC/AC inverter. The common two-stage topologies consist of a DC/AC grid-connected three-phase full-bridge voltage

source inverter with various kinds of DC/DC PV connected converters, such as the topology illustrated in Fig. 2.4 [2.11].

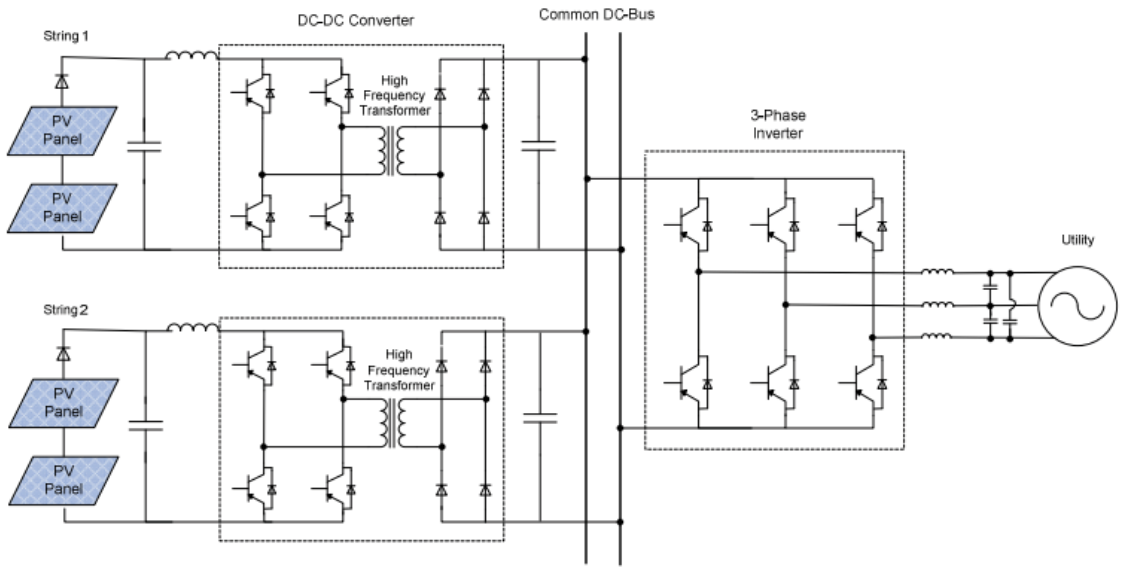

Fig. 2.4 Multi-string PV topology with high-frequency transformer-based isolation

Similar to PV systems with DC power generation, for fuel cell integration, cascaded DC/DC and DC/AC converters are also needed to supply normal customer load demand or feed power into the grid. The DC/AC converter can be either single-phase or three-phase depending on the type of utility. A fuel cell system with power electronic converter interfacing with a three-phase utility system is shown in Fig. 2.5.

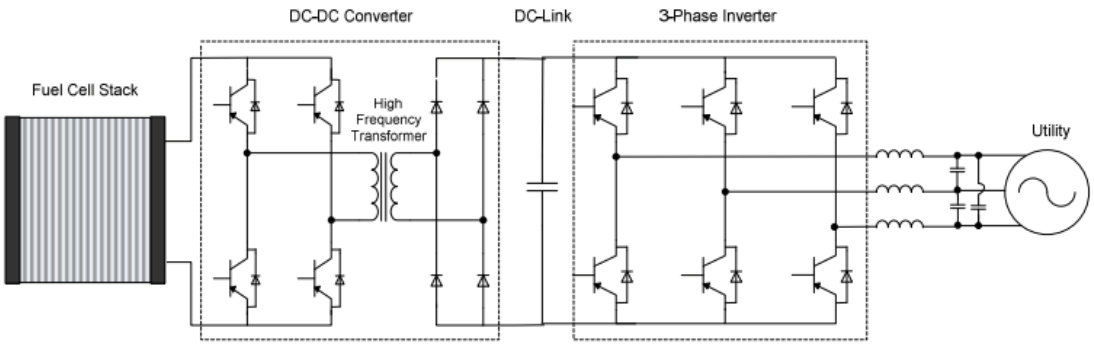

Fig. 2.5 Cascaded DC/DC and DC/AC converter topology

For microturbine integration, there are several types according to the converter topology. As shown in Fig. 2.6(a), it shows microturbine configurations with DC-link power converters. Fig. 2.6(b) shows microturbine configurations with a high frequency AC-link power converter. Fig. 2.6(c) shows the power electronic converter topology of Fig.2.6(a) configurations [2.11]. It can be concluded that for integration of the microturbine, the three-phase full-bridge converter is also needed for AC/DC or DC/AC conversion.

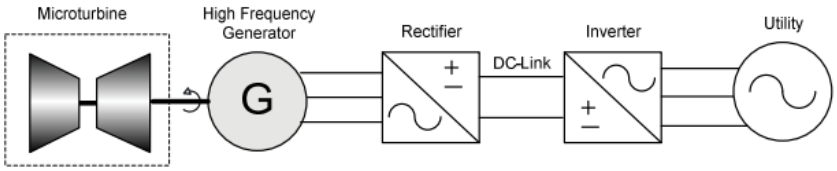

(a)

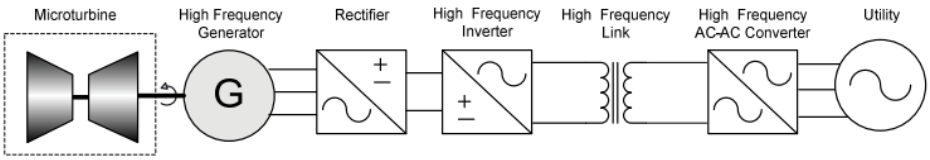

(b)

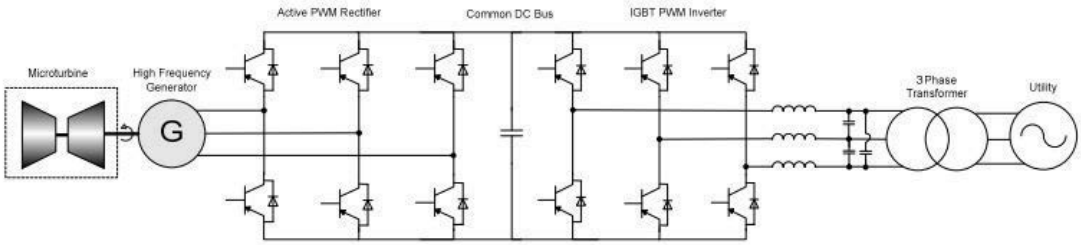

(c)

Fig. 2.6 Microturbine configurations, (a) Microturbine configurations with DC-link power converters, (b) Microturbine configurations with a high frequency AC-link power converter, (c) Power electronic converter topology

There are other kinds of distributed generations, such as flywheel systems and internal combustion engines. Flywheel systems can be combined together with the other

renewable DG sources to smooth the load fluctuations. The most common configuration for supplying these energies to the grid is also the back-to-back converter.

In conclusion, for renewable energy sources with AC/DC power conversion, the three-phase full-bridge AC/DC converter is most generally applied, though the entire topology varies accordingly with different kinds of connection and ancillary circuits. The control target and requirements vary with different kinds of DG integration. For instance, tracking the maximum power point of a PV array is an essential part of a PV system. For grid-connected DC/AC inverter such as wind turbine, constant current control and constant power control are two main control modes. It is still controversial if an inverter should be allowed to regulate voltage during grid-connected operation.

Besides, the development of more DG integrations with the grid requires AC/DC converters with more advanced functions in regard with the costs, power quality and system reliability improvement, such as reactive power compensation and fault ride through [2.12]. For example, the conventional three-phase full-bridge DC/AC converters in renewable energy systems are designed for specific applications with limited flexibility due to fixed size and functions, it will be disconnected from the grid during abnormal grid conditions or power outages. If a large number of DGs come back online simultaneously after the grid outage or being disconnected because of grid disturbance, another grid disturbance may be triggered [2.13]-[2.15].

This issue has been more serious and urgent with a growing number of renewable energy integrations in utility systems today. To overcome this issue, the concept of advanced smart inverters was proposed to provide multi-functions and various ancillary services, which represent a significant opportunity to improve the stability, reliability, and efficiency of the electric power distribution system [2.13]-[2.16].

2.2.2 Control strategies of three-phase full-bridge AC/DC converter

As reviewed, DGs are often connected with a DC common bus through an AC/DC rectifier, then interfaced to a common AC bus (utility) or AC load through a DC/AC inverter for power feed or power supply. While the power flows from the AC bus or the

utility to the ESS or battery bank of EVs, it supplies power through the AC/DC rectifier to DC bus and then flows to the ESS or battery bank of EVs through the DC/DC converter. The fast development of renewable energy systems also leads to more stringent requirements of AC/DC converters and more advanced control strategies that can deliver better system reliability and power quality [2.16]. Whether for integration of distributed power generation or power supply from ESS or DC bus, high power quality, excellent steady and dynamic performance are becoming important for AC/DC converter control.

For distributed generations, the most popular AC/DC converters are three-phase pulse width modulation (PWM) converters as shown in Fig. 2.7. A large number of three-phase full-bridge AC/DC converters have been utilized with bidirectional power flow ability. This topology has several advantages, such as low harmonic distortion of input currents, bidirectional power flow, high power factor and stable dc-link voltage and reduced DC filter capacitor size [2.17-2.19]. It is usually used as the power interface between distributed generations, utility grid, and ESS or loads to realize the bidirectional power flow with AC/DC conversion, as shown in Fig. 2.8.

Various control strategies have been studied on this kind of PWM rectifiers. A popular method for indirect active and reactive power control is the voltage oriented control (VOC), which is based on the current vector orientation based on the grid voltage vector. The implementation of this method requires an inner current loop with a proper modulator to guarantee high dynamic and static performances [2.20]. However, the overall configuration and performance of the VOC control system largely relays on the quality of the applied current control strategy [2.21].

Another popular control strategy is the switching table based direct power control (STDPC) by which the converter switching states are appropriately selected based on a preset switching table designed according to the instantaneous errors between the reference and estimated values of active and reactive powers, and voltage vector location. [2.22-2.26]. Compared with the VOC method, the STDPC does not require an

inner current loop and modulator. The coordinate transformation is also eliminated, as illustrated in Fig.2.9. While large power ripples and variable switching frequency are the two main disadvantages. Though several different switching tables are proposed to improve the performance, it requires the sampling frequency to be high enough to achieve acceptable performance [2.27-2.29].

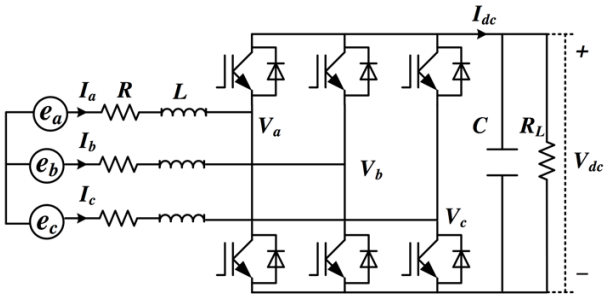

Fig. 2.7 Three phase PWM AC/DC converter

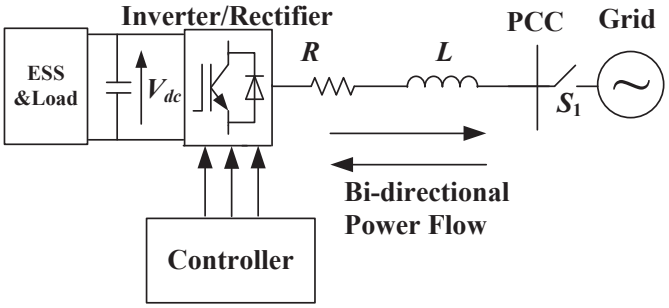

Fig. 2.8 Grid-connected AC/DC converter for bidirectional power flow

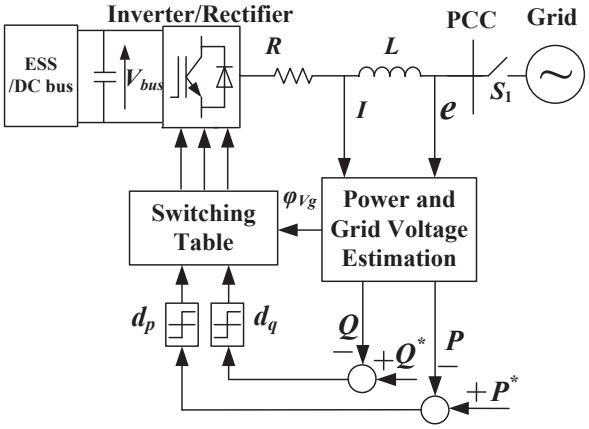

Fig. 2.9 Block diagram of conventional switching table based DPC

Various other control methods, such as the fuzzy logic based DPC, model predictive control (MPC), and the space vector modulation (SVM) control, etc., also have drew more attentions in recent years. The fuzzy logic based DPC is similar to the direct torque control (DTC) that is applied for motor drive control. Since the fuzzy logic based DPC does not require coordinate transformation and phase lock loop, and is implemented by using of virtual flux, thus it is an algorithm simple for application [2-30]. The active and reactive powers through measuring the input current and the estimated virtual flux are calculated, and instantaneously performs power control by using the hysteresis comparator and the predesigned switching table, which is similar to the STDPC control. The main advantages of this method are the fast and excellent power dynamics during instant change of the load or changes in the instantaneous reference with low sensitivity to non-ideal supply voltages, and no need for a pulse width modulator [2.31]. Meanwhile, the disadvantages are obvious. Since the magnitudes of the power ripples are in relation to the magnitude of the DC-side voltage, a high sampling frequency is needed due to implementation of hysteresis comparators, and the switching frequency also varies. A very-high-performance processor is needed in order to act fast enough within a short control period [2.32].

Since the predictive control strategy was proposed to reduce the torque and power ripples in electrical machine control systems [2.33]-[2.39], it can also be employed in power converter control. It is an attractive alternative for the control of power converters because of its excellent dynamic and steady state performances. Various kinds of control schemes have been developed under the predictive control, such as the deadbeat predictive control, hysteresis-based predictive control, trajectory-based predictive control, and MPC [2.40]-[2.46]. Among them, the MPC is a very prospective and flexible control scheme that has raised much interest in recent years [2.47]-[2.55].

The application of MPC techniques to power electronics can be classified into two main categories: (a) continuous control set MPC, and (b) finite control set MPC (FCS-MPC). In the first category, a modulator generates the switching states starting from the continuous output of the predictive controller. While the FCS-MPC approach

takes advantage of the limited number of switching states of the power converter to solve the optimization problem. A discrete model is used to predict the behaviour of system for every actuation sequence up to the prediction horizon. The switching state that minimizes a predefined cost function is finally selected to be applied in the next sampling instant [2.54]. It should be noted that with multi-vector control strategies, more than one switching state in one sampling instant may be selected. The main advantage of FCS-MPC is the direct application of the control action to the converter with consideration of future behaviour, without requiring any modulation stage [2.56].

In terms of FCS-MPC based control of the three-phase full-bridge AC/DC converter, the converter model is used to predict the system behaviour, and a cost function is employed to select the optimal switching states. The control objectives of MPC can vary by revising the cost function according to the application [2.57]. The control block and principle of MPC based DPC (MPDPC) are given as shown in Fig. 2.10. When compared with switching table based DPC, the MPDPC can reduce the power ripples, thus more sinusoidal line current can be achieved. Also, the MPDPC can reduce the harmonic pollution of the power system caused by rectifiers. However, due to the limited number of available converter states, namely only 8 vectors, and only one vector being selected in one sampling period, the results are variable switching frequency, higher power ripple and the spread spectrum nature of harmonics [2.58]-[2.60]. Also, the sampling frequency has to be relatively high in order to achieve satisfactory performance.

In order to overcome the disadvantage of MPDPC and further improve the performance, more research has been focused on selecting two or three voltage vectors in one sampling period to achieve reduced ripples and constant switching frequency [2.61]-[2.70]. This has been popular in power converter control and electrical machine drives.

In [2.71], the SVM based DPC is proposed. It tracks the errors of active and reactive powers and feeds them to two separate PI regulators. As in the control block diagram in

Fig. 2.11(a), two PI regulators are used to transform the tracking errors to the SVM module and by using the SVM method, a constant switching frequency can be realized.

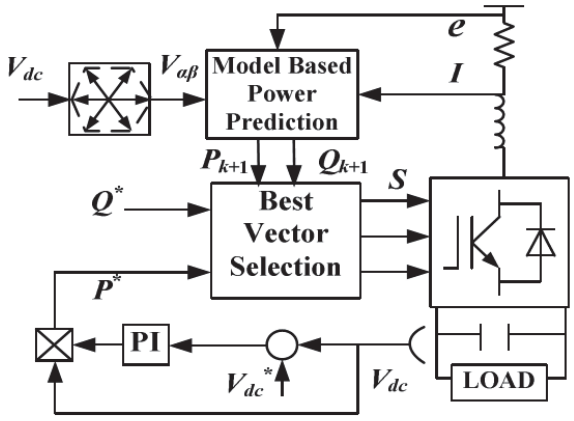

Fig. 2.10 Control block of MPDPC.

Not only can this method effectively reduce power ripples, but it also has the advantage of a fixed switching frequency. However, the dynamics with relation to the instant load change need to adjust an adequate gain owing to the influence from the gain of the PI controller. Since the complicate coordinate transformation and the PI controller are still needed, it will no doubt increase the tunning effort and control complexity.

To overcome these disadvantages, the improved SVM based direct power control (ISVMDPC) was proposed in [2.72] as shown in Fig. 2.11(b). Based on the predictive control strategy, the two separate PI regulators and coordinate transformation module are replaced by the predictive model of converter that could transfer active power error and reactive power error to V_α and V_β, respectively, and then the same SVM block is used for pulse generation.

Differing from SVMDPC, in [2.61] and [2.73], the three-vector based approach using prediction value of power slope to calculate the duration of each voltage vector has been discussed, and the adjacent two none-zero vectors are selected based on the sector location. Then the least square method is employed to calculate the duration time of

each vector as per the block diagram as illustrated in Fig. 2.12. However, it might select incorrect voltage vectors based on the conventional vector sequence tables using vector location information, which results in the negative value of optimal duration time. As a result, the action time is normally forced to zero if a negative value is calculated or forced to the maximum value, resulting in control failures and performance deterioration.

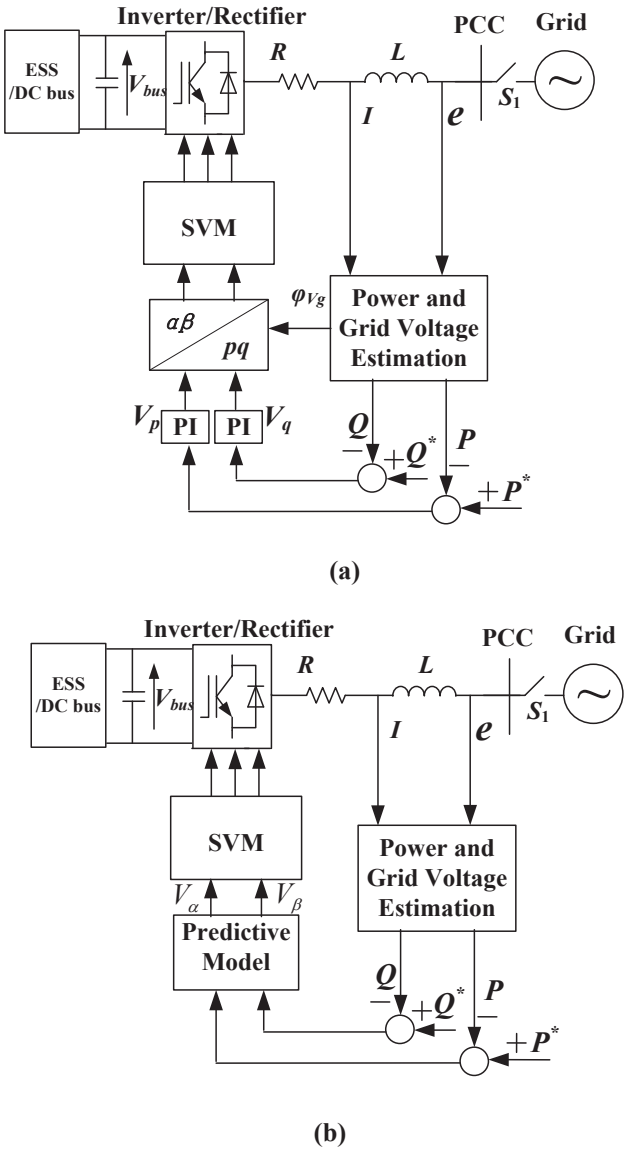

Fig. 2.11 Block diagram of SVMDPC-based power regulation (a) CSVMDPC (b) ISVMDPC

In order to solve this issue, some improved methods have been proposed [2.61]-[2.65]. In [2.62], a novel method of voltage vector selection is developed, and

global optimal voltage vectors are selected by means of cost function minimization, since the conventional control method in [2.61] limits the converter operation range to a small power angle, it constraints the active power that one can transfer from the AC side to the DC side. In [2.63] and [2.64], the modified vector selection table is proposed based on the case study. It reselected the none-zero vector based on the revised vector sequence table whenever negative time values appear, and the duration time should be recalculated with reselected vectors. Though the performance could be improved by more accurate vector selection, it is no doubt that the complexity and calculation burden will obviously increase as the vector selection and duration time calculation process repeat when the duration time is negative.

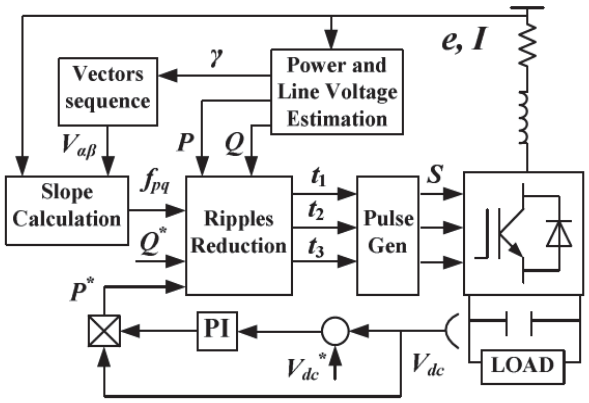

Fig. 2.12 Control block of PDCC

References [2.65] and [2.66] propose an improved predictive DPC method eliminating sector information of the grid voltage and the voltage vector selection process. However, the equivalent reconstruction of switch signals is needed and the calculation of duration time is more complex. More recently, the MPC method is employed in [2.67]-[2.71] to select voltage vectors with cost function to improve the performance without using the sector information. However, all the adjacent vector pairs need to be evaluated to select the best pair.

For duration time calculation, the least square minimization method is generally used. However, it requires calculation of the power slope of selected none-zero vector, and

the duration time calculation equation is complex, which will increase the computational burden. For various kinds of MPC based control methods mentioned above, since two control objectives are combined in one cost function, the mutual influence during dynamic instant is difficult to eliminate and less considered with the current control methods.

In conclusion, for three-phase full-bridge AC/DC converter, several control strategies have been compared and each method has great influence on converter performance with its advantages and disadvantages. Whether for the single vector based MPDPC control method or the multiple vector based method, there are still some issues such as the mutual influence of two control objectives and the control complexity needed to be solved. The main target of the thesis will focus on the advanced control of three-phase full-bridge AC/DC converter to comprehensively improve the performance.

2.2.3 Review of DC/DC converters

In RES, the DC/DC converter is generally needed to actively control the power flow between ESS or DC bus and the DC load such as EVs while regulating the voltage or power flow direction during source and load voltage changes, it needs to be very efficient, easy to control and have redundancy, and galvanic isolation is required not only for safety reasons but also for series or parallel connections of several converters in microgrids. For power storage and feedback, a DC/DC converter must also provide bidirectional power flow. Due to the fact that input power sources and loads are not always regulated, the DC/DC converter is also required to operate in a wide range of input voltages and have the ability to deliver power over a wide power range with good power quality, which requires the converter to be fully controlled. Based on the requirement above, we can review the DC/DC converter structures and choose the most suitable one for general applications in microgrids.

The general buck-boost converter shown in Fig. 2.13 has been considered first. When power is delivered from DC link V_1 to V_2, switch S_2 is controlled. On the other hand, when power is transferred from the DC link V_2 to V_1, switch S_1 is modulated. [2.74].

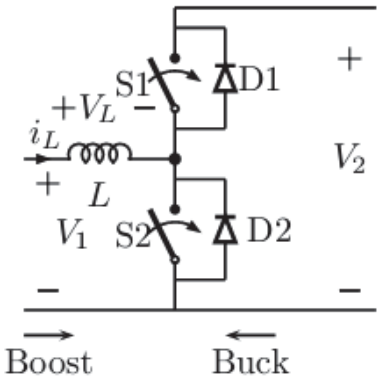

Fig. 2.13 Topology of buck-boost converter

The Buck-boost converter has simple structure and is efficient. Allowing for consideration of parasitic resistances in the inductor for practice application, which cannot be ignored in practical applications, the relationship between the output voltage V_2 and the input voltage V_1 becomes complex, resulting in difficulties to achieve a high voltage boost ratio. Besides, the galvanic isolation requirement could not be met.

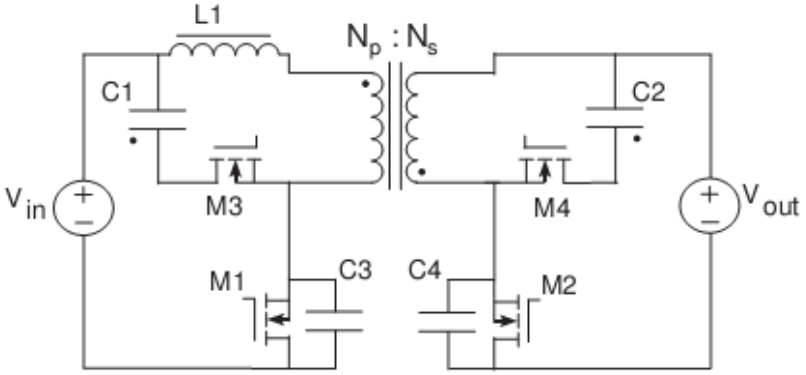

Fig. 2.14 Topology of current fed push-pull (CFPP) converter

Another topology is the current fed push-pull (CFPP) converter as shown in Fig. 2.14. This is a popular switch mode power supply topology due to its simplicity and good power-to-weight ratio. A major advantage of this topology over its voltage-fed counterpart is that it avoids staircase saturation of the transformer, which is a major failure mode of voltage-fed push-pull converters [2.74].

For high voltage ratio applications and the galvanic isolation requirement, transformer coupled bidirectional converters have been proposed. One type is the half bridge dual active converter as shown in Fig. 2.15 [2.74].

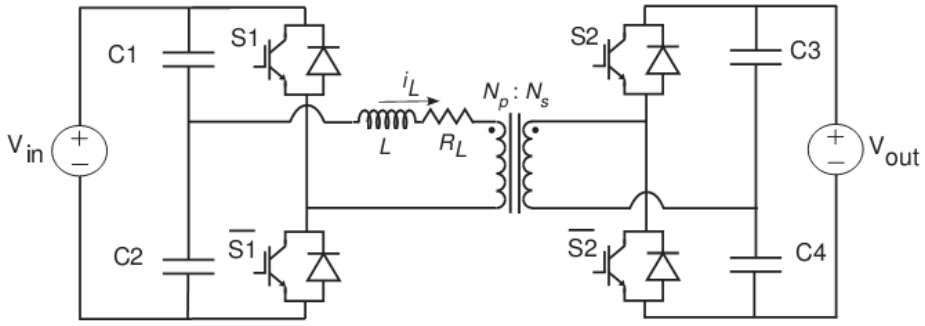

Fig. 2.15 Topology of half bridge converter

The topology is the voltage feed half bridge converter, each bridge of this converter is modulated to produce an AC waveform across the high frequency tranformer, meanwhile the filter inductance *L* limits the current between the two bridges. With higher power and voltage levels, these capacitors become expensive and bulky. As a result, the ratings of this topologies are limited to below 400 V and 2 kW.

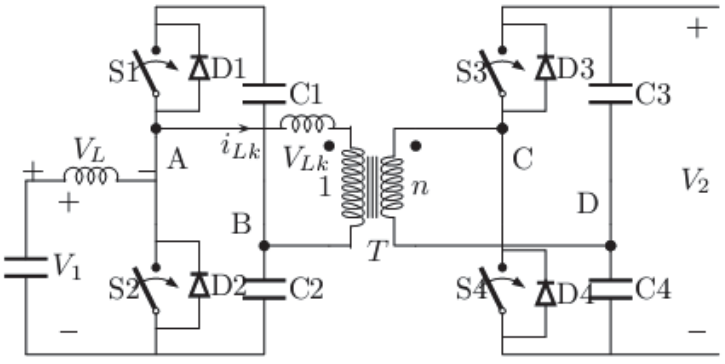

Fig. 2.16 Topology of half bridge dual active converter

Similarly, Fig. 2.16 shows the topology of current feed half bridge converter. These capacitors are required to ensure an equal voltage distribution across the two switches of

the half bridge. Furthermore, higher current rating devices are needed for lower side switches on the low voltage side of the transformer. Also, the current-fed converter has severe performance limitations such as high transient voltage in switches and an external circuit is needed to support its soft-start [2.74].

It can be concluded that though half-bridge converters offer a reduced switch count advantage in comparison with their single and three-phase bridge counterparts, the primary drawback is the size and cost of the DC capacitors required that must also sustain large ripple currents, which may increase the overall cost and risk of maintenance.

The isolated bidirectional full-bridge DC/DC converter (IBDC), which is also known as the dual active bridge (DAB) converter, has a high buck/boost voltage ratio, easy bidirectional power flow control and galvanic isolation nature [2.75]. It has single-phase topology and three-phase counterpart, as shown in Figs. 2.17 and 2.18, respectively. Its full bridge topology allows IBDC to be extended in high power applications while the transformer can boost input voltage more than 10 times. Thus it has attracted attention of many researchers for renewable energy applications. IBDC is usually chosen as a bidirectional converter for interfacing the ESS and DC bus in renewable energy systems [2.76]. They are a popular topology choice in UPS systems, fuel cell converters and even PV arrays.

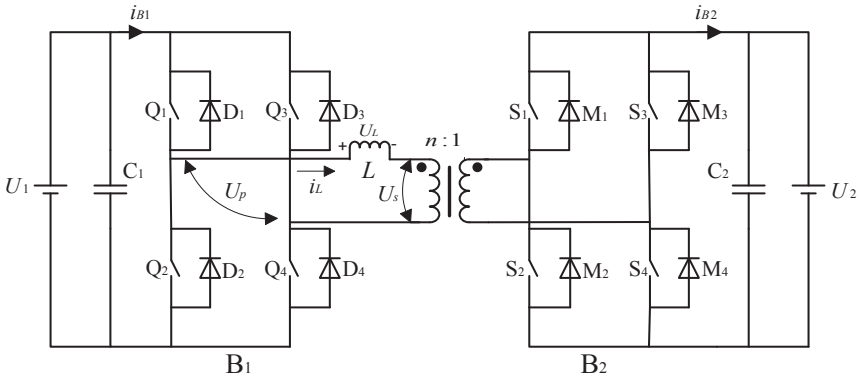

Fig. 2.17 Topology of dual active bridge converter (single phase topology)

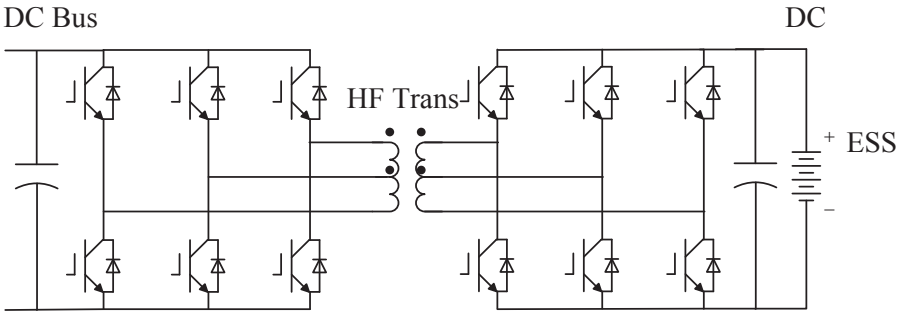

Fig. 2.18 Topology of dual active bridge converter (three phase topology)

IBDC converters have more switches (8 devices and 12 devices for the single-phase and three-phase bridges, respectively) compared to the half-bridge topology, thus they do not suffer from high capacitor ripple currents since the AC inductor current i_L in a full-bridge converter flows through the active switches (or their anti-parallel diodes) instead of flowing through the DC capacitors in a half-bridge converter.

In order to select between these two full-bridge structures, the advantages and disadvantages of each topology have been compared. Firstly, in terms of current stress, obviously, the current in the three-phase converter is shared between more phase legs than for the single-phase one, leading to lower current stress on the devices. Besides, the total power flow through the single-phase IBDC converter is AC current. To realize a constant DC bus, the capacitance is required to be large enough to absorb any oscillations in total power flow. While in comparison, the constant power flow achieved by the three-phase converter leads to a smaller DC link capacitance with lower size and cost. Also, when three-phase current flows into a transformer, the 120^o offset between the phase currents generates flux that is also offset by 120^o, which leads to flux cancellation [2.77].

Table 2.1 summarizes the reviewed converter structures and the corresponding limits of each topology that has been presented in this review. It can be seen that different converters have different appropriate voltage and power ranges. At low voltage and power levels, fly-back converter is popular, with the ratings increase beyond 100 V and

1 kW, current fed push-pull converters and half-bridges are more appropriate. While the voltage and power levels rise still further (400 V, 2 kW and above), full-bridge converters become the topology of choice [2.74].

Table 2.1 Comparisons of different kinds of DC/DC converters [2.74]

	Flyback converter	Push-pull converter	Bridge Converters	
			Half bridge	Full bridge
Voltage rating	Low (<100V)	Low (100-400V)	Low (<400V)	High (>400V)
Power rating	Low (≈500W)	Medium (>2kW)	Medium (>2kW)	High (>2kW)

2.2.4 Control theory of IBDC converter

The isolated bidirectional full-bridge DC/DC converter (IBDC) was verified to be more suitable as a DC/DC converter in RES with the advantages of high efficiency, high power density, high reliability, zero voltage switching (ZVS), wide operation range and isolation by a high-frequency transformer [2.78], [2.79]. It therefore has bright prospects in renewable energy systems and the control strategies of IBDC is worthy of discussion since different controls have a great influence on control performance.

Fig. 2.19 shows the typical single-phase topology, which consists of two full-bridge on primary and secondary sides and a high-frequency transformer. In conventional single-phase-shift control, as shown in Fig. 2.20, the gate signals of the diagonal semiconductors, e.g. (Q_1, Q_4), are the same while the gate signals of the corresponding switches in the primary and the secondary bridges are phase-shifted. This control strategy is simple and convenient as only single duty cycle is modulated. However, it results in larger current stress, larger power loss, limited ZVS region and much lower efficiency in working with a wide range of source voltage levels and lower power output, especially when the voltage amplitudes of two sides do not match, thus hindering the extension and application of IBDC in renewable energy systems that require high efficiency working in a high voltage ratio range between the input and

output ports as well as a wide input or output power range.

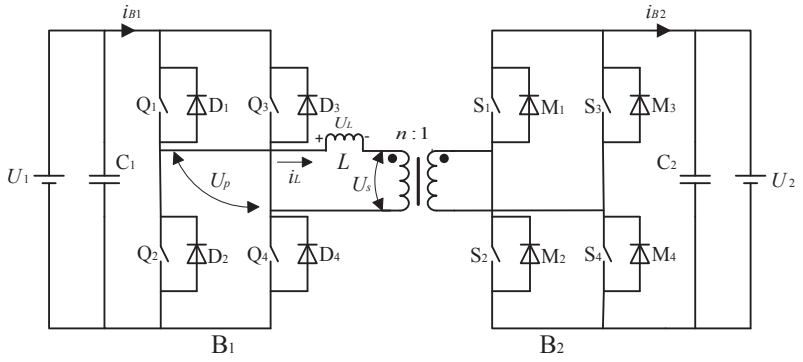

Fig. 2.19 Typical configuration of IBDC (DAB)

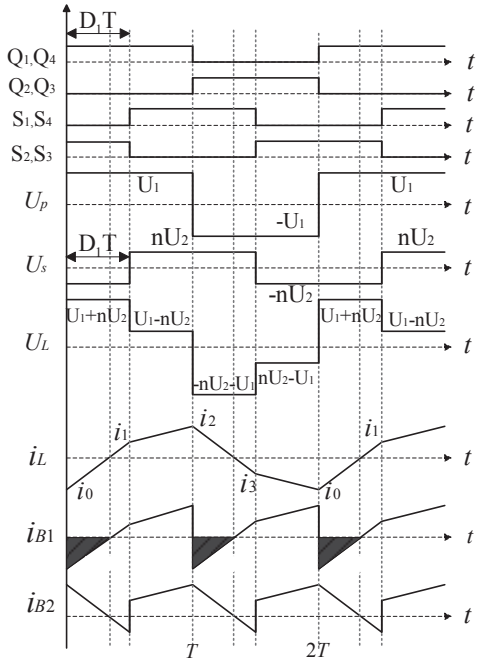

Fig. 2.20 Relevant waveforms of IBDC in CSPS control

Much effort has been done to enhance the system performance [2.80]-[2.85]. Reference [2.79] proposes and analyzes dual-phase-shift control including the phase-shift between the primary and secondary sides as well as inner phase shift of each bridge, which has two degrees of freedom to control the transmission power. Through different trajectories of phase-shift pairs in different output power reference, it can

eliminate the backflow power with the objective of minimizing the IBDC conduction losses. However, this proposal needs complex calculation in order to obtain phase-shift pairs at different power conditions, which increases the control complicity and is computationally intensive to design closed-loop feedback control. The operation with wide voltage conversion ratios and power range are also not fully considered. Reference [2.84] proposes an algorithm to implement the dual-phase-shift control to operate IBDC under ZVS in the whole operating range. However, the reduced switching loss is just a small percentage of the overall loss of IBDC, the control complexity is still a big issue. A phase-shift plus PWM is presented in [2.86]. However, the duty ratio of the gate signals of each semiconductor device is variable, and should be calculated in advance before implementing the control algorithm.

In [2.87], the extended single-phase-shift (ESPS) control is proposed to decrease the power loss and current stress compared with CSPS control, which achieves almost similar performance and lower control complexity compared with dual phase shift control. The ESPS control regulates power flow by adjusting the time sequence between the driving signals of diagonal semiconductor switches in the bridge which has a larger DC voltage, e.g. (Q_1 , Q_4) in Fig. 2.21, while the driving signals of diagonal semiconductor switches in the bridge with lower DC voltage, e.g. (S_1 , S_4), are synchronous, they also have no phase-shift angle with one of the driving signals of corresponding semiconductor switches, e.g. (Q_1 or Q_4) in the other bridge. The performance of IBDC is optimized with ESPS control and efficiency is increased in extremely low or high voltage ratio range by achieving lower backflow power and peak current. However, the operation power range with ESPS is limited to only half of the maximum power.

Recently, the MPC strategy has also been applied to the IBDC converter [2.88]-[2.93]. In [2.92], predictive current control for a single-phase IBDC is proposed. It protects the transformer from saturation even at transient conditions and increases the bandwidth of

current loop of the converter. However, the compensator that needs to be added to improve the parameter insensitivity and the proposed algorithm is only a better alternative to the classical PI based phase shift modulator, which essentially belongs to phase shift control. In [2.93], it utilizes the discrete nature of the IBDC to predicts the future behavior of the system, which has been compared to the references to calculate the cost function. The switching state that minimizes the cost function is selected for controlling the converter in the next sampling time period. It is found that the efficiencies associated with the MPC control are higher compared to that of the dual phase shift control, but the MPC based control algorithm has a problem of variable switching frequency and the required sampling frequency and computation burden is much higher than the phase shift control based method.

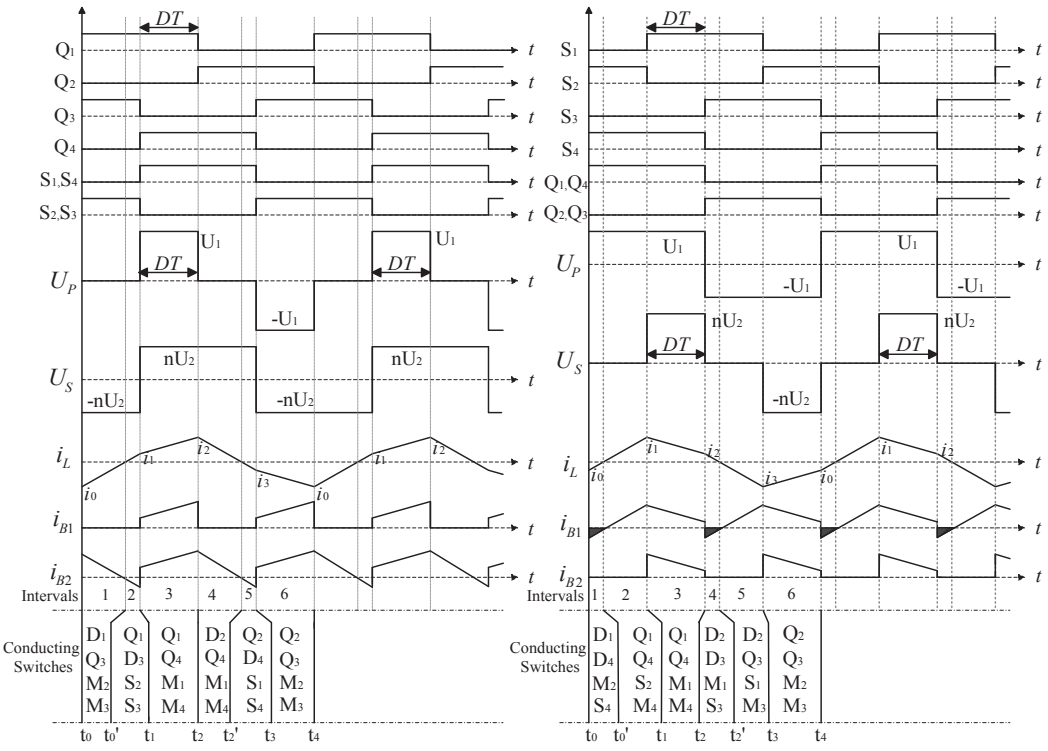

Fig. 2.21 Waveforms of IBDC in ESPS control

In conclusion, this part has reviewed the major modulation techniques for IBDC, phase-shifted modulation is the simpler and popular strategy which could be applied in renewable energy systems. For different DG connections, the control target is quite

different. For instance, in terms charging of ESS or electric vehicles, the phase-shifted modulation should be adjusted by battery management system to realize constant current charging or constant voltage charging according to charging period. While connected with DC bus, the control target is keeping the DC bus voltage steady.

2.2.5 Application of IBDC in renewable energy systems.

Although IBDC has attracted the attention of power electronic researchers for over twenty years, they have been identified as a key converter for the emerging microgrid technology more recently. IBDC with galvanic isolation has advantages such as flexibility of system configuration, safety requirements, voltage matching and galvanic isolation between the main grid and the ESS. Thus, compared with an ESS which employs a 50 or 60 Hz transformer for voltage matching and galvanic isolation. It replaces the line-frequency transformer with a high-frequency and would make the ESS more compact and flexible.

Fig. 2.22 presents a topology with series connection of IBDC and AC/DC converter in microgrids for AC/DC/DC conversion. Since the energy source and load voltage are not always regulated, an efficiency-optimized IBDC with high voltage diversity is needed and it is also a key component for batteries charging and discharging. Without IBDC connection with the ESS, the system will lack control flexibility as there is no interface and isolation between the ESS and DC bus line, since the voltage of ESS varies with capacity, it may deteriorate the system's stability.

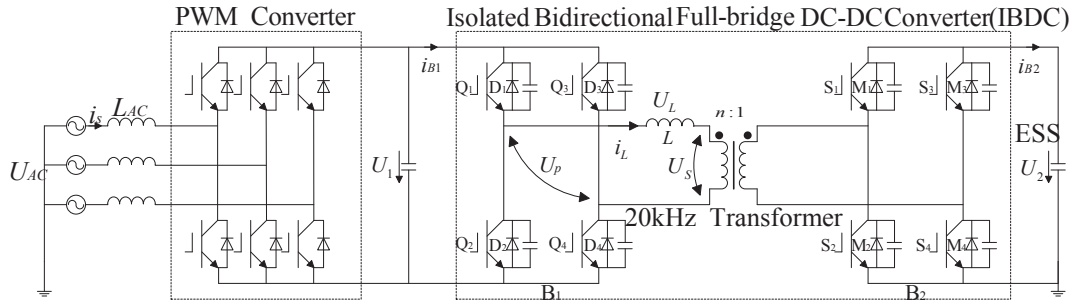

Fig. 2.22 Energy storage system based on IBDC in microgrid

The development of the IBDC for the DC/DC stage has also become one of the key factors of three-stage solid state transformer (SST), as illustrated in Fig.2.23 [2.94]. According to the research in [2.95]-[2.98], it provides a good balance between control flexibility/efficiency and system complexity. The three-stage provides the simple approach while realizing galvanic isolation, bidirectional power flow and decoupling from the utility grid [2.99]. The key feature of SST is that they can directly replace the current passive transformers while enabling management of the power flow. In addition, they ensure decoupling between the power grid and power network, and provide a DC-link that is important for the development of a hybrid microgrid.

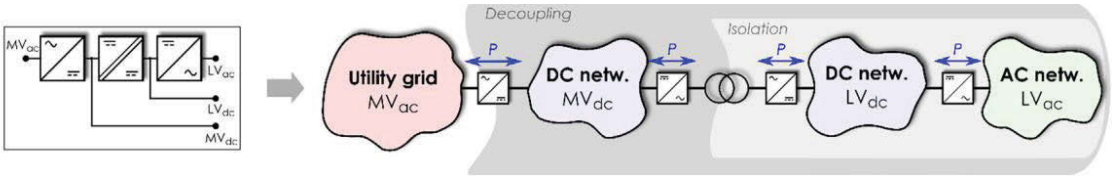

Fig. 2.23 Three stage SST network with low voltage (LV) and medium voltage (MV) DC networks

ESS, such as lithium-ion batteries, super capacitor and electric vehicles which can be considered as distributed energy storage units in a smart microgrid [2.100], should be used to smooth the power source variations. As discussed, a single-phase or three-phase IBDC converter could be selected as the interface between a high-voltage bus with distributed energy resources and a low-voltage bus with ESS in the microgrid, etc., as shown in Fig. 2.24 [2.87].

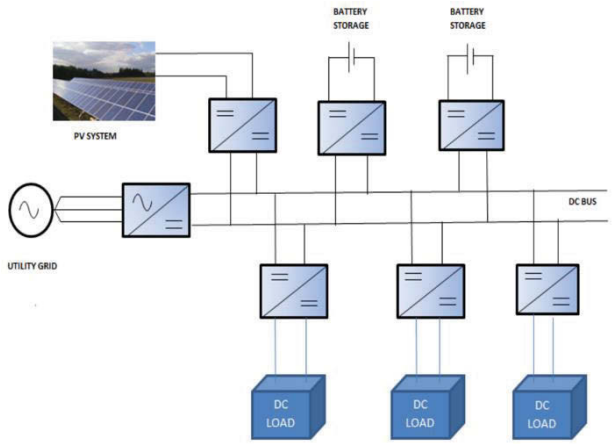

Fig. 2.24 Application of IBDC for power distribution in microgrid

2.3 The Microgrid and Topologies

The microgrid has raised many concerns in recent years due to the rapid depletion of fossil fuels, rising demand for electricity power, and government policies. Microgrids have been more important as a method of integrating DGs into the main electricity network. The microgrid is essentially defined as an integrated energy delivery system that consists of interconnected DG units, power electronic interfaces, energy storage systems and controllable loads with control devices (power flow control, frequency and voltage regulators) which may be operated autonomously and can operate in parallel with, or isolated from, the main power grid.

Generally, according to types of bus lines, there are three types of microgrids: AC bus based microgrid, DC bus based microgrid, and hybrid AC/DC microgrid. For different applications, there are various structures of microgrids according to different scenarios and integration of different kinds of ESS and DG.

A typical AC microgrid system interconnected with the medium voltage system at the point of common coupling (PCC) is shown in Fig. 2.25. The DG units and ESS are connected at some points of the distribution networks. A small isolated AC electric power system can be formed in part of the network consisting of the DG units and load circuits. Under normal conditions, the two networks are interconnected at the PCC while the loads are supplied from the local sources or, if not meeting the demand, from

the utility. If the load demand power is less than the power generated by DG units, the excess power can be exported to the utility system. In terms of the voltage and frequency standards in the microgrid, it adopts those of the conventional distribution systems [2.101].

Fig. 2.26 is an example of a hierarchical microgrid with both AC and DC links. It shows a topology of microgrid consisting of a range of DG units which are integrated into a three-level hierarchy through power electronic interfaces [2.102].

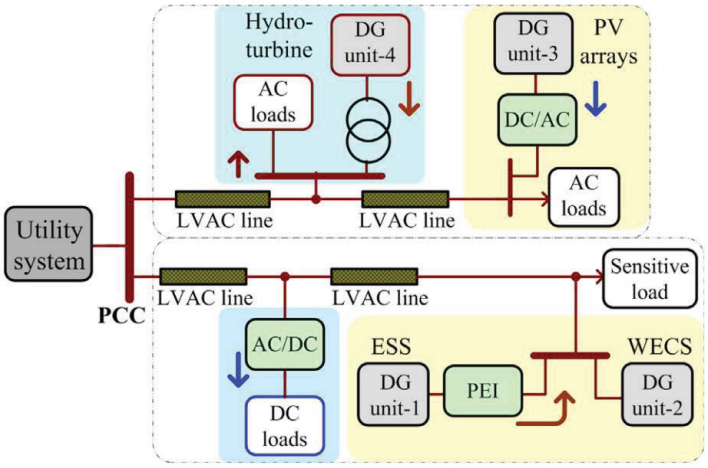

Fig. 2.25 A typical AC microgrid system

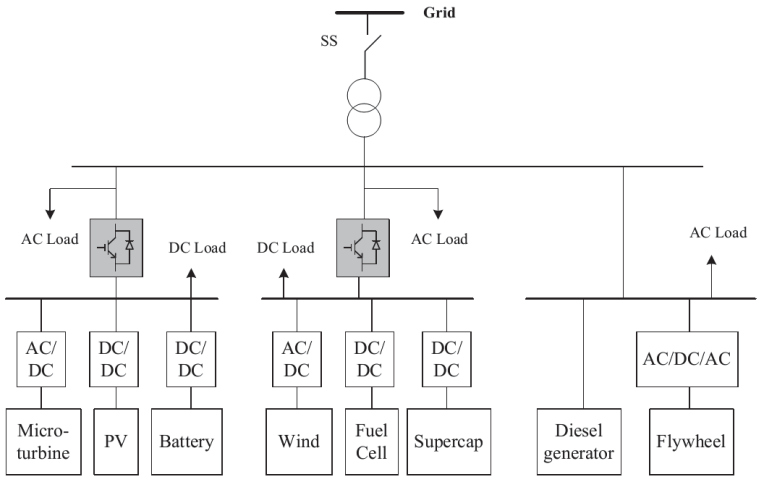

Fig. 2.26 A hierarchical microgrid with both AC and DC links

Another typical example of a hybrid microgrid is shown in Fig. 2.27. Hybrid AC/DC microgrids are considered as one of the most interesting approaches for the smart grid development in the current distribution network.

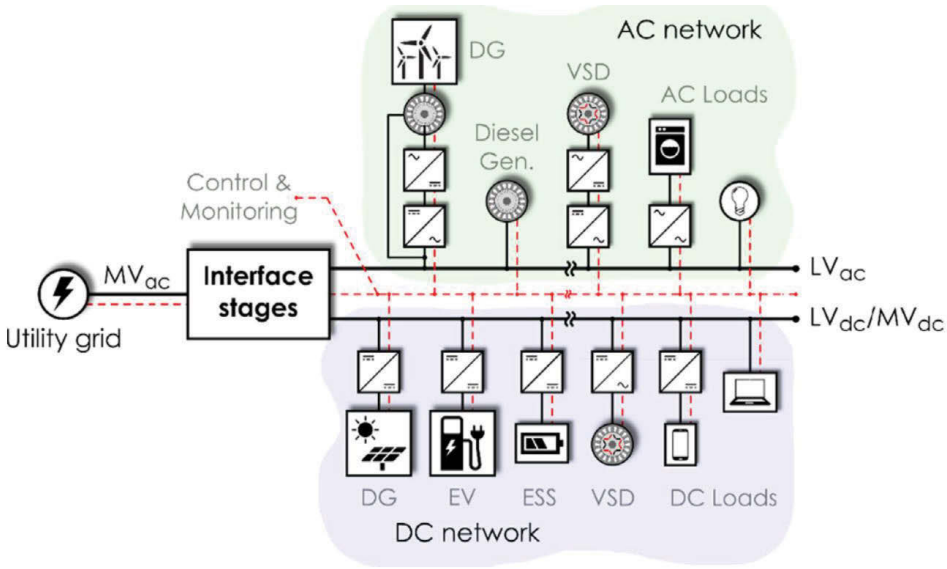

Fig. 2.27 A typical example of a hybrid microgrid configuration

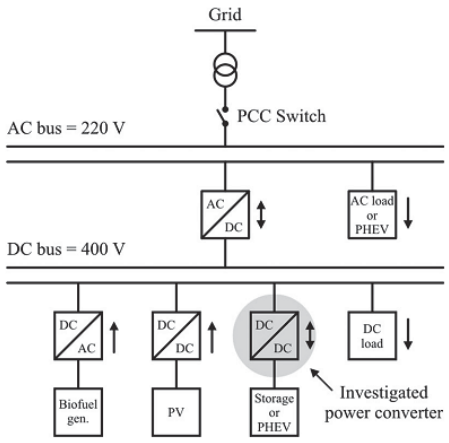

Fig. 2.28 A residential microgrid with both AC and DC links

For residential level, a microgrid with hybrid buses is shown in Fig.2.28 [2.103].

The important advantages of hierarchical microgrids are summarized in [2.94] as follows:

- Integration: AC- or DC-based devices could be directly connected with the minimum number of interface elements with reduced conversion stages and energy losses.
- Synchronization: there is no need for synchronization of generation and storage system since they are directly connected to the AC or DC network, which simplify the control devices and control efforts.
- Voltage transformation: AC-side voltage level can be simply modified by the use of transformers. The DC-side can be adjusted by the use of DC/DC converters.
- Economic feasibility: a hybrid microgrid can be developed with the addition of a power converter to the current distribution grid and the communication network for the connected devices, which reduces the overall costs.

On the other hand, this topology remains various disadvantages that need to be further researched [2.104]:

- Protection: DC protection devices have not been researched so deeply. Fault detection is more simple in AC networks thanks to the zero-crossings of the current.
- Reliability: Reliability of hybrid microgrids is lower than in AC ones as the DC-link need to be generated by the interface converter. Though the reliability of connected devices is improved since converter stage is reduced.
- Control complexity: the control of hybrid microgrids is much more complex than in its counterparts. Both control of the devices attached to the AC and DC networks and the interface power converter between them need to be regulated. It is a challenging work to ensure stable and reliable power supply in an autonomous or islanded mode.

For the DC bus based microgrid, the DC power systems have been used in industrial power distribution systems, telecommunication infrastructures and point-to-point transmissions over long distances and AC grids with different frequencies. Since most consumer equipment needs the DC power for their operation while the power from DC

output based DG units need to be converted into AC for integration, the procedure of DC/AC/DC power conversion result in substantial energy losses. With the development of power electronics, it is popular to build the DC bus based microgrid. Fig. 2.29 shows the typical DC bus based microgrid systems connected with the main systems at PCC which can be from the conventional utility grid or a high voltage DC transmission line [2.101].

The DC microgrid systems are widely applied in the area such as avionics, automotive, marine and manufacturing industries for power distribution [2.104]. The international space station, spacecraft, modern aircraft and modern electronics loads such as data centres, banks and electronics factories, require DC power supplies [2.105]. The low voltage DC microgrid can improve the power delivery efficiency and ensures a higher power quality to the customers compared with current distribution network. It is concluded in [2.106] that the DC microgrid has attractive features in terms of its simple structure, low system cost and the higher efficiency since less power converters are needed in comparison with the AC bus microgrid. However, protection issues in the low voltage DC system are still a challenging problem [2.107].

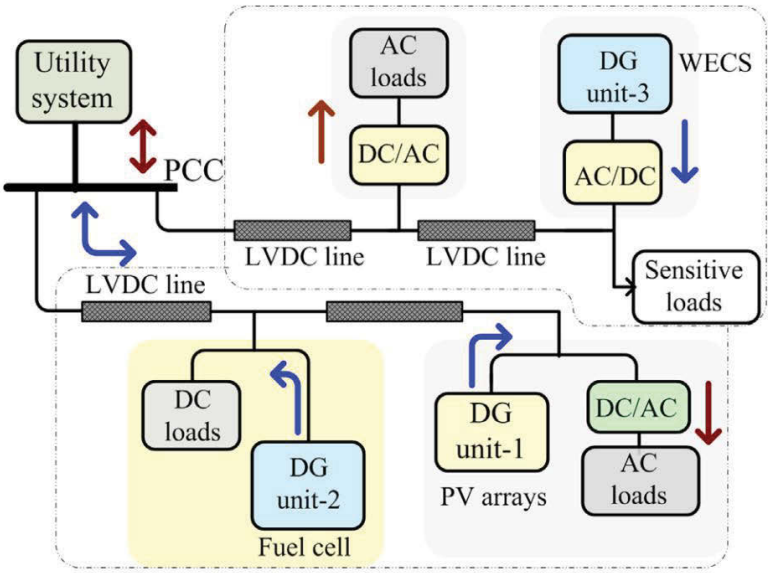

Fig.2.29 Typical DC bus based microgrid systems

In the future, the microgrid system is anticipated to incorporate more smart devices installed in the generation devices, transmission lines, substations, and distribution networks and some controllable loads. It would be a combination of both power system and information and communication system. The two networks will be embedded to form a more advanced architecture whereby the flow of power and information will be a dual-way system [2.108].

Though the common topology of the microgrid is voltage source converter based microgrid with AC bus line, the DC bus microgrid has attracted lots of attentions due to its various merits. It can be concluded that the DC bus is the simplest interconnection bus and this configuration results in high efficiency, high reliability, and no frequency or phase control requirements compared to the AC inter-connection bus. It has low distribution and transmission losses, low cost, the possibility to operate across long distances [2.109], [2.110].

In summary, though there are lots of microgrids with various structures for different applications and available resources according to literature surveys, different kinds of microgrids have similar functions and structure. Essentially, there is the H-bridge based VSC for grid synchronization, integration of DGs, and connection of AC loads and the DC/DC converter for integration of ESS and DC load or DC bus. As reviewed earlier, the three-phase full bridge converter could be used as a converter module to realize these functions. It can also be an ideal candidate for power quality improvement unit in the utility grid, which could provide ancillary services to the utility grid to improve power quality.

Thus, to find the microgrid topology for general applications and modular design with consideration given to cost, versatility, and capacity expansion, are two important issues and have not been well studied before. To realize the full functions of microgrids, it should consist of ESS with galvanic isolation, AC/DC conversion for power feed-back and grid synchronization, DC/DC conversion for power regulation of DC bus and ESS, AC/DC converter for integration of distributed generations and static bypass switch, etc.

2.4 Summary of the Chapter

As reviewed, the development of PEI still remains a challenge, especially for microgrid applications, and the control strategies of the three-phase full-bridge converter are also a hot topic in the literature regarding the improvement of their performance by regulating the power flow with good dynamic and steady state performance, fixed switching frequency, mutual influence elimination and lower sampling frequency, etc. The challenges of the current power converter interfaces need more functions and ancillary services for RES applications.

REFERENCES

[2.1] J. M. Guerrero, J. C. Vasquez, J. Matas, L. G. de Vicuna, M. Castilla, "Hierarchical control of droop-controlled AC and DC microgrids—A general approach toward standardization", *IEEE Trans. Ind. Electron.*, vol. 58, no. 1, pp. 158-172, Jan. 2011.

[2.2] S. Anand and B. G. Fernandes, "Steady state performance analysis for load sharing in DC distributed generation system", *Proc. 10th Int. Conf. Environ. Electr. Eng*., pp.1 -4 2011

[2.3] A. Kwasinski, "Quantitative evaluation of DC microgrids availability: Effects of system architecture and converter topology design choices", IEEE Trans. Power Electron., vol. 26, no. 3, pp.835 -851 2011

[2.4] Y. Zhang and H. Ma, "Theoretical and experimental investigation of networked control for parallel operation of inverters", IEEE Trans. Ind. Electron., vol. 59, no. 4, pp.1961 -1970 2012

[2.5] S.K, Zhang, Y. Xing, et al., “A distributed control strategy based on DC bus signaling for modular photovoltaic generation systems with battery energy storage”, Power Electronics, IEEE Transactions on, 2011, 26 (10): 3032-3045

[2.6] S.V. Iyer, M.N. Belur and M.C. Chandorkar, "A generalized computational method to determine stability of a multi inverter microgrid", *IEEE Trans. Power Electron.*, vol. 25, no. 9, pp.2420 -2432 2010

[2.7] F. Blaabjerg, M. Liserre, and K. Ma, “Power electronics converters for wind turbine systems,” *IEEE Trans. Ind. Appl.*, vol. 48, no. 2, pp. 708– 719, Mar./Apr. 2012

[2.8] J. R. Rodriguez, J. W. Dixon, J. R. Espinoza, J. Pontt, and P. Lezana, “PWM regenerative rectifiers: State of the art,” *IEEE Trans. Ind. Electron.*, vol. 52, no. 1, pp. 5–22, Feb. 2005.

[2.9] F. Blaabjerg, R. Teodorescu, M. Liserre, and A. Timbus, “Overview of control and grid synchronization for distributed power generation systems,” *IEEE Trans. Ind. Electron.*, vol. 53, no. 5, pp. 1398–1409, Oct. 2006.

[2.10] S. Chakraborty, B. Kramer and B. Kroposki, “A review of power electronics interfaces for distributed energy systems toward achieving low-cost modular design,” *Renewable and Sustainable Energy Reviews*, vol. 13, no. 9, pp. 2323-2335, 2009

[2.11] W. Kramer, S. Chakraborty, B. Kroposki, H. Thomas, "Advanced power electronic interfaces for distributed energy systems—I: System and topologies", *National Renewable Energy Laboratory Golden CO Tech. Rep. NREL/TP-58142672*, 2008-Mar.

[2.12] L. Hassaine, E. OLias, J. Quintero, and V. Salas, “Overview of power inverter topologies and control structures for grid connected photovoltaic systems,” *Renewable and Sustainable Energy Reviews*, vol. 30, pp. 796–807, Feb. 2014

[2.13] J. Li and K. Corzine, "Development of grid-connected inverters for micro-grid", *Power Systems Conference (PSC), 2014 Clemson University. IEEE*, pp. 1-6

[2.14] R. I. Bojoi, L. R. Limongi, D. Roiu, and A. Tenconi, “Enhanced power quality control strategy for single-phase inverters in distributed generation systems,” *IEEE Trans. Power Electron.*, vol. 26, no. 3, pp. 798–806, Mar. 2011

[2.15] Z. Ming, L. Ximei, and P. Lilin, “The ancillary services in China: An overview and key issues,” *Renewable and Sustainable Energy Reviews*, vol. 36, pp. 83–90, Aug. 2014

[2.16] T. Strasser, F. Andren, J. Kathan, C. Cecati, C. Buccella, P. Siano*, et al.*, “A review of architectures and concepts for intelligence in future electric energy systems,” *IEEE Trans. Ind. Electron.,* vol. 62(4), pp. 2424-2438, 2015

[2.17] B. Singh, B. N. Singh, A. Chandra, K. Al-Haddad, A. Pandey, D. P. Kothari, "A review of three-phase improved power quality ac–dc converters", *IEEE Trans. Ind. Electron.*, vol. 51, no. 3, pp. 641-660, Jun. 2004

[2.18] F. Blaabjerg, R. Teodorescu, M. Liserre, and A. Timbus, "Overview of control and grid synchronization for distributed power generation systems," *IEEE Trans. Ind. Electron.*, vol. 53, no. 5, pp. 1398–1409, Oct. 2006

[2.19] S. Chakraborty, B. Kramer and B. Kroposki, "A review of power electronics interfaces for distributed energy systems toward achieving low-cost modular design," *Renewable and Sustainable Energy Reviews*, vol. 13, no. 9, pp. 2323-2335, 2009

[2.20] M. Malinowski, M.P. Kazmierkowski, and A.M. Trzynadlowski, "A comparative study of control techniques for PWM rectifiers in AC adjustable speed drives," *IEEE Trans. Power Electron.*, vol. 18, no. 6, pp. 1390–1396, Nov. 2003

[2.21] M. P. Kazmierkowski, L. Malesani, "Current control techniques for three-phase voltage-source PWM converters: A survey", *IEEE Trans. Ind. Electron.*, vol. 45, pp. 691-703, Oct. 1998

[2.22] J. Alonso-Martinez, J. E. Carrasco, and S. Arnaltes, "Table-based direct power control: A critical review for microgrid applications," *IEEE Trans. Power Electron.*, vol. 25, no. 12, pp. 2949–2961, Dec. 2010

[2.23] J. Hu, J. Zhu, and D. G. Dorrell, "A Comparative Study of Direct Power Control of AC/DC Converters for Renewable Energy Generation," in Proc. *IEEE IECON Conf.*, pp. 3453–3458, 2011

[2.24] Y. Zhang, Z. Li, Y. Zhang, W. Xie, Z. Piao, and C. Hu, "Performance improvement of direct power control of PWM rectifier with simple calculation," *IEEE Trans. Power Electron.*, vol. 28, no. 7, pp. 3428–3437, Jul. 2013

[2.25] T. Noguchi, H. Tomiki, S. Kondo, and I. Takahashi, "Direct power control of PWM converter without power-source voltage sensors," *IEEE Trans. Ind. Appl*, vol. 34, no. 3, pp. 473–479, May/Jun. 1998

[2.26] L. Xu, D. Zhi, and L. Yao, "Direct power control of grid connected voltage source converters," in *Proc. IEEE Power Eng. Soc. Gen. Meet.*, 2007, pp. 1–6

[2.27] A. Bouafia, F.Krim, and J.-P. Gaubert, "Fuzzy-logic-based switching state selection for direct power control of three-phase PWM rectifier," *IEEE Trans. Ind. Electron*.,vol. 56, no. 6, pp. 1984–1992, Jun. 2009

[2.28] J. Rodriguez et al., "Predictive current control of a voltage source inverter," *IEEE Trans. Ind. Electron*.,vol. 54, no. 1, pp. 495–503, Feb. 2007

[2.29] D. E. Quevedo, R. P. Aguilera, M. A. Perez, P. Cortes, and R. Lizana, "Model predictive control of an AFE rectifier with dynamic references," *IEEE Trans. Power Electron*., vol. 27, no. 7, pp. 3128–3136, Jul. 2012

[2.30] M. Malinowski, M. P. Kazmierkowski, S. Hansen, F Blaabjerg, and G. D Marques, "Virtual flux based direct power control of three-phase PWM rectifiers," *IEEE Trans. Ind. Appl.*, vol.37, no. 4, pp.1019–1027, Jul./Aug. 2001

[2.31] P. Antoniewicz, M. P. Kazmierkowski, "Virtual flux based predictive direct power control of ac/dc converters with on-line inductance estimation", *IEEE Trans. Ind. Electron.*, vol. 55, no. 12, pp. 4381-4390, Dec. 2008

[2.32] M. Malinowski, M. P. Kazmierkowski, S. Hansen, F. Blaabjerg, G. D. Marques, "Virtual-flux-based direct power control of three-phase PWM rectifiers", *IEEE Trans. Ind. Appl.*, vol. 37, no. 4, pp. 1019-1027, Jul./Aug. 2001

[2.33] N. R. N. Idris, A. H. M. Yatim, "Direct torque control of induction machines with constant switching frequency and reduced torque ripple", *IEEE Trans. Ind. Electron.*, vol. 51, no. 4, pp. 758-767, Aug. 2004

[2.34] M. Pacas, J. Weber, "Predictive direct torque control for the PM synchronous machine", *IEEE Trans. Ind. Electron.*, vol. 52, no. 5, pp. 1350-1356, Oct. 2005

[2.35] I. Sarasola, J. Poza, M. A. Rodriguez, G. Abad, "Predictive direct torque control of brushless doubly fed machine with reduced torque ripple at constant switching frequency", *Proc. IEEE ISIE'07 Conf.*, pp. 1074-1079, 2007

[2.36] J. Beerten, J. Verveckken, J. Driesen, "Predictive direct torque control for flux and torque ripple reduction", *IEEE Trans. Ind. Electron.*, vol. 57, no. 1, pp. 404-412, Jan. 2010

[2.37] L. Tang, L. Zhong, M. F. Rahman, "A novel direct torque control for interior permanent-magnet synchronous machine drive with low ripple in torque and flux-a speed-sensorless approach", *IEEE Trans. Ind. Appl.*, vol. 39, no. 6, pp. 1748-1756, Nov./Dec. 2003

[2.38] M. Zhang, X. Xiao, Y. Li, "Predictive direct torque control of PM synchronous motors based on an area voltage vector table", *J. Tsinghua Univ.*, vol. 48, no. 1, pp. 25-30, Jan. 2008

[2.39] F. Morel, L.-S. Xuefang, J. M. Retif, B. Allard, C. Buttay, "A comparative study of predictive current control schemes for a permanent-magnet synchronous machine drive", *IEEE Trans. Ind. Electron.*, vol. 56, no. 7, pp. 2715-2728, Jul. 2009.

[2.40] J. Hu, J. Zhu, G. Platt, and D. G. Dorrell, “Multi-objective model-predictive control for high power converters,” *IEEE Trans. Energy Convers.,* vol. 28, no. 3, pp. 652-663, Sep. 2013

[2.41] R. Kennel, A. Linder, "Predictive control of inverter supplied electrical drives",*Proc. Conf. Record Power Electronics Specialists*, pp. 761-766, 2000-Jun.

[2.42] D. W. Clarke, "Advances in model-based predictive control", *Advances in Model-Based Predictive Control*, pp. 3-21, 1994, Oxford Univ. Press

[2.43] R. Vargas, U. Ammann, J. Rodrguez, J. Pontt, "Reduction of switching losses and increase in efficiency of power converters using predictive control", *Proc. IEEE PESC*, pp. 1062-1068, 2008-Jun.-1519

[2.44] S. Bibian, H. Jin, "High performance predictive dead-beat digital controller for dc power supplies", *Proc. IEEE APEC'01 Conf.*, pp. 67-73, 2001

[2.45] P. Falcone, F. Borrelli, H. E. Tsengz, J. Asgari, D. Hrovat, "A hierarchical model predictive control framework for autonomous ground vehicles", *Proc. Amer. Control Conf. (ACC)*, pp. 3719-3724, Jun. 2008

[2.46] J.C. Kantor, C.E. Garcia, B. Carnahan, "An overview of industrial model predictive control technology", *Proc. Chemical Process Control-V*, pp. 232-256, 1997

[2.47] Y. Zhang and W. Xie, “Low complexity model predictive control—Single vector based approach,” *IEEE Trans. Power Electron.*, vol. 29, no. 10, pp. 5532–5541, Oct. 2014.

[2.48] Z. Song, C. Xia, and T. Liu, “Predictive current control of three-phase grid- connected converters with constant switching frequency for wind energy systems,” *IEEE Trans. Ind. Electron.*, vol. 60, no. 6, pp. 2451–2464, Jun. 2013

[2.49] R. P. Aguilera, P. Lezana, and D. E. Quevedo, “Finite-control-set model predictive control with improved steady-state performance,” *IEEE Trans. Ind. Electron.*, vol. 9, no. 2, pp. 658–667, May 2013

[2.50] P. Cortes *et al.*, “Model predictive control of an inverter with output LC filter for UPS applications,” *IEEE Trans. Ind. Electron.*, vol. 56, no. 6, pp. 1875–1883, Jun. 2009

[2.51] S. Vazquez, C. Montero, C. Bordons, and L. G. Franquelo, “Model predictive control of a VSI with long prediction horizon,” in *Proc. IEEE Int. Symp. Ind. Electron.*, Jun. 2011, pp. 1805–1810

[2.52] J. Hu, J. Zhu, and D. G. Dorrell, “A Comparative Study of Direct Power Control of AC/DC Converters for Renewable Energy Generation,” in Proc. *IEEE IECON Conf.*, pp. 3453–3458, 2011

[2.53] S. Vazquez, C. Montero, C. Bordons, and L. G. Franquelo, “Model predictive control of a VSI with long prediction horizon,” in *Proc. IEEE Int. Symp. Ind. Electron*., Jun. 2011, pp. 1805–1810

[2.54] P. Cortes, M. Kazmierkowski, R. Kennel, D. Quevedo, and J. Rodriguez, “Predictive control in power electronics and drives,” *IEEE Trans. Ind. Electron.*, vol. 55, no. 12, pp. 4312–4324, Dec. 2008

[2.55] S. Vazquez *et al.*, “Model predictive control: A review of its applications in power electronics,” *IEEE Ind. Electron. Mag.*, vol. 8, no. 1, pp. 16–31, Mar. 2014

[2.56] J. Rodríguez, M. P. Kazmierkowski, J. R. Espinoza, P. Zanchetta, H. Abu-Rub, H. A. Young, C. A. Rojas, "State of the art of finite control set model predictive control in power electronics", *IEEE Trans. Ind. Informat.*, vol. 9, no. 2, pp. 1003-1016, May 2013

[2.57] J. Hu, J. Zhu, G. Platt, et al., “Model-predictive direct power control of AC/DC converters with one step delay compensation”, IECON 2012 - 38th Annual Conference on IEEE Industrial Electronics Society, IEEE, 2012: 4892-4897

[2.58] S. Kouro, P. Cortes, R. Vargas, U. Ammann, and J. Rodriguez, “Model predictive control—A simple and powerful method to control power converters,” *IEEE Trans. Ind. Electron*., vol.56, no. 6, pp. 1826–1838, Jun. 2009

[2.59] A. Bouafia, J.-P. Gaubert, and F. Krim, “Predictive direct power control of three-phase pulse width modulation (PWM) rectifier using space-vector modulation (SVM),” *IEEE Trans. Power Electron*., vol. 25, no. 1, pp. 228–236, Jan. 2010

[2.60] R. Portillo, S. Vazquez, J. I. Leon, M. M. Prats, and L. G. Franquelo,“Model based adaptive direct power control for three-level NPC converters,” *IEEE Trans. Ind. Inform*., vol. 9, no. 2, pp. 1148–1157,May2013

[2.61] S. Aurtenechea, M. A. Rodriguez, E. Oyarbide, and J. R. Torrealday,“Predictive control strategy for DC/AC converters based on direct power control,” *IEEE Trans. Ind. Electron.*, vol. 54, no. 3, pp. 1261–1271, Jun. 2007

[2.62] R. P. Aguilera, D. E. Quevedo, S. Vazquez, and L. G. Franquelo, “Generalized predictive direct power control for AC/DC converters,” in *Proc. ECCE Asia 2013*, Jun., pp.1215–1220

[2.63] J. Hu and Z. Q. Zhu, “Investigation on switching patterns of direct power control strategies for grid-connected DC–AC converters based on power variation rates,” *IEEE Trans. Power Electron*., vol. 26, no. 12, pp. 3582–3598, Dec. 2011

[2.64] J. Hu and Z. Zhu, “Improved voltage-vector sequences on dead-beat predictive direct power control of reversible three-phase grid-connected voltage-sourced converters,” *IEEE Trans. Power Electron.*, vol. 28, no. 1, pp. 254–267, Jan. 2013

[2.65] Z. Song, W. Chen, and C. Xia, “Predictive direct power control for three-phase grid-connected converters without sector information and voltage vector selection,” *IEEE Trans. Power Electron.*, vol. 29, no. 10, pp. 5518–5531, Oct. 2014

[2.66] Z. Song, Y. Tian, W. Chen, Z. Zou, and Z. Chen, “Predictive duty cycle control of three-phase active-front-end rectifiers,” *IEEE Trans. Power Electron*., vol. 31, no. 1, pp. 698–710, Jan. 2016

[2.67] Y. Zhang, Y. Peng, and H. Yang, “Performance improvement of two-vectors-based model predictive control of PWM rectifier,” *IEEE Trans. Power Electron.*, vol. 31, no. 8, pp. 6016–6030, 2016

[2.68] Y. Zhang, W. Xie, Z. Li, and Y. Zhang, “Low-complexity model predictive power control: Double-vector-based approach,” *IEEE Trans. Ind. Electron.*, vol. 61, no. 11, pp. 5871–5880, 2014

[2.69] Y. Zhang, W. Xie, Z. Li, and Y. Zhang, “Model predictive direct power control of a PWM rectifier with duty cycle optimization,” *IEEE Trans. Power Electron.*, vol. 28, no. 11, pp. 5343–5351, Nov. 2013

[2.70] D. Choi, K. Lee, "Dynamic performance improvement of AC/DC converter using model predictive direct power control with finite control set," *IEEE Trans. Ind. Electron.,* vol. 62, pp. 757-767, 2015

[2.71] J. Restrepo, J. Viola, J.M. Aller, A. Bueno, “A simple switch selection state for SVM direct power control”, IEEE ISIE 2006, 2006, pp. 1112–1116

[2.72] A. Bouafia, J.P. Gaubert, F. Krim, “Predictive direct power control of three-phase pulse width modulation (PWM) rectifier using space-vector modulation (SVM)”, *IEEE Trans. Power Electron*., 2010, 25, (1), pp. 228–236

[2.73] S. Kwak and J.-C. Park, “Switching strategy based on model predictive control of VSI to obtain high efficiency and balanced loss distribution,” *IEEE Trans. Power Electron.*, vol. 29, no. 9, pp. 4551–4567, Sep. 2014

[2.74] Y. Du, X. Zhou, S. Bai, S. Lukic, A. Huang, "Review of non-isolated bi-directional DC–DC converters for plug-in hybrid electric vehicle charge station application at municipal parking decks", *Proc. IEEE Appl. Power Electron. Conf.*, pp. 1145-1151, 2010-Feb.

[2.75] S. Inoue and H. Akagi, “A bidirectional isolated dc–dc converter as a core circuit of the next-generation medium-voltage power conversion system,” *IEEE Trans. Power Electron.*, vol. 22, no. 2, pp. 535–542, Mar. 2007

[2.76] S. Inoue and H. Akagi, “A bidirectional DC–DC converter for an energy storage system with galvanic isolation,” *IEEE Trans. Power Electron.*,vol. 22, no. 6, pp. 2299–2306, Nov. 2007

[2.77] S. Engel, N. Soltau, H. Stagge, R. W. De Doncker, "Dynamic and balanced control of three-phase high-power dual-active bridge DC–DC converters in DC-grid applications", *IEEE Trans. Power Electron.*, vol. 28, pp. 1880-1889, Apr. 2013

[2.78] H. Bai and C. Mi, “Eliminate reactive power and increase system efficiency of isolated bidirectional dual-active-bridge DC-DC converter using novel dual-phase-shift control,” *IEEE Trans. Power Electron*., vol. 23, no. 6, pp. 2905-2914, Nov. 2008

[2.79] G. G. Oggier, G. O. Garc´ıa, and A. R. Oliva, “Switching control strategy to minimize dual active bridge converter losses,” *IEEE Trans. Power Electron*., vol. 24, no. 7, pp. 1826–1838, Jul. 2009

[2.80] H. Bai, Z. Nie, and C. Mi, “Experimental comparision of traditional phase-shift, dual-phase-shift, and model-based control of isolated bidirectional dc-dc converters,” *IEEE Trans. Power Electron.*, vol. 25, no. 6, pp. 1444–1449, Jun. 2010

[2.81] F. Krismer and J. W. Kolar, “Efficiency-optimized high current dual active bridge converter for automotive applications,” *IEEE Trans. Ind. Electron.*,vol. 59, no. 7, pp. 2745–2760, Jul. 2012

[2.82] B. Zhao, Q. Song, and W. H. Liu, “Power characterization of isolated bidirectional dual-active-bridge DC–DC converter with dual-phase-shift control,” *IEEE Trans. Power Electron.*, vol. 27, no. 9, pp. 4172 - 4176, Sep. 2012

[2.83] H. Zhou and A. M. Khambadkone, “Hybrid modulation for dual active bridge bi-directional converter with extended power range for ultracapacitor application,” *IEEE Trans. Ind. Appl*., vol. 45, no. 4, pp. 1434–1442, Jul. 2009

[2.84] G. G. Oggier , G. O. Garcia, and A. R. Oliva, "Modulation strategy to operate the dual active bridge DC-DC converter under soft switching in the whole operating range", *IEEE Trans. Power Electron.*, vol. 26, no. 4, pp.1228 -1236, Apr. 2011

[2.85] F. Krismer, J. Biela, and J. W. Kolar, "Performance optimization of a high current dual active bridge with a wide operating voltage range," in *Proc. IEEE Power Electron. Spec. Conf. (PESC)*, 2006, pp. 1–7

[2.86]. D. H. Xu, C. H. Zhao, and H. F. Fan, "A PWM plus phase-shift control bidirectional DC–DC converter," *IEEE Trans. Power Electron.*, vol. 19, no. 3, pp. 666–675, May 2004

[2.87] I. Syed, W. Xiao, "Modeling and control of dab applied in a PV based DC microgrid", 2012 *IEEE International Conference on Power Electronics Drives and Energy Systems*, December 16-19, 2012.

[2.88] H. Bai, Z. Nie, C. Mi, "Experimental comparision of traditional phase-shift dual-phase-shift and model-based control of isolated bidirectional dc-dc converters", *IEEE Trans. Power Electron.*, vol. 25, no. 6, pp. 1444-1449, Jun. 2010

[2.89] Y. Xie, R. Ghaemi, J. S. Freudenberg, "Implicit model predictive control of a full bridge DC–DC converter", *IEEE Trans. Power Electron.*, vol. 24, no. 12, pp. 2704-2713, Dec. 2009

[2.90] Y. Xie, R. Ghaemi, J. Sun, J. S. Freudenberg, "Model predictive control for a full bridge DC/DC converter", *IEEE Trans. Control Syst. Technol.*, vol. 20, no. 1, pp. 164-172, Jan. 2012

[2.91] Y. Xie, R. Ghaemi, J. Sun, J. Freudenberg, "Comparative evaluation of linear and nonlinear model predictive control for a isolated high power DC/DC converter", *American Control Conference*, pp. 938-943, 2010

[2.92] S. Dutta, S. Hazra, S. Bhattacharya, "A digital predictive current mode controller for single phase dual active bridge isolated DC to DC converter", *IEEE Trans. Ind. Electron.*, vol. 63, no. 9, pp. 5943-5952, Sep. 2016

[2.93] P. Akter, M. Uddin, S. Mekhilef, N. M. L. Tan, H. Akagi, "Model predictive control of bidirectional isolated DC–DC converter for energy conversion system", *Int. J. Electron.*, vol. 102, no. 8, pp. 1407-1427, 2015

[2.94] E. Unamuno, J.A. Barrena, "Hybrid ac/dc microgrids—part I: review and classification of topologies". *Renew Sustain Energy Rev*, 52 (2015), pp. 1251–1259

[2.95] H. Qin, J.W. Kimball, "A comparative efficiency study of silicon-based solid state transformers", In: *Proceedings of the IEEE energy conversion congress and exposition (ECCE)*; 2010. pp. 1458–1463

[2.96] G. Ortiz, “High-power DC-DC converter technologies for smart grid and traction applications,” Ph.D. dissertation, Power Electron. Syst. Lab., Swiss Federal Inst. Technol., Zürich, Switzerland, 2014

[2.97] J.A. Martinez-Velasco, S. Alepuz, F. González-Molina, J. Martin-Arnedo, “Dynamic average modeling of a bidirectional solid state transformer for feasibility studies and real-time implementation”, *Electr Power Syst Res* 2014;117:143–53

[2.98] G. Ortiz, H. Uemura, D. Bortis, J.W. Kolar, O. Apeldoorn, “Modeling of softswitching losses of IGBTs in high-power high-efficiency dual-active-bridge DC/DC converters”, *IEEE Trans Electron Dev* 2013;60(2):587–97

[2.99] S. Falcones, X. Mao, R. Ayyanar, “Topology comparison for Solid State Transformer implementation”, In: *Proceedings of the IEEE PES general meeting*; 2010; pp. 1–8

[2.100] X.J. Wang, W.Q. Tian, H.J. He, M. Huang, J.C. Jiang, H.Y. Han, “The application of electric vehicles as mobile distributed energy storage units in smart grid”, In Proc. Power Energy Eng. Conf., Wuhan, China, Mar. 2011, 1–5

[2.101] J. J. Justo, F. Mwasilu, J. Lee, J.-W. Jung, "AC microgrids versus DC-microgrids with distributed energy resources: A review", *Renew. Sustain. Energy Rev.*, vol. 24, pp. 387-405, Aug. 2013

[2.102] M. Fazeli. “Wind generator-energy storage control schemes for autonomous grid”, PhD thesis, University of Nottingham, 2011

[2.103] L. Roggia, L. Schuch, J. E. Baggio, C. Rech, J. R. Pinheiro, "Integrated full-bridge-forward dc-dc converter for a residential microgrid application", *IEEE Trans. Power Electron.*, vol. 28, no. 4, pp. 1728-1740, Apr. 2013

[2.104] J. Lago, M. L. Heldwein, "Operation and control-oriented modeling of a power converter for current balancing and stability improvement of DC active distribution networks", *IEEE Trans. Power elctron.*, vol. 26, no. 3, pp. 877-885, Mar. 2011

[2.105] R. Noroozian , M. Abedia , G. B. Gharehpetian , and S. H. Hosseini , “ Combined operation of DC isolated distribution and PV systems for supplying unbalanced AC loads,” *Renewable Energy*, vol. 34 , no.3 , pp. 899 – 908, Mar. 2009

[2.106] L. Xu, D. Chen, "Control and operation of a DC microgrid with variable generation and energy storage", *IEEE Trans. Power Del.*, vol. 26, no. 4, pp. 2513-2522, Oct. 2011

[2.107] D. Salomonsson, L. Soder, A. Sannino, "Protection of low-voltage DC microgrids",*IEEE Trans. Power Del.*, vol. 24, no. 3, pp. 1045-1053, Jul. 2009.

[2.108] L. Nikonowicz, J. Milewski, "Virtual power plants—General review: Structure application and optimization", *J. Power Technol.*, vol. 92, no. 3, pp. 135-149, 2012

[2.109] R. S. Balog and P. T. Krein, “Bus selection in multibus DC microgrids,” *IEEE Trans. Power Electron*., vol. 26, no. 3, pp. 860–867, Mar. 2011

[2.110] J. Chen, J. Chen, R. Chen, X. Zhang, and C. Gong, “Decoupling control of the non-grid-connected wind power system with the droop strategy based on a DC micro-grid,” in *Proc. World Non-Grid-Connected Wind Power Energy Conf*., 2009, pp. 1–6

Chapter 3

APPLICATION OF THREE-PHASE FULL-BRIDGE CONVERTER IN RENEWABLE ENERGY SYSTEMS

3.1 Introduction

In recent years, due to the energy crisis and remarkable potential in renewable energies, much attention has been paid to the microgrids systems, which are local electricity networks that integrate distributed generations (DGs), energy storage systems (ESS), and various of loads by means of active network management with various kinds of power electronic interfaces (PEI).

Today, the conventional renewable energy systems and microgrids are facing challenges which are required to be extremely flexible, reliable and expandable. Most topologies of microgrids are AC bus based microgrids with the disadvantages of control complexity, capacity expansion, and efficiency, which hinders the promotion of renewable energy systems. Through discussions on the application of three-phase full-bridge converter in renewable energy systems, this chapter proposes a multi-functional modular microgrid topology, which has a fully symmetrical and modular circuit structure, and offers galvanic isolation to ESS from the DGs and loads, with advantages of convenient manufacturing process, transport, installation, maintenance, capacity expansion, and upgradability. Firstly, different kinds of operation modes are analyzed. Then, the control strategies of each modules, such as direct power control (DPC), model predictive control (MPC), and dual-phase-shift control and voltage droop control for different power flow conditions are discussed. Finally, the optimal control strategies of microgrids in each operation mode will be fully researched.

The three-phase full-bridge converter is widely applied as an AC/DC bidirectional converter in renewable energy systems (RES) for DG integration or AC power supply

or power feed. This topology is also a popular candidate when applied as a DC/DC converter with series connection by a high-frequency transformer for ESS power charge/discharge. The conventional three-phase full-bridge converter based PEI in RES can serve basic functions of power conversion and energy feeding. Since it is designed for specific applications and has limited flexibility due to fixed size and functions, it will be disconnected from the grid during abnormal grid conditions or power outage. If a large number of DGs come back online simultaneously after a grid outage or being disconnected because of a grid disturbance, another grid disturbance might be triggered. Today, this issue has drawn more attention with the wide distribution of renewable energy systems. The IEEE P1547a standard for interconnecting DG has been amended to allow inverter-based generation to participate in voltage regulation. Some proactive policys to update interconnection requirements, e.g. California Rule 21, have been proposed to meet these reactive power capabilities with increased solar installation amounts.

More recently, the advanced smart inverter concept has been proposed, and this should help prevent the reoccurrence of a grid disturbance immediately after an outage. Therefore, the issue with more and more DG integration into the utility grid requires a smart inverter to provide certain ancillary services and local voltage support functions such as voltage and frequency fault ride-through, and reactive power compensation, etc. to improve the power quality.

The smart inverter offers the required adaptability and flexibility for modern power supply systems. However, the proposed smart inverter or advanced inverter concept only focused on the specific application, such as photovoltaic (PV) system or just focused on the general application in the utility grid for the AC/DC conversion only and the DC/DC conversion realization with smart converter in the microgrids has not been considered. Besides, the development of more DG integration in microgrids needs the PEI to have more features, such as wireless communication, advanced control strategies and plug-play features. Thus this chapter proposes a new concept of smart converter

with general power conversion application and advanced features which has the inherit advantage in renewable energy systems or microgrids.

3.2 Proposal of Microgrids Topology with Modular Design

Today, renewable energy systems are required to be extremely reliable, expandable and flexible. Many types of renewable energy are not stable and discontinuous since they vary with the environment and weather conditions, such as PV and wind power, therefore the load power demand cannot be met by renewable generation seamlessly [3.1-3.2]. Due to discontinuous and variable power generation, it is difficult to connect the DGs directly to the AC power system. Besides, voltage oscillation and protection issues should be required as well.

To solve these problems, the microgrids with inclusion of ESS' have been gaining more and more attention each day [3.3-3.4]. A microgrid is generally considered as a small-scale grid with the ability to control as either a grid-connected or an islanded system. The advantages of microgrids are their capacities to generate clean energy and convenient integration of DG sources to the utility grid with the power management ability inside the system. Meanwhile, it could also provide more auxiliary service for the main gird. For the development of renewable energy in the future, the traditional power system can no longer meet the requirement of the future power system anymore and thus energy saving, clean energy, modular design, and smart microgrid systems become more popular [3.5-3.6].

Though there are various microgrid structures for various applications and available resources, different kinds of microgrids with various structures limit their applications. The module functions in microgrids could essentially be similar, due to the AC/DC conversion for grid synchronization, integration of DGs to the utility grid, power supply of AC loads and the DC/DC conversion for integration of ESS or DC bus. In the review of last chapter, the DC bus has the advantages of high reliability, high efficiency, and no requirements of frequency or phase control in comparison with the AC bus design with the benefits of low costs, low transmission and distribution losses, and the ability to

operate across long distances [3.7]. Nowadays, the development of more DG integration in microgrids requires more advanced functions in terms of the costs, ancillary services, plug-and-play ability, and power quality and reliability improvement.

In [3.5], the authors proposed a novel uninterruptible power supply (UPS) system with DC bus. However, only single-phase-bridge converters are analyzed and the concept remains only at the stage of UPS without any consideration of microgrid function realization and control. In [3.8], a DC bus-based PV generation system was presented. The DC/DC converter module are the key elements of the system with modular design and the same ratings. However, the AC/DC converter module and other distributed generation are not considered. In [3.9] and [3.10], the hierarchical microgrids with both AC and DC links, and DC and AC microgrids are compared with a similar structure. It can be concluded that most of the microgrid systems do not consider the PEI module in relation to the whole microgrid topology, which makes the microgrid system lack flexibility and universality.

This part extends the modular concept to microgrid topology and designs a novel topology of DC bus microgrid system with modular structure and wireless communication ability based on three-phase full-bridge converter modules. All the functions in the microgrid can be easily realized with this topology. The control of the identical converter modules is analysed. Compared to the conventional microgrid topologies, this topology can be used for various different applications with little modification. The fully modular circuit design has the advantages of convenient manufacturing, transport, installation, maintenance, capacity expansion, and upgrade. Also, the hierarchical control strategies for the system level, to make it more efficient, are discussed.

3.2.1 Topology of proposed microgrids

To realize the general microgrid functions, the system should consist of DGs, ESS, utility grid, and loads, and power electronic converters should have the capability of four quadrant power flow control. The microgrids can be controlled in either island or grid-connected mode.

Fig. 3.1 illustrates the block diagram of proposed microgrid topology, which consists of several identical three-phase full-bridge AC/DC converters as PEI modules to realize multiple functions in the microgrid. Filters, high frequency transformers, inductors and other external circuit elements, e.g. the static bypass switch, will be added depending on the operational power. To connect any modules in a free selectable order and to update the system scale conveniently, standardized interfaces of PEI have to be defined to communicate with each of the modules and exchange information between each other as well as the microgrid control centre [3.11]. The wireless communication between each converter module and the upper control level is assumed to employ 4G, wifi, or zigbee communication techniques. With wireless communication, not only can each converter module communicate with each other, but also each converter module can be controlled by a local microgrid control centre, which is controlled by a regional control centre through ethernet or wireless communication, as illustrated in Fig. 3.1, which has more advantages in a remote area.

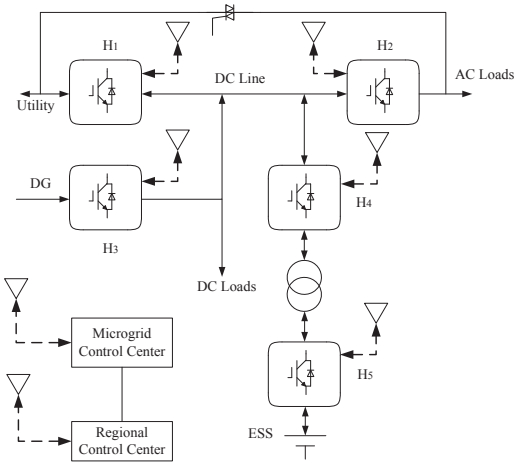

Fig. 3.1 Block diagram of proposed multi-functional modular microgrid system

Due to the modular structure of the proposed microgrid, it could realize the functions of various kinds of power converters and extends to a group of modular microgrid systems. For example, converter module H_1 or H_3 and H_2 could form an AC/DC/AC

converter to provide power to the AC load. H_1 and H_3 can form an AC/DC/AC frequency converter to integrate DG source to the utility grid. H_1 or H_3, H_4, and H_5 can form a bidirectional charger/discharger for delivering the grid power or DG power to ESS. H_2, H_4, and H_5 can form a DC/DC/AC power circuit for various kinds of loads supply. Due to the modular design of the proposed microgrid topology, the single microgrid could be applied as a microgrid module to be widely integrated into smart microgrid groups with the advantage of convenient manufacturing process, transport, installation, maintenance, capacity expansion and upgrade. In addition, it should be noted that the three-phase converter module can disable one leg for single phase AC power supply or power generation to meet various kinds of scenarios.

There are significant benefits to setting up communication between converter modules and the micorgrid control center, and regional transmission organizations or independent system operators. The PEI module is required to have the ability to receive commands or send status information through wireless communication to improve system reliability and stability, react immediately during emergencies, or respond automatically to price signals from the regional control center. It is reliable to design a PEI with a modular and scalable structure that will allow various kinds of DG sources to have the same power electronic converter module, leading to reduction of the cost due to the high quantity of these modules, which will be discussed in the latter part of this thesis.

When compared to the conventional microgrid topology, the proposed microgrid system has a fully modular design and symmetrical structure. The high-frequency transformer can also provide galvanic isolation as a safety requirement to ESS from the utility and loads, which can also reduce the weight and volume. The bidirectional power flow between the main grid and ESS and DGs could be virtually controlled. The pulse width modulation control algorithm and high frequency phase-shift modulation can make the microgrid system more efficient.

3.2.2 Operation modes of proposed microgrids

When the microgrid is not working or the bypass switch is on, the utility grid supply power to the load directly. When bypass switch is turned off, the microgrids can be operated in several different modes according to the power flow direction in the microgrid and utility grid connection status.

While the utility grid is connected, the microgrid system operates in grid-connected status. The operation mode varies according to the power flow direction.

A. Utility/microgrid power-supply mode

While the microgrid and the utility are working well, the bypass switch is in the off position. Converter modules H_1 and H_3 operate in the rectifier mode, and module H_2 operates in the inverter mode, while power supplies from the utility and DG units to the AC and DC load through the H_1 and H_2 module, as illustrated in Fig.3.2. Meanwhile, converters H_4 and H_5 and the high-frequency three-phase transformer form a DC/DC charger to absorb power from the DC bus in order to charge the ESS.

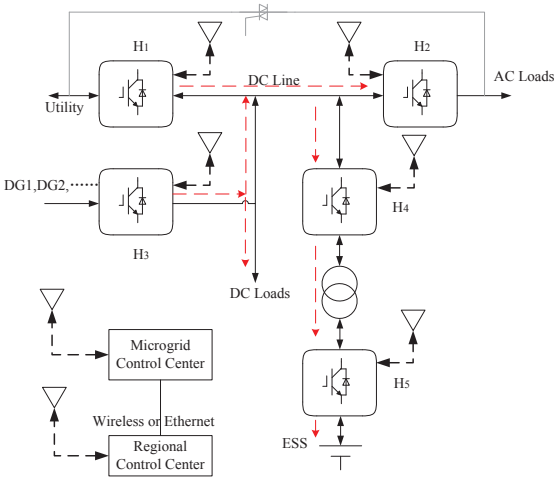

Fig. 3.2 Utility/microgrids power-supply mode, Grid-connected status

B. DG/ESS power-feed mode

While the grid needs to absorb power from the ESS or DGs and the power-feed function is selected, the microgrid operates in the DG/ESS power-feed mode. When module H_1 operates in the inverter state and module H_3 operates in the rectifier state, the renewable energy from the DG units flows to the grid for power feed. Also, converters H_4 and H_5 and the high-frequency transformer T form a DC/DC discharger to absorb electrical power from the ESS to the utility grid, as illustrated in Fig.3.3.

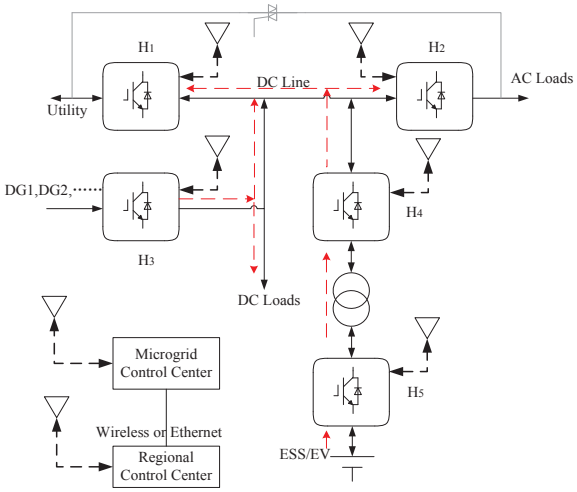

Fig. 3.3 DG& ESS power supply mode: Grid-connected status

C. DG power-generation mode

While the utility grid is disconnected, the microgrid system operates in the island mode. While the utility grid is abnormal and the DG generation is normal, i.e. converter H_1 stops working, converter H_3 operates in the rectifier mode and H_2 in the inverter mode, modules H_4 and H_5 and the high-frequency three-phase transformer form a discharger/charger based on the energy consumption level of the loads, as shown in Fig. 3.4. When the power consumption exceeds the amount of DG generation, the ESS is discharged to supplement power to the load, which can complement energy for the system. When the load has lower energy consumption, the ESS can also absorb excess power from the DGs.

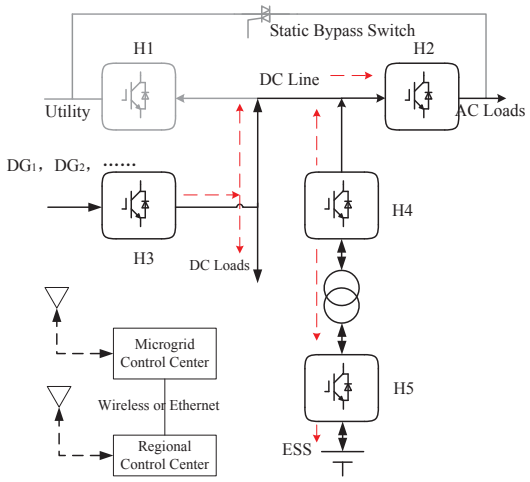

Fig. 3.4 DG power supply mode. Island status

D. ESS power-feed mode

While both the grid and DGs are abnormal and the ESS is selected for UPS, the microgrid works in the ESS power-feed mode, as shown in Fig. 3.5. When modules H_1 and H_3 are disabled and module H_2 operates in the inverter mode, modules H_4 and H_5 and the high-frequency transformer form a discharger, and the power flows from the ESS to the DC bus to supply power to the DC and AC loads.

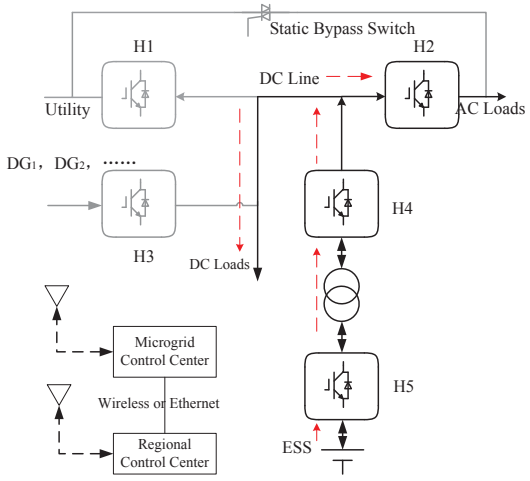

Fig. 3.5 DG power feed mode, Island status

Due to the modular design of the proposed microgrid topology with series or parallel connection, the microgrid can expand the capacity and vary the topology conveniently to form a group of microgrids. Thus, power sharing in parallel connected modules is discussed below.

E. Power sharing in parallel connected modules

As the power rating for single converter module are limited, for high power applications, parallel connections of the converter modules are required, as shown in Fig. 3.6. Thus, power sharing of the paralleling connection of converters should be considered. The droop control method has been widely used for autonomous power sharing between parallel connected AC/DC converters. More discussion of Droop control method can be referenced in [3.12]-[3.14].

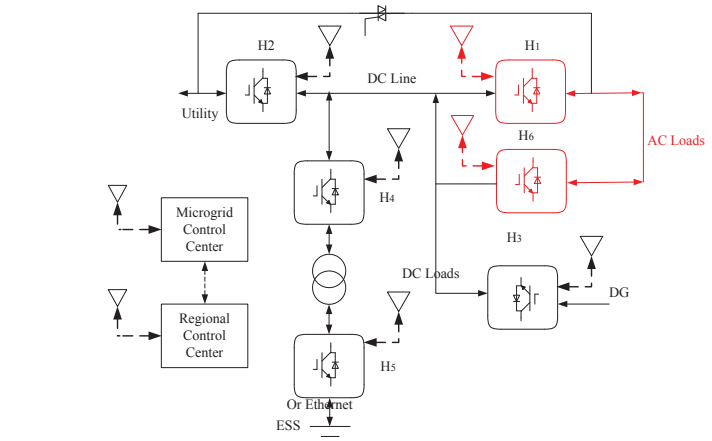

(a)

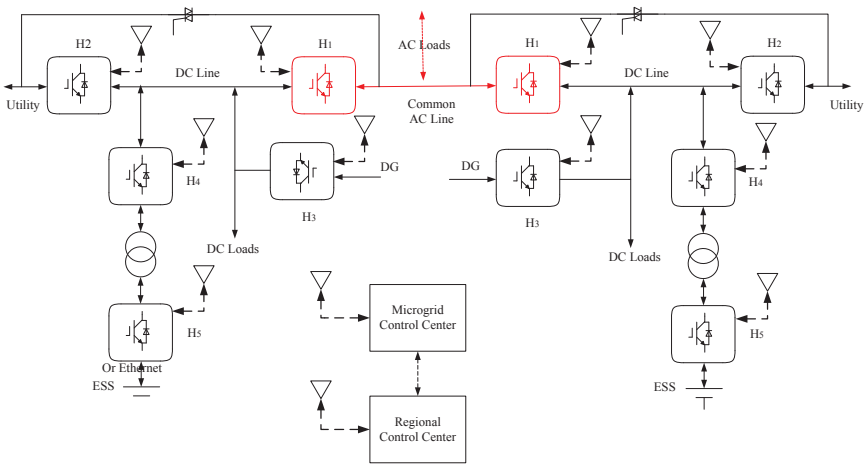

(b)

Fig. 3.6 Parallel power supply mode

The performance of the control strategy has been verified in simulation using Matlab/Simulink, as presented in Fig. 3.7, the parameter of system is the same as in [3.12].

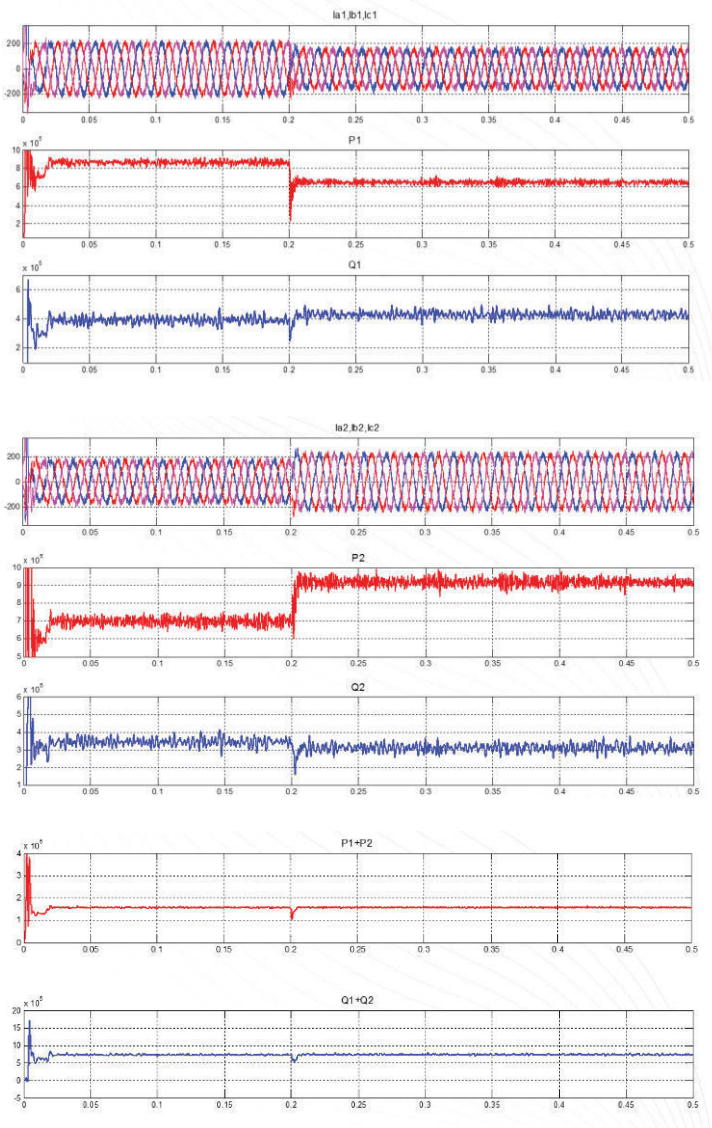

Fig. 3.7 Power sharing with droop control method

As can be concluded from the simulation results, the DG1 and DG2 together supply all the active and reactive power required by the local loads and the common load according to their frequency and voltage droop characteristics. Although the power consumption of local Load 1 decreases from 850 kW to about 650 kW at 0.2 s, Load 2

increases from 700 kW to 800 kW to meet the sum active power supply, and the sum consumption of *Load 1* and *Load 2* about active power keeps constant almost all the time. For sum reactive power consumption, it also keeps constant. The details of droop control method will not be fully discussed due to space limitation.

3.2.3 Control design of the converter module in proposed microgrids.

Most renewable energy resources require an inverter to convert DC from the generating resource to the same voltage and frequency of the AC distribution system. The three-phase full-bridge based converter in the proposed microgrid topology is mainly used as the power interface of grid and DG systems or loads to realize bidirectional power flow with AC/DC conversion. It should be noted that for single-phase AC load power supply or DG power generation, one leg of the three phase converter just needs to be disabled.

The smart inverter concept has become popular recently due to features such as the reactive power compensation, four quadrant power flow, fault ride-through capability, and grid support when there are voltage dips or swells, which can improve grid stability and provide cost reduction and performance improvement [3.15], [3.16]. This will be discussed in the following section.

For the AC/DC conversion of converter module, as reviewed, one of the most popular control methods is the switching table based DPC. It has no inner current loop and the switching states are selected from a predesigned switching table according to the instantaneous errors between the reference and estimated values of reactive and active powers, and the location of the voltage vector. Also, the space vector modulation control, model predictive control and fuzzy logic based direct power control, etc., have attracted much interest in recent years.

The MPC control for the power electronics converter is a significant solution for the control of converter modules in microgrids with several important merits, including the lack of need for a modulator, fast dynamic response, easy inclusion of constraints and

system nonlinearities, ability to incorporate nested control loops in a single loop, and flexibility to include other system performance requirements in the controller. The MPC based DPC control of the converter module with bidirectional power flow between ESS and AC source in the proposed microgrid is shown in Fig. 3.8.

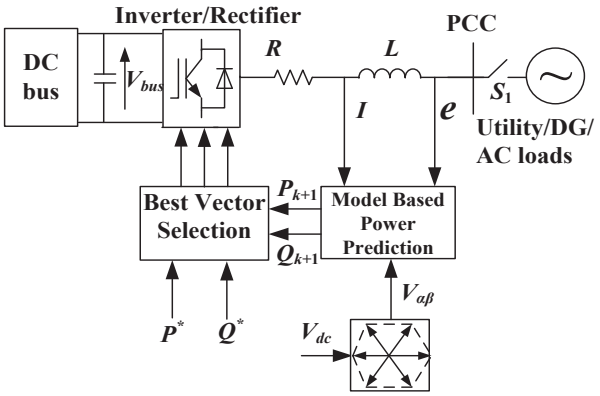

Fig. 3.8 MPC based DPC for bidirectional power flow between the ESS and the utility grid

The dynamic behaviour when there is a load change with the same parameter as [3.17] in simulation is shown in Fig. 3.9**Fig.** (a) and (b). The ESS starts to feed the active power of 4000 W to the grid at 0.04 s while the reactive power keeps at 0 Var. Then, from 0.08 s to 0.12 s, the ESS supplies 2000 Var reactive power to the grid while the active power remains steady. At 0.12 s, the grid supplies the active power of 5000 W to the ESS while the reactive power remains steady at 0 Var. It can be seen that both the conventional and MPC-based DPC work well for bidirectional power flow. The MPC-based DPC yields better performance with the advantages of quicker dynamic response and lower total harmonic distortion (THD).

As discussed in the previous microgrid topology working modes section, two converter modules connected in series by the high-frequency transformer for charging/discharging power between the DC bus and ESS are known as the isolated bidirectional full-bridge DC/DC converter (IBDC), as shown in Fig.3.10. It has a three-phase input and output bridge which are composed of two converter modules. The power flow is regulated by adjusting the phase-shift angle φ between the gating signals of corresponding legs of the output bridge and the input bridge. Compared with the

single-phase topology, the three-phase topology leads to a smaller input and output current ripples with interleaved control, smaller size of output filter and input DC bus capacitor, and therefore higher converter power density.

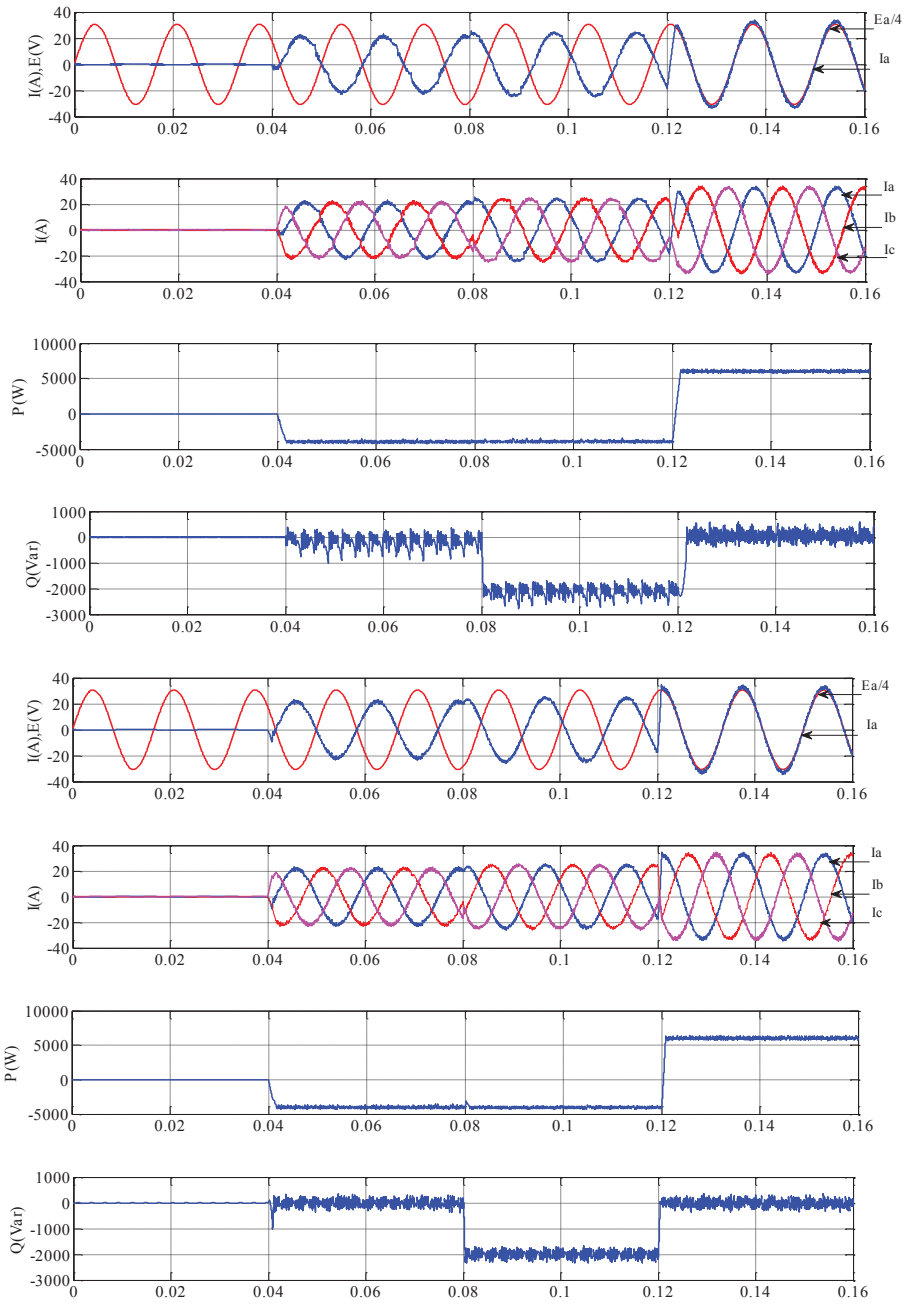

Fig. 3.9 Control performance with bidirectional power flows
(a) Conventional DPC, (b) MPC-based DPC

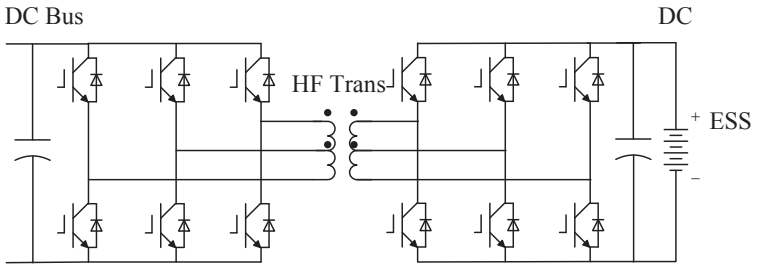

Fig. 3.10 Typical configuration of DC/DC power transmission in proposed microgrids

The high-frequency transformer in the proposed microgrids topology can bring the benefits of smaller size, galvanic isolation, and lower weight. In addition, the high-frequency transformer enables a high output/input voltage ratio and can prevent fault propagation. Therefore, a low-voltage energy system can be used for high DC voltage applications, which is very important for integrating different kinds of ESS. For lower power level DC/DC power conversion, the single-phase DAB can be realized simply by disabling one leg of each bridge to realize higher power conversion efficiency.

Fig. 3.11 presents the simulation results of power flow from the ESS to DC bus through a single phase DAB converter with galvanic isolation using phase-shift control, and then flow to the AC grid through a three-phase full-bridge inverter with MPC based DPC control, the overall system realizes the DC/DC/AC conversion, when the load active power reference changes at 0.5 s from 3000 W to 4000 W, and the referenced reactive power is set to be 0 W. The DC bus voltage is always kept constant at 300 V as shown in Fig. 3.11(e) although the load changes at 0.5 s. By MPC control, the current waveform has lower active and reactive power ripples with unity power factor. Meanwhile, the dynamic response of the whole system maintains good performance.

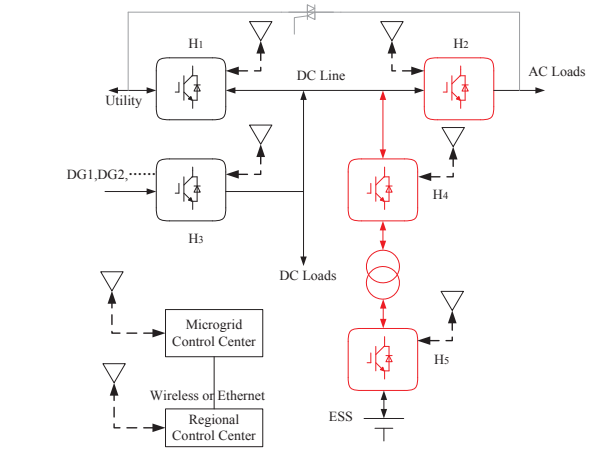

(a)

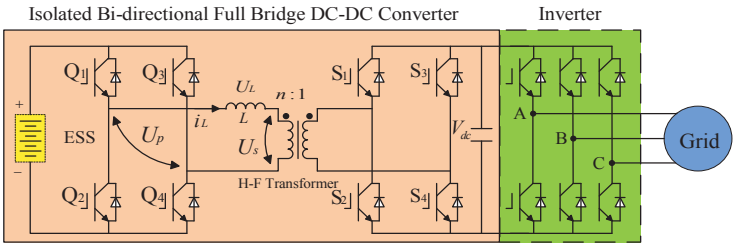

(b)

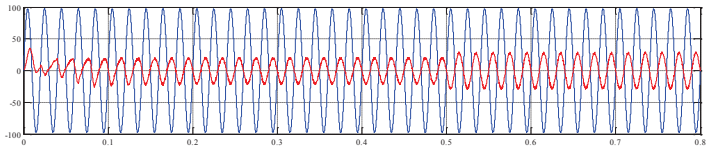

(c)

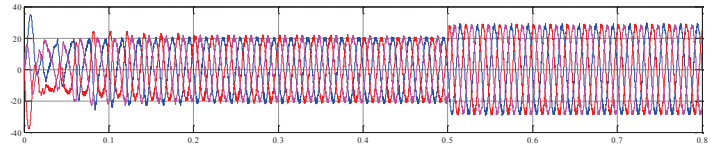

(d)

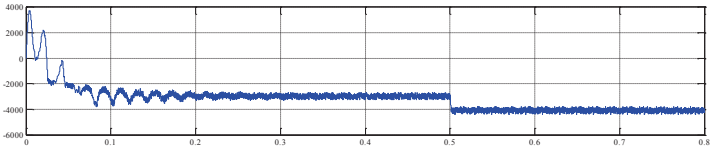

(e)

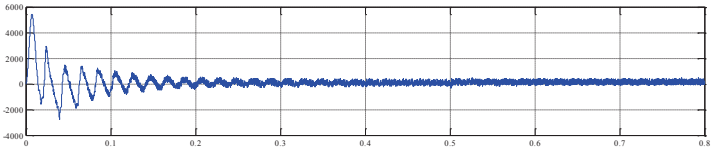

(f)

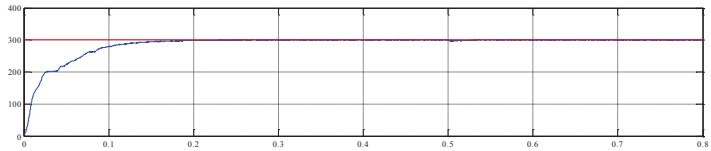

(g)

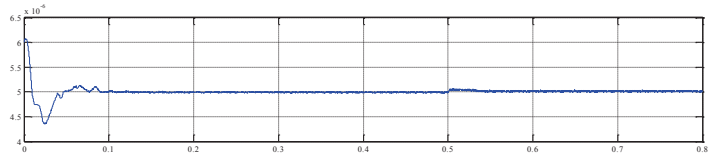

(h)

Fig. 3.11 (a) Series connection for DC/DC/AC conversion (b) Power converter topology (c) Voltage and current of phase A (d) Three phase current (e) Output active power (f) Output reactive power (g) Voltage of DC bus (h) Phase shift ratio of IBDC converter

3.2.4 Control design of microgrid system

In the proposed microgrid, different control modes will lead to different control objectives. To select the control mode for each module, the control design at the system level should be conducted first. The regional control centre operates the individual local controllers of each converter module in the same way that the converter works for different modes, such as the energy storing, power supply and power feed to the grid or load. Recently, the hierarchical control for the microgrid control in both grid-connected and islanded modes has been popular for consideration of different control levels [3.19]. To address the power sharing issues between the ESS, DGs, grid and load in the proposed microgrid, a control structure divided into hierarchical levels would be applied as shown in Fig.3.12.

Firstly, at a higher level, the sensor information from each converter module should be sent to the control centre by wireless communication. The regional control centre would select the operation mode either manually or automatically based on the microgrid operation status, such as the status of DGs, grid, and the ESS, and the load consumption level. Then the controller for each converter module should be regulated according to the determined working status of the module, such as the rectifier/inverter mode for AC/DC conversion, and charging/discharging mode for DC/DC conversion. Finally, at the bottom layer, the control strategies for different modules working in specific status will be implemented and the pulse signals will be generated to drive the switching devices of each module. For example, while the system is working in DG/ESS power-feed mode or utility/microgrid power-supply mode, the current of grid is operated by the grid-connected converter module working in the rectifier/inverter status, and the power factor can be adjusted. While for DG power-generation mode or ESS power-supply mode, the voltage of DC bus is adjusted by the IBDC converter composed by two modules.

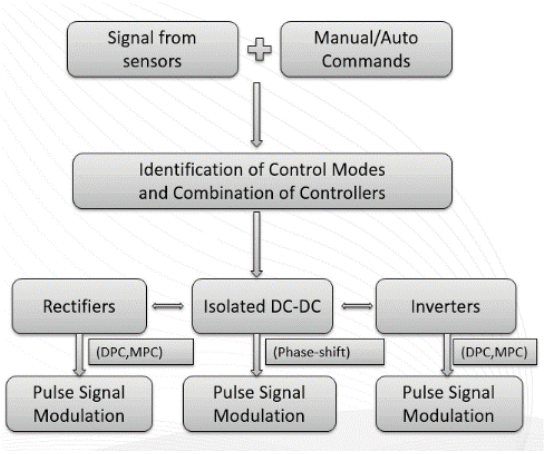

Fig.3.12 Control system design loop for proposed microgrid system

3.3 Challenges of Current PEI in Renewable Energy Systems.

In 2015, the United States experienced persistent growth in total PV capacity with expected new installations reaching almost 9,000 MW [3.20]. Meanwhile, the scheduled capacity additions consist largely of renewable resources while the fossil fuel based generation is anticipating increased reduction globally. The more reliance on variable, weather-dependent, and distributed power sources instead of traditional ones, will introduce more complications and issues in the regulation of distribution systems. With the advent of more and more grid integrations of small-scale DGs, e.g. residential solar PV inverters, utility power systems are experiencing divergent grid modernization with a transition towards a decentralized and distributed grid structure [3.21]. Thus, some issues appear more frequently and could not be ignored as they were previously.

In early times with low-penetration of renewable energy systems, PEI serves basic functions of power conversion and energy feeding, and will be disconnected from the grid during abnormal grid conditions or power outage [3.22]. Since in the past, grid tied PV systems were rare, and the inverter was required to produce a unity power factor and get out of the way quickly if anything bad happened as there were no requirements for ride through in response to grid voltage or frequency excursions. Today, with more and more grid integrations of small-scale distributed energy resources (DERs), such as residential solar PV and wind turbine, the issue of power quality at the interconnection point becomes eminent [3.23], as the frequency and voltage of the power system are

affected when any type of DER is brought on-line or taken off-line. Electricity system must be maintained with a constant frequency and voltage on the system. Since voltage and frequency disturbances beyond a specified range pose a risk to system stability. If a large number of DERs come back online simultaneously after a grid outage or being disconnected due to grid disturbance, another grid disturbance may be triggered. For instance, as seen in California and Hawaii, local power system impact cannot be ignored in areas where PV capacity exceeds 10% of a typical day's peak load. Existing regulatory structures in the US did not adequately address ride through requirements and requirements were written as "must disconnect" not as "must remain connected".

Another example is the "50.2 Hz problem" in Europe. During the first half year of 2011, PV constituted 3.5% of the electricity generation in Germany. With increased penetration of PV, the increase of system frequency has higher risk to trigger disconnection of a large amount of PV capacity from the grid at the same time. If frequency were to rise above the maximum level of existing PV interconnection standards (50.2 Hz), several gigawatts of PV capacity would be disconnected simultaneously. In worst-case, 9 GW of solar capacity might be disconnected simultaneously, while the European grid was able to withstand the instantaneous loss of a maximum of 3 GW of capacity with the design. This issue became known as the "50.2 Hz problem" [3.24]. To solve this problem, in 2012, the German government requested newly-installed PV systems reduce their output or shut down smoothly during high frequency events.

We can get the net demand curve (also called the net load curve) for the utility by using the electricity demand curve minus the PV generation curve [3.24]. The net demand curve means the amount of electricity consumption that need to be supplied by the utility. With increased distributed solar capacity on-line, the net demand curve becomes more shape. This phenomenon is known as the 'duck curve' because of its duck-like shape (see Fig.3.13). With increase of PV generation, the belly of the duck becomes larger since PV generation is higher during noon. Thus there is an increased

need to ramp conventional generating resources down at sunrise and to ramp them back up quickly at sunset.

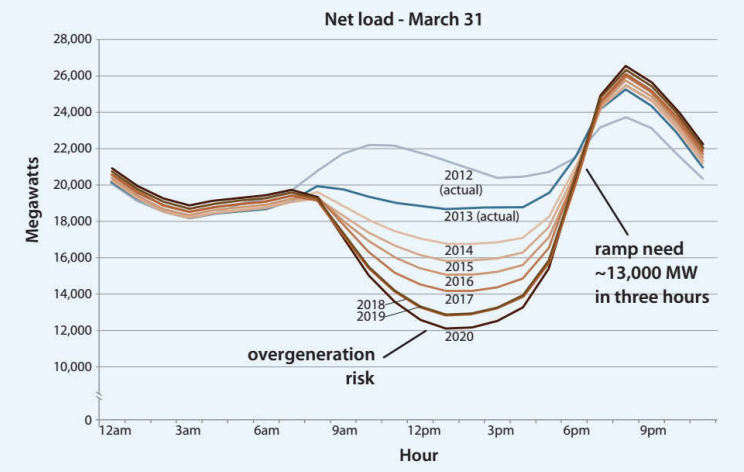

Fig 3.13 An Illustration of California's Current and Estimated Net Load Curve - often referred to as the 'duck curve' [3.24]

To solve these issues, the power industry has an initiative to develop a set of standardized inverter functions to facilitate the deployment of large quantities of distributed generations and to mitigate the frequency issue associated with the parallel tripping of solar PV inverters.

AC/DC bidirectional converters are essential components of power generations, whether at the utility scale or in smaller systems. With DER connected into distribution networks at higher voltage levels, the requirements become more complicated and the PEI are being developed to meet these requirements. Furthermore, autonomous operations of emerging microgrids are seeking new control functionalities of power converters. The development of microgrids requires the PEI in microgrids with more advanced functions with regard to the costs, rescale, power quality and system reliability improvement [3.25]. These issues have brought increasing attention to develop more advanced functions for improving power system performances [3.26-3.28].

Apart from providing advanced functions with revised standards and being more

reliable, more efficient, more compact and less costly, new utility and industry applications have demanded smart features associated with power electronics, especially power inverters, hence the term “smart inverter”. The smart inverter, as it is envisioned, employs both the grid and DER to solve the issue in relation to the growing popularity of DER intelligently [3.24-3.30]. Put simply, the future smart inverter in renewable systems should help prevent the large scale grid disturbance issue immediately after an outage and thereby improve power quality and system stability. The increasing DER integration in the grid provides novel PEI a chance to solve these issues.

3.3.1 Review of the smart inverter

Apart from continuous self-driven motivations of being more reliable, more efficient, more compact and less costly, new utility and industry applications have demanded smart features associated with power electronics, especially power inverters for renewable energy systems, hence the term “smart inverter” or “advanced inverter” has been proposed in recent years, and several forums or conferences have been held to discuss this concept. Smart inverter is developed to provide multi-functions and various ancillary services to improve the stability, reliability, and efficiency of the electric power distribution system. Advanced inverter functions introduced in [3.30] are listed as follows:

- The “riding through” capability in terms of minor disturbances in the frequency or voltage.
- Regulating the real and reactive power output of DERs.
- The ability to prevent the reoccurrence of a grid disturbance immediately after a grid interruption.
- These advanced functions could feasibly respond either autonomously or to the commands sent by system operators.

To capture the technological features of smart inverters, in Dec 2014, modifications to the Electric Tariff Rule 21 were proposed by the Pacific Gas and Electric Company, Southern California Edison Company, and San Diego Gas & Electric Company. After

the latest modifications, “smart inverters” should have the following functions [3.31]:

- Bidirectional power flow for delivering AC power and DC power for different applications, such as PV power to the AC grid or charging the energy storage system from the grid.
- Control of reactive power so as to regulate the voltage at its terminals.
- Ability to deliver power in four quadrants. Either positive or negative real power and reactive power could be regulated flexibly.
- Ability to monitor voltage and frequency at the terminals and react autonomously to alleviate abnormal conditions: to increase active power supply if the frequency is low and to increase reactive power if the voltage is low.
- Through a communication link, to regulate real and reactive power and to charge/discharge storage systems according to commands from the utility operator.

CA rule 21 approves smart inverter functionality. CA rule 21 Phase 1 autonomous behaviors approved in Dec. 2015 includes voltage and frequency ride through, real and reactive power control and return to service behaviours/ramp rate control. Hawaiian Electric Inc. implements mandatory ride through requirements in Jan 2015. CA rule 21 Phase 2 is about bidirectional communication standards for inverters. Still in development, it is moving toward consensus on data models and protocols, including IEC 61850 data model and IEEE 2030.5 protocol.

California Public Utilities Commission has also initiated a smart inverter working group to investigate the new requirements for inverter-based solar PV and energy storage. In January 2014, the Smart Inverter Working Group (SIWG) released “Recommendations for Updating the Technical Requirements for Inverters in Distributed Energy Resources”. The proposal is the result of a one year joint effort of the California Public Utilities Commission (CPUC), California Energy Commission (CEC) and the Smart Inverter Working Group (SIWG) [3.32].

In February 2014, The Electric Power Research Institute (EPRI) published “Common

Functions for Smart Inverters, Version 3" as a recommendation for the future smart inverters' functionalities. The effort began in 2009 with the participation of more than 500 individuals representing inverter manufacturers including system & solution providers, utilities and universities all over the world. A common set of functions and the way that each function should be implemented are defined. Also, it should be noted that the recommendations are about common grid functions for smart inverter only and communication standards are not proposed.

The US Department of Energy has launched an effort to develop advanced PV inverter systems with intelligent, interactive, and dispatchable functions so that solar power can be integrated into grid management. A few IEEE and IEC standards are under revision or new development. IEEE 1547, the recommended interconnection standard for distributed generations below 10 MVA, is currently under full revision. IEEE 2030 and its series are under development to provide a guide for smart grid interoperability of DERs operation in power system. IEC TC57 WG17 is developing the communication standards for integrating DERs into the IEC 61850 body of communication standards. The IEC technical report, IEC/TR 61850-90-7, describes advanced functions for power converters in DER systems, which will be adopted in the new edition of IEC 61850-7-420, the first standard for DER object modeling [3.33].

As reviewed, smart inverter or advanced inverter development so far is still slow and primarily limited to the utility grid with high penetration of renewable energy sources, such as PV and wind turbine. However, the DC/DC conversion in renewable energy systems, which is also quite important for realizing the general applications in microgrids, has not been mentioned. Besides, the smart features of the advanced inverter or smart inverter are vague and have not been comprehensively analyzed, and smart converter applications with multiple functions in proposed microgrids are yet to be investigated. Thus, this chapter proposes a smart converter concept with smart features and modular design which provides inherited advantages for renewable energy systems.

3.4 Proposal of Smart Converter

3.4.1 Smart converter concept

With the extension of advanced smart inverter applications to any type of power electronics based renewable energy systems and distributed generations for both bidirectional AC/DC and DC/DC conversions, the concept of smart converter has been proposed and common and standardized functions of the smart converter become necessary.

Beyond the fundamental functionalities, there are also more smart functions for the converter as shown in Fig. 3.14, which is proposed in this paper as the smart converter concept.

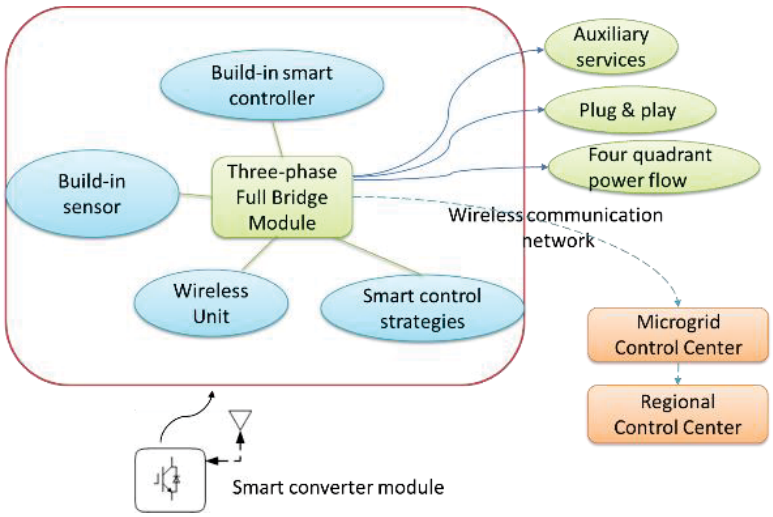

Fig. 3.14 Smart converter for distributed generations

The smart converter should realize real-time communication and monitoring of the microgrid status, such as the ability to receive commands from a microgrid control centre, and the capability to improve the utility power quality and microgrid stability through providing ancillary services. The concept of the smart converter and applications of the smart converter in microgrids is discussed below.

A. Smart converter hardware

Basically, a smart converter is a power electronics-based module with controllable switches to form a three-phase full-bridge for DC to AC conversion or, conversely,

converting AC to DC, so that most of DGs can be integrated into the renewable energy systems.

Through series connection of smart converter modules with additional high-frequency transformer to form a DAB converter as discussed in the literature review, the bidirectional DC/DC conversion can also be realized without redesign of the smart converter module, and thus the multi-function energy conversion can be realized by smart converter modules in renewable energy systems.

For signal collecting, processing and communication, the smart sensor, built-in processor and wireless communication unit are included in the smart converter module, which is shown in Fig. 3.15.

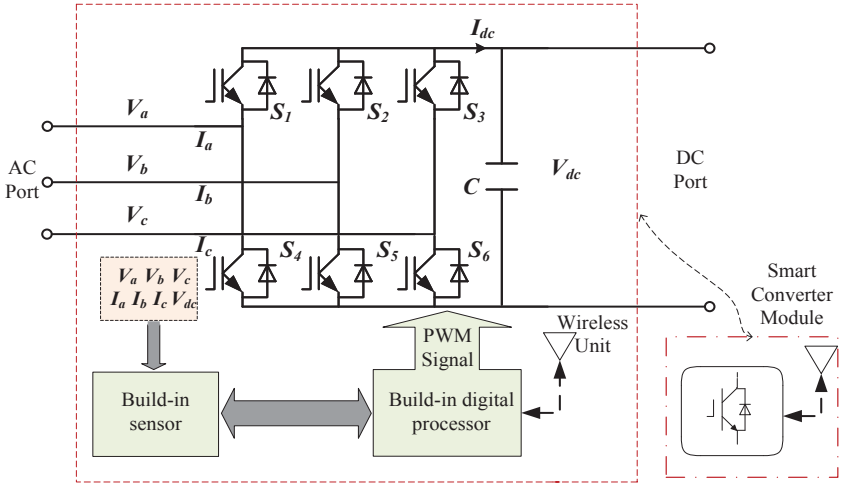

Fig. 3.15 Smart converter hardware

B. Modular structure

Whilst there are lots of benefits DERs can offer, the main factor for a decision of DERs installations largely depends on the initial cost. It is shown that the PEI can occupy up to 40% of the total cost of the renewable energy system [3.34].

To reduce the production and development cost and to meet the demand of different DERs, a standardized converter with modular design is required. Application of modular power electronics is a method to reduce the costs and is becoming a trend of converter development. Since the converter modules can be applied for different scenarios, it is possible for massive production to reduce the costs of testing, design,

installation and maintenance work for various applications [3.34]. It can be realized by designing standardized interfaces of hardware and communication standards. Series or parallel connection of smart converter modules can easily integrate different DERs into a renewable energy system and form a microgird to realize various functions.

With standardized interfaces and modular design, the smart converter can be scaled independently. The renewable energy system would be completely adaptive with size, components, configuration and the control strategy. Therefore, the DER is flexible to be quickly integrated and optimized according to different applications.

The feasibility analysis of applications of the smart converter module in each kind of renewable energy system will be discussed in the following section.

C. Smart control strategies

For smart converter control, multi-functionalities could be realized by advanced control algorithms to adapt to a dynamic environment. Not only hardware modularity but also control modularity in a smart converter should be achieved as an integrated power electronics building block.

For bidirectional AC/DC conversion, advanced control strategies, such as MPC and fuzzy logic control, can be applied with built-in digital signal processors. For DC/DC conversion function, since two smart converter modules can be connected in series with an additional high-frequency transformer to form a dual active bridge converter, the buck-boost mode with various voltage ratio and bidirectional power flow can be realized, which has been verified in the previous section. The advanced control for DC/DC conversion, such as dual-phase-shift control and MPC, could also be applied. For parallel connection or series connection of smart converter modules, the droop control strategy can be employed to realize automatic reactive and active power sharing. With advanced control strategies, the smart converter can realize advanced features as will be discussed in the next section.

3.4.2 Auxiliary functions of the smart converter

From the utility/grid perspective, the smart converter technologies can be used to provide smart features such as frequency/voltage fault ride-through, and reactive power compensation, which can contribute to grid stability, increase system efficiency, and improve power quality.

A. Reactive power compensation

Usually, capacitors are used for reactive power compensation in power systems to eliminate phase differences between current and voltage, decrease line losses, adjust sags and swells in voltage levels, and improve both distribution efficiency and power quality. The geographic proximity to the load or substation and cost are the main factors influencing the efficacy of reactive power control. Thus, DERs are an ideal source for providing reactive power because of their distributed location.

As reactive power compensation needs to be controlled at the system level with load forecasting and restrictions such as power rating and voltage levels, the smart converter, with the inherited advantages of wireless communications and smart control strategies e.g. predictive control, becomes necessary. In remote areas, it is quite difficult to provide traditional, centralized reactive power compensations, and thus the reactive power compensation provided by smart converters would have a better value with inherited advantages.

B. Four quadrant power flow

Four quadrants power flow is an important function for power quality adjustment and power sharing control in microgrids. Power flow in four quadrants, that is, positive/negative reactive power and positive/negative active power, is the basic function of smart converters to provide ancillary services.

For instance, by regulating the active and reactive power of the DER through smart control strategies, smart converters can conveniently help the grid maintain stability by

controlling voltage and frequency within specified limits during an abnormal frequency or voltage instant. The fault ride-through also requires four quadrant power flow.

C. Fault ride through

Ride-through ability requires a grid-connected converter to appropriately respond to a temporary fault or condition in the distribution line to which the converter is connected. As discussed, the conventional PV inverters are designed to monitor a typical fault and immediately disconnect from the line when detecting a fault. Although some inverter standards are revised to allow some ride-through of restricted periods with limited frequency and voltage range, this function is not widely updated in conventional converters [3.35], though in most cases it only requires an update to the software.

In response to a typical condition, the ride through function executes the disconnection action in the situation of the serious permanent fault, while preventing disconnection in the situation of temporary or isolated events [3.35]. This improves grid reliability by continuing to supply power and support the grid

With four quadrant power flow controlled by smart control strategies and built-in sensors, the smart converter has the ability to realize fault ride-through function, which is another main feature of the smart converter. For example, through modulation of the active power supplied, the lower or higher frequency can be achieved, similar to the reactive power and voltage regulation. Voltage and frequency ride-through functions are the most important features needed to improve grid stability. These functions can be controlled remotely with the smart converter through standard communication codes and interface.

D. Standard communication & Plug and play feature

As previously mentioned, there are significant benefits if establishing standard communications among DER converters, the regional control centre, grid operators, and regional transmission organizations as well as the residential microgrid control centre. Smart converters should be able to receive commands from the control centres to

improve the power quality, and respond appropriately to market pricing signals and instructions of emergency processing.

For renewable energy systems, the standard communication interface aids the design of the smart converter with flexible, modular, easy-to-use, multi-functional blocks, which can alleviate the difficulty of DER and energy storage system integration. If each side of the converter interface supports device self-identification and system resources assignment, the plug-and-play function is reliable for smart converter applications in microgrids.

3.4.3Application of smart converter for various scenarios in microgrids

It is feasible to apply smart converter modules as the same power electronic components in renewable energy systems, and the application for different DERs is illustrated in Fig.3.16 [3.36]. For renewable energy integration, the PEI with modular design is becoming a trend. The efficient and popular power electronic topology for PV and other renewable energy systems is the DC/AC inverter cascaded with isolated DC/DC converter. The wind turbine and micro-turbine systems generate AC output variable frequency which should be converted into power frequency for grid-connection. In addition, the back-to-back converter is the main method to deliver the output power from wind turbine and micro-turbine systems. The smart converter with modular design allows for a reduction in cost due to the large application number of smart converter modules. It can be concluded that the smart converter could be installed for various DER applications with quite small modifications, as illustrated in Fig. 3.16.

To well connect each module in a complex renewable energy system, standardized interfaces of hardware and software design of the smart converter would allow reaction to linked neighbour modules and the seamless sharing of information with each other.

It is predicted that flexible and modular power converters and standardized communication and controls will provide lots of advantages in hardware and software for the integration of renewable energy systems. The wide applications of the smart converter modules maintain the flexibility of the microgrids system design, which is

comparable to the customized design strategies. Thus, modular, flexible, reliable and low cost DER integration can be implemented with less effort in the design, updates and scalability. Furthermore, smart converter based microgrid systems can be easily modified, rescaled and expanded with the modular design, such as the application in the proposed modular microgrid.

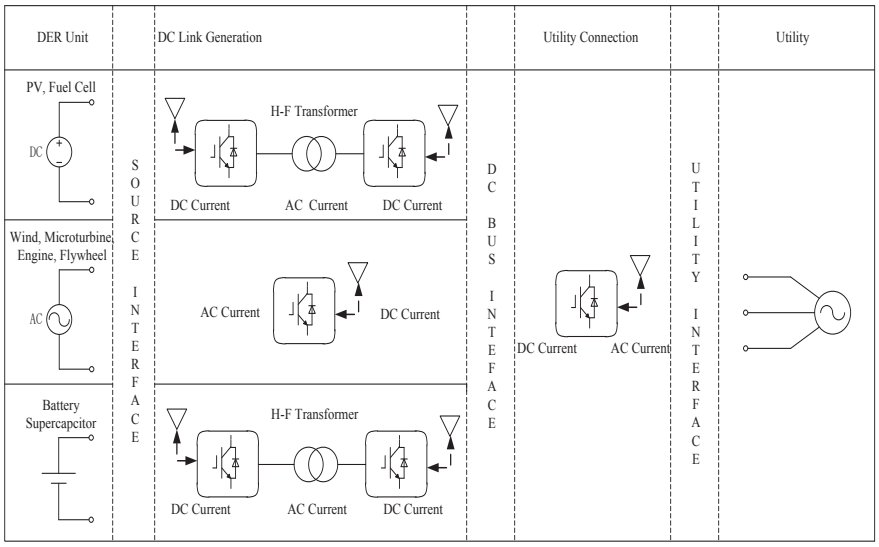

Fig.3.16 Smart converter module for various DERs

3.4.4 Conclusion of discussion

As can be seen, the three-phase two-level full-bridge converter has a wide application in microgrids or individual renewable energy systems. Regardless whether the conventional AC/DC converter, smart inverter or proposed smart converter is employed, the control strategies are of vital importance in providing advanced functions and ancillary services in renewable energy systems. Thus, for better control performance, the following chapter will focus on control strategies of the three-phase two-level full-bridge converter and comprehensive research with advanced controls with be conducted.

3.5 Summary of the Chapter

This chapter proposes a multi-functional microgrid topology with modular design and wireless communication ability. The operation modes of proposed microgrids are analysed in detail, and the control strategies of power modules and systems are introduced. With the modular design and advanced control strategies, it can readily expand its capacity with identical converter modules, with reduced cost and increased system redundancy. In addition, multiple microgrids with modular topology can form a group of smart microgrids in the future. For the three-phase full-bridge identical converter module, which is the basic PEI module in the proposed microgrids, this chapter discussed the challenges of the current converter for renewable energy system applications and reviewed the advanced smart inverter in renewable energy systems. Then, the smart converter concept has been proposed and comprehensively analysed. Basically, it is a three-phase full-bridge converter module with build-in smart controller and sensors as well as wireless communication units, which is mainly applied as the PEI modules in renewable energy systems. It is designed to provide ancillary services such as reactive power compensation, fault ride-through, and plug-play ability. The feasibility of smart converter modular applications in various renewable energy systems is analysed. Overall, it has great advantages for applications in renewable energy systems or applied as a basic PEI module in proposed microgrids, thus control strategies of three-phase full-bridge converter is worth comprehensive research.

Therefore, the following chapter will focus on control strategies of three-phase two-level full-bridge converter and comprehensive research with advanced controls with be conducted.

REFERENCES

[3.1] A. F. Zobaa, and C. Cecati, “A comprehensive review on distributed power generation,” in *Proc. Int. Symp. on Power Electron., Electr. Drives, Automat. and Motion*, Jun. 11-13, 2008.

[3.2] H. Farhangi, “The path of the smart grid,” *IEEE Power and Energy Mag.*, vol. 8, no. 1, pp. 18-28, Jan./Feb. 2010.

[3.3] H. Zhou, T. Bhattacharya, D. Tran, T. S. T. Siew, and A. M. Khambadkone, "Composite energy storage system involving battery and ultracapacitor with dynamic energy management in microgrid applications," Power Electronics, IEEE Transactions on, vol. 26, pp. 923-930, 2011.

[3.4] L. Roggia, L. Schuch, J. E. Baggio, etc., “Integrated full-bridge-forward dc-dc converter for a residential microgrid application,” IEEE Trans. Power Electronics., vol. 28, no. 4, pp. 1728-1740, April 2013.

[3.5] B. Zhao, Q. Song, W. Liu, and Y. Xiao, “Next-generation multi- functional modular intelligent ups system for smart grid,” *Industrial Electronics, IEEE Transactions on*, vol. 60, no. 9, pp. 3602–3618, Sept 2013.

[3.6] T. Strasser, F. Andren, J. Kathan, C. Cecati, C. Buccella, P. Siano*, et al.*, "A Review of Architectures and Concepts for Intelligence in Future Electric Energy Systems," *Industrial Electronics, IEEE Transactions on,* vol. 62(4), pp. 2424-2438, 2015.

[3.7] J. J. Justo, F. Mwasilu, J. Lee, and J-W. Jung, "AC microgrids versus DC-microgrids with distributed energy resources: A review." *Renewable and Sustainable Energy Reviews*, vol. 24, pp. 387-405, Aug. 2013.

[3.8] K. Sun, L. Zhang, Y. Xing, and J. M. Guerrero, “A distributed control strategy based on DC bus signaling for modular photovoltaic generation systems with battery energy storage”, *IEEE Trans. Power Electron.*, vol. 26, no. 10, pp. 3032–3045, Oct. 2011.

[3.9] Jackson John Justo, “AC-microgrids versus DC-microgrids with distributed energy resources: A review,” *Renewable and Sustainable Energy Reviews* pp.387–405, 2013.

[3.10] N.W.A. Lidula, A.D. Rajapakse, “Microgrids research: A review of experimental microgrids and test systems,” *Renewable and Sustainable Energy Reviews* pp.186–202, 2011.

[3.11] S. Chakraborty, B. Kramer and B. Kroposki, "A review of power electronics interfaces for distributed energy systems toward achieving low-cost modular design", *Renewable and Sustainable Energy Reviews*, vol. 13, no. 9, pp. 2323-2335, 2009.

[3.12] Y. Li, D. M. Vilathgamuwa, and P. C. Loh, "Design, analysis, and real-time testing of a controller for multibus microgrid system," *IEEE Trans. Power. Electronics*, vol. 19, no. 5, pp. 1195-1204, Sep. 2004.

[3.13] K. D. Brabandere, B. Bolsens, J. V. Keybus, A. Woyte, J. Driesen, and R. Belmans, "A voltage and frequency droop control method for parallel inverters," IEEE Trans. Power. Electron., vol. 22, no. 4, pp. 1107-1115, Jul. 2007.

[3.14] M. C. Chandorkar, D. M. Divan, and R. Adapa, "Control of parallel connected inverters in standalone ac supply systems," IEEE Trans. Ind. Appl., vol. 29, no. 1, pp. 136-143, Jan./Feb. 1993.

[3.15] B. Zhao, Q. Yu and W. Sun, "Extended-phase-shift control of isolated bidirectional DC-DC converter for power distribution in microgrid," IEEE Trans. Power Electronics, vol. 27, pp. 4667-4680, Nov. 2012.

[3.16] L. Hassaine, E. OLias, J. Quintero, and V. Salas, "Overview of power inverter topologies and control structures for grid connected photovoltaic systems," *Renewable and Sustainable Energy Reviews*, vol. 30, pp. 796–807, Feb. 2014.

[3.17] X. Shi, J. Zhu, L. Li, et al. "Model predictive control of PWM AC/DC converters for Bi-directional power flow control in microgrids". *Power Engineering Conference (AUPEC)*, 2015 Australasian Universities. IEEE, 2015: 1-4.

[3.18] X. Shi, J. Jiang, and X. Guo, "An efficiency-optimized isolated bidirectional dc-dc converter with extended power ranger for energy storage systems in microgrids," *Energy*, vol. 6, pp. 27–44, 2012

[3.19]. J. M. Guerrero, P. C. Loh, M. Chandorkar, T.-L. Lee, "Advanced control architectures for intelligent microgrids—Part I: Decentralized and hierarchical control", *IEEE Trans. Ind. Electron.*, vol. 60, no. 4, pp. 1254-1262, Apr. 2013.

[3.20] *Solar Industry Data*. Available at: www.seia.org/research-resources/solarindustry-data, accessed in Dec. 2014

[3.21] F. Wang, J. Duarte, M. Hendrix, "Grid-interfacing converter systems with enhanced voltage quality for microgrid application;concept and implementation", *IEEE Trans. Power Electron.*, vol. 26, no. 12, pp. 3501-3513, Dec. 2011.

[3.22] S. X. Carvajal, J. Serrano, and S. Arango, "Colombian ancillary services and international connections: Current weaknesses and policy challenges," *Energy Policy*, vol. 52, pp. 770–778, Jan. 2013.

[3.23] P. Komor, A. Hoke, and R. Kempener, "Seven Steps to a Smarter Grid," *The Electricity Journal*, vol. 27, no. 2, pp. 61–67, Mar. 2014.

[3.24] Time P O. Advanced Inverter Functions To Support High Levels of Distributed Solar[J]. Accessed Feb. 2017: http://www.oregonrenewables.com/Publications/NREL-smart-inverters-62612.PDF

[3.25] L. Hassaine, E. OLias, J. Quintero, and V. Salas, "Overview of power inverter topologies and control structures for grid connected photovoltaic systems," *Renewable and Sustainable Energy Reviews*, vol. 30, pp. 796–807, Feb. 2014.

[3.26] J. Li and K. Corzine, "Development of grid-connected inverters for micro-grid",*Power Systems Conference (PSC), 2014 Clemson University. IEEE*, pp. 1-6

[3.27] R. I. Bojoi, L. R. Limongi, D. Roiu, and A. Tenconi, "Enhanced power quality control strategy for single-phase inverters in distributed generation systems," *IEEE Trans. Power Electron.*, vol. 26, no. 3, pp. 798–806, Mar. 2011.

[3.28] Z. Ming, L. Ximei, and P. Lilin, "The ancillary services in China: An overview and key issues," *Renewable and Sustainable Energy Reviews*, vol. 36, pp. 83–90, Aug. 2014.

[3.29] J. Rocabert, A. Luna, F. Blaabjerg, and P. Rodriguez, "Control of power converters in AC microgrids," *IEEE Trans. Power Electron*., vol. 27, no. 11, pp. 4734–4749, 2012.

[3.30] S Appert: "Advanced inverter technologies report", California public utilities commission, 18 January 2013, http://www.cpuc.ca.gov/WorkArea/DownloadAsset.aspx?id=3342

[3.31] California Public Utilities Commission (CPUC). (2014). "Interim Decision Adopting Revisions to Electric Tariff Rule 21 for Pacific Gas and Electric Company, Southern California Edison Company, and San Diego Gas & Electric Company to Require "Smart" Inverters." Decision 14-12-035. San Francisco, CA: California Public Utilities Commission. Accessed Feb. 2016: http://docs.cpuc.ca.gov/PublishedDocs/Published/G000/M143/K827/143827879.PDF

[3.32] Smart Inverter Working Group (SIWG), "Recommendations for Updating the Technical Requirements for Inverters in Distributed Energy Resources," SIWG Rule 21 Recommendations for the California Public Utilities Commission (CPUC). Jan 2014.

[3.33] Y. Xue and et al., “Towards next generation photovoltaic inverters,” in Proc. 2011 IEEE Energy Conversion Congress and Exposition (ECCE), Phoenix, Arizona, USA, Sept. 17-22, 2011, pp. 2467-2474.

[3.34] S. Chakraborty, B. Kramer and B. Kroposki, "A review of power electronics interfaces for distributed energy systems toward achieving low-cost modular design", *Renewable and Sustainable Energy Reviews*, vol. 13, no. 9, pp. 2323-2335, 2009.

[3.35] W. Zhang et al., “Survey on fault-tolerant techniques for power electronic converters,” *IEEE Trans. Power Electron.*, vol. 29, no. 12, pp. 6319-6331, Dec. 2014.

[3.36] W. Kramer, S. Chakraborty, B. Kroposki, H. Thomas, "Advanced power electronic interfaces for distributed energy systems—I: System and topologies", *National Renewable Energy Laboratory Golden CO Tech. Rep. NREL/TP-58142672*, Mar. 2008

Chapter 4

MULTI-FUNCTIONAL MODEL PREDICTIVE CONTROL OF THREE-PHASE FULL-BRIDGE AC/DC CONVERTER

4.1 Introduction

Nowadays, renewable energy sources (RES) are important to satisfy the growing energy demand and reduce reliance on fossil fuels [4.1]. The three-phase full-bridge converter is a popular option for integration of renewable energy sources [4.2], active power filters, electric drives and energy storage systems (ESS) due to its advantages such as four-quadrant power flow control, natural power factor correction, flexible DC-link voltage adjustment, and relatively low DC filter capacitance when compared with the uncontrolled AC/DC converters [4.3]-[4.5]. The fast development of renewable energy systems also leads to more stringent requirements of AC/DC converters and more advanced control strategies that can deliver better system reliability and power quality [4.6].

The direct power control (DPC) and voltage-oriented control (VOC) are two typical control methods [4.7]-[4.12]. As reviewed, the VOC controls has good dynamic response and stability in steady-state, but the inner loop current controller has a large influence on system performance [4.13]. The DPC can control the active and reactive powers directly by selecting an appropriate space voltage vector from the preset switching table according to the instantaneous errors between the reference and instantaneous values of active and reactive powers, and the voltage vector position [4.14]. This control has a simple control algorithm and does not need an internal controller while retaining good dynamic performance. However, the control accuracy cannot be guaranteed. To improve the performance of the conventional switching table, the improved switching table based DPC (STDPC) has been proposed with a revised

switching table. The improved STDPC in [4.15]-[4.16] can achieve lower current harmonic distortion, and the switching actions are less compared with the conventional switching table. However, to achieve acceptable performance, a high sampling frequency is required.

The model predictive control (MPC) is a flexible control method that allows easy inclusion of system nonlinearities and constraints [4.17]-[4.28]. In the MPC based DPC (MPCDPC) scheme, the system model and cost function of errors between the reference and measured active and reactive powers are evaluated for a finite set of voltage space vectors, and the voltage space vector that minimizes the cost function is selected for actuation [4.29]-[4.33]. This approach is more accurate compared with the STDPC. The control objectives of cost function can vary relatively according to different applications. For instance, in the conventional MPCDPC, the active and reactive powers are simultaneously controlled with a single cost function, but it has a one-step-delay arising from computation and communication processes in the digital implementation [4.34]-[4.36]. The concept of multi-objective control was proposed to compensate the one-step-delay while maintaining the system stability and reducing the average switching frequency [4.37]. This approach, however, only contributes to improving the system steady-state performance. During the transient state, if one control objective experiences a large change in the power reference value, relatively more weight is put on that changed objective due to parametric coupling of the cost function. Afterwards, the voltage vector that is more likely to adjust this objective to the reference value would be selected based on the cost function. This influences the control of the other control target since these two control objectives could not be completely decoupled according to the converter model. This deteriorates the dynamic performance of active power and reactive power control, and also causes the output voltage waveform distoration, especially when using the cost function consisting of square terms [4.38]-[4.40]. This mutual influence issue exists in most MPC methods and the problem is more likely to occur in the systems with significant change of power usage. This may impose more stress on load system and decrease the efficiency and operational

performance of the system [4.41]. A modulated MPC scheme with vector duty cycle calculation was proposed in [4.41] to eliminate this mutual influence. However, it is not designed for the conventional single vector based MPC method. In addition, the steady-state performance was not considered, and the proposed method is not a general approach for eliminating the mutual influence.

In order to solve the aforementioned issues, this chapter proposed an advanced multi-functional MPC to improve both the dynamic and steady state performances simultaneously by adding a proposed mutual influence elimination term in the cost function while considering the dynamic and steady state performance simultaneously in the novel cost function. Not only can the novel control improve the steady-state performance by one-step-delay compensation while improving the corresponding system deterioration issue such as switching frequency increment, but it can also improve the dynamic performance by eliminating the mutual influence between the active and reactive powers.

4.2. Three-phase Full-bridge AC/DC Converter Control

4.2.1 Mathematical model of three-phase full-bridge converter.

Fig. 4.1 illustrates the topology of a three-phase AC/DC converter that can be operated for bidirectional power conversion. The three-phase full-bridge unit is connected to the AC side via three inductors L and resistors R. At the DC side, a DC load or DC bus is connected to the bridge in parallel to a capacitor C, where e_a, e_b, and e_c are the three-phase AC source voltages; V_a, V_b, and V_c the AC terminal voltages of the three-phase bridge; and I_a, I_b, and I_c the three-phase currents. Fig. 4.2 shows the voltage space vectors.

In the stationary reference frame, the AC source voltage vector and current vector in the αβ-coordinate system can be calculated by the following transformation:

$$e_{\alpha\beta} = \begin{bmatrix} e_\alpha \\ e_\beta \end{bmatrix} = \frac{2}{3}\begin{bmatrix} 1 & -1/2 & -1/2 \\ 0 & \sqrt{3}/2 & -\sqrt{3}/2 \end{bmatrix}\begin{bmatrix} e_a \\ e_b \\ e_c \end{bmatrix} \tag{4.1}$$

$$I_{\alpha\beta}=\begin{bmatrix} I_\alpha \\ I_\beta \end{bmatrix}=\frac{2}{3}\begin{bmatrix} 1 & -1/2 & -1/2 \\ 0 & \sqrt{3}/2 & -\sqrt{3}/2 \end{bmatrix}\begin{bmatrix} I_a \\ I_b \\ I_c \end{bmatrix} \tag{4.2}$$

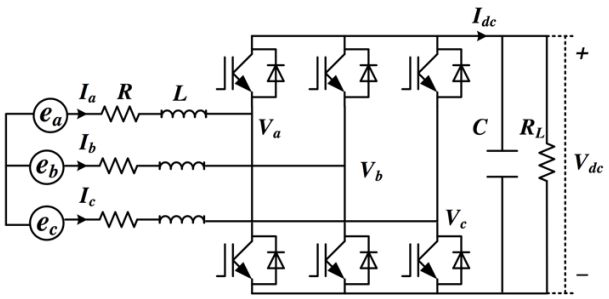

Fig. 4.1 AC/DC three-phase converter structure

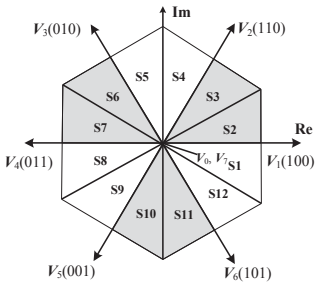

Fig. 4.2 Voltage space vectors

In a balanced three-phase system, the line currents can be calculated in stationary reference frame as follows:

$$e_{\alpha\beta}=L\frac{dI_{a\beta}}{dt}+RI_{a\beta}+V_{\alpha\beta} \tag{4.3}$$

where $\boldsymbol{e}_{\alpha\beta}$, $\boldsymbol{V}_{\alpha\beta}$, $\boldsymbol{I}_{\alpha\beta}$ are the input source voltage vector, the three-phase converter input voltage vector and the line current vector, respectively.

For each switching state and the corresponding voltage space vector, $V_{i\alpha}$ and $V_{i\beta}$ are calculated as follows,

$$\begin{bmatrix} V_{i\alpha} \\ V_{i\beta} \end{bmatrix}=\frac{2}{3}V_{dc}\begin{bmatrix} S_{ia}-\frac{1}{2}(S_{ib}+S_{ic}) \\ \frac{\sqrt{3}}{2}(S_{ib}-S_{ic}) \end{bmatrix} \tag{4.4}$$

where S_{ia} , S_{ib} and S_{ic} are the switching states of the converter.

For sinusoidal and balanced three phase line voltage,

$$\overline{e} = e_\alpha + je_\beta = |\overline{e}|\, e^{j\omega t} \tag{4.5}$$

From (4.1), the following expression can be deduced as

$$\frac{d}{dt}\begin{bmatrix} e_\alpha \\ e_\beta \end{bmatrix} = \omega \cdot \begin{bmatrix} -e_\beta \\ e_\alpha \end{bmatrix} \tag{4.6}$$

TABLE 4.1 Converter switching states and corresponding output voltage vectors

V_i	S_{ia}	S_{ib}	S_{ic}	$V_{i\alpha}$	$V_{i\beta}$
$\boldsymbol{V_0}$	0	0	0	0	0
$\boldsymbol{V_1}$	1	0	0	$2V_{dc}/3$	0
$\boldsymbol{V_2}$	1	1	0	$V_{dc}/3$	$V_{dc}/\sqrt{3}$
$\boldsymbol{V_3}$	0	1	0	$-V_{dc}/3$	$V_{dc}/\sqrt{3}$
$\boldsymbol{V_4}$	0	1	1	$-2V_{dc}/3$	0
$\boldsymbol{V_5}$	0	0	1	$-V_{dc}/3$	$-V_{dc}/\sqrt{3}$
$\boldsymbol{V_6}$	1	0	1	$V_{dc}/3$	$-V_{dc}/\sqrt{3}$
$\boldsymbol{V_7}$	1	1	1	0	0

The exchange of active and reactive powers at the grid side can be derived as

$$\begin{bmatrix} P \\ Q \end{bmatrix} = \frac{3}{2}\begin{bmatrix} e_\alpha & e_\beta \\ e_\beta & -e_\alpha \end{bmatrix}\begin{bmatrix} I_\alpha \\ I_\beta \end{bmatrix} \tag{4.7}$$

4.2.2 Switching table based direct power control.

The conventional switching table based DPC (STDPC) scheme is based on the instantaneous active and reactive powers to form the control loops, as described in [4.9]. The voltage vector of the pulse width modulation (PWM) rectifier is chosen from a preset switching table. It is formulated according to the digitized signals *dp* and *dq* from the tracking errors between the referenced and estimated values of active and reactive power, respectively, which are supplied according to the fixed band non-linear hysteresis comparators and the power source voltage vector location, θn, in the α–β

plane associated to a preset switching table. The block diagram of STDPC-based power regulation is shown in Fig. 4.3, while for the DC-link voltage control, usually a PI-based external control loop is applied to generate the active power reference.

The control strategy is implemented in the stationary reference frame without the requirement of a coordinate transformation. It is also popular and quite easy to implement and STDPC is often regarded as a benchmark to which new strategies are compared. The main disadvantages are the variable switching frequency and high power ripples, and thus, a high sampling frequency is required to achieve a satisfactory performance. The conventional switching table is presented in Table 4.2.

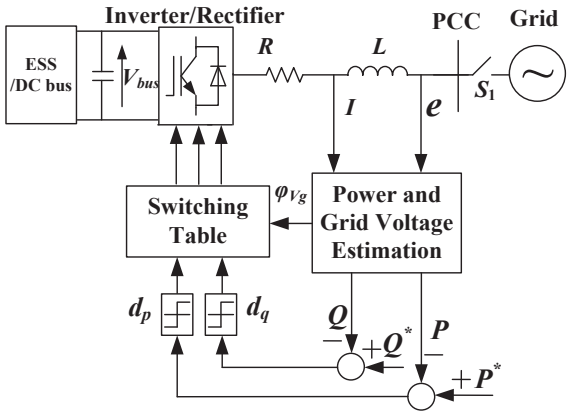

Fig. 4.3 Block diagram of conventional DPC-based power regulation

TABLE 4.2 Conventional switching table of STDPC

d_P	d_Q	θ_1	θ_2	θ_3	θ_4	θ_5	θ_6	θ_7	θ_8	θ_9	θ_{10}	θ_{11}	θ_{12}
1	0	V_6	V_7	V_1	V_0	V_2	V_7	V_3	V_0	V_4	V_7	V_5	V_0
	1	V_7	V_7	V_0	V_0	V_7	V_7	V_0	V_0	V_7	V_7	V_0	V_0
0	0	V_6	V_1	V_1	V_2	V_2	V_3	V_3	V_4	V_4	V_5	V_5	V_6
	1	V_1	V_2	V_2	V_3	V_3	V_4	V_5	V_5	V_5	V_6	V_6	V_1

TABLE 4.3 Improved switching table of STDPC [4.15]

d_P	d_Q	θ_1	θ_2	θ_3	θ_4	θ_5	θ_6	θ_7	θ_8	θ_9	θ_{10}	θ_{11}	θ_{12}
1	0	V_5	V_6	V_6	V_1	V_1	V_2	V_2	V_3	V_3	V_4	V_4	V_5
	1	V_3	V_4	V_4	V_5	V_5	V_6	V_6	V_1	V_1	V_2	V_2	V_3
0	0	V_6	V_1	V_1	V_2	V_2	V_3	V_3	V_4	V_4	V_5	V_5	V_6
	1	V_1	V_2	V_2	V_3	V_3	V_4	V_4	V_5	V_5	V_6	V_6	V_1

It should be noted that there are several other improved switching table proposed to improve the performance. For instance, switching tables like Table 4.3 and Table 4.4 are proposed with the novel switching table to improve the quality of line current and dynamic performances.

TABLE 4.4 Improved switching table of STDPC [4.16]

d_P	d_Q	θ_1	θ_2	θ_3	θ_4	θ_5	θ_6	θ_7	θ_8	θ_9	θ_{10}	θ_{11}	θ_{12}
1	0	V_5	V_6	V_6	V_1	V_1	V_2	V_2	V_3	V_3	V_4	V_4	V_5
	1	V_7	V_7	V_0	V_0	V_7	V_7	V_0	V_0	V_7	V_7	V_0	V_0
0	0	V_6	V_1	V_1	V_2	V_2	V_3	V_3	V_4	V_4	V_5	V_5	V_6
	1	V_1	V_2	V_2	V_3	V_3	V_4	V_4	V_5	V_5	V_6	V_6	V_1

In this chapter, the generally used improved switching Table 4.3 is selected for further discussion and performance comparison.

4.2.3 SVM based direct power control

The main disadvantage of STDPC is variable switching frequency and high power ripples. With the space vector modulation (SVM) approach based DPC (SVMDPC), the average voltage vector of the converter is generated by integrating linear voltage vectors in a fixed period which contributes to constant switching frequency.

As illustrated in Fig.4.4(a), without using the hysteresis comparators and a switching table as STDPC, the conventional SVMDPC (CSVMDPC) inputs the tracking errors of the active and reactive powers into two separate PI regulators. The PI regulators are used to transform the input tracking errors to V_α and V_β in stationary reference frame, which are further delivered to the SVM module for switching signals generation. Since it requires two PI regulators to generate a reference value of V_α and V_β, the transient and steady-state performances are highly sensitive to the PI control parameters. Much tuning effort is anticipated to ensure the system stability and steady-state performance. Also, the coordinate transformation complicates the system control design and results in

larger computing efforts. The improved SVM based DPC (ISVMDPC) as shown in Fig. 4.4(b) and other kinds of fixed switching frequency approach will be fully researched and compared in another chapter.

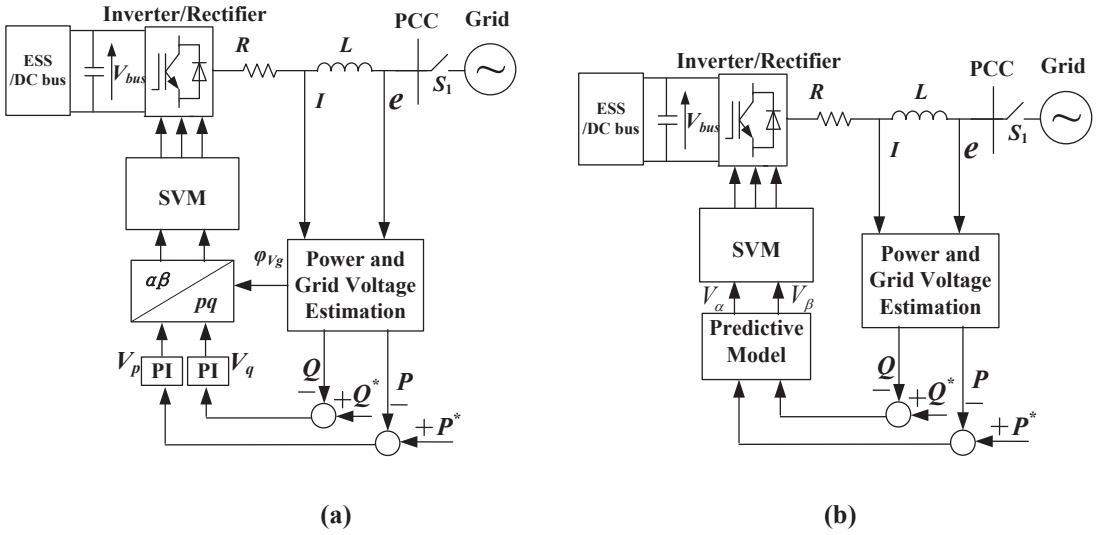

Fig. 4.4. Block diagram of SVMDPC-based power regulation (a) CSVMDPC (b) ISVMDPC

4.2.4 Model predictive based DPC

The predictive control is a popular for power electronic converters due to its robustness and performances. Another advantage of the predictive control is that it is easy to include various constraints to improve the specific performance.

The MPCDPC is proposed based on the discrete system model, which is used to predict the change of power behaviour at the time instant (k+1) for different voltage vectors. Then, it applies the voltage vector that minimizes the cost function to the converter. Fig. 4.5 illustrates the block diagram of MPC.

The differential equation of active and reactive powers can be derived from (4.7) as

$$\frac{d}{dt}\begin{bmatrix} P \\ Q \end{bmatrix} = \frac{3}{2}\left(I_\alpha \frac{d}{dt}\begin{bmatrix} e_\alpha \\ e_\beta \end{bmatrix} + \frac{dI_\alpha}{dt}\begin{bmatrix} e_\alpha \\ e_\beta \end{bmatrix} + I_\beta \frac{d}{dt}\begin{bmatrix} e_\beta \\ -e_\alpha \end{bmatrix} + \frac{dI_\beta}{dt}\begin{bmatrix} e_\beta \\ -e_\alpha \end{bmatrix} \right) \tag{4.8}$$

The instantaneous active and reactive powers can be derived by substituting (4.3) and (4.6) into (4.8) as

$$\frac{d}{dt}\begin{bmatrix} P_i \\ Q_i \end{bmatrix} = -\frac{R}{L}\begin{bmatrix} P_i \\ Q_i \end{bmatrix} + \omega\begin{bmatrix} -Q_i \\ P_i \end{bmatrix} + \frac{3}{2L}\begin{bmatrix} \left(|\bar{e}|^2 - \mathrm{Re}\left(\bar{e}\bar{V}_i^*\right)\right) \\ -\mathrm{Im}\left(\bar{e}\bar{V}_i^*\right) \end{bmatrix} \tag{4.9}$$

where $\bar{V}_i$ represents the i-th voltage space vector, and P_i and Q_i the corresponding active and reactive power, respectively.

If assuming that the tracking error of the DC-bus voltage is constant over one sampling period, the instantaneous active power at the next sampling instant (k+1) can be predicted using a linear extrapolation. Thus, at the end of sampling period T_s, the predictive P and Q for each converter switching state can be expressed as:

$$\begin{bmatrix} P_i^{k+1} \\ Q_i^{k+1} \end{bmatrix} = T_s\left(-\frac{R}{L}\begin{bmatrix} P_i^k \\ Q_i^k \end{bmatrix} + \omega\begin{bmatrix} -Q_i^k \\ P_i^k \end{bmatrix} + \frac{3}{2L}\begin{bmatrix} \left(|\bar{e}|^2 - \mathrm{Re}\left(\bar{e}\bar{V}_i^*\right)\right) \\ -\mathrm{Im}\left(\bar{e}\bar{V}_i^*\right) \end{bmatrix}\right) + \begin{bmatrix} P_i^k \\ Q_i^k \end{bmatrix} \tag{4.10}$$

The MPC controller can compare the active and reactive powers of each converter switching state, and choose the one leading to the least value of the cost function as defined in

$$J_i = (P^* - P_i^{k+1})^2 + (Q^* - Q_i^{k+1})^2 \tag{4.11}$$

where i ranging from 0 to 7 indicates the voltage vectors.

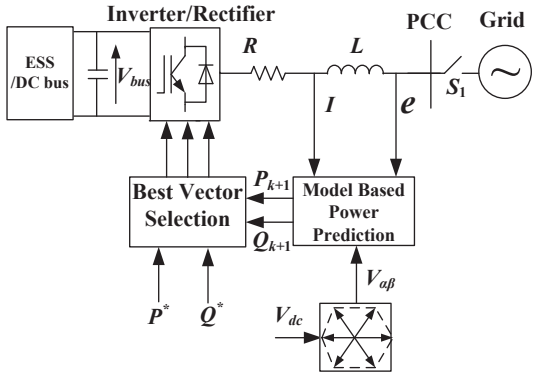

Fig. 4.5 Block diagram of MPC-based power regulation

It should be noted that there are several different forms of cost functions. The two main forms are the sum of the square and absolute values from the error of the active

and reactive powers, which is employed to select the best vector among the 8 vectors to implement. When using the cost function with absolute value form, it has balanced control due to the relatively smaller mutual interference between the two control objectives. However, it sacrifices the dynamic performance with longer response time. While for the cost function with square terms, though the dynamics is better, the mutual influence occurs which cannot be ignored when there is a step change of one control objective.

4.3 Proposal of Multi-functional MPC

The conventional MPCDPC of three-phase AC/DC converters usually suffers from parametric coupling between active and reactive powers. A change of the reference of either the active or reactive power will affect the response of the other, leading to poor dynamic response. The steady-state performance of the conventional MPC is affected by one-step-delay arising from computation and communication processes in the digital implementation, which also should be considered simultaneously. This chapter proposes an advanced multi-functional MPC for three-phase full-bridge AC/DC converters. With proposed control method, both the steady and dynamic performances of the converter can be improved simultaneously. It has multiple functions such as one-step-delay compensation, power ripple improvement, switching frequency reduction for steady state performance improvement, and mutual influence elimination for dynamic performance improvement. The simulation and experimental results are obtained to verify the advancement of the proposed control in comparison with other control methods.

4.3.1 Steady state performance improvement

The conventional MPC inherits two main disadvantages which may influence the system dynamic and steady state performances. The first one is the influence of one-step-delay, which could cause large power ripples that deteriorate the system steady

state performance [4.34], [4.35]. The second one is the dynamic mutual influence between active and reactive powers due to control of two targets in one cost function, which degrades the system's dynamic performance. The design loop of the proposed control is illustrated schematically in Fig. 4.6. With the redesigned cost function and additional objective terms in consideration with switching frequency reduction, one step delay compensation and mutual influence elimination, the proposed multi-functional MPC can improve both the dynamic and steady state performance of the three-phase converter simultaneously, in comparison with the conventional MPC. For different control aspects, the key is to choose proper weighting factors to get a reasonable tradeoff among various control objectives.

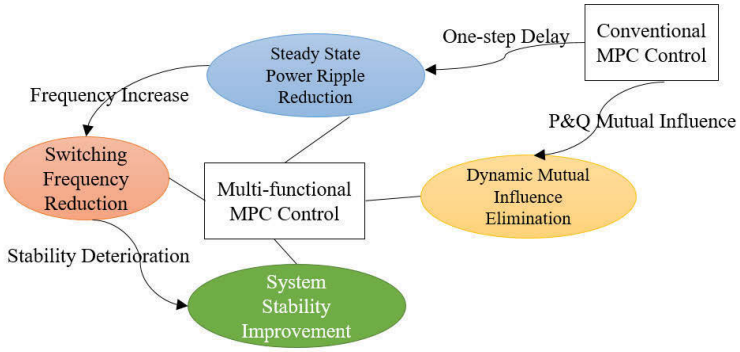

Fig. 4.6 Advanced control design in comparison with CMPC

A. One-step-delay compensation

For steady-state performance, the most significant influence is caused by the one-step-delay in discrete-time digital implementation, as shown in Fig. 4.7. The implementation on digital solutions are limited by computation delays that affect the predictive control performances. The one-step-delay issue exists when using (4.11) for real system control, which increases the system power ripples in the steady state, and causes errors in power prediction. Taking the active power as an example, as illustrated in Fig. 4.7, P^k is the sampled data at the k-th instant, and T_c the computing time of the control strategy. After the best voltage vector V_i^{k+1} is determined using P^k and P^*, it will be applied at the (k+1)-th instant while the active power variables at the (k+1)-th instant

is changed to P^{k+1}, which would be usually different from P^k because of the application of V_i^k. Therefore, the vector chosen at the (k+1)-th instant may no longer be the best one, and the one-step-ahead prediction value P^{k+2} that is acquired from the converter model should be used in the cost function instead of P^{k+1} to calculate the best vector for the (k+1)-th instant. Likewise, the Q^{k+2} acquired through the prediction model should be used in cost function instead of Q^{k+1} for the best vector selection.

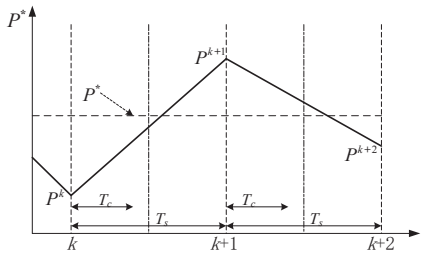

Fig. 4.7 Data processing in digital implementation

With one-step-delay compensation, the cost function should defined as,

$$J_i = (P^* - P_i^{k+2})^2 + (Q^* - Q_i^{k+2})^2 \tag{4.12}$$

B. Switching frequency reduction and system stability compensation

While applying the one-step-delay compensation, it is known that the switching frequency increases significantly [4.21]. The power losses of the converter increase with the increase of switching frequency, especially in high power applications. The switching frequency can be reduced by seeking the minimum possible state changes of each switch [4.37]. Taking the switching state "000" as an example, Fig. 4.8 shows the possible vector switching patterns. It can be seen that there are four patterns according to the number of switches, i.e. the zero, one-state, two-state, and three-state changes. To reduce the switch state change, the vector leading to the least leg switch changes is preferred.

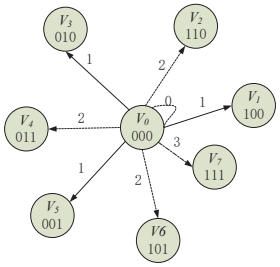

Fig. 4.8 Switching paths of vectors

According to the analyses above, the cost function (4.12) can be revised to

$$J_i = (P^* - P_i^{k+2})^2 + (Q^* - Q_i^{k+2})^2 + \lambda_1 \left(\sum_{i=a,b,c} \left| D_i^{k+1} - D_i^k \right| \right) \tag{4.13}$$

where D_i^k and D_i^{k+1} represent the switching state of phase i ($i = a, b, c$) bridge leg in the k-th and (k+1)-th control periods, respectively; $D_i^k = 0$ or 1, where 1 means that the upper switch is on and the lower one is off, and 0 otherwise; λ_1 is the weighting factor. Thus, by redesigning the cost function as (4.13), the switching frequency reduction can be realized.

As indicated in Fig. 4.6, the system control stability may deteriorate with the application of the switching frequency reduction method, resulting in quite large power and current ripples. A solution is introduced in [4.6] to predict the variables behaviour with N steps ahead, by controlling the prediction value at the (k+N)-th ($N > 1$) instant. The active and reactive powers at the (k+N)-th instant are linearly predicted from the value at the (k+1)-th and (k+2)-th instants. This could help reduce the system power ripples, especially when λ_1 is too large. Finally, for the steady state performance improvement, the cost function (4.13) can be further revised [4.37]

$$J_i = (P^* - P_i^{k+2})^2 + (Q^* - Q_i^{k+2})^2 + \lambda_1 \left(\sum_{i=a,b,c} \left| D_i^{k+1} - D_i^k \right| \right) + \lambda_2 \left(\left| P^* - P_i^{k+N} \right| + \left| Q^* - Q_i^{k+N} \right| \right) \tag{4.14}$$

where λ_2 is the weighting factor in relation with system stability, P_i^{k+N} and Q_i^{k+N} are the active and reactive powers at the (k+N)-th instant with linear extrapolation for the prediction horizon. However, even at this stage with the revised cost function (4.14),

only the steady state performance is improved while the dynamic mutual influence has not been considered.

4.3.2 Mutual influence elimination strategy

In the aforementioned cost functions, the control objectives, namely the active and reactive powers, are combined in one equation and are controlled at the same time to achieve the minimum cost function value. If one objective significantly changes in a large-scale system using MPC control with the aforementioned cost function, the control target is focused on the changing objective, while the other objective is less controlled and the transient performance would deteriorate significantly. The interaction becomes larger while the variation amount of the two control factors becomes larger, especially in high power applications. Due to such influence, the issue of dynamic performance deterioration should also be taken into account.

To eliminate the mutual interference issue and enhance the dynamic performance of the conventional MPC, a novel objective terms is proposed in this paper, which can be used as a general approach to eliminate the mutual influence in MPC by balancing the *P* and *Q* control, which could also be used in various areas with MPC control and will be verified in Chapter 6. The eliminating term M that eliminates the mutual influence can be expressed as:

$$M = \lambda \left| (Q^* - Q_i^{k+2})(P^* - P_i^{k+2}) \right| \tag{4.15}$$

where λ is the weighting factor of mutual influence elimination, which is chosen in consideration of the system's rated active and reactive powers. At the instant of step change of P^* or Q^*, the vector that may incur a large mutual influence on the other control objective would be less considered. Also, the constraint *M* would have almost no influence on steady state performance.

Then, the cost function (4.16) for improving steady performance could be further reorganized by adding this term in the cost function to eliminate the mutual interference, resulting in the revised final cost function as

$$J_i = (P^* - P_i^{k+2})^2 + (Q^* - Q_i^{k+2})^2 + \lambda \left| (Q^* - Q_i^{k+2})(P^* - P_i^{k+2}) \right| + \lambda_1 \left(\sum_{i=a,b,c} \left| D_i^{k+1} - D_i^k \right| \right) + \lambda_2 \left(\left| P^* - P_i^{k+N} \right| + \left| Q^* - Q_i^{k+N} \right| \right) \quad (4.16)$$

In (4.16), each term has a corresponding weighting factor. By selecting proper weighting factors, good dynamic and steady state performance can be balanced in a systematic way. To the best knowledge of the authors, this is the first time in the literature where steady-state and dynamic performance improvements are implemented simultaneously. It should be noted that the proposed method for eliminating mutual influence could be used as a general solution to solve mutual influence of two control objectives in one cost function for various MPC applications, such as electrical drive.

In summary, the proposed multi-functional MPC method chooses the voltage vector according to the cost function which takes the dynamic performance and steady performance into account. The effects of each vector on active and reactive power regulation will then be compared and the selected voltage vector will have minimum cost function value to the system.

4.4 Numerical Simulation and Experimental Verification

4.4.1 Numerical Simulation

The AC/DC converter control has been numerically simulated using the MATLAB/Simulink tool for each control method. The main system parameters used in the simulation are listed in Table 4.5. The sampling frequency for each control method remains the same at 20 kHz.

For simplicity, the conventional switching table based DPC method and conventional MPCDPC methods without one-step-delay compensation are denoted as “CDPC” and “CMPC-I”, respectively, as benchmarks for comparison. The conventional MPC with only one-step-delay compensation and stability enhancement is denoted as “CMPC-II”, the conventional MPC with only proposed mutual influence elimination is denoted as “MMPC-I”, and the proposed multi-functional MPC with both steady state and dynamic performance improvement as “MMPC-II”.

For convenience, the power flow from the AC power supply to the DC load is defined as positive. To analyse both the steady state and dynamic performances for each of the control strategies, the P^* steps up from 0 W to 4000 W at 0 s while the Q^* remains 0 Var. After that, the active power changes to -5000 W at 0.02 s and the reactive power increases to 3000 Var at 0.04 s. At 0.06 s, the active power changes from -5000 W to 7000 W, while the reactive power steps down to -4000 Var at 0.08 s. At 0.1 s, the active power decreases from 7000 W to 0 W.

TABLE 4.5 Electrical parameter of simulation

Resistance of reactor	R	510 mΩ
Inductance of reactor	L	4.2 mH
DC-bus capacitor	C	3500 uF
Load resistance	R_L	50 Ω
Source voltage	e	110 V(peak)
Source voltage frequency	f	50 Hz
DC-bus voltage	V_{dc}	300 V
Weighting factor	λ	0.02
Weighting factor	λ_1	100
Weighting factor	λ_2	55

A. Steady-State Performance

To compare the steady state performance, the AC three-phase input current and reactive power of the system are depicted from 0 s to 0.04 s to show the detailed power ripples. As we can see in Fig. 4.9, both the active and reactive powers track their reference values with good accuracy and stability for each control method.

From Fig. 4.9(a), it is shown that the power ripple is reduced and the line currents are more sinusoidal with the CMPC-I method. With one-step-delay compensation, the performance is further improved with the CMPC-II method.

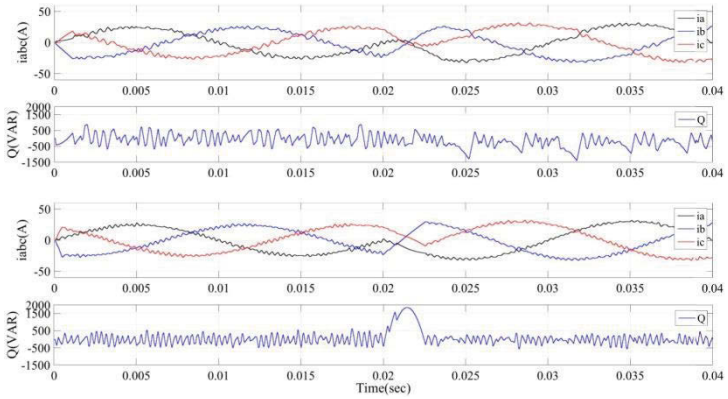

(a)

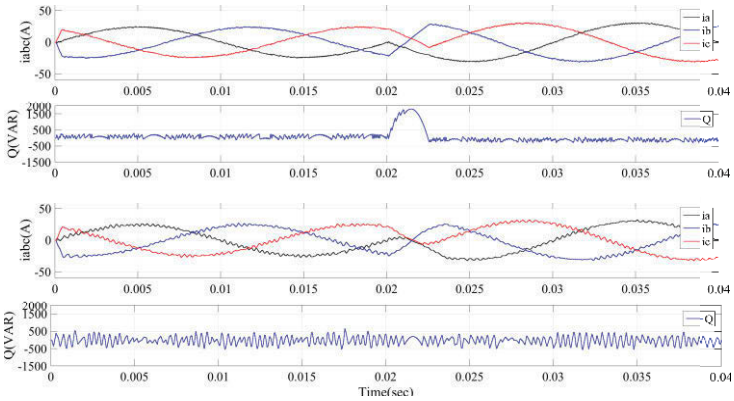

(b)

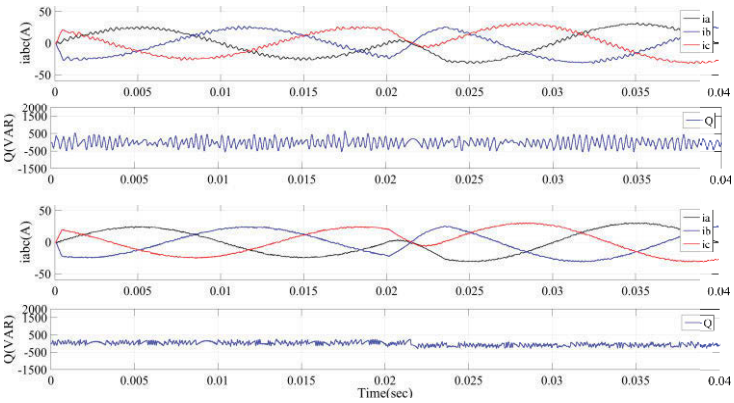

(c)

Fig. 4.9 Steady-state performance comparison. From top to bottom. (a) CDPC three-phase currents, CDPC reactive powers, CMPC-I three-phase currents, CMPC-I reactive powers, (b) CMPC-II three-phase currents, CMPC-II reactive powers, MMPC-I three-phase currents, MMPC-I reactive powers; (c) MMPC-I three-phase currents, MMPC-I reactive powers, MMPC-II three-phase currents, MMPC-II reactive powers;

Take the steady state of P at -5000 W and Q at 0 Var as an example. The active power ripple of CDPC is as high as 209.6 W and the reactive power ripple is 323.1 Var. It should be noted that power ripple is defined as the standard deviation of the power, which is universal definition in this thesis. By comparison, the active power ripple of

CMPC-I is reduced to be around 143.2 Var, while the active power ripple significantly decreases to 244.3 Var, and the current waveform is more sinusoidal compared with the CDPC control. With the CMPC-II method, the power ripple of active power is further decreased to 77.7 W, and the active power ripple is only 81.3 Var, which is the best performance in the steady state, as shown in Fig. 4.9(b). With the MMPC-I method, the steady state performance is similar to the CMPC-I method as expected, since only dynamic performance is improved with the MMPC-I method as discussed before.

With the MMPC-II control, the ripples of active and reactive powers in the steady state are also improved when compared with the CMPC-I and MMPC-I method, and it is almost the same as the CMPC-II control, as shown in Fig. 4.9(c), which aligns well with the theoretical analysis.

As discussed previously, with one-step-delay compensation the switching frequency increases significantly, which correspondingly increases the switching losses. To compare the switching frequency reduction performance of different kinds of methods, the switching frequency can be evaluated by counting the total state changes of one phase leg in a fixed period and divided by 2. The comparison was conducted at 0.05 s as an example. The sample period of the frequency calculation is every 0.01 s. It can be seen that the CMPC-I and MMPC-I control have lower switching frequency due to the lack of one-step-delay compensation. With one-step-delay compensation and corresponding frequency reduction, the switching frequency of the CMPC-II method is 3201 Hz. The MMPC-II control also has similar a frequency in comparison with CMPC-II, which verifies that MMPC-II has a switching frequency reduction ability compared with CMPC-II.

The quantitative comparison of steady state performance including current total harmonic distortion (THD), average switching frequency and active and reactive power ripple at P = -5000 W, Q = 0 Var are presented in Table 4.6.

In conclusion, both the CMPC-II and MMPC-II control methods have the best steady-state performance with lower active power and reactive power ripple, and more sinusoidal waveform.

B. Dynamic performance

To compare the dynamic performance, transient responses of active power and reactive power with each method are simulated, as presented in Fig. 4.10. At the transient instant, the sector where has mutual influence is marked in dashed circles. The following comparisons of active power overshoot and reactive power overshoot take the instant of 0.06 s and 0.02 s as an example. As shown in Fig. 4.10(a), there is no obvious mutual influence between the active and reactive powers with the CDPC control since the control of P and Q are decoupled; the active power overshoot is 580 W and reactive power overshoot is 600 Var. By comparison, the mutual influence of active and reactive powers with the CMPC-I and CMPC-II are apparently of similar performance when there are step changes of P and Q during dynamic instants, as shown in dashed circles in Fig. 4.10(b) and (c). For instance, the P and Q overshoot of CMPC-I are as high as 1855 W and 2020 Var, respectively.

With MMPC-I and MMPC-II, it shows much better dynamic performance by eliminating mutual influence, as shown in Fig. 4.10(d) and (e). For instance, the active power overshot is 310 W and reactive power overshot is 170 Var with the MMPC-II method, which is significantly improved in comparison with the CMPC-I and CMPC-II methods. It should be noted that MMPC-II has better dynamic performance in comparison with MMPC-I due to the improvement of simultaneous steady-state performance.

With the proposed MMPC-I and MMPC-II methods, the mutual influence between active and reactive powers is eliminated. There is almost no overshoot in both reactive and active powers at step change conditions in comparison with CDPC and CMPC and it retains almost the same tracking ability with less response time. The quantitative comparison is shown in Table 4.6, where the active power overshoot and reactive power overshoot value are taken at the instances of 0.06 s and 0.02 s as an example, respectively.

It can be concluded from simulation results that the proposed MMPC-II is the best one among these control methods in consideration of the steady state and dynamic performance at the same time.

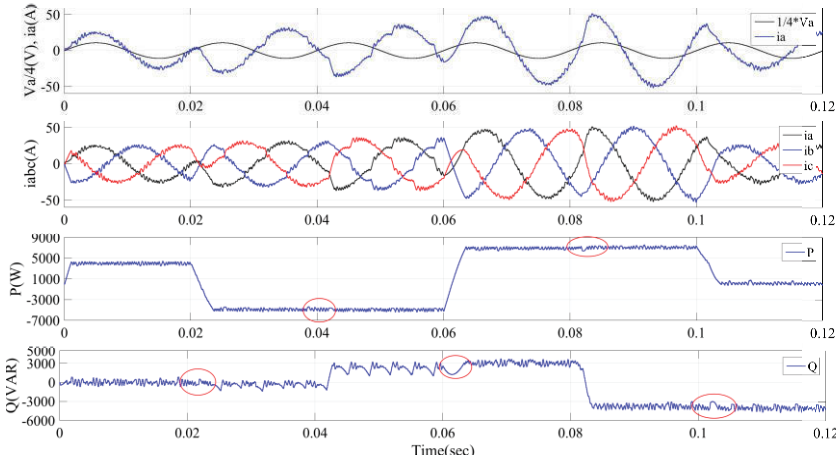

(a)

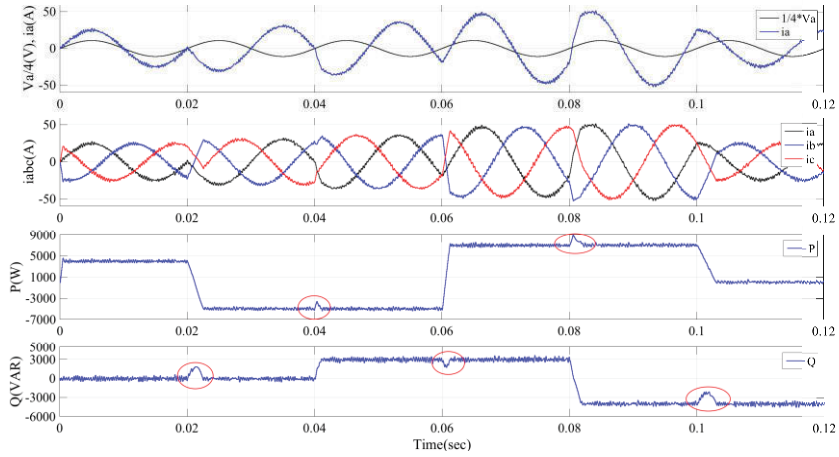

(b)

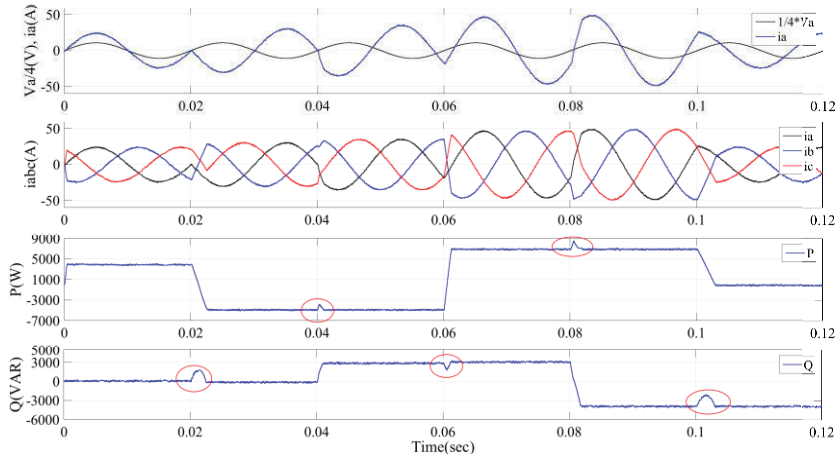

(c)

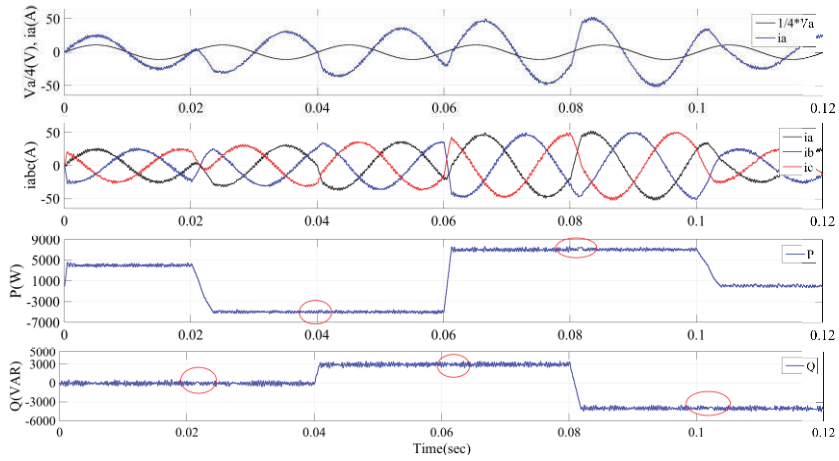

(d)

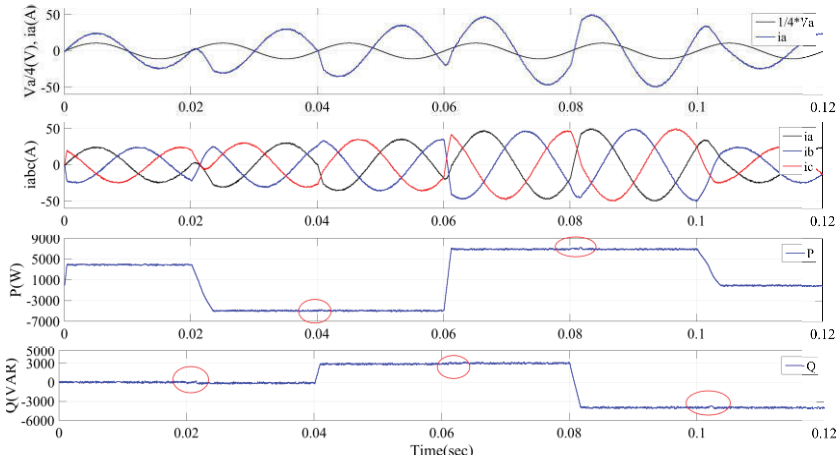

(e)

Fig. 4.10. Dynamic performance. From top to bottom, AC voltage, three-phase currents, active power and reactive power, (a) CDPC, (b) CMPC-I, (c) CMPC-II, (d) MMPC-I, (e) MMPC-II

TABLE 4.6 Quantitative comparison of simulation results

Control	*THD* (%)	*Prip* (W)	*Qrip* (Var)	*fsw* (Hz)	*P Overshoot* (W)	*Q Overshoot* (Var)	*Response* (s)
CDPC	7.95	209.6	323.1	1472	600	580	0.0036
CMPC-I	5.92	143.2	244.3	1908	2020	1855	0.0025
CMPC-II	2.69	77.7	81.3	3201	1561	1812	0.0027
MMPC-I	5.33	152.3	224.3	1952	541	185	0.0033
MMPC-II	2.76	81.8	83.1	3291	310	170	0.0032

4.4.2 Experimental prototype setup

In order to verify the performances of proposed multi-functional MPC algorithm, a scaled down prototype is constructed. Experiments were carried out on a prototyping

platform based on Texas Instruments C2000 control board with TMS320F28335 floating-point DSP that controls a three-phase full-bridge converter. The full bridge is constructed with an intelligent power module (IPM) and the series number is 6MBP50RA, which includes 6 IGBT switches and corresponding driving circuits.

A photo of this prototyping platform is presented in Fig. 4.11 with two main parts: the main circuit part and the control circuit part. The main circuit includes the IPM, three-phase inductors, three-phase isolation transformer and adjustable transformer and DC load. The control circuit includes the voltage and current sensing circuit, signal conditioning circuit, power supply circuit and protection circuit as well as the DSP control board.

For control strategy design, the control program is designed based on the Matlab Target Support Package™ TC2 tool, which integrates MATLAB® and Simulink® with Texas Instruments™ DSP tools and C2000™ processors. Then, with the automatic code generation function of the Target Support Package™ TC2 tool box, the C code of the designed control strategy is generated directly into the Code Composer Studio which is connected with the C2000 control board. The code is then downloaded and run automatically in TMS320F28335 floating-point DSP directly. To change the control system parameter while running the experimental setup, the real time data exchange (RTDX) function is used to exchange data in real time from host and controller using the specified RTDX channel.

Fig. 4.11 Laboratory experimental prototype

4.4.3 Experimental results

To compare the dynamic and steady state performances of existing and proposed methods, a series of experiments have been done. The sampling frequency for each control method remains the same at 20 kHz. The system parameters are tabulated in Table 4.7.

TABLE 4.7 Electrical parameter of experimental prototype

Resistance of reactor	R	500 mΩ
Inductance of reactor	L	22 mH
DC-bus capacitor	C	680 uF
Load resistance	R_L	34 Ω
Source voltage	e	110 V(peak)
Sampling Period	Ts	$50\mu s$
Source voltage frequency	f	50 Hz

A. Comparison of steady-state performance and dynamic performance under the step change of reactive power

For the steady-state performance, the current THD, power ripple of reactive power and active power and switching frequency comparison at steady state of P equal to 450 W and Q equal to 0 Var, have been conducted with each control method. To compare the dynamic-state performance with Q step change of each control method, keep P^* steady at 450 W and change the Q^* from 550 Var to 0 Var at 0.2 s.

Fig. 4.12(a) shows the upper switch driving signal of one leg, input line voltage V_{ab}, and input current i_a and i_b with the CDPC method. It can be verified that both P and Q track their references successfully during the whole test time period. The current THD is 8.52% as shown in Fig. 4.13(a). The P ripple is 38.56 W, and the Q ripple is 38.7 Var. The average switching frequency f_{sw} is 1720 Hz. For the dynamic performance, as shown in Fig. 4.12(a), the CDPC method tracks the reference successfully within 0.0041 s and there is no obvious mutual influence between the P and Q control. The P overshoot when Q changes from 550 Var to 0 Var at 0.2 s is 68 W.

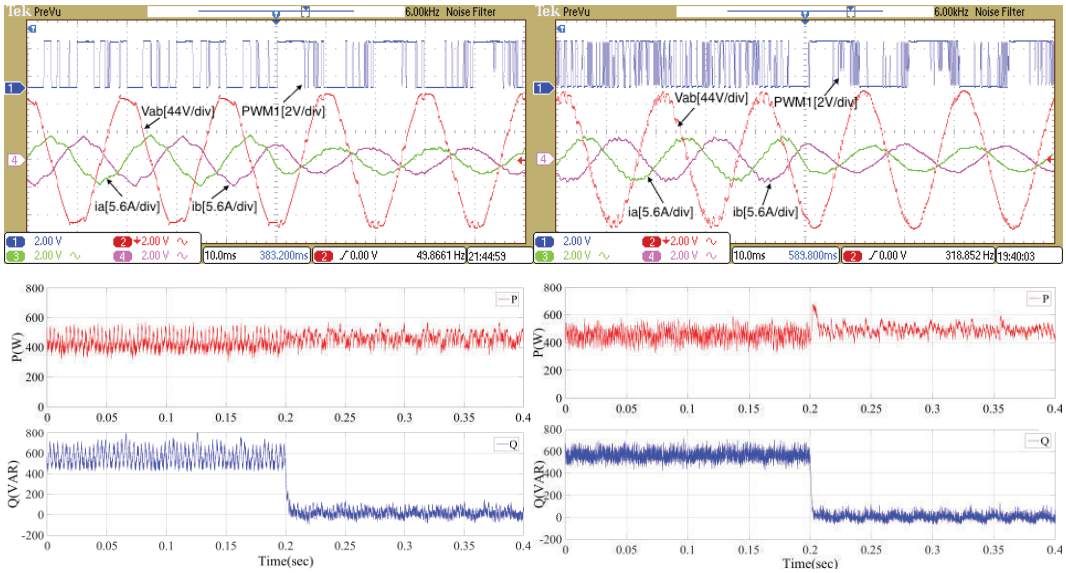

(a) (b)

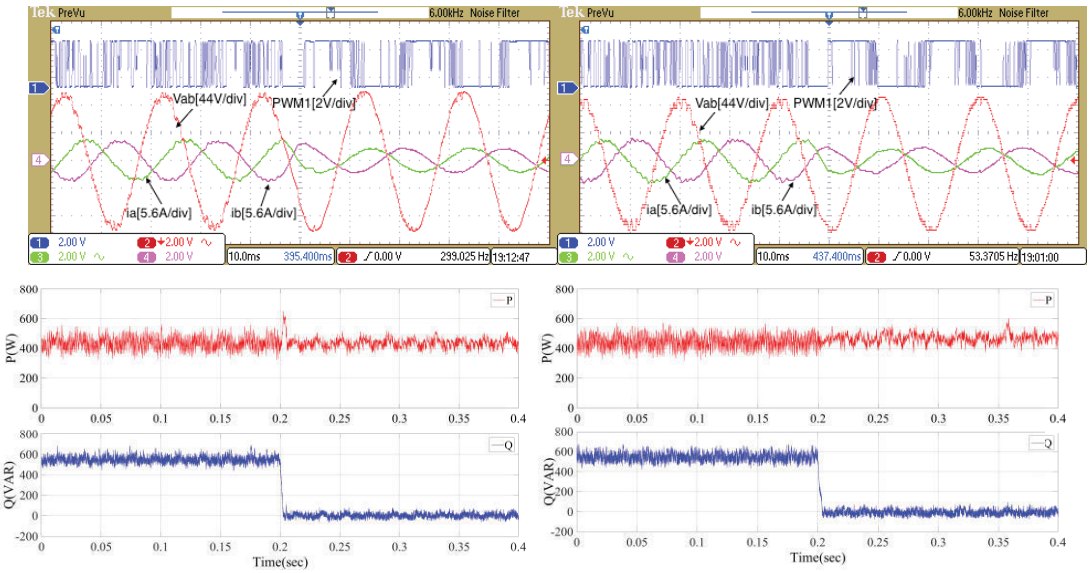

(c) (d)

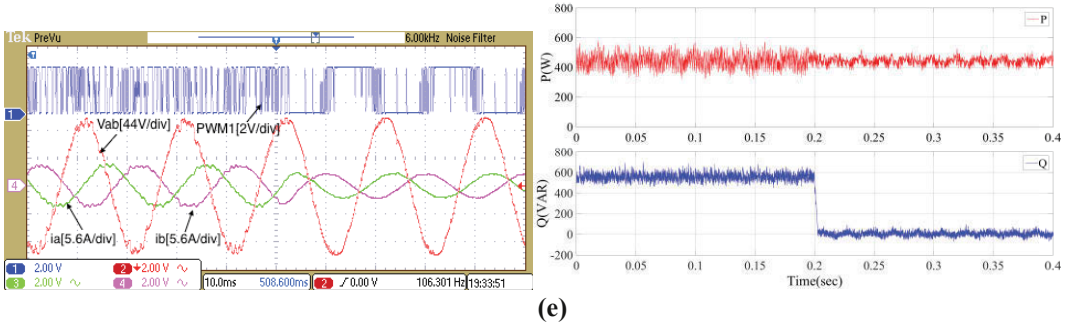

(e)

Fig. 4.12 Experimental performance when *P*=450 W, *Q* changes from 550 Var to 0 Var. Top: PWM signal, V_{ab}, i_a and i_b, Bottom: active power and reactive power, (a) CDPC, (b) CMPC-I, (c) CMPC-II, (d) MMPC-I, (e) MMPC-II.

For comparison, the experiment with CMPC-I method is shown in Fig. 4.12(b). It can be observed that the steady state performance is slightly improved in comparison with CDPC. The current THD is decreased to 6.94% as shown in Fig. 4.13(b), and the P ripple is decreased to 30.59 W while the Q ripple is reduced to 31.57 Var. The average switching frequency f_{sw} is 2520 Hz. The dynamic performance of CMPC-I shows that the response time is 0.0027s, while the influence on P is significant while Q changes from 550 Var to 0 Var. The P overshoot is dramatically increased to 231 W at 0.2 s.

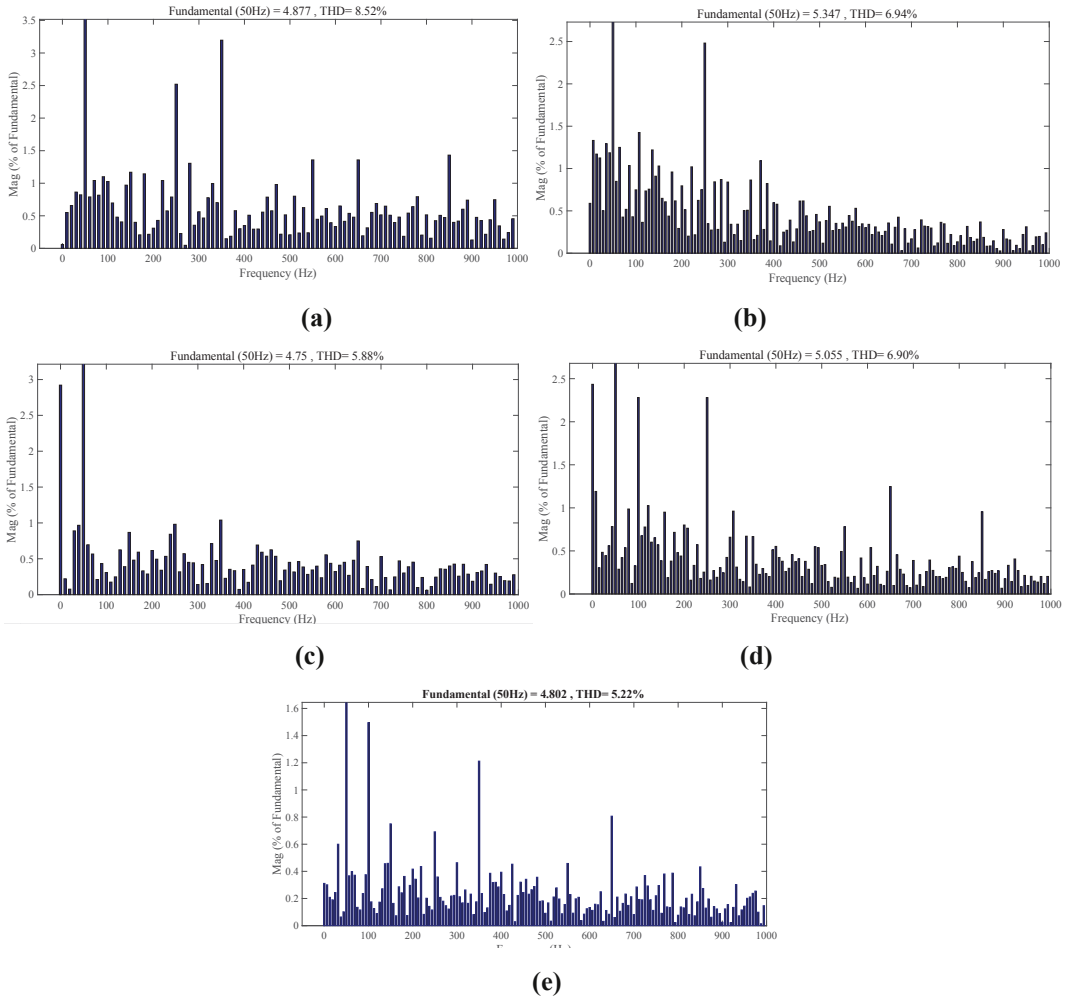

Fig. 4.13 Harmonic spectra of grid current when P=450 W and Q=0 Var. (a) CDPC. (b) CMPC-I. (c) CMPC-II (d) MMPC-I (e) MMPC-II

Similarly, the experimental results with the CMPC-II method are shown in Fig. 4.12(c). It can be seen that the steady-state performance is further improved in comparison with CMPC-I. The THD is 5.88% as shown in Fig. 4.13(c). The P ripple is

28.67 W, and the Q ripple is decreased to 22.87 Var. The average switching frequency f_{sw} is 3410 Hz. For the dynamic performance of the CMPC-II method, the result indicates that the response time is 0.0032 s, and the P overshoot is also as high as 201 W while Q has the step change at 0.2 s.

The experimental results with proposed MMPC-I are shown in Fig. 4.12(d). The THD is 6.9% as shown in Fig. 4.13(d). The P ripple is 32.82 W, and the Q ripple is 27.43 Var. The average switching frequency f_{sw} is 2650 Hz. It can be concluded that the steady state performance is similar to that of the CMPC-I method, which is deteriorated when compared with the CMPC-II control. While for the dynamic performance, the influence on the active power overshoot is significantly decreased to 71 W at the instance of Q step change when compared with the CMPC-I and CMPC-II method.

The experimental results with proposed MMPC-II method are shown in Fig. 4.12(e). The THD is 5.22% as shown in Fig. 4.13(e). The active power ripple is 22.12 W, and the reactive power ripple 22.49 Var. The average switching frequency is 3760 Hz. It can be seen that the steady state performance shows significant improvement in comparison with the CMPC-I, which is similar to the CMPC-II. For the dynamic performance of the MMPC-II method, the P overshoot is significantly decreased to the lowest value of 49 W during the transient period due to the simultaneous mutual influence elimination and steady state performance improvement in comparison with CMPC-II and MMPC-I methods.

B. Comparison of dynamic-state performance with P step change

To compare the influence on Q control when P has a step change, he experimental results with each control method have also been presented when Q reference keeps at 200 Var, and P reference steps up from 200 W to 400 W, as shown in Fig. 4.14. With CDPC, the Q overshoot is 133 Var during the active power step change, as shown in Fig. 12(a). It is increased to 163 Var and 141 Var with the CMPC-I and CMPC-II method as

shown in Fig. 4.14(b) and (c), while with the proposed MMPC-I and MMPC-II control strategies, the *Q* overshoot is significantly decreased to 45 Var and 49 Var, as shown in Fig. 4.14(d) and (e), respectively, which verifies the simulation results well and validates the effectiveness of the proposed MMPC strategy.

The quantitative comparisons of steady-state and dynamic performance are presented in Table 4.8, which aligns well with the theoretical analysis and simulation results, and well verifies the proposed method with multi-functions.

TABLE 4.8 Quantitative comparison of steady-state and dynamic-state performance

Control	*THD* *(%)*	*Prip* (W)	*Qrip* (Var)	*fsw* (Hz)	*P overshoot* (W)	*Q overshoot* *(Var)*	*Response* *(s)*
CDPC	8.52	38.56	38.7	1720	68	133	0.0041
CMPC-I	6.94	30.59	31.57	2520	231	163	0.0027
CMPC-II	5.88	28.67	22.87	3410	201	141	0.0032
MMPC-I	6.90	32.82	27.43	2650	71	45	0.0039
MMPC-II	5.22	22.12	22.49	3760	49	49	0.0038

4.5 Summary of the Chapter

In this chapter, the control strategy of the three-phase full-bridge AC/DC converter has been comprehensively discussed. The advantage and disadvantages of STDPC and current MPC based DPC control have been analysed. The conventional MPC based DPOC of three-phase AC/DC converters usually suffers from parametric coupling between two control objectives. A change in reference of either the active or reactive power will affect the other, leading to poor dynamic response. The steady-state performance of the conventional MPC is affected by one-step-delay arising from computation and communication processes in the digital implementation, which also should be considered simultaneously. With the analyses of mutual influence in MPC based control strategy, a novel constraint which could be generally used to eliminate the mutual influence of two control objectives has been proposed.

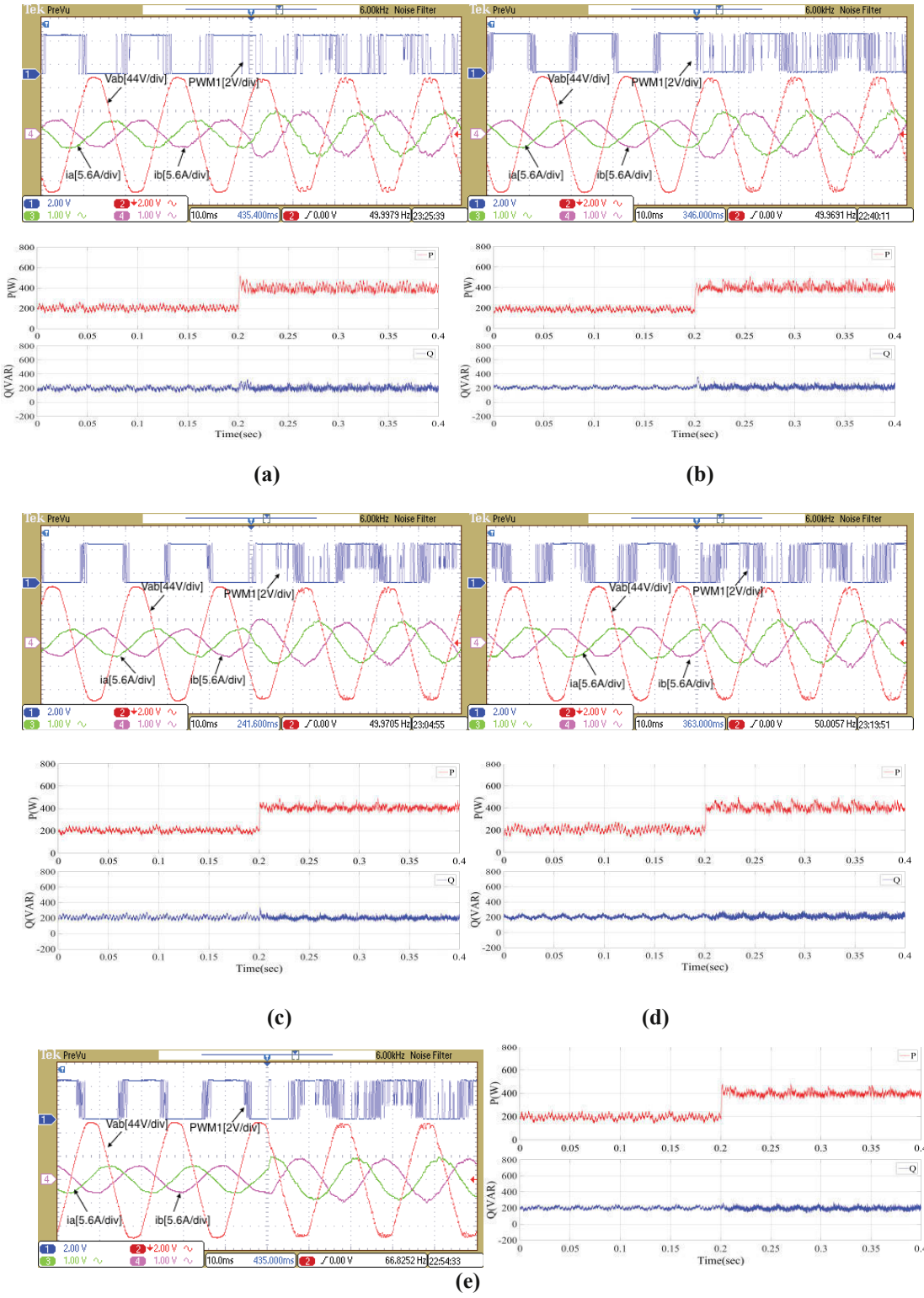

Fig. 4.14 Experimental performance when *Q*=200 Var, *P* changes from 200 W to 400 W. Top: PWM signal, V_{ab} , i_a and i_b . Bottom: active power and reactive power. (a). CDPC. (b) CMPC-I. (c) CMPC-II (d) MMPC-I (e) MMPC-II

Meanwhile, to achieve good dynamic and steady state performance simultaneously, a multi-functional MPC based control strategy of three-phase AC/DC converters to

improve the steady-state and dynamic performances simultaneously has been proposed. It has multiple functions such as one-step-delay compensation, power ripple reduction, switching frequency reduction for steady state performance improvement, and mutual influence elimination for dynamic performance improvement. The steady-state and dynamic-state performances of CDPC, CMPC-I, CMPC-II, MMPC-I and MMPC-II for bidirectional power flow control of the AC/DC converter are compared with both simulation and experimental results. The proposed MMPC-I and MMPC-II methods have been verified to be able to eliminate the mutual influence of two control objective, namely active and reactive power. The proposed MMPC-II method has demonstrated its superior dynamic and steady state performances in comparison with conventional STDPC and MPDPC methods by simultaneously reducing power ripples and eliminating the mutual influence of active and reactive powers during the transient.

REFERENCES

[4.1] J. M. Carrasco, L. G. Franquelo, J. T. Bialasiewicz, E. Galvan, R. C. Portillo Guisado, M. A. M. Prats, J. I. Leon, and N. Moreno-Alfonso, "Power-electronic systems for the grid integration of renewable energy sources: A survey," *IEEE Trans. Ind. Electron.*, vol. 53, no. 4, pp. 1002– 1016, Jun. 2006

[4.2] F. Blaabjerg, M. Liserre, and K. Ma, "Power electronics converters for wind turbine systems," *IEEE Trans. Ind. Appl.*, vol. 48, no. 2, pp. 708– 719, Mar./Apr. 2012

[4.3] J. R. Rodriguez, J. W. Dixon, J. R. Espinoza, J. Pontt, and P. Lezana, "PWM regenerative rectifiers: State of the art," *IEEE Trans. Ind. Electron.*, vol. 52, no. 1, pp. 5–22, Feb. 2005

[4.4] F. Blaabjerg, R. Teodorescu, M. Liserre, and A. Timbus, "Overview of control and grid synchronization for distributed power generation systems," *IEEE Trans. Ind. Electron.*, vol. 53, no. 5, pp. 1398–1409, Oct. 2006

[4.5] S. Chakraborty, B. Kramer and B. Kroposki, "A review of power electronics interfaces for distributed energy systems toward achieving low-cost modular design," *Renewable and Sustainable Energy Reviews*, vol. 13, no. 9, pp. 2323-2335, 2009

[4.6] T. Strasser, F. Andren, J. Kathan, C. Cecati, C. Buccella, P. Siano*, et al.*, "A review of architectures and concepts for intelligence in future electric energy systems," *IEEE Trans. Ind. Electron.,* vol. 62(4), pp. 2424-2438, 2015

[4.7] J. Alonso-Martinez, J. E. Carrasco, and S. Arnaltes, "Table-based direct power control: A critical review for microgrid applications," *IEEE Trans. Power Electron.*, vol. 25, no. 12, pp. 2949–2961, Dec. 2010

[4.8] Y. Zhang, Z. Li, Y. Zhang, W. Xie, Z. Piao, and C. Hu, "Performance improvement of direct power control of PWM rectifier with simple calculation," *IEEE Trans. Power Electron.*, vol. 28, no. 7, pp. 3428–3437, Jul. 2013

[4.9] J. Hu, J. Zhu, and D. G. Dorrell, "A Comparative Study of Direct Power Control of AC/DC Converters for Renewable Energy Generation," in Proc. *IEEE IECON Conf.*, pp. 3453–3458, 2011

[4.10] T. Noguchi, H. Tomiki, S. Kondo, and I. Takahashi, "Direct power control of PWM converter without power-source voltage sensors," *IEEE Trans. Ind. Appl*, vol. 34, no. 3, pp. 473–479, May/Jun. 1998

[4.11] L. Xu, D. Zhi, and L. Yao, "Direct power control of grid connected voltage source converters," in *Proc. IEEE Power Eng. Soc. Gen. Meet.*, 2007, pp. 1–6

[4.12] M. Malinowski, M.P. Kazmierkowski, and A.M. Trzynadlowski,"A comparative study of control techniques for PWM rectifiers in AC adjustable speed drives," *IEEE Trans. Power Electron.*, vol. 18, no. 6, pp. 1390–1396, Nov. 2003

[4.13] P. Antoniewicz and M. Kazmierkowski, "Virtual-flux-based predictive direct power control of ac/dc converterswith online inductance estimation," *IEEE Trans. Ind. Electron*.,vol. 55, no. 12, pp. 4381–4390, Dec.2008

[4.14] J. Hu, J. Zhu, and D. Dorrell, "In-depth study of direct power control strategies for power converters, *IET Power Electronics*," vol. 7, no. 7, 2014, pp. 1810–1820

[4.15] A. Bouafia, J.-P. Gaubert, and F. Krim, "Analysis and design of new switching table for direct power control of three-phase PWM rectifier," in *Proc. 13th Power Electron. Motion Control Conf.*,2008, pp.703–709.

[4.16] A. Baktash, A. Vahedi, and M. A. S. Masoum, "Improved switching table for direct power control of three-phase PWM rectifier," in *Proc. Australasian Univ. Power Eng. Conf.*, 2007, pp. 1–5.

[4.17] Y. Zhang, W. Xie, Z. Li, and Y. Zhang, "Model predictive direct power control of a PWM rectifier with duty cycle optimization," *IEEE Trans. Power Electron.*, vol. 28, no. 11, pp. 5343–5351, Nov. 2013.

[4.18] Y. Zhang and W. Xie, "Low complexity model predictive control—Single vector based approach," *IEEE Trans. Power Electron.*, vol. 29, no. 10, pp. 5532–5541, Oct. 2014.

[4.19] Z. Song, C. Xia, and T. Liu, "Predictive current control of three-phase grid- connected converters with constant switching frequency for wind energy systems," *IEEE Trans. Ind. Electron.*, vol. 60, no. 6, pp. 2451–2464, Jun. 2013.

[4.20] R. P. Aguilera, P. Lezana, and D. E. Quevedo, "Finite-control-set model predictive control with improved steady-state performance," *IEEE Trans. Ind. Electron.*, vol. 9, no. 2, pp. 658–667, May 2013.

[4.21] M. Preindl, E. Schaltz, and P. Thøgersen,"Switching frequency reduction using model predictive direct current control for high-power voltage source inverters," *IEEE Trans. Ind. Electron.*, vol. 58, no. 7, pp. 2826–2835, Jul. 2011.

[4.22] P. Cortes *et al.*, "Model predictive control of an inverter with output LC filter for UPS applications," *IEEE Trans. Ind. Electron.*, vol. 56, no. 6, pp. 1875–1883, Jun. 2009.

[4.23] S. Vazquez, C. Montero, C. Bordons, and L. G. Franquelo, "Model predictive control of a VSI with long prediction horizon," in *Proc. IEEE Int. Symp. Ind. Electron.*, Jun. 2011, pp. 1805–1810.

[4.24] J. Hu and Z. Zhu, "Improved voltage-vector sequences on dead-beat predictive direct power control of reversible three-phase grid-connected voltage-sourced converters," *IEEE Trans. Power Electron.*, vol. 28, no. 1, pp. 254–267, Jan. 2013.

[4.25] Z. Song, W. Chen, and C. Xia, "Predictive direct power control for three-phase grid-connected converters without sector information and voltage vector selection," *IEEE Trans. Power Electron.*, vol. 29, no. 10, pp. 5518–5531, Oct. 2014.

[4.26] R. O. Ramirez, J. R. Espinoza, F. Villarroel, E. Maurelia, and M. E. Reyes, "A novel hybrid finite control set model predictive control scheme with reduced switching," *IEEE Trans. Ind. Electron.*, vol. 61, no. 11, pp. 5912–5920, Nov. 2014.

[4.27] J. Rodriguez, M. P. Kazmierkowski, J. R. Espinoza, P. Zanchetta, H. Abu-Rub, H. A. Young, and C. A. Rojas, "State of the art of finite control set model predictive control in power electronics," *IEEE Trans. Ind. Informat.*, vol. 9, no. 2, pp. 1003–1016, May 2013.

[4.28] U. Maedera, F. Borrelli, and M. Morari, "Linear offset-free model predictive control," *Automatica*, vol. 45, no. 10, pp. 2214–2222, Oct. 2009.

[4.29] S. A. Larrinaga, M. A. Rodriguez, E. Oyarbide and J. R. T. Apraiz, "Predictive control strategy for DC/AC converters based on direct power control," *IEEE Trans. Ind. Electron.,* vol. 54, pp. 1261-1271, June 2007.

[4.30] P. Cortes, M. Kazmierkowski, R. Kennel, D. Quevedo, and J. Rodriguez, "Predictive control in power electronics and drives," *IEEE Trans. Ind. Electron.*, vol. 55, no. 12, pp. 4312–4324, Dec. 2008.

[4.31] S. Kwak and J.-C. Park, "Switching strategy based on model predictive control of VSI to obtain high efficiency and balanced loss distribution," *IEEE Trans. Power Electron.*, vol. 29, no. 9, pp. 4551–4567, Sep. 2014.

[4.32] S. Vazquez *et al.*, "Model predictive control: A review of its applications in power electronics," *IEEE Ind. Electron. Mag.*, vol. 8, no. 1, pp. 16–31, Mar. 2014.

[4.33] S. Vazquez, J.A. Sanchez, J.M. Carrasco, J.I. Leon, and E. Galvan,"A model-based direct power control for three-phase power converters," *IEEE Trans. Ind. Electron.*, vol. 55, no. 4, pp. 1647–1657, Apr. 2008.

[4.34] P. Cortes, J. Rodriguez, C. Silva, and A. Flores, "Delay compensation in model predictive current control of a three-phase inverter," *IEEE Trans. Ind. Electron.*, vol. 59, no. 2, pp. 1323–1325, Feb. 2012.

[4.35] Y. Zhang, J. Zhu, and W. Xu, "Analysis of one step delay in direct torque control of permanent magnet synchronous motor and its remedies," in *Proc. Int. Electr. Mach. Syst. Conf.*, 2010, pp. 792–797.

[4.36] H. Abu-Rub, J. Guzinski, Z. Krzeminski, and H. A. Toliyat, "Predictive current control of voltage source inverters," *IEEE Trans. Ind. Electron.*, vol. 51, no. 3, pp. 585–593, Jun. 2004.

[4.37] J. Hu, J. Zhu, G. Platt, and D. G. Dorrell, "Multi-objective model-predictive control for high power converters," *IEEE Trans. Energy Convers.,* vol. 28, no. 3, pp. 652-663, Sep. 2013.

[4.38] D. Zhi and L. Xu, "Direct power control of DFIG with constant switching frequency and improved transient performance," *IEEE. Trans. Energy Convers.*, vol. 22, no. 1, pp. 110–118, Mar. 2007.

[4.39] D. E. Quevedo, R. P. Aguilera, M. A. Perez, P. Cortes, and R. Lizana, "Model predictive control of an AFE rectifier with dynamic references," *IEEE Trans. Power Electron.*, vol. 27, no. 7, pp. 3128–3136, Jul. 2012.

[4.40] P. Cortes, J. Rodriguez, P. Antoniewicz, and M. Kazmierkowski, "Direct power control of an AFE using predictive control," *IEEE Trans. Power Electron.*, vol. 23, no. 5, pp. 2516–2523, Sep. 2008.

[4.41] D. Choi, K. Lee, "Dynamic performance improvement of AC/DC converter using model predictive direct power control with finite control set." *IEEE Trans. Ind. Electron.,* vol. 62, pp. 757-767, 2015.

Chapter 5

REVERSIBLE PREDICTIVE DUTY CYCLE CONTROL OF AC/DC FULL-BRIDGE CONVERTER

5.1 Introduction

As verified in the last chapter, the switching table based direct power control (STDPC) method has the disadvantages of higher current distortion and variable switching frequency. To solve this issue, without using a predefined switching table, model predictive based DPC (MPDPC) is applied widely. The complete model of the three-phase converter and its future behavior are taken into account with several advantages such as fast dynamic response, no need of modulator, and flexibility to include other system requirements and constraints in the controller [5.1]-[5.10], which was verified in the last chapter. It therefore can achieve better dynamic and steady state performance compared with the STDPC method.

However, since the errors between the reference and measured active and reactive powers are evaluated for a finite set of voltage space vectors in the cost function, the best one that minimizes the cost function is selected for actuation in each control period. Due to a limited number of available converter states, namely 8 vectors, and only one vector selected in one sampling period, it results in variable switching frequency, higher power ripple and rich harmonics inherent with the strategy thereby complicating further filter design [5.11]-[5.13]. Also, the sampling frequency has to be relatively high in order to achieve satisfactory performance. These disadvantages cancel the merits of MPDPC for the three-phase full-bridge converter application in renewable energy systems (RES).

In order to overcome the disadvantage of MPDPC and further improve the performance, recently more efforts have been made to select two or three vectors in one

sampling period to achieve ripple reduction and constant switching frequency [5.14]-[5.23]. The three-vector-based approaches have been applied in the power converter control and electrical machine drives. In [5.14] and [5.15], the conventional predictive duty cycle control (CPDCC) with three-vector based approach using prediction value of power slope to calculate the duration time of selected voltage vector has been proposed, the best adjacent two none-zero vector is selected based on the sector information. The least square method is employed to calculate the duration time of each vector. However, it is found that the selection method widely used, e.g. the one presented in [5.14], might select incorrect voltage vectors based on the conventional vector sequence table and this will further result in the negative value of optimal duration time. Normally, the action time is forced to zero whenever a negative value is calculated or forced to maximum value, resulting in control failures and performance deterioration. To solve this problem, some methods have been proposed [5.16]-[5.20]. In [5.17], a novel method of optimal voltage vector selection is developed by selecting global optimal voltage vectors with cost function minimization, since the conventional control method in [5.15] constrains the converter operation range to a small power angle, which limits the active power transfer from AC to DC side. In [5.18] and [5.19], the reason of wrong vector selection with the CPDCC method is analyzed and a modified vector selection table is proposed based on the specified case study. The none-zero voltage vectors are reselected based on the revised vector sequence table whenever negative time values appear, and then the duration time would be recalculated with reselected vectors. Though the performance could be improved, it is no doubt that the complexity and calculation burden will increase obviously as the vector selection and duration time calculation repeat when the duration time is negative. References [5.20] and [5.21] propose an improved predictive DPC method eliminating sector information of the grid voltage and the voltage vector selection process. However, the equivalent reconstruction of switch signals is needed and the calculation of duration time is complex. The model predictive control (MPC) method is employed in [5.22]-[5.26] to avoid the wrong selection of voltage vectors to improve the performance without using

the sector information. However, all the adjacent vector pairs need to be evaluated using cost function to select the best pair [5.22]-[5.24].

This chapter firstly analyzes the CPDCC method and improved PDCC (IPDCC) method, the disadvantages and advantages of each method are discussed, and then proposes a reversible PDCC (RPDCC) method based on the fact that the active and reactive power slope of reverse vector pairs are symmetric with respect to the active and reactive power slope of zero vectors, respectively. With RPDCC, the reverse vector is selected to replace the original none-zero vector whose calculated duration time is negative with the CPDCC method, and then the negative duration time could change to be positive with the same value, as the duration time of the zero vector has been verified to meet the boundary condition the same as the CPDCC method according to the theoretical analyses. It is simply derived without recalculation. Thus, there is no need to recalculate the power slope and duration time as the IPDCC method, which reduces the control complexity obviously. Finally, the simulation results and experimental results also verify that RPDCC achieves better steady and dynamic performance than the CPDCC and IPDCC methods.

5.2 Three Vectors based Predictive Duty Cycle Control Approach

5.2.1 Mathematical model of conventional predictive duty cycle control

Fig. 5.1(a) illustrates the topology of the three-phase full-bridge AC/DC converter, and Fig. 5.1(b) a diagram showing the voltage space vectors. The three-phase full bridge unit is connected to either the main grid or an AC load via a choke consisting of three series-connected inductors L and resistors R. At the DC side, a DC load or DC bus is connected to the full bridge in parallel to a capacitor C, where e_a, e_b, and e_c are the three-phase AC source voltages; v_a, v_b and v_c the AC terminal voltages of the three phase bridge; and i_a, i_b, and i_c the three-phase currents.

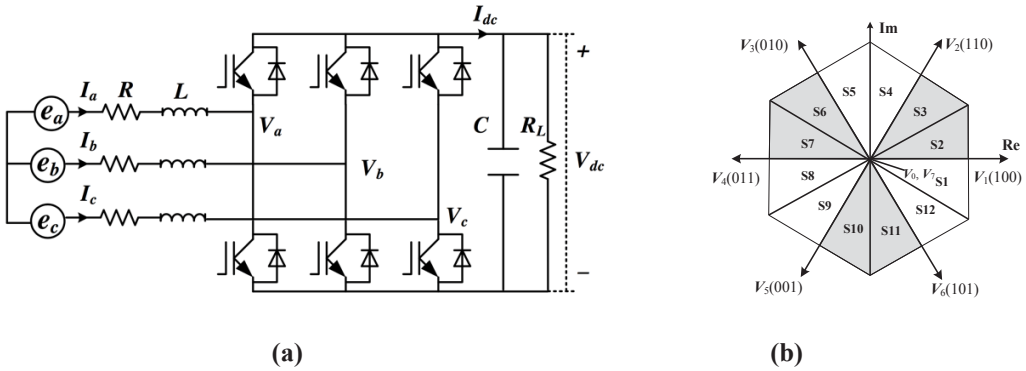

(a) **(b)**

Fig. 5.1 (a) AC/DC three-phase converter structure, and (b) Voltage space vectors

In stationary reference frame, the AC source voltage vector and current vector in the αβ-coordinate system can be calculated by the following transformation:

$$e_{\alpha\beta} = \begin{bmatrix} e_\alpha \\ e_\beta \end{bmatrix} = \frac{2}{3}\begin{bmatrix} 1 & -1/2 & -1/2 \\ 0 & \sqrt{3}/2 & -\sqrt{3}/2 \end{bmatrix}\begin{bmatrix} e_a \\ e_b \\ e_c \end{bmatrix} \tag{5.1}$$

$$I_{\alpha\beta} = \begin{bmatrix} I_\alpha \\ I_\beta \end{bmatrix} = \frac{2}{3}\begin{bmatrix} 1 & -1/2 & -1/2 \\ 0 & \sqrt{3}/2 & -\sqrt{3}/2 \end{bmatrix}\begin{bmatrix} I_a \\ I_b \\ I_c \end{bmatrix} \tag{5.2}$$

In a balanced three-phase system, the line currents can be calculated by solving the differential equation as follows:

$$e_{\alpha\beta} = L\frac{dI_{a\beta}}{dt} + RI_{a\beta} + V_{\alpha\beta} \tag{5.3}$$

where $e_{\alpha\beta}$, $V_{\alpha\beta}$, $I_{\alpha\beta}$, and I_L are the input source voltage vector, the three-phase converter input voltage vector, the line current vector, and load current, respectively. The active and reactive power exchange with the grid can be calculated as

$$\begin{bmatrix} P \\ Q \end{bmatrix} = \frac{3}{2}\begin{bmatrix} e_\alpha & e_\beta \\ e_\beta & -e_\alpha \end{bmatrix}\begin{bmatrix} I_\alpha \\ I_\beta \end{bmatrix} \tag{5.4}$$

Firstly, the CPDCC proposed in [5.15] is discussed as below. Fig. 5.2 shows the block diagram of the conventional predictive duty cycle control strategy. The sector information and active and reactive power slopes are both important for PDCC implementation. The selection of two none-zero voltage vectors is based on the sector information, as shown in Table 5.1. The selection of the two voltage vectors in each

sector was based on the location of the grid voltage vector, to which the two adjacent active vectors were selected together with either V_0 or V_7 according to the rule of minimum commutation numbers. Duration times are calculated based on corresponding power slopes of the selected none-zero vector pair and zero vector.

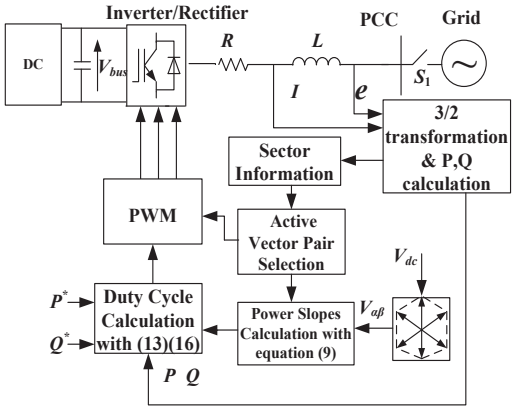

Fig. 5.2 Block diagram of PDCC for the AC/DC converter

TABLE 5.1 Conventional voltage-vectors' sequences for predictive DPC [5.15]

Vector sequence	Sector number (S_n)											
	S_1	S_2	S_3	S_4	S_5	S_6	S_7	S_8	S_9	S_{10}	S_{11}	S_{12}
V_a	V_1	V_1	V_2	V_2	V_3	V_3	V_4	V_4	V_5	V_5	V_6	V_6
V_b	V_6	V_2	V_1	V_3	V_2	V_4	V_3	V_5	V_4	V_6	V_5	V_1
V_c	V_7	V_7	V_0	V_0	V_7	V_7	V_0	V_0	V_7	V_7	V_0	V_0

The differential equation matrix of active and reactive powers can be derived from (5.3) and (5.4) as

$$\frac{d}{dt}\begin{bmatrix} P \\ Q \end{bmatrix} = \frac{3}{2}\left(I_\alpha \frac{d}{dt}\begin{bmatrix} e_\alpha \\ e_\beta \end{bmatrix} + \frac{dI_\alpha}{dt}\begin{bmatrix} e_\alpha \\ e_\beta \end{bmatrix} + I_\beta \frac{d}{dt}\begin{bmatrix} e_\beta \\ -e_\alpha \end{bmatrix} + \frac{dI_\beta}{dt}\begin{bmatrix} e_\beta \\ -e_\alpha \end{bmatrix} \right) \tag{5.5}$$

For the sinusoidal and balanced three phase line voltage,

$$\overline{e} = e_\alpha + je_\beta = |\overline{e}|\, e^{j\omega t} \tag{5.6}$$

From (5.6), the following expression can be deduced as

$$\frac{d}{dt}\begin{bmatrix} e_\alpha \\ e_\beta \end{bmatrix} = \omega \cdot \begin{bmatrix} -e_\beta \\ e_\alpha \end{bmatrix} \tag{5.7}$$

The instantaneous active and reactive power variation can be calculated by substituting (5.1) and (5.7) into (5.5) as

$$\begin{cases} \dfrac{dP_i}{dt} = -\dfrac{R}{L}P - \omega Q + \dfrac{3}{2L}\left|\bar{e}\right|^2 - \dfrac{3}{2L}\mathrm{Re}\left(\bar{e}\bar{V}_i^*\right) \\ \dfrac{dQ_i}{dt} = -\dfrac{R}{L}Q + \omega P - \dfrac{3}{2L}\mathrm{Im}\left(\bar{e}\bar{V}_i^*\right) \\ \delta_{pi} = \dfrac{dP_i}{dt} \quad \delta_{qi} = \dfrac{dQ_i}{dt} \end{cases} \tag{5.8}$$

Where δ_{pi} and δ_{qi} are the active and reactive power slopes of each voltage space vector, $\bar{V}_i$ represents the voltage space vector, i=0,1,2…7. For every switching state and the corresponding voltage space vector, $V_{i\alpha}$ and $V_{i\beta}$ are calculated as follows,

$$\begin{bmatrix} V_{i\alpha} \\ V_{i\beta} \end{bmatrix} = \frac{2}{3}V_{dc}\begin{bmatrix} S_{ia} - \dfrac{1}{2}(S_{ib} + S_{ic}) \\ \dfrac{\sqrt{3}}{2}(S_{ib} - S_{ic}) \end{bmatrix} \tag{5.9}$$

where S_{ia} , S_{ib} and S_{ic} are the switching states of the converter.

If the tracking error of the DC-bus voltage is assumed constant over two successive sampling periods, the instantaneous active power at the next sampling instant (k+1) can be estimated using a linear extrapolation. Thus, at the end of sampling period T_s, the predictive active and reactive powers for each converter switching state can be expressed as:

$$\begin{bmatrix} P_i^{k+1} \\ Q_i^{k+1} \end{bmatrix} = T_s\left(-\frac{R}{L}\begin{bmatrix} P_i^k \\ Q_i^k \end{bmatrix} + \omega\begin{bmatrix} -Q_i^k \\ P_i^k \end{bmatrix} + \frac{3}{2L}\begin{bmatrix} \left(\left|\vec{e}\right|^2 - \mathrm{Re}\left(\vec{e}\vec{V}_i^*\right)\right) \\ -\mathrm{Im}\left(\vec{e}\vec{V}_i^*\right) \end{bmatrix}\right) + \begin{bmatrix} P_i^k \\ Q_i^k \end{bmatrix} \tag{5.10}$$

For CPDCC, two adjacent none-zero vectors are selected according to power source voltage vector location, namely sector information. For instance, if source voltage vector locates at section S_2 or S_3, the adjacent none-zero vectors V_1 and V_2 should be selected. Assuming the power slopes are constant for a small sampling period, the powers at the end of the sampling period can be predicted as

$$\begin{cases} P^{k+1} = P^k + 2(\delta_{pa}t_a + \delta_{pb}t_b + \delta_{pc}t_c) \\ Q^{k+1} = Q^k + 2(\delta_{qa}t_a + \delta_{qb}t_b + \delta_{qc}t_c) \end{cases} \tag{5.11}$$

where $\delta_{p1}, \delta_{p2}, \delta_{p3}$ are the active power slopes of two adjacent none-zero voltage vectors V_I, V_{II} and one zero voltage vector, $\delta_{q1}, \delta_{q2}, \delta_{q3}$ the reactive power slopes, t_a, t_b and t_c the corresponding durations of two adjacent none-zero voltage vectors and zero vector, respectively, and satisfy the boundary condition $t_a + t_b + t_c = T_s / 2$. For CPDCC, the key is to calculate the optimal duty ratios. The error between predicted value and the reference value can be calculated as

$$\begin{cases} P_{err} = P^* - \left[P^k + 2(\delta_{pa}t_a + \delta_{pb}t_b + \delta_{pc}t_c) \right] \\ Q_{err} = Q^* - \left[Q^k + 2(\delta_{qa}t_c + \delta_{qb}t_c + \delta_{qc}t_c) \right] \end{cases} \tag{5.12}$$

where P^* is the active power reference and Q^* the reactive power reference. Then the least square optimization is utilized to minimize the power errors, as

$$J = P_{err}^2 + Q_{err}^2 \tag{5.13}$$

$$\begin{cases} \dfrac{\partial J}{\partial t_a} = 0 \\ \dfrac{\partial J}{\partial t_b} = 0 \end{cases} \tag{5.14}$$

The optimal application durations can be obtained as follows

$$\begin{cases} t_a = \left[(P^* - P^k)(\delta_{qb} - \delta_{qc}) + (Q^* - Q^k)(\delta_{pc} - \delta_{pb}) + T_s(\delta_{pb}\delta_{qc} - \delta_{pc}\delta_{qb}) \right] / 2m \\ t_b = \left[(P^* - P^k)(\delta_{qc} - \delta_{qa}) + (Q^* - Q^k)(\delta_{pa} - \delta_{pc}) + T_s(\delta_{qa}\delta_{pc} - \delta_{qc}\delta_{pa}) \right] / 2m \\ t_c = T_s / 2 - t_a - t_b \end{cases} \tag{5.15}$$

where

$$m = (\delta_{qb} - \delta_{qc})\delta_{pa} + (\delta_{qc} - \delta_{qa})\delta_{pb} + (\delta_{qa} - \delta_{qb})\delta_{pc} \tag{5.16}$$

Once t_a, t_b and t_c are calculated, switch duty cycles can thus be obtained and switching signals are generated. It should be noted that the calculated the voltage vector action time based on (5.15) may be negative or over $T_s / 2$. With the CPDCC method,

the actual action time is normally forced to zero whenever a negative value is calculated or possibly forced to $T_s/2$ when the calculated time is over than $T_s/2$, resulting in performance deterioration.

5.2.2 Improved predictive duty cycle control with novel vector sequence

To analyse the reason for the wrong vector selection and corresponding negative duration time, the power slope of each vector with the converter parameters given in Table 5.4 has been illustrated. Fig. 5.3(a) and (b) depict the variation rates of instantaneous active/reactive powers with each converter voltage vector throughout the 12 sectors under the conditions that P is equal to 450 W and -450 W at unity power factor, respectively.

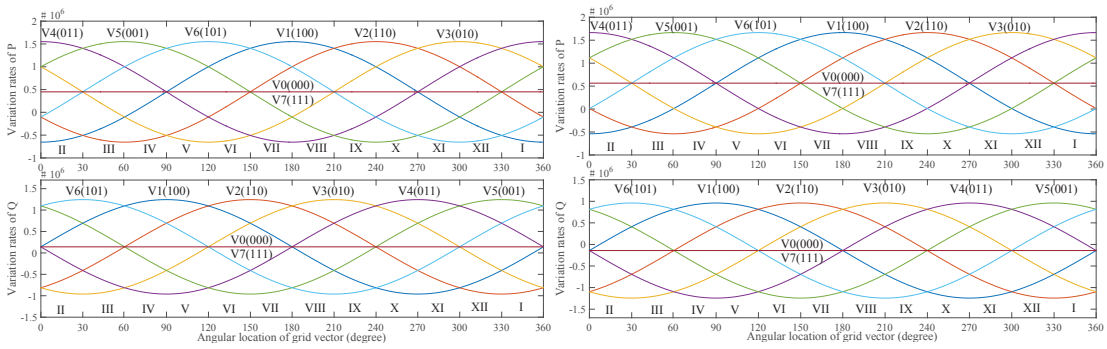

(a) **(b)**

Fig. 5.3. Active and reactive power variation rates by using each converter voltage vector throughout 12 different sectors. (a) P =450 W, Q =0 Var. (b) P =-450 W, Q =0 Var.

Firstly, taking sector V in Fig. 5.3(a) as an example, V_3, V_2, and V_7 are selected based on Table 5.1. It is seen that with such a voltage-vectors' sequence, the instantaneous active power can be regulated properly by combining selected vectors with their predicted duration times, since although V_2 and V_3 remain the active power decreased during the entire sector, V_7 could produce a positive active power variation during the whole sector V. By comparison, during the latter part of sector V, as illustrated in Fig. 5.3(a), all the three selected voltage vectors have a positive reactive power variation rate. Therefore, the instantaneous reactive power cannot be controlled properly with the positive values of predicted duration times. As a result, the negative duration time is

calculated to meet the instantaneous reactive power regulation. The same phenomena can also be observed in the other odd sectors in Fig. 5.3(a)

Similarly, as shown in Fig. 5.3(b), taking sector IV as an example, V_2, V_3, and V_0 are selected according to Table 5.1. Although active power could be regulated properly during the whole sector, the reactive power slope of each vector remains negative at the initial part of sector IV, which cannot be precisely controlled. Thus the negative duration time is calculated. The same phenomenon can be observed in the other even sectors in Fig. 5.3(b).

While for different reactive power outputs, Fig. 5.4(a) and (b) depict the variation rates of active/reactive powers using each voltage vector throughout the 12 sectors under the conditions that P is equal to -350 W, Q is equal to 200 Var and -200 Var, respectively, it can be seen that the same issues also exist, which results in negative duration time and control failure.

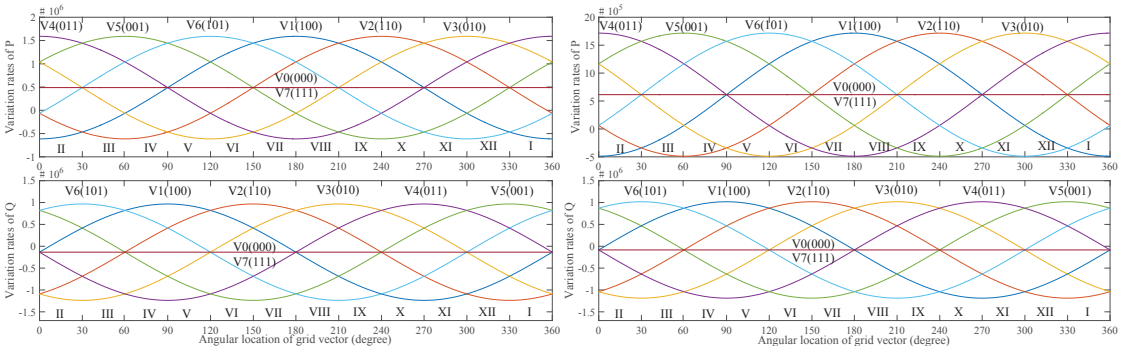

(a) **(b)**

Fig. 5.4. Active and reactive power variation rates by using each converter voltage vector throughout 12 different sectors. (a) P =-350 W, Q =200 Var. (b) P =-350 W, Q =-200 Var.

With CPDCC, predicted negative duration times will be forced to zero, resulting in control failure. Associated solutions have been proposed [5.18] with an improved sequence as shown in Table 5.2, which is based on the case study and analyses of power slope variation with different power status. The improved sequence as shown in Table 5.2 is used as an additional vector sequence table when the calculated t_b is negative. The vector is reselected based on the second vector sequence Table 5.2, after reselection of the none-zero vector, the corresponding power slopes are calculated again with (5.8), then the optimal durations are recalculated using (5.15), which means the whole control

algorithm is almost repeated once. It is no doubt that the control performance such as power ripple could be improved, while the hardware system with higher computing capacity is required because of the complexity of the algorithm

TABLE 5.2 Improved Voltage-vectors' sequences for predictive DPC [5.18]

Vector sequence	Sector number (S_n)											
	S_1	S_2	S_3	S_4	S_5	S_6	S_7	S_8	S_9	S_{10}	S_{11}	S_{12}
V_a	V_1	V_1	V_2	V_2	V_3	V_3	V_4	V_4	V_5	V_5	V_6	V_6
V_b	V_2	V_6	V_3	V_1	V_4	V_2	V_5	V_3	V_6	V_4	V_1	V_5
V_c	V_7	V_7	V_0	V_0	V_7	V_7	V_0	V_0	V_7	V_7	V_0	V_0

5.2.3 Proposed reversible predictive duty cycle control

The proposed reversible predictive duty-cycle-control method solves the issue of negative durations without repeating the calculation procedure. The selection of two adjacent vector pairs and the calculation of duration times is the same as the CPDCC method. However, while calculated duration time is negative for the none-zero vector, the reverse vector is selected and the positive value of that calculated could be applied without recalculation. The implementation time of the zero-vector is also verified to meet the boundary condition $t_a + t_b + t_c = T_s / 2$ .The principle is very simple in calculation and easy to implement. Theoretical analyses of the proposed method are presented as follows and the switching frequency reduction discussion and one-step-delay compensation method is applied.

A. Theoretical analyses

It can be concluded from (5.9) that

$$\begin{cases} V_{0\alpha} = V_{0\alpha} = V_{7\alpha} = V_{7\alpha} = 0 \\ V_{1\alpha} = -V_{4\alpha} \quad V_{1\beta} = -V_{4\beta} \\ V_{2\alpha} = -V_{5\alpha} \quad V_{2\beta} = -V_{5\beta} \\ V_{3\alpha} = -V_{6\alpha} \quad V_{3\beta} = -V_{6\beta} \end{cases} \tag{5.17}$$

Substituting (5.17) into (5.8), the power slope of the zero vector can be derived as follows,

$$\begin{cases} \delta_{p0} = \delta_{p7} = -\dfrac{R}{L}P - \omega Q + \dfrac{3}{2L}\left|\overline{e}\right|^2 \\ \delta_{q0} = \delta_{q7} = -\dfrac{R}{L}Q + \omega P \end{cases} \tag{5.18}$$

Taking V_1 and the reverse V_4 vector as an example, the power slope relations with the zero vector can be derived,

$$\begin{cases} \delta_{p1} = \delta_{p0} - \dfrac{3}{2L}\mathrm{Re}\left(\overline{e}\overline{V}_1^*\right) \\ \delta_{p4} = \delta_{p0} - \dfrac{3}{2L}\mathrm{Re}\left(\overline{e}\overline{V}_4^*\right) \\ \delta_{p1} + \delta_{p4} = 2\delta_{p0} \end{cases} \tag{5.19}$$

Similarly, for all the none-zero vectors, the relations of the original vector and corresponding reverse vector pair could be derived as follows.

$$\begin{cases} \delta_{p1} = 2\delta_{p0} - \delta_{p4} \quad \delta_{q1} = 2\delta_{q0} - \delta_{q4} \\ \delta_{p2} = 2\delta_{p0} - \delta_{p5} \quad \delta_{q2} = 2\delta_{q0} - \delta_{q5} \\ \delta_{p3} = 2\delta_{p0} - \delta_{p6} \quad \delta_{q3} = 2\delta_{q0} - \delta_{q6} \end{cases} \tag{5.20}$$

If the selected vector is V_a, its reverse vector is named as V_{-a} and the corresponding active and reactive power slope are δ_{-pa} and δ_{-qa}, respectively. Similarly, for V_b, its reverse vector is V_{-b} .the power slope relation of V_a, V_b and V_{-a}, V_{-b} could be derived as follows.

$$\begin{cases} \delta_{pa} = 2\delta_{p0} - \delta_{-pa} \quad \delta_{qa} = 2\delta_{q0} - \delta_{-qa} \\ \delta_{pb} = 2\delta_{p0} - \delta_{-pb} \quad \delta_{qb} = 2\delta_{q0} - \delta_{-qb} \end{cases} \tag{5.21}$$

While the calculated duration based on (5.15) has a negative value, for instance, t_a is negative, t_b is positive, then substitute δ_{pa} and δ_{qa} from (5.21) into (5.12),

$$\begin{cases} P_{err} = P^* - \left\{P^k + 2\left[(2\delta_{p0} - \delta_{-pa})t_a + \delta_{pb}t_b + \delta_{pc}t_c\right]\right\} \\ Q_{err} = Q^* - \left\{Q^k + 2\left[(2\delta_{q0} - \delta_{-qa})t_a + \delta_{qb}t_b + \delta_{qc}t_c\right]\right\} \end{cases} \tag{5.22}$$

Then, it could be written as follows,

$$\begin{cases} P_{err} = P^* - \left\{P^k + 2\left[\delta_{-pa}(-t_a) + \delta_{pb}t_b + \delta_{pc}(t_c + 2t_a)\right]\right\} \\ Q_{err} = Q^* - \left\{Q^k + 2\left[\delta_{-qa}(-t_a) + \delta_{qb}t_b + \delta_{qc}(t_c + 2t_a)\right]\right\} \end{cases} \tag{5.23}$$

Then the durations could be correspondingly rescheduled as follows without recalculation using equation (5.15), though the none-zero vector is reselected.

$$t_a^{'} = -t_a \quad t_b^{'} = t_b \quad t_c^{'} = t_c + 2t_a \tag{5.24}$$

It means that the reverse vector V_{-a} could be selected to replace V_a to achieve the positive duration time while $t_a < 0$, and the corresponding duration time is $-t_a$. Meanwhile, the duration of the zero vector is adjusted to be $t_c + 2t_a$ to ensure the dead-beat control performance. Similarly, while $t_b < 0$, the reverse vector V_{-b} should be selected to replace V_b to achieve the positive duration time. The vector reselection and corresponding duration times for different conditions are presented in Table 5.3.

It should be noted that although the duration time is rearranged, duration times for each vector still meet the following equation.

$$t_a^{'} + t_b^{'} + t_c^{'} = T_s / 2 \tag{5.25}$$

Thus, calculation of $t_c^{'}$ could be easily as follows under any conditions,

$$t_c^{'} = T_s / 2 - |t_a| - |t_b| \tag{5.26}$$

With the RPDCC method, the action time of the none-zero vector do not need to be forced to 0 or to $T_s / 2$, but remains its abstract value, resulting in improvement of system performance.

Compared with the IPDCC method, there is no need to recalculate the power slope of active power and reactive power. The recalculation of duration time using equation (5.15) is eliminated, though the none-zero vector is reselected. Thus the computation work and control complexity are reduced. Both the negative duration time of t_a and t_b can be adjusted, which could further improve the steady and dynamic performance.

TABLE 5.3 Voltage selection for proposed RPDCC

Selection	$t_a>0, t_b>0$	$t_a<0, t_b>0$	$t_a>0, t_b<0$	$t_a<0, t_b<0$
$t_a^{'}$	t_a	$-t_a$	t_a	$-t_a$
$t_b^{'}$	t_b	t_b	$-t_b$	$-t_b$
$t_c^{'}$	t_c	t_c+2t_a	t_c+2t_b	$t_c+2t_a+2t_b$
$V_a^{'}$	V_a	V_{-a}	V_a	V_{-a}
$V_b^{'}$	V_b	V_b	V_{-b}	V_{-b}

B. 3 + 3 Voltage-Vectors' Sequence

In the proposed method, three voltage vectors consisting of two none-zero vectors V_a and V_b and one zero vector V_c are applied within each control period T_s. To implement the three vectors, the 3 + 3 voltage-vectors' sequence is applied, as illustrated in Fig. 5.5. It can be seen that the second subsequence is totally symmetrical to the first one with reverse applying order. In this way, the power ripple is reduced when compared with the none-symmetrical vector sequence [5.19].

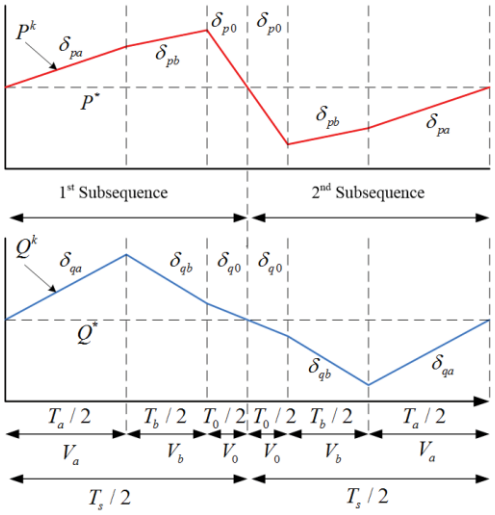

Fig. 5.5 Active and reactive power changes using 3 + 3 voltage-vectors' sequence

C. Vector Sequence and Switching Frequency Reduction Based on the Minimum-Switching-Loss Approach

With consideration of vector sequence to achieve minimal jumps between each of the vectors during implementation, the frequency reduction and lower switching loss can be

achieved. There are mainly two aspects regarding vector sequence after vector reselection of the proposed RPDCC method for switching frequency reduction.

Firstly, an appropriate zero vector to produce minimal switching jumps while switching between the none-zero vector and the null vector should be selected. For instance, if voltage vector “100” and “110” is selected as the two none-zero voltage vectors with the “110” as the second vector, the preferred zero voltage vector will be “111” rather than “000.” Secondly, sequence of two selected none-zero vectors should be exchanged dynamically to achieve minimal jumps between previous vector sequences in each period. For instance, if the vectors during the last cycle is with “100” at the end, while the vectors to be applied in next cycle are “110” and “010”, therefore “110” instead of “010” should be applied firstly. Obviously, the duration of each vector application should be changed in accordance with vector sequence change. Due to space limitations, the switching frequency reduction will not be fully discussed in this paper.

D. Design of One-step-delay compensation.

The one-step-delay compensation is different for the three-vectors-based approach. Thus the one step delay compensation is needed in the proposed method. Firstly, the converter voltage V is reconstructed from the applied active voltage vectors and corresponding durations as

$$V = V_a^{'} d_a^{'} + V_b^{'} d_b^{'} \tag{5.27}$$

Where $d_a^{'}=2t_a^{'}/T_s$ and $d_b^{'}=2t_b^{'}/T_s$, they are the duty ratio of the selected two none-zero vectors. By substituting (5.27) into (5.10), the prediction value P^{k+1} and Q^{k+1} at the (k+1)th instant could be achieved.

Then the values of P_i^{k+2} and Q_i^{k+2} can be derived for each none-zero voltage vector with P^{k+1} and Q^{k+1}, the equation for predicting P_i^{k+2} and Q_i^{k+2} are similar to (5.10), which are expressed as (5.28).

$$\begin{bmatrix} P_i^{k+2} \\ Q_i^{k+2} \end{bmatrix} = T_s \left(-\frac{R}{L}\begin{bmatrix} P_i^{k+1} \\ Q_i^{k+1} \end{bmatrix} + \omega \begin{bmatrix} -Q_i^{k+1} \\ P_i^{k+1} \end{bmatrix} + \frac{3}{2L}\begin{bmatrix} \left(|\vec{e}|^2 - \mathrm{Re}\left(\vec{e}\vec{V}_i^{*}\right)\right) \\ -\mathrm{Im}\left(\vec{e}\vec{V}_i^{*}\right) \end{bmatrix} \right) + \begin{bmatrix} P_i^{k+1} \\ Q_i^{k+1} \end{bmatrix} \tag{5.28}$$

The cost function used to calculate the optimal duration time could be revised

$$J = (P^* - P_i^{k+2})^2 + (Q^* - Q_i^{k+2})^2 \tag{5.29}$$

The control design of the proposed RPDCC method is illustrated schematically in Fig. 5.6.

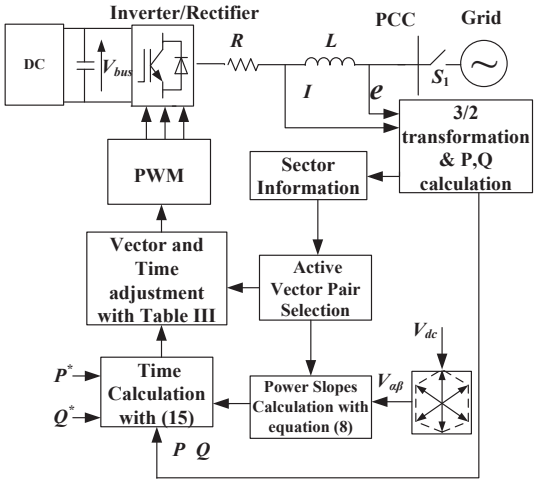

Fig. 5.6 Block diagram of the IPDCC for the AC/DC converter

5.3 Numerical Simulation and Experimental Verification

5.3.1 Numerical simulation

The AC/DC converter control with each control method has been numerically simulated using the MATLAB/Simulink tool. The electrical parameters used in the simulation are listed in Table 5.4.

TABLE 5.4 Electrical Parameter of Power Circuit

Resistance of reactor	R	510 mΩ
Inductance of reactor	L	4 mH
DC-bus capacitor	C	680 uF
Load resistance	R_L	34 Ω
Source voltage	e	36 V(peak)
Source voltage frequency	f	50 Hz
DC-bus voltage	V_{dc}	120 V

The compensation method proposed in previous Section is also applied for CPDCC in the following simulation and experiments. For convenience, the power flow from the

AC power supply to the DC load is defined as positive. It should be noted that the simulation results of each control method are in same simulation circumstance.

A. Steady state performance comparisons

To compare the steady-state performance, the AC three-phase input current and instantaneous active and reactive powers of the system are depicted to show the detailed performance of each control method. For a detailed analysis of different vector sequences and corresponding duration time calculation methods, the none-zero vector pair selection and calculated duration time are also presented. As we can see from Fig. 5.7, the active power reference remains at 450 W and reactive power reference remains at 0 Var. Both the active and reactive powers track their reference values with good accuracy and stability with each control method.

From Fig. 5.7(a), it can be seen that the ripples of both active and reactive powers are quite high with the CPDCC method. As shown, the P ripple is 19.82 W and Q ripple 17.34 Var. The current total harmonic distortion (THD) is as high as 6.46%. As we can see from Fig. 5.7(a), the none-zero vector pair selection is strictly according to the sector information based on Table 5.1. There is no adjustment at any circumstances. It is the negative value of duration time obtained by this method that causes the significant AC current notches and the active and reactive power pulsations. By comparison, with improved vector selection sequence, IPDCC reselects the none-zero vector V_b with Table 5.2 when the calculated duration time t_b is negative with the selected vector pair based on Table 5.1. The none-zero vector V_a remains the same as that of the CPDCC method, and then the duration time with the new vector V_b is recalculated, which almost eliminates the appearance of the negative value of t_b. Therefore, it can achieve much better results than that by the CPDPC method. For example, the THD is significantly decreased to 2.26%, the P ripple is significantly reduced to 8.92 W, and

the Q ripple to 5.51 Var, as shown in Fig. 5.7(b), which validates the superiority of the IPDCC method.

With the proposed RPDCC method, the steady state performance can be further improved without recalculating the duration time. The reverse vector of the original selected vector based on Table 5.1 is selected whenever there exits a negative duration time, and thus, the selection of both vectors V_a and V_b could be adjusted. As shown in Fig. 5.7(c), the current THD is further decreased to only 1.71% with the MPDCC-I method and the current waveform is more sinusoidal compared with that by the IPDCC control. The active and reactive power ripples are further decreased to 6.06 W and 4.64 Var, respectively.

For bidirectional power flow, the steady-state performance at P=-350 W and Q=200 Var with each method is compared. As can be seen from Fig. 5.8, similar results could be achieved. The quantitative comparison of steady state performance including of current THD and active and reactive power ripple are presented in Table 5.5.

In conclusion, both the IPDCC and RPDCC control method can improve the steady-state performance significantly when compared with CPDCC method, and RPDCC has the best steady-state performance.

B. Dynamic state performance comparisons

For dynamic-state performance comparison, transient responses of active and reactive powers under step change with each method are numerically simulated, as shown in Fig. 5.9. The active power reference value steps up from 250 W to 450 W at 0.01 s while the reactive power reference remains at 350 Var at the beginning, and is changed to -300 Var at 0.03 s.

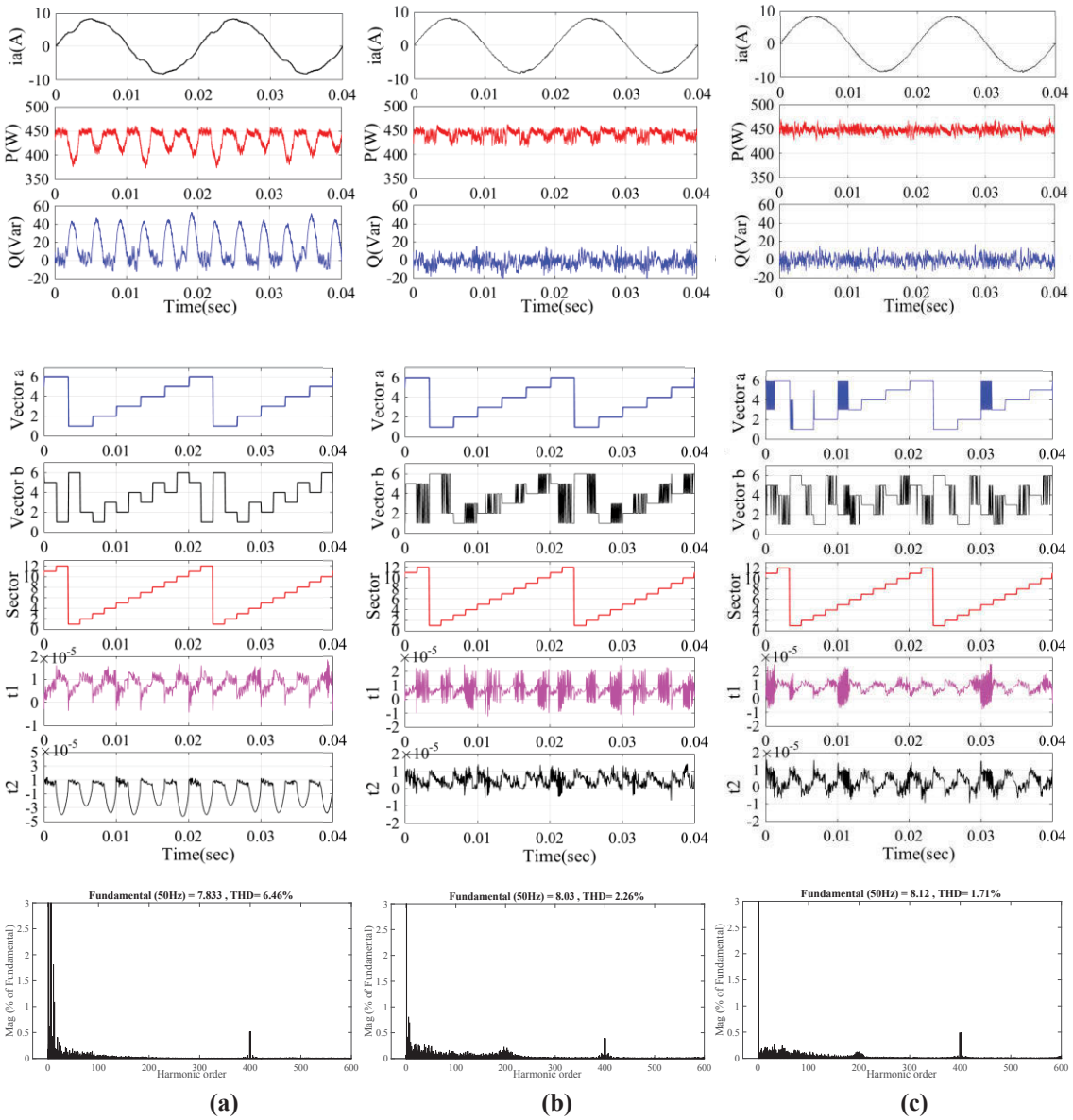

Fig.5.7 Steady-state performance at *P*=450 W, *Q*=0 Var. Top to bottom: i_a, *P* and *Q*, $V_a^{'}$, $V_b^{'}$, sector, t_a, t_b, THD analyses of i_a, (a) PDPC, (b) IPDCC, and (c) RPDCC

For each control method, both the active and reactive powers can track their reference values with good accuracy and stability, showing good dynamic response. There also exist some apparent differences between these methods. For instance, at 0.01 s when *P* has a step change, the dynamic response time with the PDPC method and IPDCC method is quite high in comparison with the RPDCC method as shown in Fig. 5.9. Meanwhile, the *Q* overshoot when *P* has a step change and *P* overshoot when *Q* has a step change are also reduced with the RPDCC method, especially at 0.03 s in Fig. 5.9. The quantitative comparisons of dynamic performance are presented in Table 5.5.

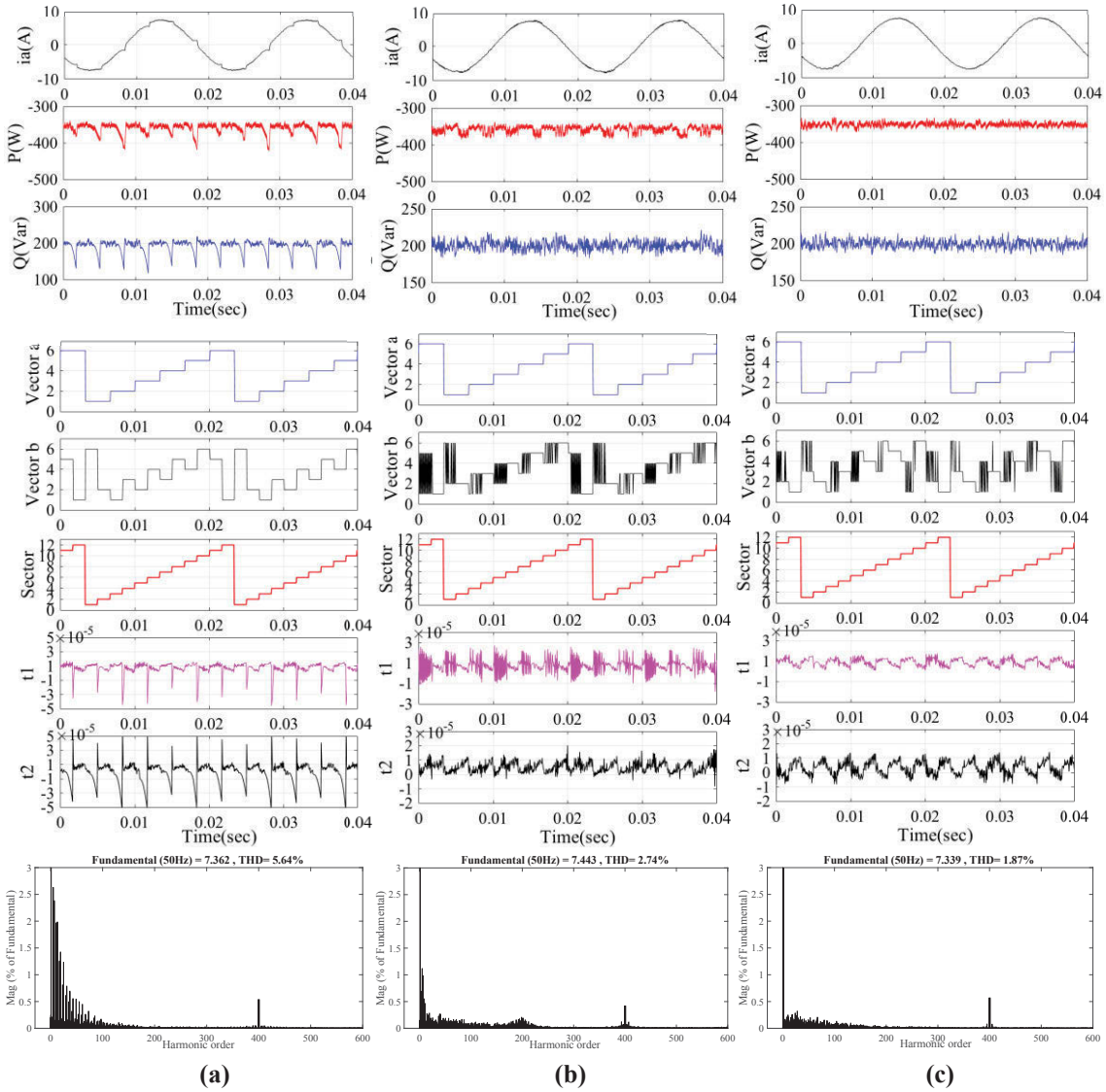

Fig.5.8 Steady-state performance at *P*=-350 W, *Q*=200 Var. Top to bottom: i_a, *P* and *Q*, $V_a^{'}$, $V_b^{'}$, sector, t_a, t_b, THD analyses of i_a, (a) PDPC, (b) IPDCC, and (c) RPDCC

In conclusion, the proposed RPDCC is the best one among these control methods when considering the steady-state and dynamic-state performance at the same time, while the complexity of the control algorithm is reduced in comparison with the IPDCC method.

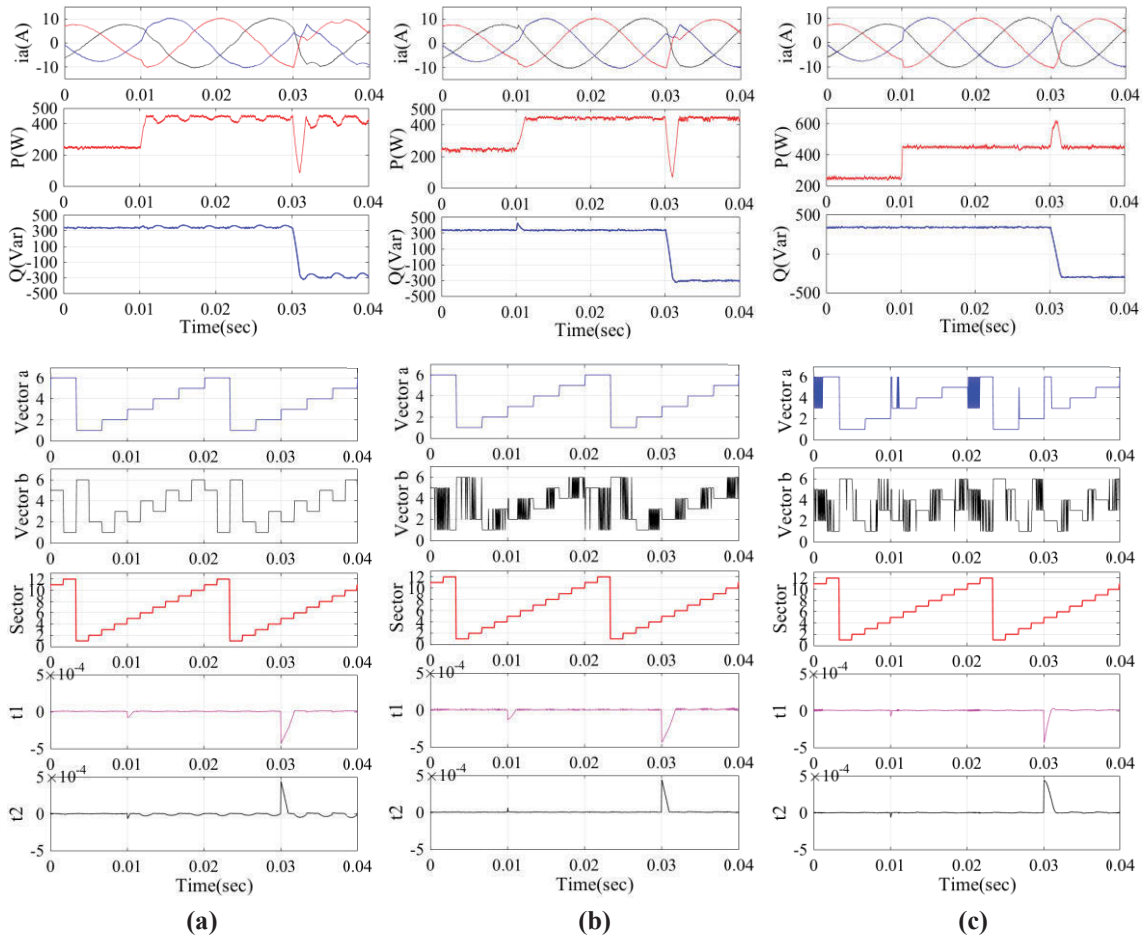

Fig. 5.9 Dynamic-state performance comparison, Top to bottom: i_a, *P* and *Q*, $V_a^{'}, V_b^{'}$, sector, t_a, t_b, where (a) PDPC, (b) IPDCC, and (c) RPDCC

TABLE 5.5 Quantitative comparison of simulation results

Control method	*P=450 W Q=0 Var*			*P=-350 W Q=200 Var*			*Response (at 0.01 s)*	*Over shoot*	*Response (at 0.03 s)*	*Over shoot*
	THD(%)	*Prip* (W)	*Qrip*(Var)	*THD(%)*	*Prip* (W)	*Qrip* (Var)	*Time*(s)	*Q*(Var)	*Time*(s)	*P*(W)
PDCC	6.46	19.82	17.34	5.64	14.17	17.05	0.001	25	0.0017	370
IPDCC	2.26	8.92	5.51	2.74	9.30	5.49	0.0012	79	0.0021	380
NIPDCC	1.71	6.06	4.64	1.87	5.59	4.77	0.00015	22	0.0014	171

5.3.2 Experimental Verification

To verity the effectiveness of the proposed methods, a scaled down prototype is constructed. The system parameter is presented in Table 5.6. The comparison is also divided into steady state comparison and dynamic response comparison.

TABLE 5.6 Electrical parameter of prototype

Resistance of reactor	R	500mΩ
Inductance of reactor	L	22 mH
DC-bus capacitor	C	680 uF
Load resistance	R_L	34 Ω
Source line voltage	e	120 V
Sampling frequency	fs	20kHz
Source voltage frequency	f	50 Hz

A. Comparison of steady-state performance

To compare the steady state performance of each control method, the THD, ripples of active and reactive powers at the steady state of P being equal to 450 W and Q equal to 0 Var have been measured and calculated with each control method. The sampling frequency for each method is the same at 10 kHz.

Fig. 5.10 shows the input phase to phase voltages, V_{ab} and V_{bc}, and input currents, i_a and i_b, of each control method. The detailed analyses have been presented based on the experimental data acquired from oscilloscope to PC, such as the instant active power, reactive power, and harmonic spectra analyses of i_b.

The active and reactive powers can track their reference values successfully with each control method, while the steady-state performance varies significantly. With the PDCC method, the ripples of P and Q are 36.88 W and 38.03 Var, respectively, and the current THD is 7.69% as shown in Fig. 5.10(a). By comparison, the performance is much improved with IPDCC as shown in Fig. 5.10(b). The power ripples and THD are decreased dramatically, which aligns well with the theoretical analyses. With the proposed RPDCC, the current THD is further decreased to 4.64%, and the reactive power ripples are also decreased obviously to 22.08 Var by comparison to the IPDCC method, which verifies the simulation results well. The steady state of P equal to 200 W and Q being equal 350 Var are also presented as shown in Fig. 5.11, and the quantitative comparisons of each control method is presented in Table IV.

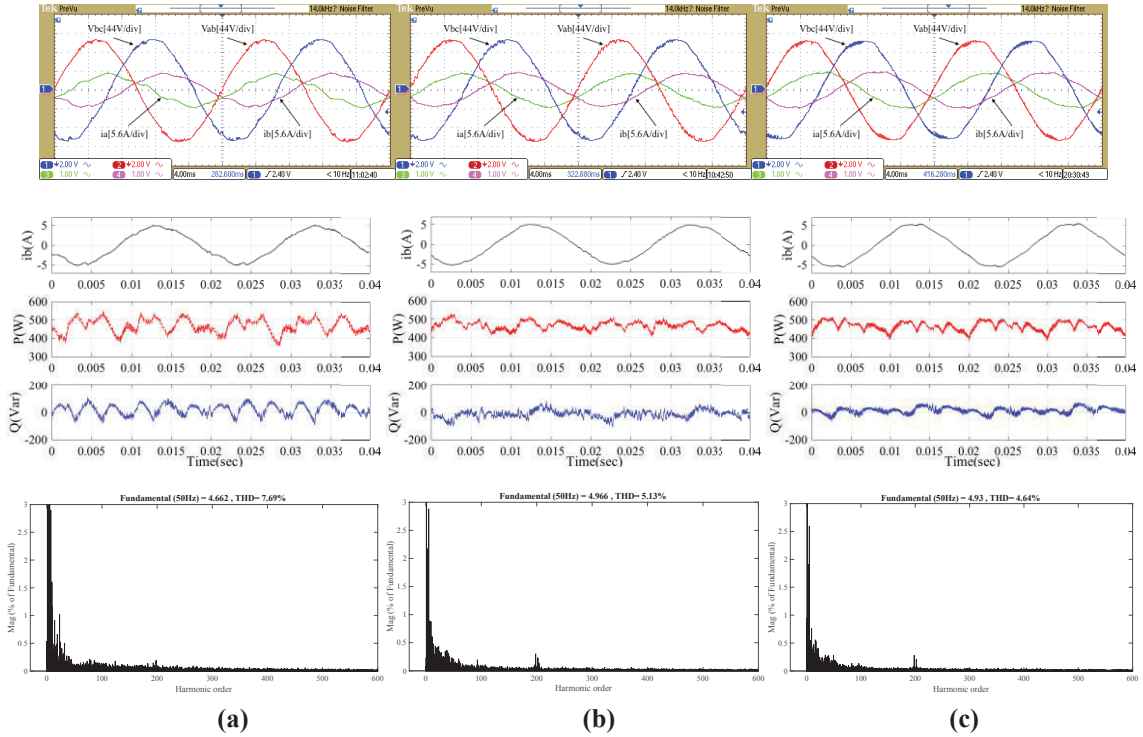

(a) (b) (c)

Fig. 5.10. Steady-state performance at *P*=450 W, *Q*=0 Var; From top to bottom, experimental figure, i_b, *P* and *Q*, THD of i_b, where (a) PDPC, (b) IPDCC, and (c) RPDCC

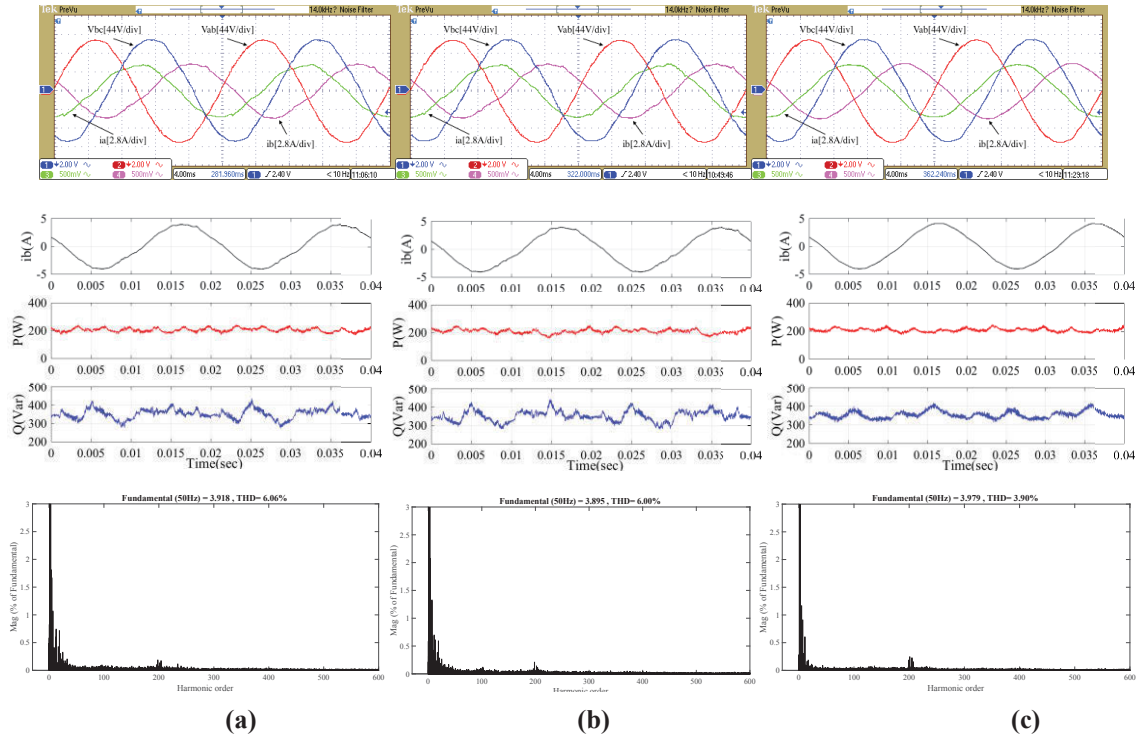

(a) (b) (c)

Fig.5.11. Steady-state performance at *P*=200 W, *Q*=350 Var; From top to bottom, experimental figure, i_b, *P* and *Q*, THD of i_b, where (a) PDPC, (b) IPDCC, and (c) RPDCC

B. Comparison of dynamic-state performance

The dynamic performance of each method is also compared comprehensively with a series of experimental results. Firstly, the active power steps change from 250 W to 450 W, while the reactive power remains at 350 Var.

Fig. 5.12 shows the experimental results of dynamic performance for each control method. It is shown that each method tracks the reference value accurately with similar quick response during the dynamic instant, which validates the reference tracking ability of the proposed RPDCC method. However, it is seen that the response time is quite different between these methods. As shown in Fig. 5.12(a), the response time when P changes from 250 W to 450 W at 0.1 s is 0.0051 s and it decreases to 0.0015 s with the IPDCC method. However, with the proposed RPDCC method, it is further decreased to only 0.0008 s, as can be seen from Fig. 5.12(c), which validates the superiority of dynamic response in comparison with the conventional methods. The quantitative comparisons of each control method are presented in Table 5.7.

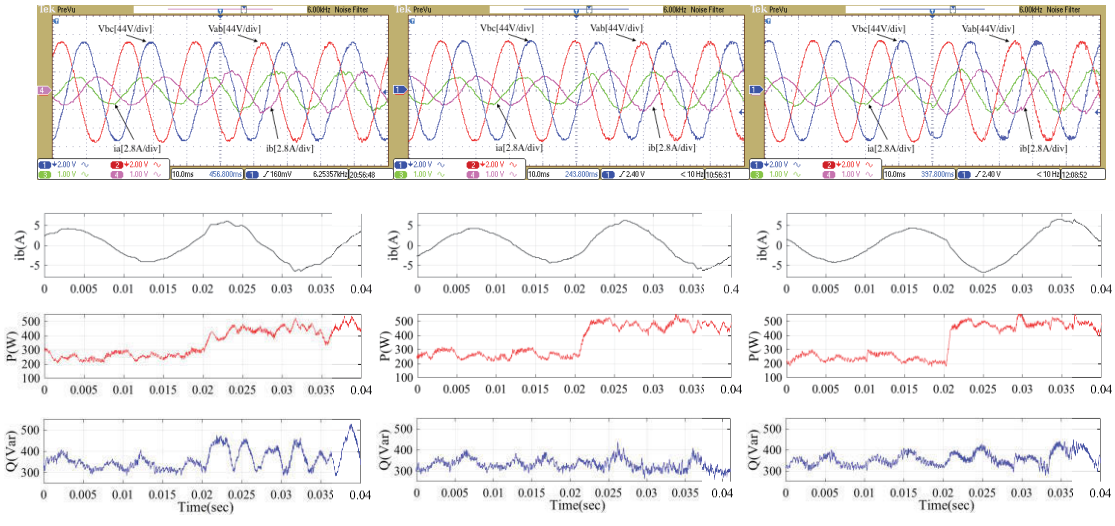

Fig.5.12. Dynamic-state performance when P changes from 250 W to 450 W, Q=300 Var; Top: Experimental figure; Bottom: i_b, P and Q; where (a) PDPC, (b) IPDCC, and (c) RPDCC

C. System parameter redundancy.

The robustness of the proposed RPDDC is examined through a series of experiments while the line inductance has different value with the real one. As shown in Fig. 5.13(a), when the inductance used in the control from 50% to 200% of the real one (20 mH) are applied for comparison, the active and reactive powers ripples increase and the positive offset in the reactive power appears. However, if the inductance used in the control increases to 30 mH and 40 mH, there is slight influence on the reactive power ripple and positive offset in the active power appears, as shown in Fig. 5.13(c) and (d), respectively. The results indicate that the accuracy of inductance has a slight influence on the steady state performance of the proposed RPDDC while the system stability is not influenced at least in the range of -50% and 100% inductance variations.

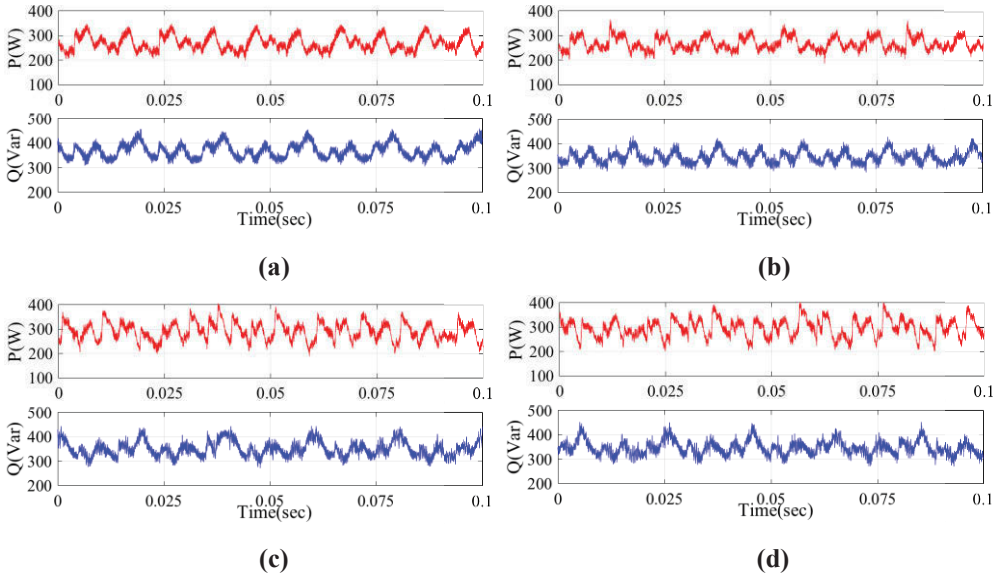

Fig. 5.13 Responses of active power and reactive power for proposed RPDDC when the actual inductance in control differs from the real value; (a) 10 mH, (b) 20 mH, (c) 30 mH, and (d) 40 mH

TABLE 5.7 Quantitative comparisons of experimental results

Control	*P=450 W Q=0 Var*			*P=200 W Q=350 Var*			*Response*
	THD(%)	*Prip* (W)	*Qrip*(Var)	*THD*(%)	*Prip* (W)	*Qrip* (Var)	*Time*
CPDCC	7.69	36.88	38.03	6.06	14.34	26.6	0.0051
IPDCC	5.13	22.54	27.7	6.0	15.18	27.57	0.0015
RPDCC	4.64	24.86	22.08	3.9	12.08	19.57	0.0008

5.4 Summary of the Chapter

This chapter proposes a novel predictive duty-cycle-control strategy of three-phase AC/DC converters with improved performance. In comparison with CPDCC, the reverse none-zero vector is selected with RPDCC when the calculated duration time is negative. Differing from IPDCC, the reselection of none-zero voltage vector pair using a second switching table is avoided and recalculation of duration time with the new vector pair is eliminated. Duration time only needs to be calculated once, which is a simple algorithm for application. The principles of vector pair selection, theoretical analyses of duration calculation and control delay compensation design are fully discussed.

Comprehensive comparisons by simulation and experimental results are conducted to compare the performance of proposed RPDCC with conventional methods. The results validate the superior dynamic and steady state performance of the proposed RPDCC method. While the IPDCC method can improve the steady state performance by decreasing power ripples and current THD in comparison with the CPDCC method, the proposed RPDCC achieves even better steady-state performance with a simpler algorithm. In terms of dynamic state performance, the RPDCC method also has better performance in relation to dynamic response time and power overshoot when compared with the CPDCC and IPDCC methods.

REFERENCES

[5.1] S.Vazquez, J.A.Sanchez, J.M.Carrasco, J.I.Leon, and E.Galvan, "A model-based direct power control for three-phase power converters," *IEEE Trans. Ind. Electron.*, vol. 55, no. 4, pp. 1647–1657, Apr. 2008

[5.2] P. Antoniewicz and M. P. Kazmierkowski, "Virtual flux predictive direct power control of three phase AC/DC converter," in *Proc. Human Syst.Interactions*, 2008, pp. 510–515

[5.3] S. Vazquez *et al.*, "Model predictive control: A review of its applications in power electronics," *IEEE Ind. Electron. Mag.*, vol. 8, no. 1, pp. 16–31, Mar. 2014

[5.4] C. Xia, T. Liu, T. Shi, and Z. Song, "A simplified finite-control-set model- predictive control for power converters," *IEEE Trans. Ind. Informat.*, vol.10, no. 2, pp. 991–1002, May 2014

[5.5] R. Aguilera, P. Lezana, and D. Quevedo, "Finite-control-set model predictive control with improved steady-state performance," *IEEE Trans. Ind. Informat*., vol. 9, no. 2, pp. 658 –667, May 2013

[5.6] S. Kwak, U.-C. Moon, and J.-C. Park, "Predictive-control-based direct power control with an adaptive parameter identification technique for improved AFE performance," *IEEE Trans. Power Electron.*, vol. 29, no. 11, pp. 6178–6187, Nov. 2014

[5.7] J. Rodriguez, M. P. Kazmierkowski, J. R. Espinoza, P. Zanchetta, H. Abu-Rub, H. A. Young, and C. A. Rojas, "State of the art of finite control set model predictive control in power electronics," *IEEE Trans. Ind. Informat.*, vol. 9, no. 2, pp. 1003–1016, May 2013

[5.8] J. Hu, J. Zhu, G. Platt, and D. G. Dorrell, "Multi-objective model-predictive control for high powerconverters," *IEEE Trans. Energy Convers.,* vol. 28, no. 3, pp. 652-663, Sep. 2013

[5.9] D. E. Quevedo, R. P. Aguilera, M. A. Perez, P. Cortes, and R. Lizana, "Model predictive control of an AFE rectifier with dynamic references," *IEEE Trans. Power Electron.*, vol. 27, no. 7, pp. 3128–3136, Jul. 2012

[5.10] P. Cortes, J. Rodriguez, C. Silva, and A. Flores, "Delay compensation in model predictive current control of a three-phase inverter," *IEEE Trans. Ind.Electron.*, vol. 59, no. 2, pp. 1323–1325, Feb. 2012

[5.11] S. Kouro, P. Cortes, R. Vargas, U. Ammann, and J. Rodriguez, "Model predictive control—A simple and powerful method to control power converters," *IEEE Trans. Ind. Electron*., vol.56, no. 6, pp. 1826–1838, Jun. 2009

[5.12] A. Bouafia, J.-P. Gaubert, and F. Krim, "Predictive direct power control of three-phase pulse width modulation (PWM) rectifier using space-vector modulation (SVM)," *IEEE Trans. Power Electron*., vol. 25, no. 1, pp. 228–236, Jan. 2010

[5.13] R. Portillo, S. Vazquez, J. I. Leon, M. M. Prats, and L. G. Franquelo, "Model based adaptive direct power control for three-level NPC converters," *IEEE Trans. Ind. Inform*.,vol. 9, no. 2, pp. 1148–1157, May 2013

[5.14] S. Kwak and J.-C. Park, "Switching strategy based on model predictive control of VSI to obtain high efficiency and balanced loss distribution," *IEEE Trans. Power Electron.*, vol. 29, no. 9, pp. 4551–4567, Sep. 2014

[5.15] S. Aurtenechea, M. A. Rodriguez, E. Oyarbide, and J. R. Torrealday, "Predictive control strategy for DC/AC converters based on direct power control," *IEEE Trans. Ind. Electron.*, vol. 54, no. 3, pp. 1261–1271, Jun. 2007

[5.16] P. Antoniewicz and M. P. Kazmierkowski, "Virtual-flux-based predictive direct power control of AC/DC converters with online inductance estimation," *IEEE Trans. Ind. Electron*, vol. 55, no. 12, pp. 4381–4390, Dec. 2008

[5.17] R. P. Aguilera, D. E. Quevedo, S. Vazquez, and L. G. Franquelo, "Generalized predictive direct power control for AC/DC converters," in *Proc. ECCE Asia 2013*, Jun., pp.1215–1220

[5.18] J. Hu and Z. Q. Zhu, "Investigation on switching patterns of direct power control strategies for grid-connected DC–AC converters based on power variation rates," *IEEE Trans. Power Electron*., vol. 26, no. 12, pp. 3582–3598, Dec. 2011

[5.19] J. Hu and Z. Zhu, "Improved voltage-vector sequences on dead-beat predictive direct power control of reversible three-phase grid-connected voltage-sourced converters," *IEEE Trans. Power Electron.*, vol. 28, no. 1, pp. 254–267, Jan. 2013

[5.20] Z. Song, W. Chen, and C. Xia, "Predictive direct power control for three-phase grid-connected converters without sector information and voltage vector selection," *IEEE Trans. Power Electron.*, vol. 29, no. 10, pp. 5518–5531, Oct. 2014

[5.21] Z. Song, Y. Tian, W. Chen, Z. Zou, and Z. Chen, "Predictive duty cycle control of three-phase active-front-end rectifiers," *IEEE Trans. Power Electron*., vol. 31, no. 1, pp. 698–710, Jan. 2016

[5.22] Y. Zhang, Y. Peng, and H. Yang, "Performance improvement of two-vectors-based model predictive control of PWM rectifier," *IEEE Trans. Power Electron.*, vol. 31, no. 8, pp. 6016–6030, 2016

[5.23] D. Choi, K. Lee, "Dynamic performance improvement of AC/DC converter using model predictive direct power control with finite control set." *IEEE Trans. Ind. Electron.,* vol. 62, pp. 757-767, 2015

[5.24] Y. Zhang, W. Xie, Z. Li, and Y. Zhang, "Low-complexity model predictive power control: Double-vector-based approach," *IEEE Trans. Ind. Electron.*, vol. 61, no. 11, pp. 5871–5880, 2014

[5.25] Y. Zhang and Y. Peng, "Model predictive current control with optimal duty cycle for three-phase ac/dc converters," in *IEEE International Power Electronics and Application Conference and Exposition*, 2014, pp. 837–842

[5.26] Y. Zhang, W. Xie, Z. Li, and Y. Zhang, "Model predictive direct power control of a PWM rectifier with duty cycle optimization," *IEEE Trans. Power Electron.*, vol. 28, no. 11, pp. 5343–5351, Nov. 2013

Chapter 6

MODEL PREDICTIVE CONTROL BASED DUTY CYCLE CONTROL WITH MUTUAL INFLUENCE ELIMINATION AND SIMPLIFIED CALCULATION

6.1 Introduction

Due to a limited number of available converter states and only one switching vector selected in one sampling period, the conventional model predictive control based direct power control (MPDPC) results in a variable switching frequency and the spread spectrum nature of harmonics inherent with the strategy thereby complicating filter design [6.1]-[6.8]. To overcome the disadvantages of conventional MPDPC, in the last chapter, the conventional predictive duty cycle control (CPDCC) method with the three vectors based approach and corresponding improved predictive duty cycle control (IPDCC) are discussed comprehensively. In order to solve the calculated negative duration time of CPDCC and high control complexity, the reversible predictive duty cycle control (RPDCC) method is proposed, which further improves the dynamic and steady state performance without increasing the control complexity. However, there are still some inherent disadvantages that cannot be ignored. Firstly, the mutual influence of two control objectives cannot be eliminated by using the above control methods, and this mutual influence issue is more likely to occur particularly in higher power systems, which is difficult to solve. Secondly, the calculated negative duration time cannot be totally eliminated with IPDCC and RPDCC, as it means incorrect vector selection should also exist, which results in performance deterioration [6.9]-[6.15]. Thirdly, the computational burden is still high with the least square error minimization method for duration time calculation, since it is very complex requiring a power slope calculation and least square minimization. The hardware system is required to have higher

computing capacity to due to complexity of the control algorithm. These methods can only work well with the three vector based approach, which limits the application to a two vector based approach.

To solve these issues, in this chapter, the model predictive control (MPC) is applied for vector selection instead of using the sector information and the novel simplified calculation method of duty cycle is proposed. Firstly, the MPC based vector selection is implemented without using the sector information to avoid incorrect vector selection since the future behavior is taken into account. Then, the previously proposed mutual influence method in Chapter 4 is integrated in the MPC based vector selection to eliminate the mutual influence, as MPC has the flexibility to include other constraints in the controller. In addition, the proposed simplified duty cycle calculation method is applied to reduce the computational burden and eliminate the negative duration time. The proposed reverse vector selection method could also be integrated with the model predictive based method by using the conventional power error minimization method for duration time calculation, which has been verified to have universality. The improved space vector modulation (SVM) based DPC (SVMDPC) has also been analyzed and discussed [6.16], which can be used as a bench mark for performance comparison.

Firstly, the two-vector based predictive control with simplified calculation is proposed and compared with the conventional two vector based approach. Then, the improved SVMDPC is analyzed and compared with the proposed three vector based approach with mutual influence elimination. The comprehensive comparisons using various methods by simulation and experimental results are conducted.

6.2 Model Predictive based Duty Cycle Control – Two Vector Based Approach

6.2.1 Conventional two vector based approach

The conventional two-vector based model predictive duty cycle control (MPDCC) proposed in [6.17] is discussed below. The duty cycles of the best none-zero and zero

vectors are computed based on the selected active voltage vectors and corresponding power slopes.

According to the converter model equation in Chapter 5, at the end of the sampling period T_s, the predicted active and reactive powers for each converter switching state can be expressed as:

$$\begin{bmatrix} P_i^{k+1} \\ Q_i^{k+1} \end{bmatrix} = T_s \left(-\frac{R}{L} \begin{bmatrix} P_i^k \\ Q_i^k \end{bmatrix} + \omega \begin{bmatrix} -Q_i^k \\ P_i^k \end{bmatrix} + \frac{3}{2L} \begin{bmatrix} \left(|\bar{e}|^2 - \mathrm{Re}\left(\bar{e}\bar{V}_i^* \right) \right) \\ -\mathrm{Im}\left(\bar{e}\bar{V}_i^* \right) \end{bmatrix} \right) + \begin{bmatrix} P_i^k \\ Q_i^k \end{bmatrix} \tag{6.1}$$

The power slope can be derived as:

$$\begin{cases} \dfrac{dP_i}{dt} = -\dfrac{R}{L} P - \omega Q + \dfrac{3}{2L} |\bar{e}|^2 - \dfrac{3}{2L} \mathrm{Re}\left(\bar{e}\bar{V}_i^* \right) \\ \dfrac{dQ_i}{dt} = -\dfrac{R}{L} Q + \omega P - \dfrac{3}{2L} \mathrm{Im}\left(\bar{e}\bar{V}_i^* \right) \\ \delta_{pi} = \dfrac{dP_i}{dt} \quad \delta_{qi} = \dfrac{dQ_i}{dt} \end{cases} \tag{6.2}$$

For the conventional MPDCC with the two vector approach, the difference of active and reactive powers with respect to a referenced value of each converter's switching state is compared and the vector leading to a minimum value of the specific cost function defined as

$$j_i = (P^* - P_i^{k+1})^2 + (Q^* - Q_i^{k+1})^2 \quad (i = 1,2,3,4,5,6) \tag{6.3}$$

is selected as the best none-zero vector.

By comparison, for CPDCC, two adjacent none-zero vectors are selected according to the sector location of the grid voltage vector. Assuming the power slopes are constant for a small sampling period, the active and reactive powers at the end of the sampling period can be predicted as

$$\begin{cases} P^{k+1} = P^k + \delta_{pa} t_a + \delta_{pb} t_b \\ Q^{k+1} = Q^k + \delta_{qa} t_a + \delta_{qb} t_b \end{cases} \tag{6.4}$$

where δ_{pa} and δ_{pb} are the active power slopes of the none-zero voltage vectors and zero voltage vector, and δ_{pa} and δ_{pb} the reactive power slopes, t_a and t_b the corresponding durations of none-zero voltage vector and zero vector, and they satisfy

the boundary condition $t_a + t_b = T_s$. To implement MPDCC, optimal duty ratios should be calculated. The error between the predicted and reference values can be calculated by

$$\begin{cases} P_{err} = P^* - \left(P^k + \delta_{pa} t_a + \delta_{pb} t_b \right) \\ Q_{err} = Q^* - \left(Q^k + \delta_{qa} t_a + \delta_{qb} t_b \right) \end{cases} \tag{6.5}$$

where P^* and Q^* are the active and reactive power references, respective. Then, the conventional least square optimization method [6.17]-[6.19] can also be utilized for MPDCC in order to minimize the power errors, as

$$\begin{cases} J = P_{err}^2 + Q_{err}^2 \\ \dfrac{\partial J}{\partial t_a} = 0 \end{cases} \tag{6.6}$$

Finally, the optimal application durations can be obtained as the following

$$\begin{cases} t_a = \dfrac{(P^* - P^k)(\delta_{pa} - \delta_{pb}) + (Q^* - Q^k)(\delta_{qa} - \delta_{qb}) + T_s(\delta_{pb}^2 + \delta_{qb}^2 - \delta_{pa}\delta_{pb} - \delta_{qa}\delta_{qb})}{(\delta_{pa} - \delta_{pb})^2 + (\delta_{qa} - \delta_{qb})^2} \\ t_b = T_s - t_a \end{cases} \tag{6.7}$$

Once t_a and t_b are calculated, the switch duty cycles can be obtained and the switch signals are generated. It should be noted that the calculated value of the voltage vector action time based on (6.7) may be negative or greater than T_s. The common practice is normally to force the action time to zero whenever a negative value is obtained or to T_s when the calculated time is greater than T_s, resulting in control failures and performance deterioration, which is similar as in Chapter 5. By using MPDCC, the power ripples can be reduced and a constant switching frequency can be obtained.

6.2.2 Simplified model predictive based duty cycle control

To simplify the duty cycle calculation, this chapter proposes a method that allocates a fraction of duty cycle in relation to the cost function, resulting to the none-zero vector

which is selected based on the MPC method, meanwhile a zero vector is utilized for the rest of the time. The principle of the simplified model predictive based duty cycle control (SMPDCC) to obtain the duty cycle is very simple in calculation and implementation. Meanwhile, the negative value of duration time is fundamentally avoided.

A. Principle of proposed SMPDCC

The proposed SMPDCC method is based on the MPC method to select the best none-zero vector and apply the none-zero and zero vectors with the novel duty cycle calculation principle without calculating the power slope of the two vectors. The best none-zero vector V_i that achieving the minimum cost function, J_i, is selected according to

$$J_i = \left|P^* - P_i^{k+1}\right| + \left|Q^* - Q_i^{k+1}\right| \ (i = 1,2,3,4,5,6) \tag{6.8}$$

Using the cost function value of the none-zero and zero vectors based on (6.8), the duration time can be directly calculated by

$$\begin{cases} k\left(\dfrac{1}{J_i} + \dfrac{1}{\lambda J_0}\right) = T_s \\ t_a = k\dfrac{1}{J_i} \quad t_b = k\dfrac{1}{\lambda J_0} \end{cases} \tag{6.9}$$

where λ is added to balance the ratio of J_0 and J_i for the duration time calculation. Usually when λ is selected in the range between 1 and 2, the system can achieve better dynamic and steady state performance. When λ is infinitely large, the control is the same as the conventional single vector based MPC method since t_b is near 0, meaning only the best vector is applied during each control period.

The corresponding duty cycles for each vector can be easily derived as

$$\begin{cases} d_a = \dfrac{\lambda J_0}{J_i + \lambda J_0} & t_a = d_a T_s \\ d_b = \dfrac{J_i}{J_i + \lambda J_0} & t_b = d_b T_s \end{cases} \tag{6.10}$$

where d_a and d_b are the duty ratio of selected none-zero and zero vectors. It should be noted that the duty cycle is simply calculated by (6.10) and directly controlled to implement the corresponding vector. Thus, the calculation of the slopes of active and reactive powers for the two vector is eliminated, which can reduce the computational burden and is simple for application. Besides, since t_a and t_b are definitely in the range of 0 to T_s in proportion with the reciprocal values of J_i and λJ_0, respectively, there is no need to do a further normalized approximation. Comparatively, the calculated value of the voltage vector action time based on the conventional MPDCC method may be outside the range of 0 to T_s during the dynamic instant and the duration time is consequently forced to zero or to T_s, resulting in control failures and performance deterioration.

B. Vector sequence and switching frequency reduction

With consideration of vector sequence to achieve minimal jumps between each of the vectors during implementation, the switching frequency and switching loss can be reduced effectively. There are mainly two aspects regarding the vector sequence for switching frequency reduction. The first one is to select an appropriate zero vector to produce minimal switching jumps while switching between the none-zero and zero vectors. For instance, if the voltage vector “100” is selected as the best active voltage vector, the best voltage vector will be “000” rather than “111”.

Another one is to exchange the sequence of none zero and zero vectors dynamically to ensure minimal jumps between the previous vector sequences. For instance, if the vectors during the last cycle is the zero vector “111” at the end, then the zero vector firstly applied and the same zero vector “111” should be selected in the next cycle to decrease the switching frequency.

C. Design of one-step-delay compensation

The influence of one-step-delay should not be disregarded for the proposed control approach. Thus, the one step ahead prediction is required for the model predictive based control method.

Firstly, the converter voltage V_i is reconstructed from the applied active voltage vectors and the corresponding durations is

$$V_i = V_a d_a \tag{6.11}$$

where $d_a = t_a / T_s$ and $d_b = t_b / T_s$, being the duty ratio of the selected two none-zero vectors. By substituting (6.11) into (6.1), the prediction values of P^{k+1} and Q^{k+1} at the ($k+1$)th time instant could be achieved.

The values of P_i^{k+2} and Q_i^{k+2} can be calculated for each none-zero voltage vector with initial states of P^{k+1} and Q^{k+1}. The equation for predicting P_i^{k+2} and Q_i^{k+2} are

$$\begin{bmatrix} P_i^{k+2} \\ Q_i^{k+2} \end{bmatrix} = T_s \left(-\frac{R}{L} \begin{bmatrix} P_i^{k+1} \\ Q_i^{k+1} \end{bmatrix} + \omega \begin{bmatrix} -Q_i^{k+1} \\ P_i^{k+1} \end{bmatrix} + \frac{3}{2L} \begin{bmatrix} \left(|\bar{e}|^2 - \mathrm{Re}\left(\bar{e} \bar{V}_i^* \right) \right) \\ -\mathrm{Im}\left(\bar{e} \bar{V}_i^* \right) \end{bmatrix} \right) + \begin{bmatrix} P_i^{k+1} \\ Q_i^{k+1} \end{bmatrix} \tag{6.12}$$

The cost function to select the best vector could be revised as

$$J_i = \left| P^* - P_i^{k+2} \right| + \left| Q^* - Q_i^{k+2} \right| (i = 0,1,2,3,4,5,6) \tag{6.13}$$

Finally, substituting P_i^{k+2} and Q_i^{k+2} into (6.13), the voltage vector pair minimizing the cost function (6.13) should be selected, and the duration time could be calculated with (6.10). The control design of the proposed SMPDCC method is illustrated schematically in Fig.6.1.

6.2.3 Numerical simulation

The AC/DC converter control with each control method has been numerically simulated with the MATLAB/Simulink toolbox. The main electrical parameters used in the simulation are listed in Table 6.1.

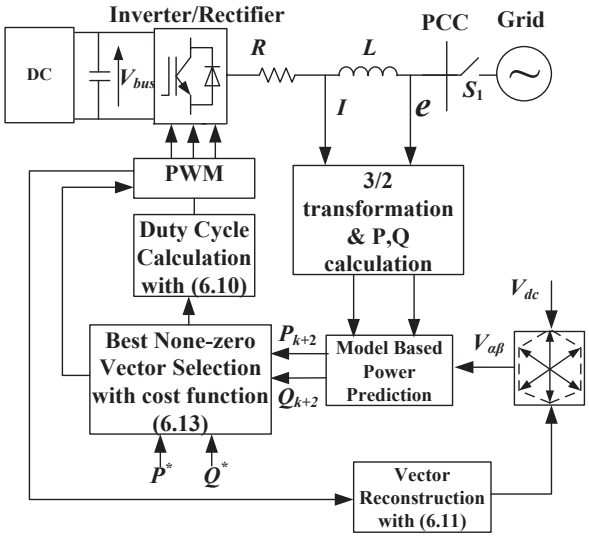

Fig.6.1 Block diagram of the SMPDCC for the AC/DC converter

TABLE 6.1 Electrical parameter of power circuit

Resistance of reactor	R	510 mΩ
Inductance of reactor	L	4 mH
DC-bus capacitor	C	680 uF
Load resistance	R_L	34 Ω
Source voltage	e	36 V(peak)
Source voltage frequency	f	50 Hz
DC-bus voltage	V_{dc}	120 V

For simplicity, the conventional MPC based DPC methods with one-step-delay compensation are used as a benchmark for comparison, which is denoted as “MPDPC”. The conventional two-vector based predictive duty cycle control in paper [6.17] is denoted as “MPDCC”, and it should be noted that the compensation method proposed is also applied for MPDCC in the following simulation and experiments. The proposed simplified model predictive based duty cycle control is denoted as “SMPDDC”. For convenience, the power flow from the AC power supply to the DC load is defined as positive. It should be noted the simulation results of each control method are in the same simulation circumstance and sampling frequency.

A. Steady state performance comparisons

To compare the steady-state performance, the AC three-phase input current, instantaneous active and reactive powers of the system are depicted to show the detailed performance of each control method, where the reactive power reference remains 200 Var and the active power reference remains at 400 W. It can be concluded from Fig. 6.2 that both the active and reactive powers track their reference values with good accuracy and stability with each control method.

From Fig. 6.2(a), it can be seen that the power ripples of both active and reactive power are large with the conventional MPDPC method with the P ripples of 11.05 W and Q ripples of 12.32 Var, respectively. The current THD is 3.77%. While by comparison, the duty cycle control achieves much better results than the MPDPC method.

For the MPDCC method, the THD significantly decreased to 1.49%, which is only half of that by the MPDPC method, and the P and Q ripples are significantly decreased to 4.87 W and 4.27 Var, respectively, which validates the superiority of the conventional duty cycle control method, as shown in Fig. 6.2(b).

With the proposed SMPDCC method, the steady performance is almost similar to that by the MPDCC method while a slight difference can be observed from the results. For instance, the Q ripple is slightly decreased to 3.98 Var with $\lambda = 1$ and the THD is decreased further to 1.43%, while P ripple is increased to 5.12 W. When $\lambda = 1.5$, the steady performance is similar to that when $\lambda = 1$ with a slight increase of the Q ripple and THD. Similar results could be achieved when P is equal to 400 W and Q equals 0 Var, as presented in Table 6.2.

It should be noted that for the conventional MPDPC, while the THD is the highest, there is a wide harmonic spectrum, which may be difficult to filter out. For the proposed SMPDCC control, the THD is further improved when compared with the conventional MPDCC. The low-order harmonic contents are much lower and the filter design should be easier.

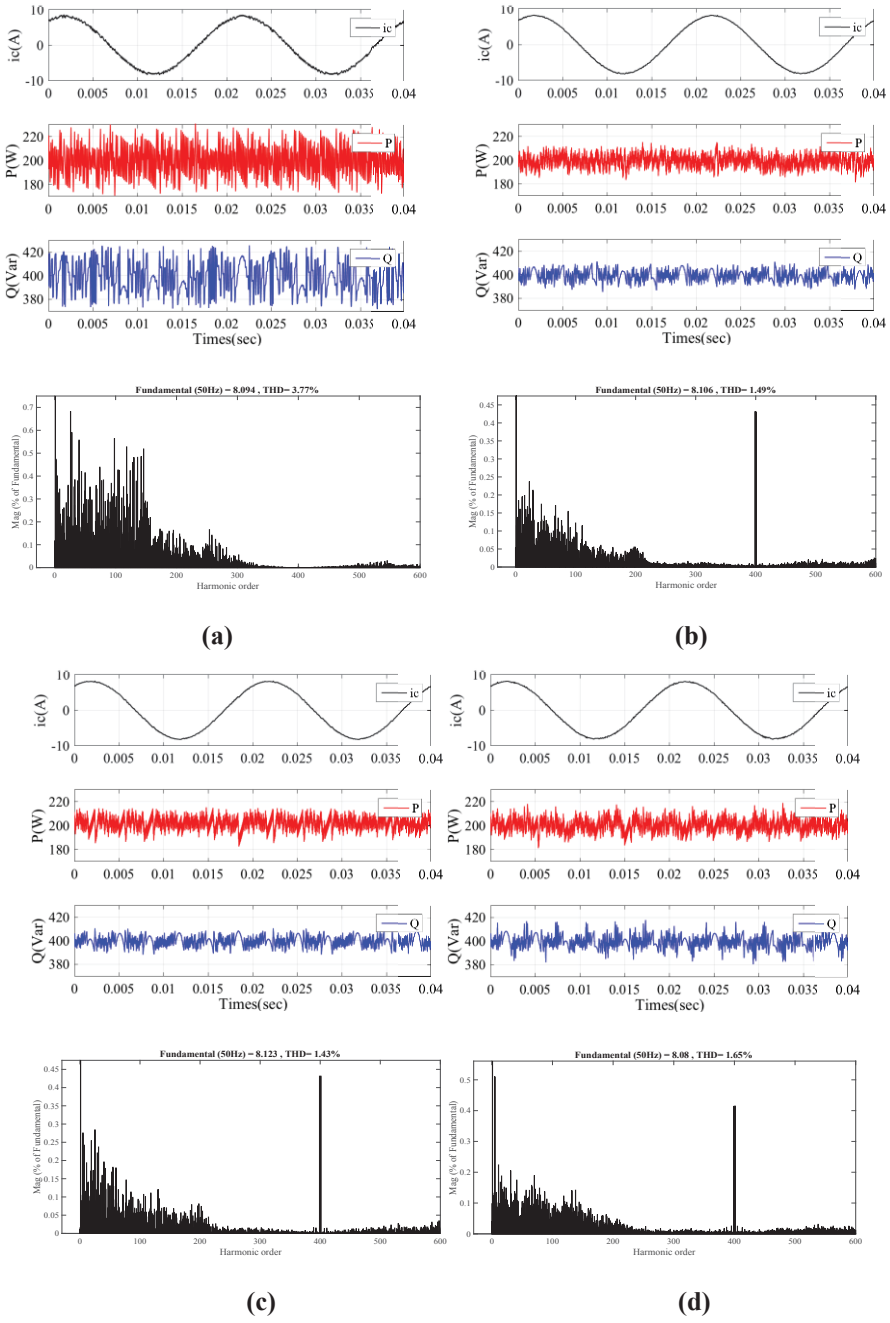

Fig.6.2 Steady-state performance at *P*=200 W, *Q*=400 Var. Top to bottom: i_c , *P* and *Q*, THD analyses of i_c , where (a) MPDPC, (b) MPDCC, (c) SMPDCC-1, and (d) SMPDCC-1.5

The quantitative comparison of steady state performance inclusive of current THD, active and reactive power ripple at two different operation states are also presented in Table 6.2.

In conclusion, both the proposed SMPDCC control methods with $\lambda = 1.5$ and $\lambda = 1$ can improve the steady-state performance significantly compared with the MPDPC

method, and their steady state performances are almost the same as that of the conventional MPDCC method.

B. Dynamic state performance comparisons

For dynamic-state performance comparison, the transient responses of active and reactive powers under step change with each method are conducted, as shown in Fig. 6.3. The active power reference value steps up from 0 W to 400 W at 0 s while the reactive power reference remains at 0 Var. After that, the active power reference changes to 100 W at 0.02 s and the reactive power reference decreases to -300 Var at 0.03 s. At 0.04 s, the active power reference steps up to 800 W, while the reactive power steps up to -400 Var at 0.06 s. At 0.11 s, the active power reference decreases to 200 W.

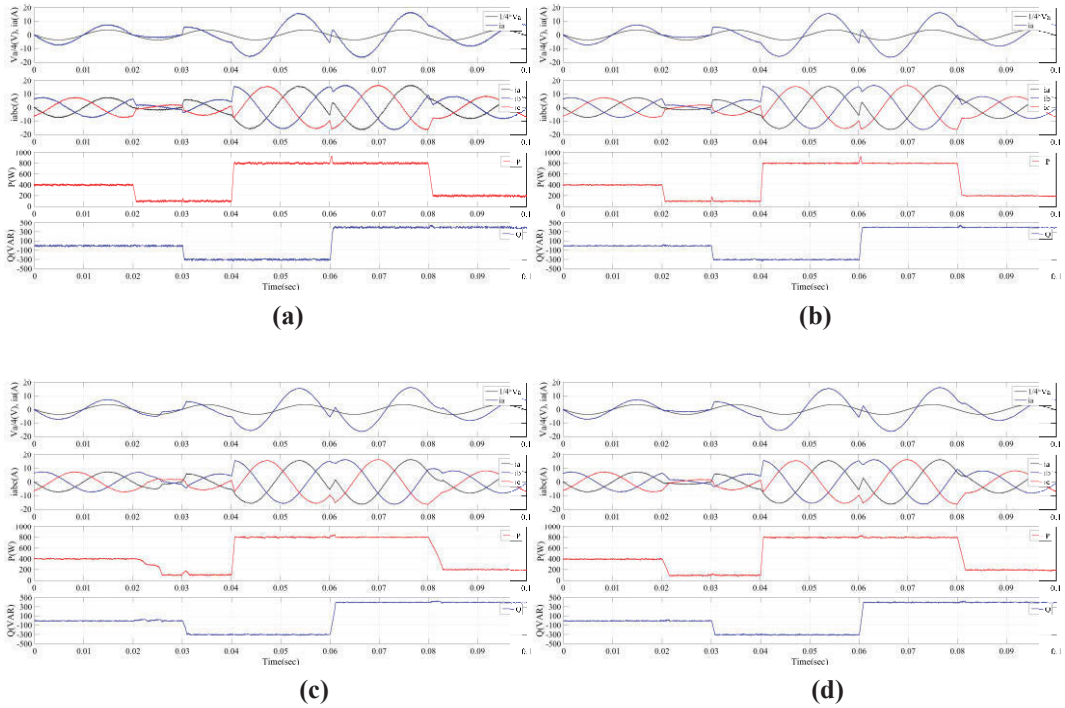

(a) **(b)**

(c) **(d)**

Fig. 6.3 Dynamic-state performance with bi-directional power flow, Top to bottom: V_a and i_a, three phase current, *P* and *Q*, where (a) MPDPC, (b) MPDCC, (c) SMPDCC-1, (d) SMPDCC-1.5

For dynamic-state performance comparison, transient responses of active power and reactive power under step change with each method are conducted, as shown in Fig. 6.3. The active power reference value steps up from 0 W to 400 W at 0 s while the reactive power reference remains at 0 Var. After that, the active power changes to 100 W at 0.02

s and, the reactive power decreases to -300 Var at 0.03 s. At 0.04 s, the active power steps up to 800 W, while the reactive power steps up to -400 Var at 0.06 s. At 0.11 s, the active power decreases to 200 W.

As shown in Fig. 6.3, all control methods can track their reference values of P and Q with good accuracy and stability, while retaining good dynamic responses. It can be seen that the overshoots of P at the instance of Q step change are apparent with both the MPDPC and MPDCC methods.

For the proposed SMPDCC method, when $\lambda = 1$, the reference tracking ability and accuracy is good. The dynamic response time at 0.02 s while P has a step change is much longer than that of MPDPC and MPDCC. However, when $\lambda = 1.5$, the problem is solved as can be seen from Fig. 6.3(d). It also shows good dynamic performance with short dynamic response time and accurate reference tracking. There is almost no overshoot of both reactive and active powers at step-change conditions in comparison with MPDPC and MPDCC.

In conclusion, the proposed SMPDCC method has simple control strategy with good dynamic and steady state performances.

TABLE 6.2 Quantitative comparison of simulation results

	P=200w Q=400var			*P=400w Q=0var*			
Control	*THD* (%)	*Prip* (W)	*Qrip* (Var)	*THD* (%)	*Prip* (W)	*Qrip* (Var)	*Response Time*
MPDPC	3.77	11.05	12.32	3.91	9.94	11.92	0.0008
MPDCC	1.49	4.87	4.27	1.93	5.37	5.47	0.0007
SMPDCC-I	1.43	5.12	3.98	1.97	6.3	5.1	0.0039
SMPDCC-II	1.65	5.3	5.28	1.99	6.25	5.29	0. 0014

6.2.4 Experimental Verification

To verity the performance of the proposed methods, a scaled down prototype is used for experimental verification. The system parameters are tabulated in Table 6.3. The comparison consists of the comparisons of dynamic response and steady state performance.

TABLE 6.3 Electrical parameters of experimental prototype

Resistance of reactor	R	500mΩ
Inductance of reactor	L	22 mH
DC-bus capacitor	C	680 uF
Load resistance	R_L	34 Ω
Source line voltage	e	105 V
Sampling frequency	fs	20kHz
Source voltage frequency	f	50 Hz

A. Comparison of steady-state performance

To compare the steady state performance of each control method, the THD and ripples of active and reactive powers at the steady state when P being equal to 200 W and Q being equal to 400 Var have been measured and calculated with each control method. T sampling frequency for each method is fixed at 10 kHz. For detailed performance comparison, the sampling frequency at 20 kHz of the MPDPC method and three vector based predictive duty cycle control (PDCC) with improved sequence in [6.15] are also implemented as a benchmark for comparison. For simplicity, the MPDPC method with 10 kHz and 20 kHz sampling frequencies are termed as MPDPC-10kHz and MPDPC-20kHz, respectively. The SMPDCC method with $\lambda = 1$ and $\lambda = 1.5$ are termed as SMPDCC-1 and SMPDCC-1.5 respectively. Fig.6.4 shows the steady-state performance of each control method with one-step-delay compensation.

Fig. 6.4(a) shows the upper pulse width modulation (PWM) driving signal of one leg, input phase to phase voltage V_{ab}, and input current i_a and i_b of the MPDPC method with 10 kHz sampling frequency. Based on the experimental data acquired from oscilloscope to PC, the instant active and reactive powers and harmonic spectrum analyses of i_a are presented. The current THD is 4.95% as shown by the harmonic spectrum of i_b. The active and reactive powers can track the reference values successfully. The P ripple is 19.55 W and the Q ripple is 22.88 Var. By comparison, the performance is improved a lot with MPDPC-20kHz as shown in Fig. 6.4(b), which is as expected since the sampling frequency is much higher with a heavier burden on the

hardware. With MPDPC-20kHz, the current THD is decreased to 3.54% and the ripples of active and reactive powers are also decreased significantly.

Though the sampling frequency is only 10 kHz, the steady-state performance of the three-vector based IPDCC approaches to the performance with MPDPC-20kHz, confirming that using duty cycle modulation has a much better result than MPDPC with the same sampling frequency. The conventional MPDCC method is also presented as shown in Fig. 6.4(c). The steady state performance is slightly deteriorated in comparison with PDCC due to the application of two vectors and is improved when compared with the single vector based MPDPC-10kHz. The proposed SMPDCC-1 and SMPDCC-1.5 are shown in Figs. 6.4(e) and (f). They both achieve slightly lower THD and Q ripples when compared with the MPDCC method, while the P ripple of the proposed method is increased, which verifies that the proposed methods are superior to MPDPC and has similar performance of MPDCC and PDCC. The quantitative comparisons of each control method are presented in Table 6.4.

As for harmonic analyses, with the proposed SMPDCC control, the low-order harmonic contents are lower, while by comparison, the conventional MPDPC has much higher harmonic contents in the low-order range, and has a wide harmonic spectrum, which increases the filter design work.

B. Comparison of dynamic-state performance

The dynamic performance of each method is also compared comprehensively with a series of experimental results. The active power step changes from 200 W to 400 W, while the reactive power remains at 400 Var. Fig. 6.5 shows the experimental results of dynamic performance for each control method.

It is shown that each method can track the reference value accurately with similar response time during the dynamic instant, which validates the reference tracking ability of the proposed MPDCC method. It is seen that the control accuracy of reactive power is deteriorated with SMPDCC-1 at the instance of P step change. Through adjustment of λ, this could be solved with SMPDCC-1, as can be seen from Fig. 6.5(f).

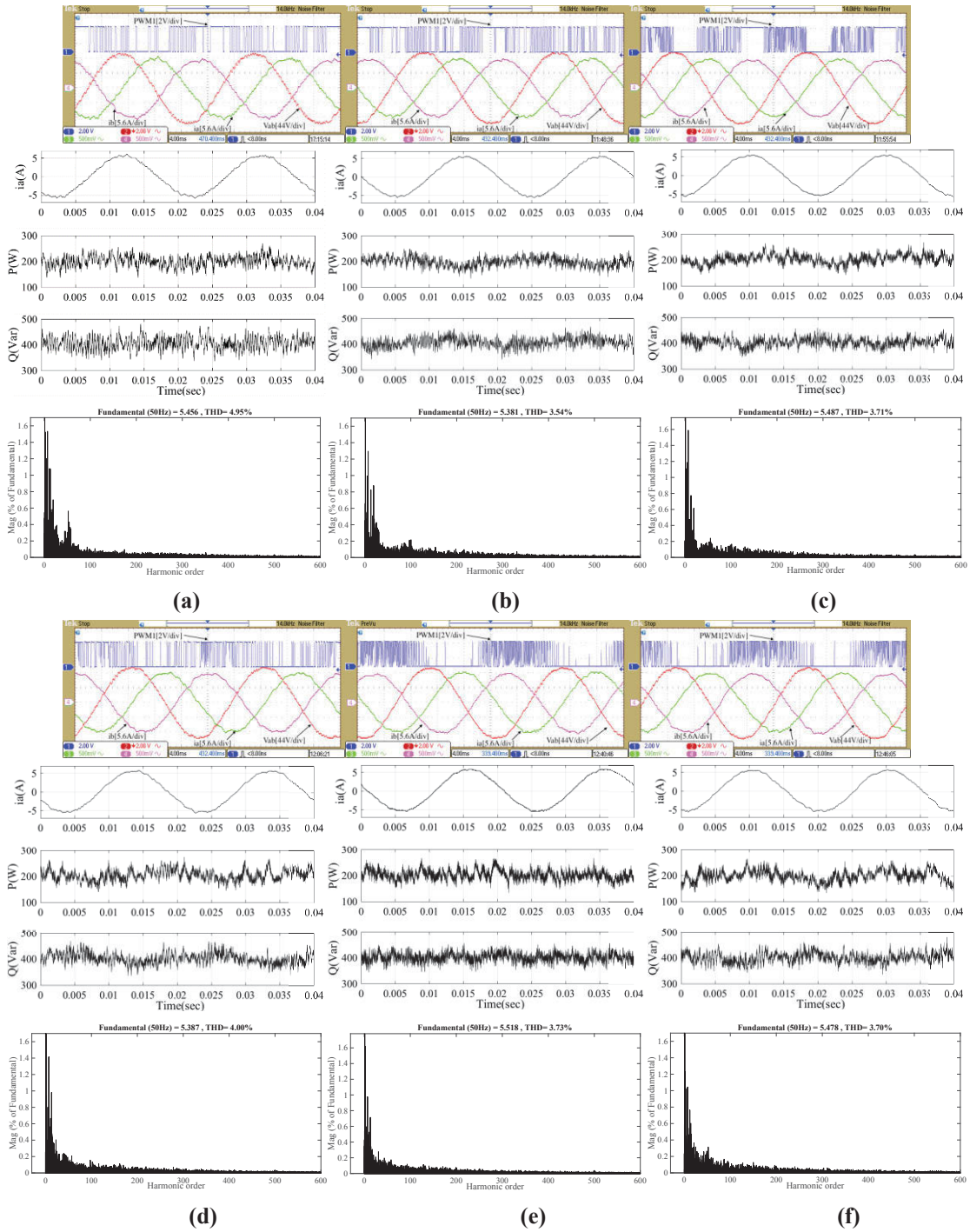

Fig.6.4 Steady-state performance at *P*=200 W, *Q*=400 Var, Top to bottom: Experimental figure, corresponding *P* and *Q*, THD analyses of i_a , where (a) MPDPC-10kHz, (b) MPDPC-20kHz, (c) IPDCC, (d) MPDCC, (e) SMPDCC-1, and (f) SMPDDC-1.5

C. System parameter redundancy

The robustness of the proposed SMPDCC is examined through a series of experiments when the inductance is different from the real one. As shown in Fig. 6.6(a),

the inductance value applied in the control is 50% of the real value (20 mH), the ripple of reactive power increases and the negative offset in the active power appears. While if inductance value used in the control increases to 30 mH and 40 mH, there is almost no influence on the reactive power ripple and positive offset in the active power will appear, as shown in Fig. 6.6(c) and (d), respectively. The results verify that the accuracy of inductance has a slight influence on the steady state performance of the proposed SMPDCC while the system stability is not influenced at least in the range of -50% and 100% inductance variations, which is superior to the conventional DPC method.

TABLE 6.4 Quantitative comparison of experimental results

Control	*fs* (Hz)	*THD* (%)	*Prip* (W)	*Qrip* (Var)
MPDPC-10kHz	10 K	4.95	19.55	22.88
MPDPC-20kHz	20 K	3.54	16.74	17.77
IPDCC	10 K	3.71	17.18	16.26
MPDCC	10K	4.00	17.49	19.52
SMPDCC-1	10 K	3.73	18.23	18.52
SMPDCC-1.5	10 K	3.70	19.21	18.34

6.2.5 Conclusion of discussions

This section proposes a novel two vector based SMPDCC strategy for three-phase AC/DC full-bridge converters. In comparison with the conventional MPDPC, two vectors are implemented during one control period, and thus a lower sampling frequency could be applied. Different from the conventional MPDCC method, the calculation of durations is much simpler and it would not be negative or exceed the range.

Comprehensive comparisons are presented to compare the performance of proposed control with the conventional MPDPC and MPDCC method. The results verify the correctness of the proposed method. Meanwhile, the superior dynamic and steady state performance of the proposed MPDCC method with fixed switching frequency, lower THD and lower power ripples are also achieved.

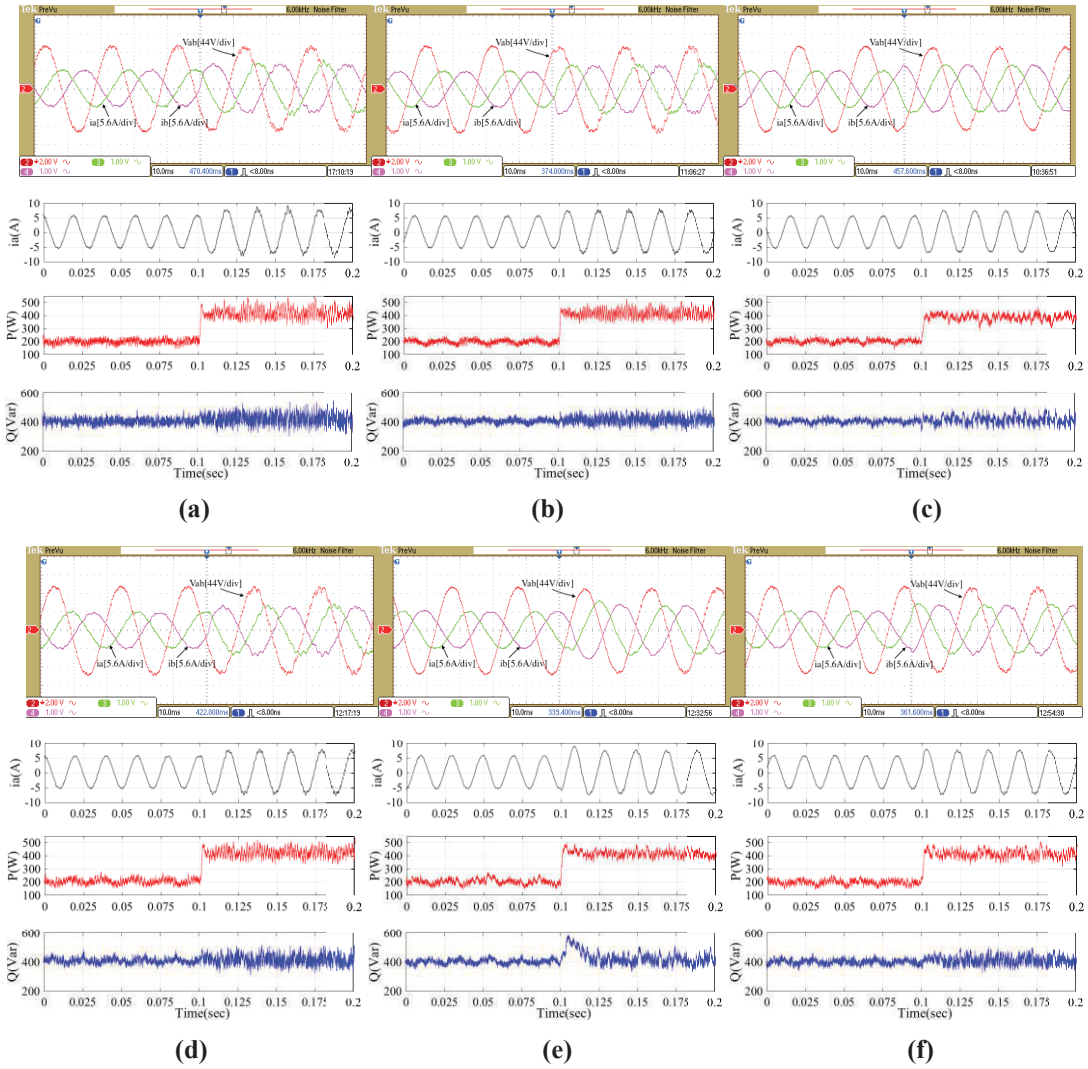

Fig.6.5 Dynamic-state performance when *P* from 200 W to 400 W, *Q*=200 Var, Top: Experimental figure. Bottom: i_a, *P* and *Q*, where (a) MPDPC-10kHz, (b) MPDPC-20kHz, (c) PDCC, (d) MPDCC, (e) SMPDCC-1, (f) SMPDCC-1.5

6.3 Improved SVM based DPC

The conventional SVMDPC (CSVMDPC) tracks the errors of active and reactive powers and puts them into two separate PI regulators. The control block diagram is illustrated in Fig. 6.7(a). The PI regulators are used to transform the input tracking errors to V_α and V_β in the stationary reference frame, and then use the SVM module to generate the switching signals. Whilst the SVMDPC introduced previously has benefits such as constant switching frequency, however the PI regulators and the

coordinate transformation increase the control complexity significantly and the transient and steady-state performances are quite sensitive to the PI control parameters.

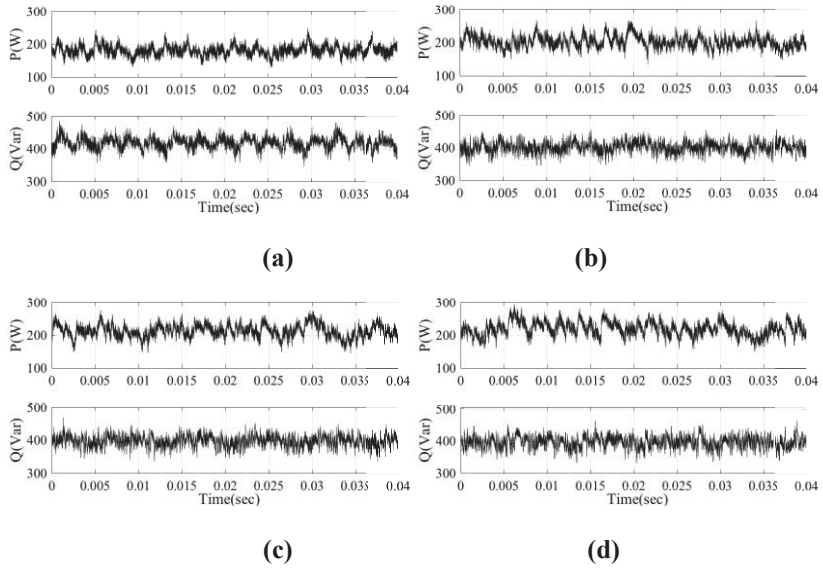

Fig.6.6 Responses of active and reactive powers for proposed SPDDC when the actual inductance in control differs from the real value, where (a) 10 mH, (b) 20 mH, (c) 30 mH, and (d) 40 mH

To solve this issue, the improved SVM based DPC (ISVMDPC) was proposed in [6.16] as shown in Fig. 6.7(b). Based on the predictive control strategy, it achieves the direct control of instantaneous active and reactive powers of the converter. With ISVMDPC, the two separate PI regulators and coordinate transformation module are replaced with a predictive model of the converter that could transfer the active and reactive power errors to V_α and V_β, respectively, which will be discussed below. Then the same SVM block is used for pulse generation.

If the sampling period T_s is assumed to be small in comparison with the period of the power-source voltage, components of $e_{\alpha\beta}$ is assumed constant over the switching period ($e_{\alpha\beta}(k+1) = e_{\alpha\beta}(k)$). According to the converter model, the variation of active and reactive powers can be obtained as follows

$$\begin{bmatrix} \Delta P \\ \Delta Q \end{bmatrix} = \frac{3}{2} \begin{bmatrix} e_\alpha & e_\beta \\ e_\beta & -e_\alpha \end{bmatrix} \begin{bmatrix} \Delta I_\alpha \\ \Delta I_\beta \end{bmatrix} \tag{6.14}$$

By neglecting the voltage drop of R, $\Delta I_{a\beta}$ can be derived in the discrete-form as

$$\Delta I_{a\beta} = \frac{T_s}{L}(e_{\alpha\beta} - V_{\alpha\beta}) \tag{6.15}$$

Substituting (6.15) into (6.14), one obtains

$$\begin{bmatrix} \Delta P \\ \Delta Q \end{bmatrix} = \frac{3T_s}{2L}\begin{bmatrix} e_\alpha & e_\beta \\ e_\beta & -e_\alpha \end{bmatrix}\begin{bmatrix} e_\alpha - V_\alpha \\ e_\beta - V_\beta \end{bmatrix} \tag{6.16}$$

To ensure the active and reactive powers equal to their references, that is, $\Delta P = P_{ref} - P^k = 0$ and $\Delta Q = Q_{ref} - Q^k = 0$, then the required reference voltage can be calculated as

$$\begin{bmatrix} V_\alpha \\ V_\beta \end{bmatrix} = \begin{bmatrix} e_\alpha \\ e_\beta \end{bmatrix} - \frac{2L_s}{3T_s|e|^2}\begin{bmatrix} e_\alpha & e_\beta \\ e_\beta & -e_\alpha \end{bmatrix} \times \begin{bmatrix} P_{ref} - P^k \\ Q_{ref} - Q^k \end{bmatrix} \tag{6.17}$$

Finally, the computed rectifier average voltage vector, in α–β or *d–q* reference frame, is converted into a sequence of switching states (adjacent voltage vectors) by the SVM technique, and a constant switching frequency can be remained.

It should be noted that the derived equation above is under static α−β coordinates. However, there exists a small offset in reactive power control, which is caused by the assumption that $e_{\alpha\beta}$ is constant over the switching period ($e_{\alpha\beta}(k+1) = e_{\alpha\beta}(k)$). To solve this issue, the average voltage vector in the rotating reference frame *d–q* could be derived similarly as above, and the offset could be eliminated, since for purely sinusoidal power-source voltages e_{dq} is constant ($e_{dq}(k+1) = e_{dq}(k)$). However, to use the SVM, transformation from rotating *d–q* coordinates to static α−β coordinates is necessary, which will increases the control complexity.

6.3 Model Predictive based Duty Cycle Control – Three Vector Based Approach

6.3.1 MPC based PDCC

The conventional PDCC discussed in Chapter 5 uses the sector information to select the none-zero vector pair, during the initial or later part of odd or even sectors for some cases, the calculated duration time is negative, which means the vector selection is

incorrect. Though the improved PDCC has been proposed before and reversible PDCC was proposed in Chapter 5 to optimize the performance, the corresponding negative duration time of each none-zero vector still exists, though not as significantly as the conventional method. This means the selected none-zero vector is still not entirely correct, which is the inherent disadvantage of these methods, and thus there are still spaces to improve the performance. Besides, since the vector selection is based on the sector information without considering the converter model and instant power change, there is no useful method to eliminate the mutual influence during the dynamic instant when there is a step change of one control objective, such as active and reactive powers.

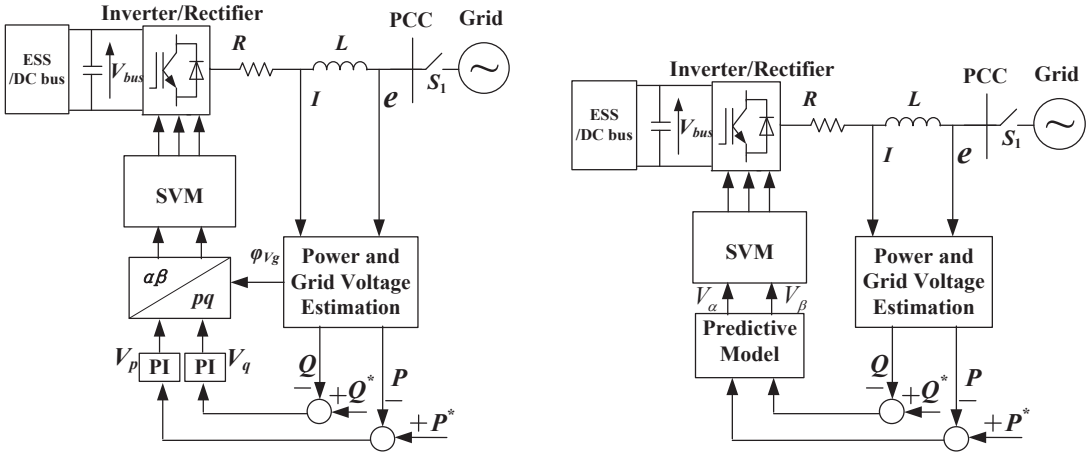

Fig. 6.7 Block diagram of SVMDPC-based power regulation, where (a) CSVMDPC, and (b) ISVMDPC

In consideration of vector selection with future behaviour, the MPC is a perfect option for the three vector based method, which leads to more accurate none-zero vector pair selection with the possibility to eliminate mutual influence, and thus better dynamic and steady state performance could be achieved.

The main difference between the MPC based PDCC (MPCPDCC) and CPDCC is on the none-zero vector pair selection procedure. Firstly, the active and reactive power differences between the referenced values of each converter switching state are compared, and the none-zero vector pair leading to the minimum sum value of the specific cost function as defined by

$$g_i = (P^* - P_i^{k+2})^2 + (Q^* - Q_i^{k+2})^2 \quad (i = 0,1,2,3,4,5,6) \tag{6.18}$$

are selected for each control cycle with consideration of one step delay compensation.

The novel cost function could be constructed as

$$g_i^{'} = g_i + g_{i+1} \quad (i = 1,2,3,4,5,6, g_7 = g_1) \tag{6.19}$$

For instance, if $g_1^{'}$ is the minimum value among all the six adjacent none-zero vector pairs, the adjacent vector pair V_1 and V_2 will be selected.

Then, according to the selected none-zero vector pair and zero vector, the power slopes of each vector could be calculated and the corresponding duration time will be derived with the same least square minimization method as discussed in Chapter 5, (which will not be repeated here).

With the calculated results of duration time, the duty cycles of switching signal can be obtained. The hardware system with higher computing capacity might be required. However, the mutual influence during the dynamic instant still has not been eliminated.

In the aforementioned cost function (6.18), the control objectives, namely the active and reactive powers, are combined in one cost function. If one objective significantly changes, the control target is focused on the changed objective, while the other objective is less controlled and the dynamic performance would deteriorate significantly. The interaction becomes larger while the variation amount of the two control factors becomes larger. This influence also exists in the CPDCC and IPDCC method in Chapter 5. During the transit period, the calculated durations change significantly and may exceed the boundary due to a large power error, which would deteriorate the control of the other objectives.

As mentioned before, one of the main advantages of MPC is that any variable and constraint term or requirement of the system could be added in the cost function to combine multiple constraints and nonlinearities to improve the system performance. The dynamic mutual influence between the active and reactive powers exists due to the control of two targets in one cost function, deteriorating the system's dynamic performance.

With consideration of eliminating the mutual influence, the proposed constraint in Chapter 4 could be applied for MPCPDCC as well. The constraint *M* is defined as follows

$$M = \lambda_1 \left| (Q^* - Q_i^{k+2})(P^* - P_i^{k+2}) \right| \tag{6.20}$$

where parameter λ_1 is the weighting factor of mutual influence elimination, which is chosen in consideration of the system's rated active and reactive powers. At the instant of step change of P^* or Q^*, the vector that may incur a large mutual influence on the other control objective would be less considered. Meanwhile, the constraint *M* would have almost no influence on the steady state performance.

Thus the cost function (6.18) for vector pair selection could be revised to

$$g_i = (P^* - P_i^{k+2})^2 + (Q^* - Q_i^{k+2})^2 + \lambda \left| (Q^* - Q_i^{k+2})(P^* - P_i^{k+2}) \right| \tag{6.21}$$

6.3.2 MPC based direct duty cycle control

The MPC based direct duty cycle (MPCDDC) control proposed in this section has two main differences in comparison with the conventional PDCC method in Chapter 5. Because the selection of two adjacent vector pairs is based on MPC, the need for the sector information is eliminated, which is the same as the MPCPDCC method proposed above, and therefore, incorrect selection of sector during sector changing instant and the resulting performance deterioration can be avoided. The mutual influence can also be eliminated. The second difference is about the duty cycle calculation method whereby the proposed method allocates a fraction of control period in relation with the cost function results to the selected none-zero vector pairs, while a zero vector is applied for the rest of the time. The principle of the proposed method to obtain the duration time is very simple in calculation and easy to implement, which is similar to the method for two vector based SMPDCC.

A. Vector sequence and switching frequency reduction

The proposed method is based on the MPC method but with a novel cost function and application of three vectors with a novel duty cycle calculation principle. To select the neighboring vector pair for the proposed duty cycle control method, a novel cost function is established as follows

$$g_i^{"} = \frac{1}{g_i} + \frac{1}{g_{i+1}} (i = 1...6, g_7 = g_1) \tag{6.22}$$

where is g_i same as (6.21), which also considers the mutual influence elimination.

According to cost function (6.22), the adjacent two none-zero vectors that can achieve maximum $g_i^{"}$ are selected. Then, the duration time is calculated by the following equations for the selected none-zero vector pairs:

$$\begin{cases} k(\frac{1}{g_i} + \frac{1}{g_{i+1}} + \frac{1}{g_0}) = T_s / 2 \\ t_a + t_b + t_c = T_s / 2 \end{cases} \tag{6.22}$$

According to (6.22), the corresponding application durations for each vector can be easily derived as follows

$$\begin{cases} t_a = \dfrac{g_{i+1} g_0}{g_i g_{i+1} + g_i g_0 + g_{i+1} g_0} \\ t_b = \dfrac{g_i g_0}{g_i g_{i+1} + g_i g_0 + g_{i+1} g_0} \\ t_c = \dfrac{g_i g_{i+1}}{g_i g_{i+1} + g_i g_0 + g_{i+1} g_0} \end{cases} \tag{6.23}$$

It should be noted that the application durations are simply calculated by (6.23) and directly allocated to the corresponding vector. There is no need to do any further normalized approximations since t_a, t_b and t_c are definitely within the range of 0 to $T_s / 2$ in proportion to the reciprocal value of the corresponding g_i.

B. Design of one-step-delay compensation

The one-step delay compensation is also needed in the proposed method. Firstly, the converter voltage V is reconstructed from the applied active voltage vectors and the corresponding durations as

$$V=V_a d_a+V_b d_b \tag{6.24}$$

where $d_a=2t_a/T_s$ and $d_b=2t_b/T_s$, being the duty ratio of the selected two none-zero vectors. By substituting (6.24) into (6.1), the prediction value P^{k+1} and Q^{k+1} at the $(k+1)$th instant could be achieved.

Then, the values of P^{k+2} and Q^{k+2} can be calculated for each none-zero voltage vector with the initial states of P^{k+1} and Q^{k+1}. Finally, substitute P^{k+2} and Q^{k+2} to (6.21), and then the voltage vector pair maximizing the cost function should be selected. According to (6.23), the duration time could be calculated directly.

The control design of the proposed MPCDDC method is illustrated schematically in Fig. 6.8. With the redesigned cost function and additional constraints, the proposed MPCDDC control could improve both the dynamic and steady state performance of the three-phase converter simultaneously.

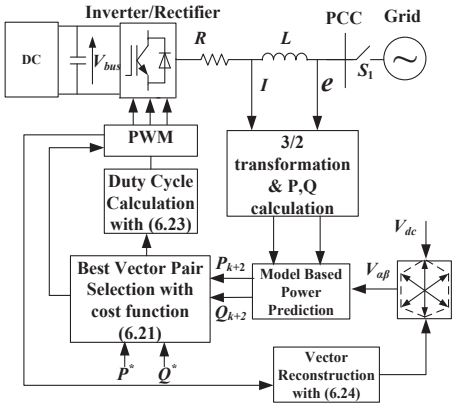

Fig.6.8 Block diagram of the MPCDDC for the AC/DC converter

6.3.3 Numerical simulation

For simplicity, the improved SVM based DPC is denoted as ISVMDPC. The proposed simplified model predictive based direct duty cycle control without mutual influence elimination is denoted as "MPCDDC-I", and the proposed simplified model predictive based direct duty cycle control with mutual influence elimination as "MPCDDC-II". The proposed MPC based duty cycle control without mutual influence constraint is denoted as MPCPDCC-I, while it is denoted as MPCPDCC-II. Since MPCPDCC cannot totally avoid the negative duration time, the reverse vector selection is added when there is negative duration time, which is denoted as RMPCPDCC-I. For convenience, the power flow from the AC power supply to the DC side is defined as positive. Each control method are in same simulation circumstance and sampling frequency, and one-step-delay compensation is added for all methods.

TABLE 6.5 Quantitative Comparison of Simulation Results

Resistance of reactor	R	510 mΩ
Inductance of reactor	L	4.2 mH
DC-bus capacitor	C	3500 uF
Load resistance	R_L	50 Ω
Source voltage	e	110 V(peak)
Source voltage frequency	f	50 Hz
DC-bus voltage	V_{dc}	300 V

A. Steady state performance comparisons

To compare the steady-state performance, the AC three-phase input current and instantaneous active and reactive powers of the system are depicted to show the detailed performance of each control method. As we can see from Fig. 6.9, both the active and reactive powers can track their reference values with good accuracy and stability for each of control methods.

From Figs. 6.9(a) and (b), it can be seen that the ripples of both the active and reactive powers are much lower with the MPCDDC-I method. The P ripple is only 5.36 W and the Q ripple 4.87 Var, respectively, when P is equal to 450 W and Q equals 0

Var. The current THD is as low as 1.64%. With the MPCDDC-II method, it has slightly better steady state performance but almost the same as that of MPCDDC-I. With the MPCDDC based method, it verifies the effectiveness of the proposed simplified MPC based methods. By comparison, with ISVMDPC, as can be seen from Fig. 6.9(c), the selected none-zero vectors do not have as significant a state change as the MPC based method, which means the switching frequency can be reduced a lot. As a result, the steady state performance is not as good as that with the MPCDDC based methods.

For instance, the THD is increased to 2.19%, and the active and reactive power ripples are increased to 7.78 W and 5.36 Var, respectively. It can also be observed from Fig. 6.9(c) that there is a positive offset of reactive power with the value of 6.93 Var, which can be attributed to the assumption that $e_{\alpha\beta}$ is constant over the switching period ($e_{\alpha\beta}(k+1) = e_{\alpha\beta}(k)$).

The MPC based vector selection with the conventional least square minimization method for duration time calculation achieved the best steady state performance. It can be seen from Figs. 6.9(d), (e) and (f) that the THD, active and reactive power ripples with the MPCPDCC based method are further decreased, which validates that the MPCPDCC based method could achieve the best steady state performance, though the control complexity is increased. Also, as can be seen from Fig. 6.9(e), with the mutual influence compensation constraint, there is almost no sacrifice on steady state performance. With the reverse vector strategy as proposed in Chapter 5, the negative duration time can be almost eliminated with the RMPCPDCC method, but there is no improvement on the steady state performance, which means the reverse vector strategy for the MPC based method is not as useful as the sector information based vector selection method.

The steady-state performance comparison at different states of P being equal to -350 W and Q being equal to 200 Var is also conducted, as shown in Fig. 6.10. A similar conclusion could be drawn.

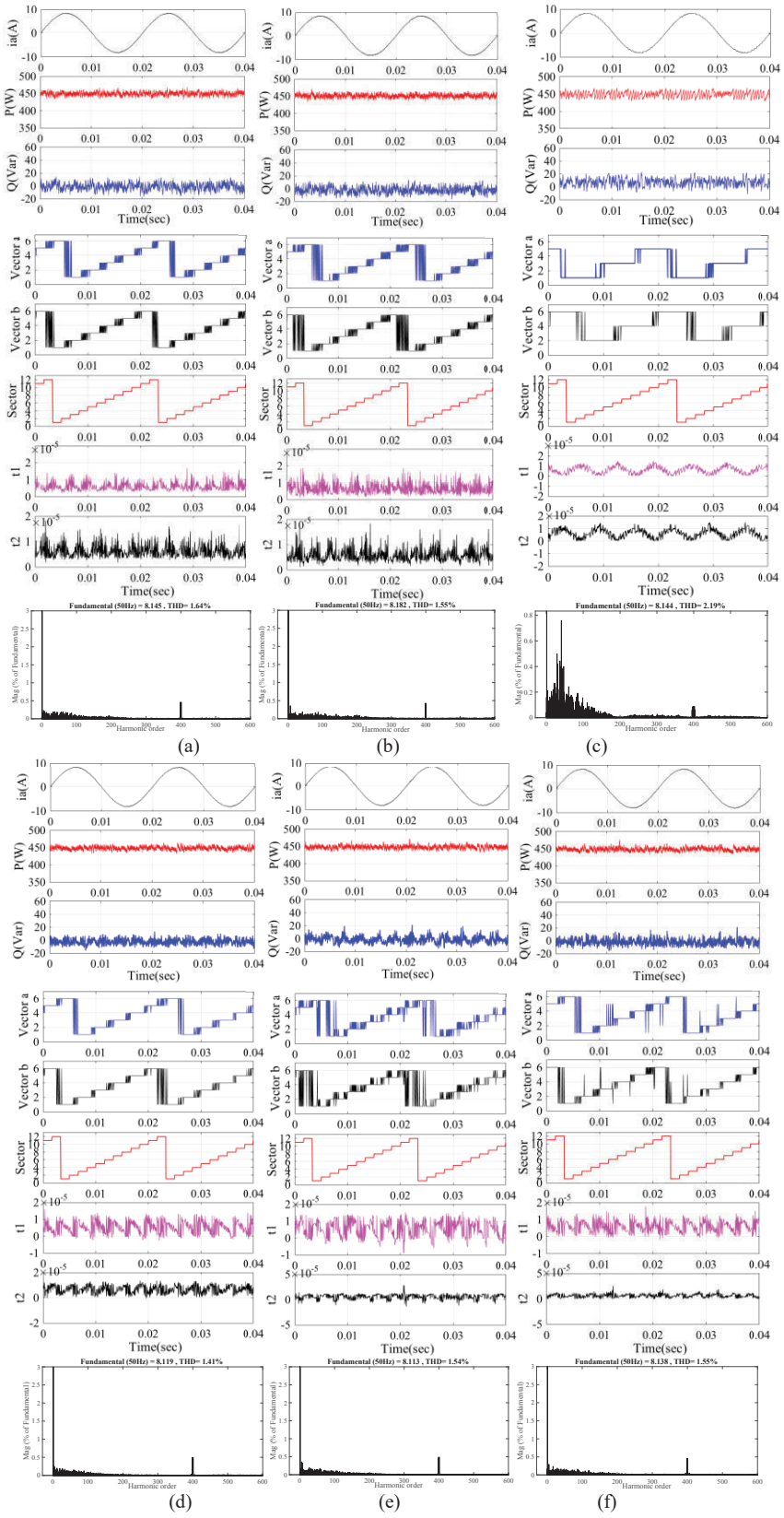

Fig.6.9 Steady-state performance at *P*=450 W, *Q*=0 Var, Top to bottom: i_a, *P* and *Q*, $V_a^{'}$, $V_b^{'}$, sector, t_a, t_b, THD analyses of i_a, where (a) MPCDDC-I, (b) MPCDDC-II, (c) ISVMPDC, (d) MPCPDCC-I, (e) MPCPDCC-II, and (f) RMPCPDCC

For a comprehensive comparison of various kinds of three-vector based control methods, quantitative comparisons of control methods with the sector information based vector selection and MPC based vector selection are presented in Table 6.6. It can be concluded that the MPC based vector selection method achieves the best steady state performance. Among these methods, the MPCDDC based method achieves similar good performance though not as good as the MPCPDCC based method with reduced control complexity. Also, there is almost no influence on the steady state performance by adding the mutual influence elimination constraints. The ISVMDPC achieves worthy performance when compared with the sector information based vector selection method, RPDCC, which is the best one in the sector information based vector selection method. However, the performance is still deteriorated compared with MPC based methods.

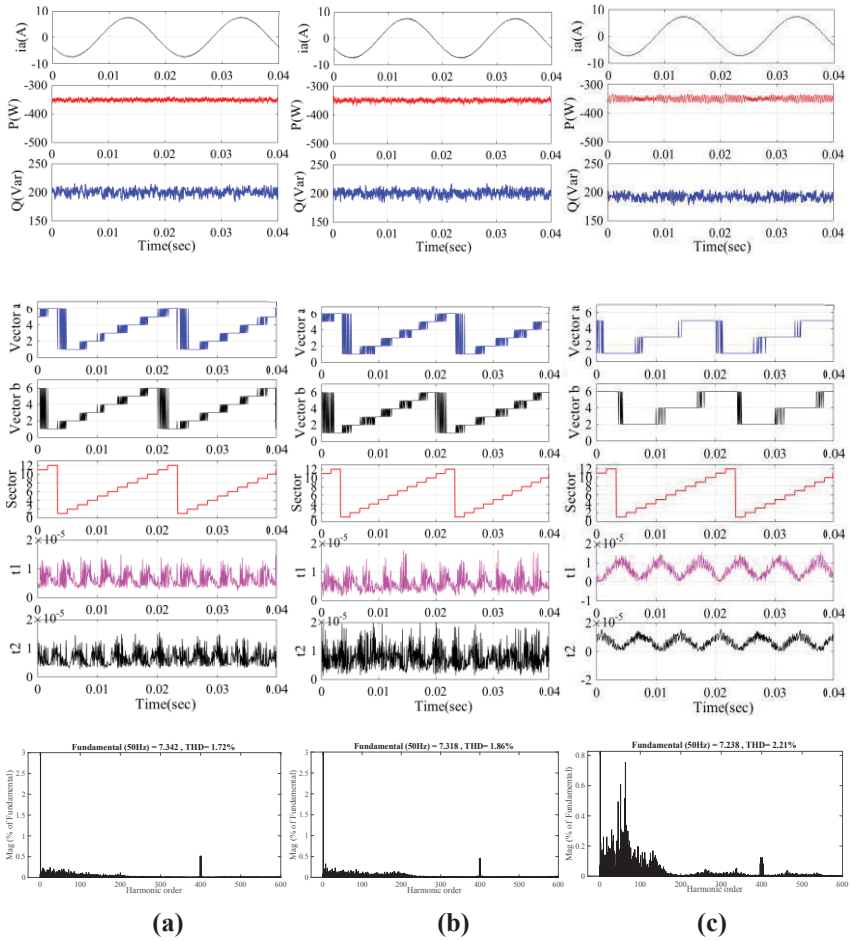

(a) **(b)** **(c)**

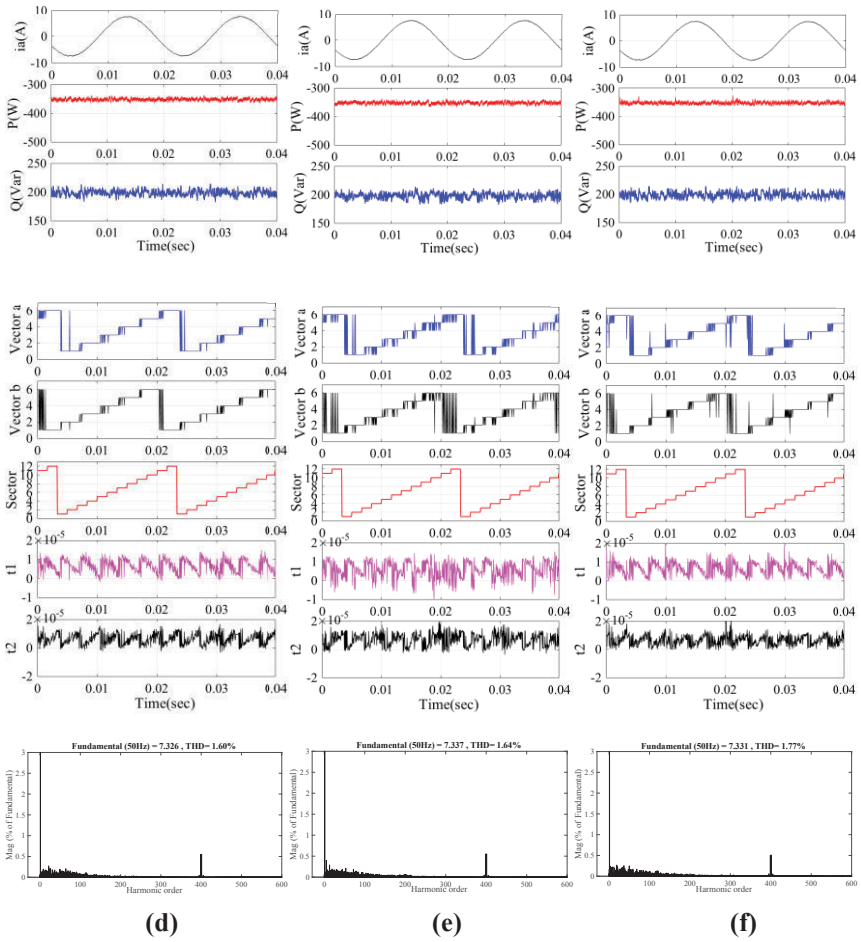

(d) **(e)** **(f)**

Fig.6.10 Steady-state performance at *P*=-350 W, *Q*=200 Var, Top to bottom: i_a, *P* and *Q*, $V_a^{'}$, $V_b^{'}$, sector, t_a, t_b, and THD analyses of i_a, where (a) MPCDDC-I, (b) MPCDDC-II, (c) ISVMPDC, (d) MPCPDCC-I, (e) MPCPDCC-II, and (f) RMPCPDCC

B. Dynamic state performance comparisons

For each control method, as can be seen from Fig. 6.11, the active and reactive powers track their reference values with good accuracy and stability. Good dynamic response could also be achieved. As shown in Fig. 6.11(a), the mutual influence on active power control is apparent with MPCDDC-I when reactive power has a step change. The *P* overshoot is as high as 147 W. By comparison, with the mutual influence elimination constraint, the mutual influence is eliminated with MPCDDC-II as shown in Fig. 6.11(b), and the *P* overshoot is decreased significantly to 22 W. The similar phenomenon happens with the MPCPDCC based method, as can be seen from Figs. 6.11(d), (e) and (f). The mutual influence is eliminated as well with MPCPDCC-II method, which further validates the effectiveness and universality of the proposed

mutual influence elimination constraint. By comparison, with the ISVMDPC method, the mutual influence is apparent, as shown in Fig. 6.11(c), which could not be eliminated.

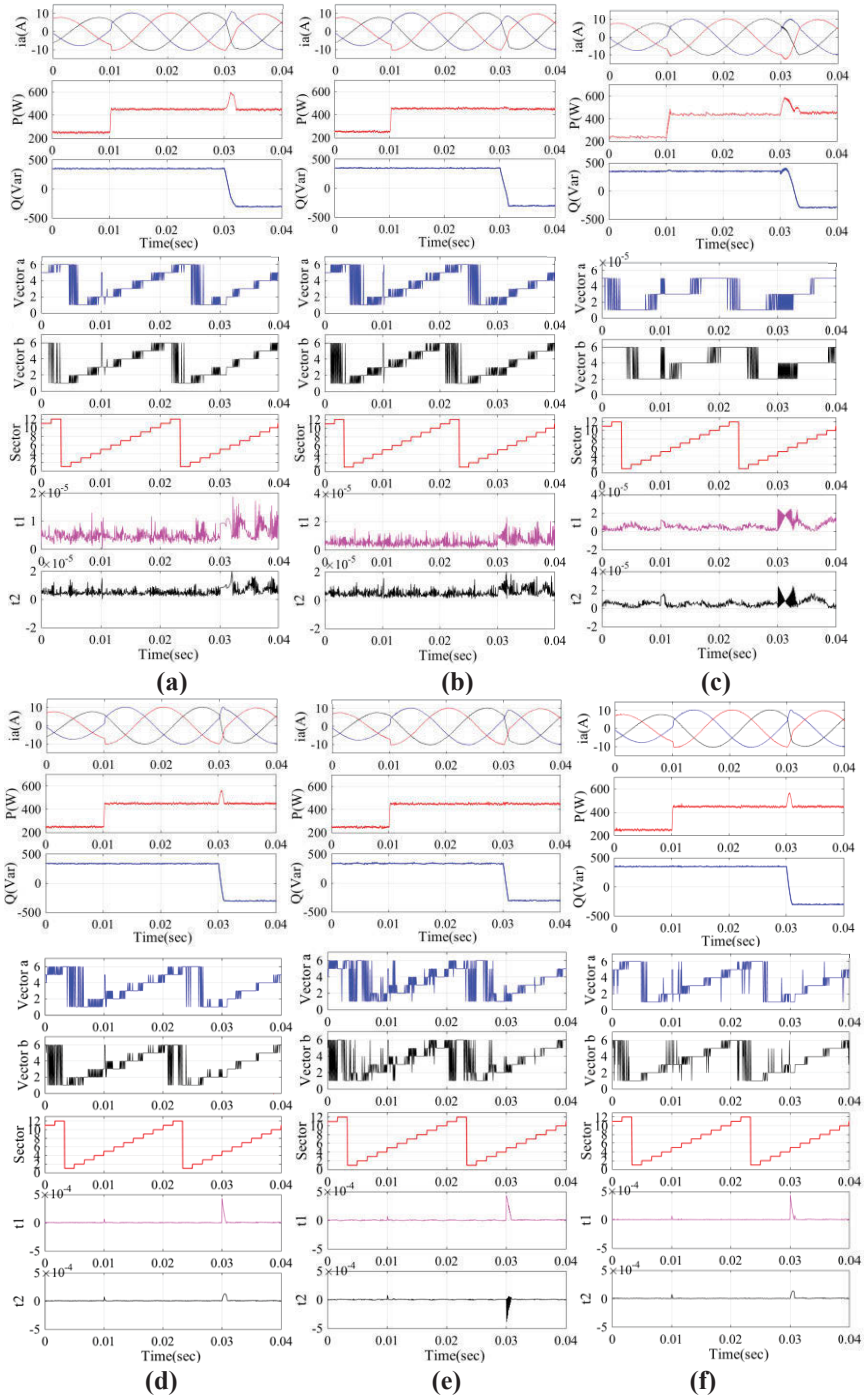

Fig.6.11 Dynamic-state performance, Top to bottom: i_a, *P* and *Q*, $V_a^{'}$, $V_b^{'}$, sector, t_a, t_b, and THD analyses of i_a, where (a) MPCDDC-I, (b) MPCDDC-II, (c) ISVMPDC, (d) MPCPDCC-I, (e) MPCPDCC-II, and (f) RMPCPDCC

TABLE 6.6 Quantitative comparison of simulation results

	P=450 W Q=0 Var			***P=-350 W Q=200 Var***			***Response***	***Overshoot***	***Response***	***Overshoot***
Control	*THD* (%)	*Prip* (W)	*Qrip* (Var)	*THD* (%)	*Prip* (W)	*Qrip* (Var)	*Time* (S)	*Q* (Var)	*Time* (S)	*P* (W)
PDCC	6.46	19.815	17.34	5.64	14.17	17.05	0.001	25	0.0017	370
IPDCC	2.26	8.92	5.51	2.74	9.30	5.49	0.0012	79	0.0021	380
RPDCC	1.71	6.06	4.64	1.87	5.59	4.77	0.00015	22	0.0014	171
MPCDDC-I	1.64	5.36	4.87	1.72	4.62	5.18	0.00014	12	0.0018	147
MPCDDC-II	1.55	5.23	4.72	1.86	5.34	5.18	0.00015	13	0.0015	22
ISVMDPC	2.19	7.78	5.36	2.21	7.11	4.86	0.0007	29.4	0.0035	143.28
MPCPDCC-I	1.41	5.05	3.86	1.6	4.67	4.69	0.00013	13	0.00093	118
MPCPDCC-II	1.54	5.31	4.81	1.64	4.9	4.85	0.00013	18	0.00093	21
RMPCPDCC	1.55	5.59	4.41	1.77	4.96	5.03	0.00014	16	0.0009	119

In terms of the response time, the MPCDDC based method has a longer response time than that of the MPCPDCC based method, but it is much shorter than that of the ISVMDPC method, especially at the instance of 0.03 s when Q has a step change. For instance, the response time with MPCDDC-I at 0.03 s is 0.0018 s, while it decreases to 0.0009 s with the MPCPDCC-I method, and it increases significantly to 0.0035 s with the ISVMDPC method.

For a comprehensive comparison of dynamic performance with various kinds of three vector based methods, the quantitative comparisons of dynamic performance are also presented in Table 6.6. It can be concluded that with the sector information based vector selection methods, the mutual influence is much higher and the response time is relatively longer, with the exception of the RPDCC method. With the MPC based vector selection method, the mutual influence is relatively lower and could be eliminated by adding the mutual influence elimination constraint. The response time is decreased especially with the MPCPDCC based method.

6.3.4 Experimental verification

To verity the effectiveness of the proposed methods, a scaled down prototype is constructed. The system parameter is presented in Table 6.7. The comparison can be divided into steady state performance comparison and dynamic response comparison.

TABLE 6.7 Electrical Parameter of Prototype

Resistance of reactor	R	500mΩ
Inductance of reactor	L	22 mH
DC-bus capacitor	C	680 uF
Load resistance	R_L	34 Ω
Source voltage	e	96 V(peak)
Sampling frequency	fs	20kHz
Source voltage frequency	f	50 Hz

A. Comparison of steady state performance

To compare the steady state performance of each control method, the THD, ripples of active and reactive powers in the steady state when P equal to 200 W and Q equal to 200 Var, respectively, have been measured and calculated with each control method. The sampling frequency for each method is fixed at 10 kHz, while the sampling frequency at 20 kHz of MPDPC method is also presented as a benchmark for further performance comparison. The MPDPC methods with sampling frequencies of 10 kHz and 20 kHz are termed as MPDPC-10k and MPDPC-20k, respectively.

Fig. 6.12(a) shows the upper PWM driving signal of one leg, input phase to phase voltage, and input current of the MPDPC method with 10 kHz sampling frequency. Further analyses have been presented based on the experimental data acquired from oscilloscope to PC, such as instant active power, reactive power and harmonic spectrum analyses of i_a. With the MPDPC method, the current THD is 5.63% as shown by the harmonic spectra of i_a. The active and reactive powers track the reference value successfully. The P ripple is 15.44 W and the Q ripple is 16.17 Var. By comparison, the performance is much improved with MPDPC-20k as shown in Fig. 6.12(b), which is as

expected since the sampling frequency is much higher. With MPDPC-20k, the current THD, the power ripples of active power and reactive power are decreased obviously.

For a comprehensive comparison, the steady state performance of IPDCC is also presented as a benchmark, as shown in Fig. 6.12(c). Though the sampling frequency is only 10 kHz, the steady state performance is similar to that of MPDPC-20k, confirming that using duty cycle modulation has much better performance than MPDPC with the same sampling frequency. The performances of proposed MPCDDC-I and MPCDDC-II are shown in Figs. 6.12(d) and 6.12(e), which are similar as expected. The proposed MPCDDC presents an even better result by achieving lower THD and power ripples than that of IPDCC and MPDPC-20k, even though the sampling frequency is only half that of MPDPC-20k. For example, the THD of MPCDDC-I is only 3.87%, the P ripple is decreased to 12.17 W and the Q ripple is only 12.58 Var. The performance with ISVMDPC is presented in Fig. 6.12(f) and it achieves a slightly better result in comparison with the MPDPC-I method by realizing lower THD and reactive power ripple, while the active power ripple is larger than that of the MPDPC based method. Finally, the experimental results with the MPCPDCC based method are presented in Figs. 6.12(g) and (h), which have the best steady state performance compared with all other kinds of methods. For example, the THD is further reduced to 3.5%, and the P and Q ripples are reduced to 5.71 W and 5.19 Var, respectively, with the MPCPDCC-II method.

The quantitative comparison of each control method is presented in Table 6.8. It should be noted that the per unit values of P and Q ripples are calculated in proportion to the nominal values of 200 W and 200 Var, respectively.

B. Comparison of dynamic state performance

The dynamic performance of each method is also compared comprehensively with a series of experimental results. Firstly, the active power step changes from 200 W to 400 W, while the reactive power remains at 200 Var. Fig. 6.13 shows the experimental results of dynamic performance for each control method.

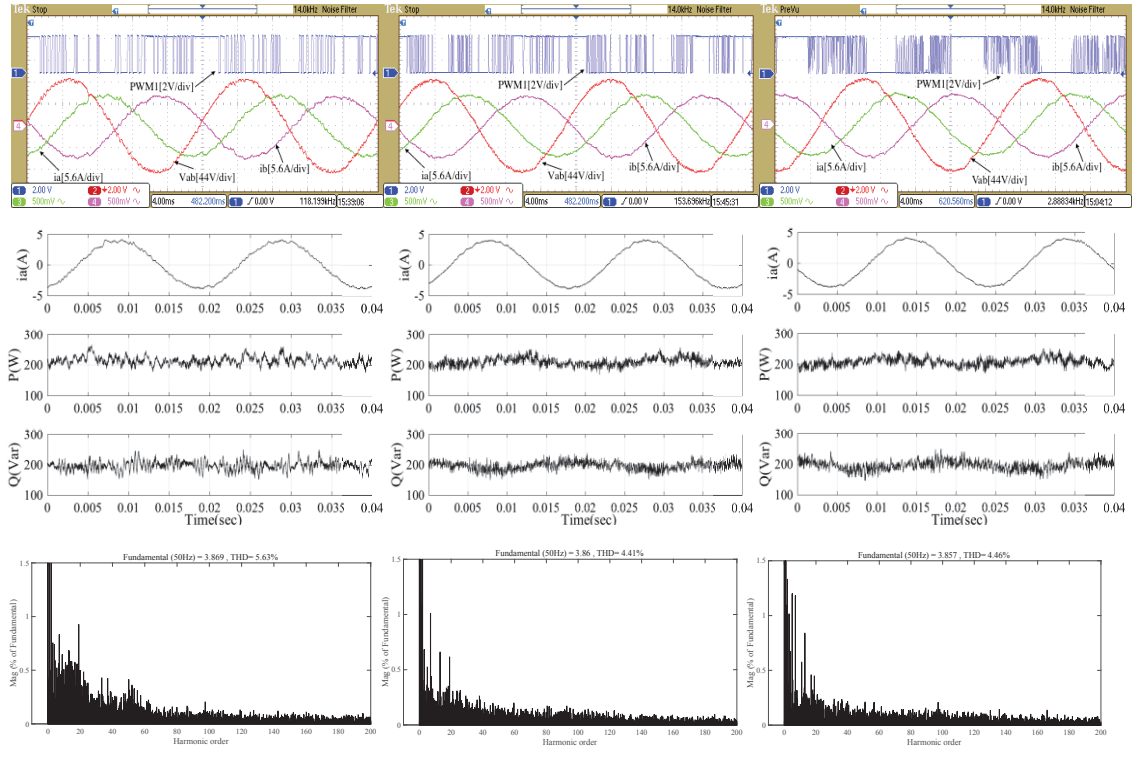
PWM1[2V/div]
ia[5.6A/div]
Vab[44V/div]
ib[5.6A/div]
ia(A)
P(W)
Q(Var)
Time(sec)

Fundamental (50Hz) = 3.869 , THD= 5.63%
Fundamental (50Hz) = 3.86 , THD= 4.41%
Fundamental (50Hz) = 3.857 , THD= 4.46%
Mag (% of Fundamental)
Harmonic order

(a) **(b)** **(c)**

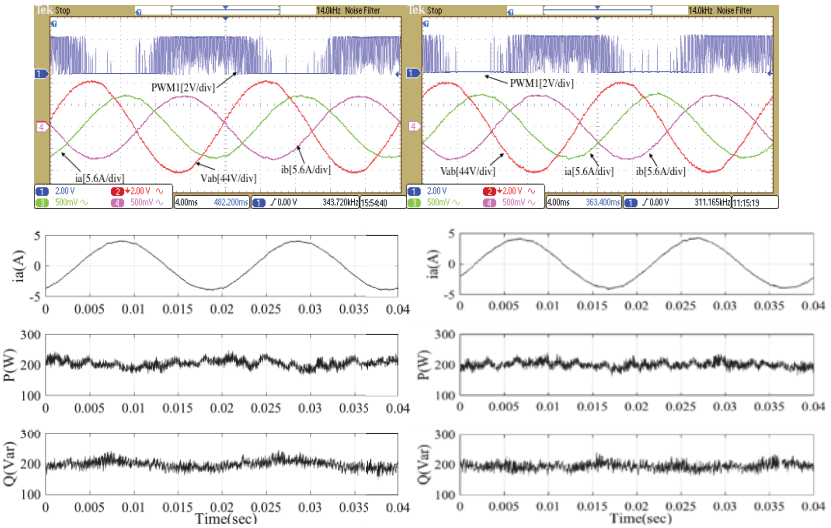
PWM1[2V/div]
ia[5.6A/div]
Vab[44V/div]
ib[5.6A/div]
ia(A)
P(W)
Q(Var)
Time(sec)

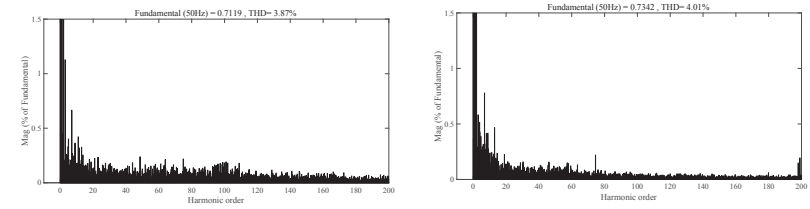
Fundamental (50Hz) = 0.7119 , THD= 3.87%
Fundamental (50Hz) = 0.7342 , THD= 4.01%
Mag (% of Fundamental)
Harmonic order

(d) **(e)**

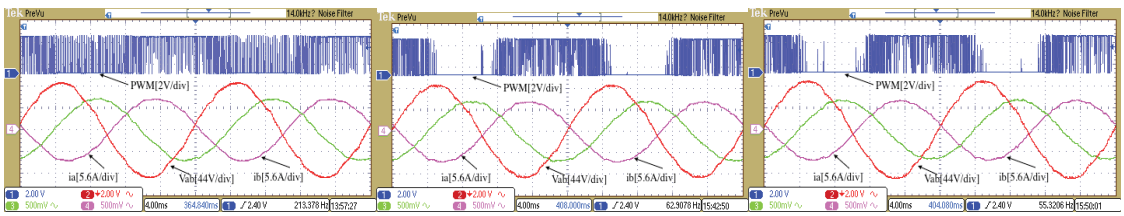
PWM[2V/div]
ia[5.6A/div]
Vab[44V/div]
ib[5.6A/div]

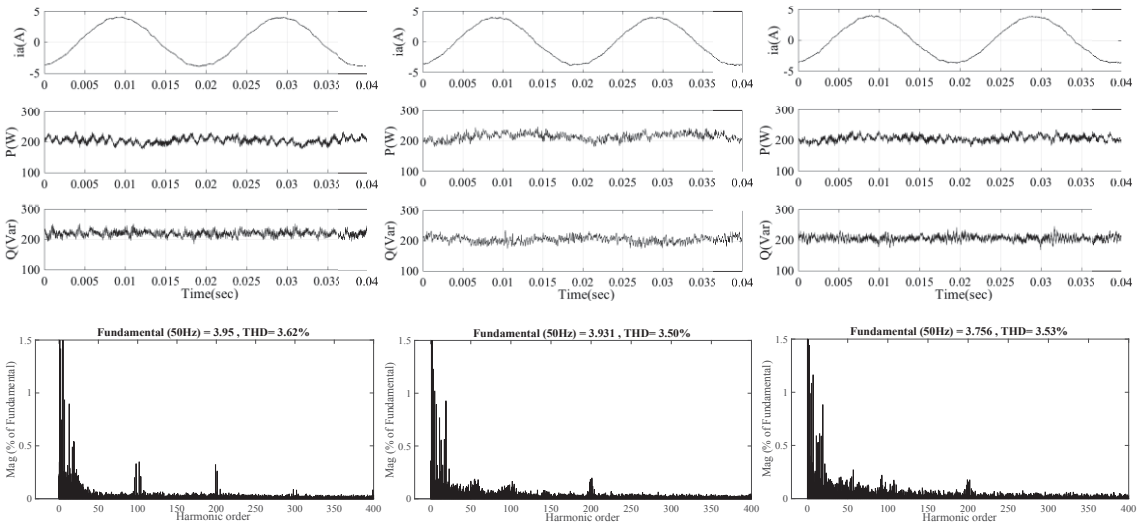

(f) **(g)** **(h)**

Fig.6.12 Steady state performance at *P*=200 W, *Q*=200 Var, Top to bottom: experimental figure, corresponding *P* and *Q*, and THD analyses of i_a, where (a) MPDPC-10k, (b) MPDPC-20k, (c) PDCC, (d) MPCDDC-I, (e) MPCDDC-II, (f) ISVMDPC, (g) MPCPDCC-I, and (h) MPCPDCC-II

Each method can track the reference values accurately with a similar quick response during the dynamic period, which validates the reference tracking ability of the proposed MPCDDC method. However, it is seen that the mutual influence on the other control objective is also apparent while there is a step change of active power. For instance, while the *P* step changes from 200 W to 400 W, the *Q* overshoots are 99.5 Var and 97.2 Var with MPDPC-10k and PDCC, respectively, as shown by the dashed circle in Figs. 6.13(a) and (c). The overshoot with ISVMDPC is 92.2 Var as shown in Fig. 6.13(f), which could not be eliminated. The same issue also exists in the proposed MPCDDC-I method. Without the mutual influence compensation, the *Q* overshoot is also as high as 69.8 Var, while with the MPCDDC-II method by adding a mutual influence compensation constraint, the *Q* overshoot is significantly decreased to 33.8 Var, as shown in Figs. 6.13(d) and (e). The same phenomenon can also be observed with the MPCPDCC based method, where the mutual influence is reduced significantly with the MPCPDCC-II method, as shown in Fig. 6.13(h).

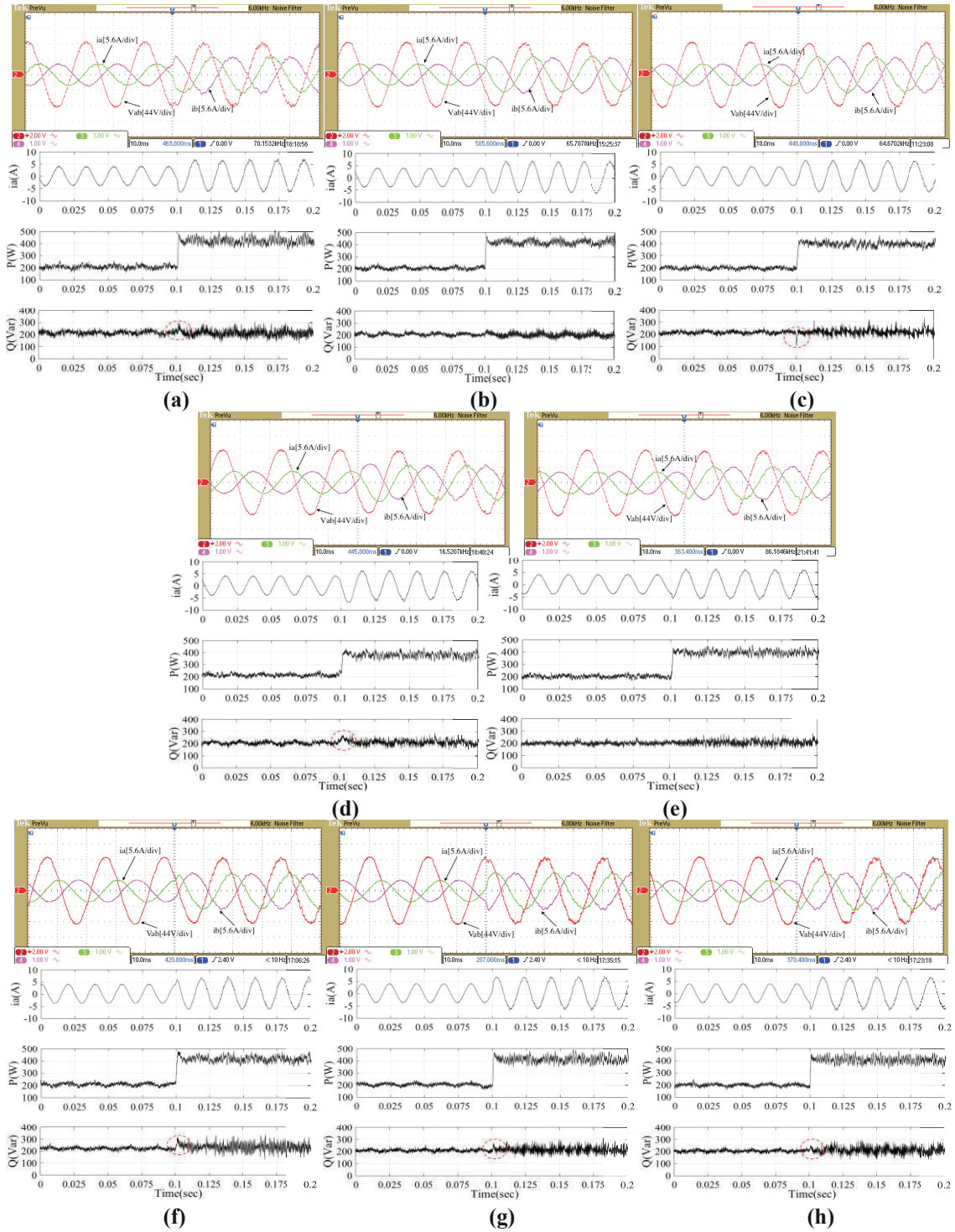

Fig. 6.13 Dynamic state performance when *P* from 200 W to 400 W, *Q*=200 Var, Top: experimental figure, Bottom: i_a, *P* and *Q*, where (a) MPDPC-10k, (b) MPDPC-20k, (c) PDCC, (d) MPCDDC-I, (e) MPCDDC-II, (f) ISVMDPC, (g) MPCPDCC-I, and (h) MPCPDCC-II

The experimental results when *Q* step changes from 450 Var to 150 Var and *P* remains at 300 W are also presented, as shown in Fig. 6.14. Similarly, it can be seen that the mutual influence also exists when *Q* has step changes with the MPDPC, IPDCC

and MPCDDC-I methods. The P overshoots are 85.5 W and 97.1 W with the MPDPC-10kHz and PDCC method, respectively, as shown by the dashed circle in Figs. 6.14(a) and (c). The P overshoot with the MPCDDC-I method is as high as 118.8 W, while with a mutual influence compensation of MPCDDC-II, the mutual influence is eliminated since the P overshoot is decreased to 49.5 W, as shown in Figs. 6.14(d) and (e). The quantitative comparison of each control method is presented in Table 6.8. Also, the per unit values of P and Q overshoots are nominalized in proportion to the nominal values of 300 W and 200 Var, respectively.

6.4 Conclusion of the Chapter

Various novel MPC based duty cycle control strategies for three-phase full-bridge AC/DC converters are proposed in this chapter. Firstly, the two vector based control method is proposed with simplified duration time calculation and comprehensively compared with other methods with simulation and experimental results. Then, the improved SVMDPC method is discussed and analysed in detail. Finally, a series of MPC based duty cycle control methods with three vector selection are proposed and analysed with mutual influence elimination ability and simplified calculation. Different from the conventional PDCC method, the selection of none-zero voltage vector pair uses the MPC method based on the proposed cost function, and thus the need for sector information is eliminated. Additional constraints could be involved easily to eliminate the mutual influence issue. The calculation of durations is much simpler and it would not be negative or exceed the range. The principles of vector pair selection, duration calculation, control delay compensation design and mutual influence elimination are discussed in detail.

Comprehensive comparisons by simulation and experimental results are presented to validate and compare the performance of various kinds of three vector based control methods. The results verify the superior dynamic and steady state performance of the proposed MPCDDC method with the advantage of fixed switching frequency, lower THD, lower power ripples and elimination of the mutual influence between active and

reactive powers during the step-change instant. Meanwhile, the control complexity is reduced. With the proposed MPCPDCC method, the best dynamic and steady state performance with the lowest power ripples and mutual influence elimination ability could be achieved.

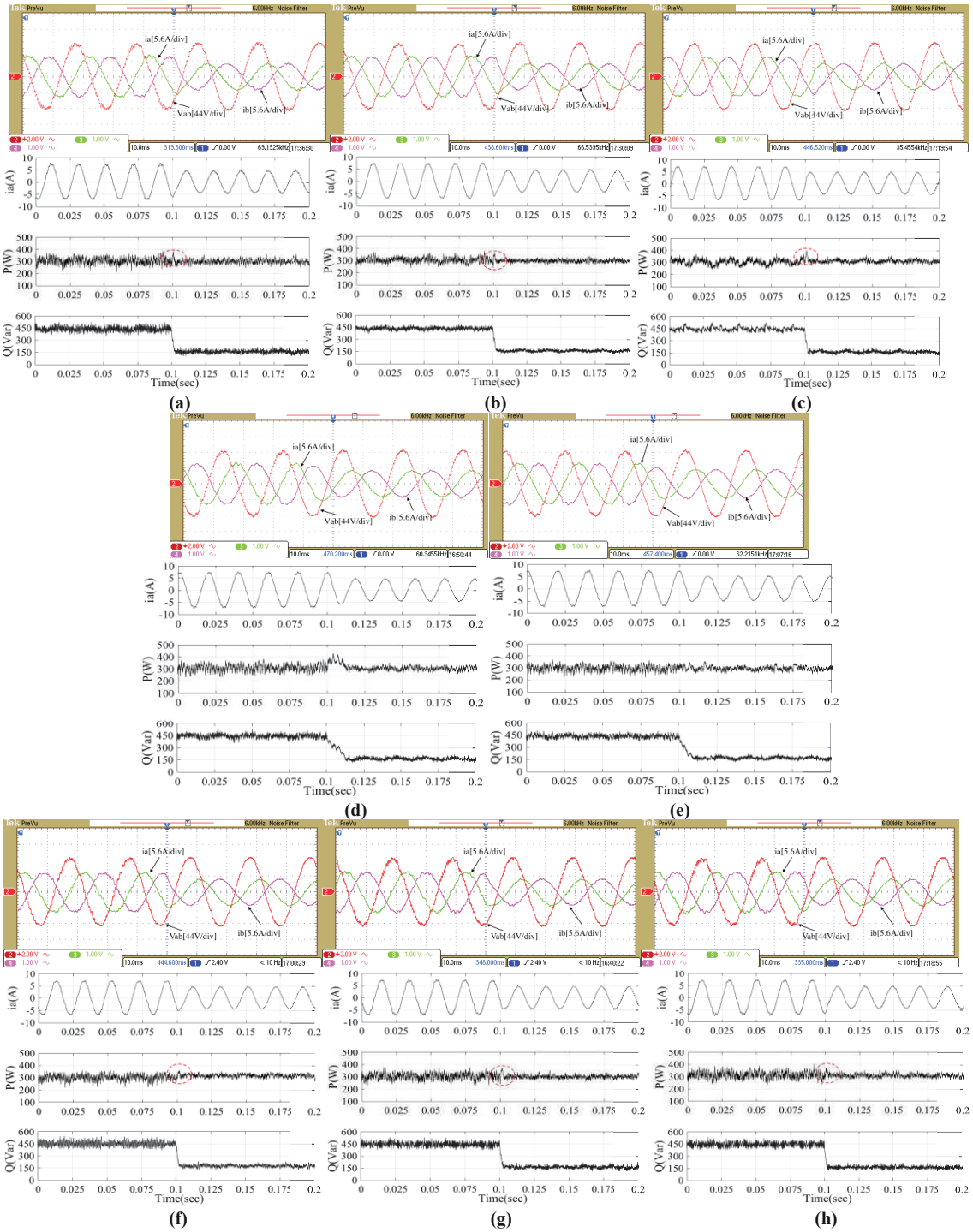

Fig. 6.14 Dynamic state performance when *Q* from 450 Var to 150 Var, *P*=300 W, Top: Experimental figure, Bottom: i_a, *P* and *Q*, where (a) MPDPC-10k, (b) MPDPC-20k, (c) PDCC, (d) MPCDDC-I, (e) MPCDDC-II, (f) ISVMDPC, (g) MPCPDCC-I, and (h) MPCPDCC-II

TABLE 6.8 Quantitative comparison of experimental results

Control	*fs* (Hz)	*THD* (%)	*Prip* (%)	*Qrip* (%)	*P* overshoot(%)	*Q* overshoot (%)
MPDPC-10k	10 K	5.63	7.72	8.09	28.5	49.75
MPDPC-20k	20 K	4.41	6.16	6.77	23.2	17.6
PDCC	10 K	4.46	6.27	7.19	32.4	48.6
MPCDDC-I	10 K	3.87	6.09	6.29	39.6	34.9
MPCDDC-II	10 K	4.01	5.07	6.29	16.5	16.9
ISVMDPC	10 K	3.62	6.21	5.69	20.3	46.1
MPCPDCC-I	10 K	3.53	5.81	5.50	24.3	38.0
MPCPDCC-II	10 K	3.5	5.71	5.19	22.1	25.0

REFERENCES

[6.1] C. Xia, T. Liu, T. Shi, and Z. Song, "A simplified finite-control-set model- predictive control for power converters," *IEEE Trans. Ind. Informat.*, vol.10, no. 2, pp. 991–1002, May 2014

[6.2] S. Vazquez *et al.*, "Model predictive control: A review of its applications in power electronics," *IEEE Ind. Electron. Mag.*, vol. 8, no. 1, pp. 16–31, Mar. 2014

[6.3] L. Tarisciotti, P. Zanchetta, A. Watson, J. Clare, M. Degano, and S. Bifaretti, "Modulated model predictive control for a three-phase active rectifier," *IEEE Trans. Ind. Appl*., vol. 51, no. 2, pp. 1610–1620, Mar./Apr. 2015

[6.4] P. Cortes, J. Rodriguez, P. Antoniewicz, and M. Kazmierkowski, "Direct power control of an AFE using predictive control," *IEEE Trans. Power Electron*., vol. 23, no. 5, pp. 2516–2523, Sep. 2008

[6.5] J. Rodriguez, J. Dixon, J. Espinoza, J. Pontt, and P. Lezana, "PWM regenerative rectifiers: State of the art," *IEEE Trans. Ind. Electron*., vol. 52, no. 1, pp. 5–22, Feb. 2005

[6.6] R. P. Aguilera, D. E. Quevedo, S. Vazquez, and L. G. Franquelo, "Generalized predictive direct power control for AC/DC converters," in *Proc. IEEE ECCE Asia Downunder*, 2013, pp. 1215–1220

[6.7] J. Hu, J. Zhu, and D. Dorrell, "In-depth study of direct power control strategies for power converters, *IET Power Electronics*," vol. 7, no. 7, 2014, pp. 1810–1820

[6.8] R. Aguilera, P. Lezana, and D. Quevedo, "Finite-control-set model predictive control with improved steady-state performance," *IEEE Trans. Ind. Informat*., vol. 9, no. 2, pp. 658 –667, may 2013.

[6.9] S. Aurtenechea, M. A. Rodriguez, E. Oyarbide, and J. R. Torrealday,"Predictive control strategy for DC/AC converters based on direct power control," *IEEE Trans. Ind. Electron.*, vol. 54, no. 3, pp. 1261–1271, Jun. 2007.

[6.10] J. Hu and Z. Q. Zhu, "Investigation on switching patterns of direct power control strategies for grid-connected DC–AC converters based on power variation rates," *IEEE Trans. Power Electron*., vol. 26, no. 12, pp. 3582–3598, Dec. 2011

[6.11] Z. Song, W. Chen, and C. Xia, “Predictive direct power control for three-phase grid-connected converters without sector information and voltage vector selection,” *IEEE Trans. Power Electron.*, vol. 29, no. 10, pp. 5518–5531, Oct. 2014

[6.12] Z. Song, Y. Tian, W. Chen, Z. Zou, and Z. Chen, “Predictive duty cycle control of three-phase active-front-end rectifiers,” *IEEE Trans. Power Electron*., vol. 31, no. 1, pp. 698–710, Jan. 2016

[6.13] D. Choi, K. Lee, "Dynamic performance improvement of AC/DC converter using model predictive direct power control with finite control set," *IEEE Trans. Ind. Electron.,* vol. 62, pp. 757-767, 2015

[6.14] Y. Zhang, Y. Peng, and H. Yang, “Performance improvement of two-vectors-based model predictive control of PWM rectifier,” *IEEE Trans. Power Electron.*, vol. 31, no. 8, pp. 6016–6030, 2016

[6.15] J. Hu and Z. Zhu, “Improved voltage-vector sequences on dead-beat predictive direct power control of reversible three-phase grid-connected voltage-sourced converters,” *IEEE Trans. Power Electron.*, vol. 28, no. 1, pp. 254–267, Jan. 2013

[6.16] A. Bouafia, J.P. Gaubert, F. Krim, “Predictive direct power control of three-phase pulsewidth modulation (PWM) rectifier using space-vector modulation (SVM)”, *IEEE Trans. Power Electron*., 2010, 25, (1), pp. 228–236

[6.17] Y. Zhang, W. Xie, Z. Li, and Y. Zhang, “Low-complexity model predictive power control: Double-vector-based approach,” *IEEE Trans. Ind. Electron.*, vol. 61, no. 11, pp. 5871–5880, 2014

Chapter 7

CONCLUSIONS AND FUTURE WORKS

7.1 Conclusions

In this thesis, the application of three-phase full-bridge converter for renewable energy systems and its control strategies have been studied comprehensively and new control strategies developed. Based on the research work presented in the thesis, the general conclusions can be drawn as the following:

(1) A review of the state of art of power converters for AC/DC conversion and DC/DC conversion with corresponding control strategies for microgrid applications, and microgrid topologies has led to the development of the isolated bidirectional full-bridge DC/-DC converters (IBDC) with high frequency transformer to provide galvanic isolation and new model predictive control (MPC) methods for effective improvement of dynamic and steady state performance of microgrids.

(2) A novel topology of microgrid with modular design by using three-phase full-bridge converter module is proposed. Various control modes and control strategies under different scenarios are analysed. A novel smart converter concept is proposed for renewable energy system applications to solve challenges of current converter.

(3) Based on a comprehensive study of control strategies for power converters, a novel advanced multi-functional MPC is developed to improve the dynamic and steady state performance simultaneously. A general utilized mutual influence elimination constraint is also proposed.

(4) Based on a comprehensive study of advantages and disadvantages of three vectors based predictive duty cycle control and corresponding improved method presented previously in the thesis, a novel reversible predictive duty cycle control

method is developed to reduce control complexity and achieve better steady and dynamic performance than the conventional and improved method.

(5) The proposed MPC for best vector selection for two and three vector based control method is applied in a microgrid, and a novel simplified duration time calculation method is proposed. An improved space vector modulation based direct power control method is studied for the purpose of comparison with the proposed methods. The novel two and three vector based method is further improved for even better performance with mutual influence elimination and simple calculation.

7.2 Future Works

The study of new advanced control strategies of smart converter for renewable energy systems and development of microgrids with more smart functions have become a trend to meet the challenges of energy depletion and more and more integration of distributed generations. Based on the progress obtained in this thesis, the continued work of this research area can be outlined as the following:

(1) Further development of smart converter prototype with wireless communication ability and using proposed advanced control strategies to research ancillary services such as reactive power compensation, fault ride-through.

(2) Application of the proposed control methods, such as mutual influence elimination and reversible vector selection to other areas with different control objectives, and further research of predictive based control strategies with more than one step prediction to further improve the performance.

(3) Further development and validation of the MPC strategy of IBDC converters for DC/DC conversion are required with each three-phase full-bridge simply controlled by the advanced controls proposed above. While the effectiveness of hypothetical control strategy is already verified by numerical simulation, further experimental validation is still required.

(4) Development of control strategies of the proposed microgrid with modular design, realizing control of each converter module with modular designed control strategies in various scenarios.

APPENDIX A:

PUBLICATIONS BASED ON THE THESIS WORK

Journal Papers:

[1] X. Shi, J. Zhu, DDC. Lu, and L. Li, “Multi-Functional model predictive control for three-phase AC/DC converters”. Under review.

[2] X. Shi, J. Zhu, DDC. Lu, and L. Li, “Model predictive based duty-cycle-control with mutual influence elimination and simple calculation for three-phase AC/DC converter”. Under review.

[3] X. Shi, J. Zhu, DDC. Lu, L. Li, and J. Zhang, “Novel predictive duty cycle control for three-phase AC/DC converters with reversible vector selection”. Under review.

[4] X. Shi, J. Zhu, DDC. Lu, and L. Li, “Predictive direct duty cycle control of three-phase AC/DC converters-two vector based approach”. Under review.

Conference Papers:

[1] X. Shi, J. Zhu, L. Li, Y. Qu, "Model predictive control of PWM AC/DC converters for Bi-directional power flow control in microgrids", *Power Engineering Conference.*, 2015.

[2] X. Shi, J. Zhu，DDC. Lu, L. Li, "Advanced multi-functional model predictive control for three-phase AC/DC converters", *Electrical Machines and Systems (ICEMS) 2016 19th International Conference on*, 2016.

[3] X. Shi, J. Zhu，DDC. Lu, L. Li, " A multi-functional modular approach to developing microgrid systems", *Electrical Machines and Systems (ICEMS) 2016 19th International Conference on*, 2016.